University of Nottingham

UK | CHINA | MALAYSIA

The roles of polyamines in ESKAPE pathogens

Thesis submitted to the University of Nottingham for the degree of Doctor of Philosophy

Samuel G. Jackson

Supervisors: Dr Laura Hobley, Professor Andrew Lovering, and Dr Philip Hill

March 2024

Abstract

Klebsiella pneumoniae and *Acinetobacter baumannii* are two of the ESKAPE pathogens that are responsible for a large number of nosocomial infections globally. Increasing levels of multidrug resistance make both organisms of critical concern for developing new therapeutic strategies. A possible approach for this is to target polyamine synthesis. Polyamines are small polycationic molecules that are derived from amino acids, that are found across all domains of life. In bacteria polyamine synthesis pathways are not conserved between species and polyamines do not have a conserved function, as they do in mammalian cells. They have been found to contribute to growth, gene expression, biofilm formation, motility, and stress resistance. Previous investigations have shown a link between polyamines and the virulence factors of *K. pneumoniae* and *A. baumannii.*

This study has shown that loss of 1, 3-diaminopropane synthesis, in *A. baumannii* impacts growth and results in a cell septation defect. Chemical complementation indicates a requirement for 1, 3-diaminopropane with other di- and triamines unable to chemically complement a Δ*ddc* 1, 3-diaminopropane null mutant. The Δ*ddc* strain also exhibited a lack of surface-associated motility, reduced biofilm formation with overproduction being observed when chemically complemented, a decreased susceptibility to aminoglycosides and attenuated virulence possibly linked to increased susceptibility to antimicrobial elements within the haemolymph of larvae. The loss of 1, 3-diaminopropane synthesis in *K. pneumoniae* had little impact, with only a reduction in biofilm formation being observed. With regard to cadaverine, deletion of the acid-inducible synthesis pathway in *K. pneumoniae* demonstrates the ability of cadaverine to contribute to growth in an acidic environment. Additionally, it suggests that cadaverine also provides protection against nitrosative stress in *K. pneumoniae* but not oxidative stress.

This study expands on the current understanding of the role of 1, 3-diaminopropane in *A. baumannii* and highlights some of the roles of 1, 3-

diaminopropane and cadaverine in *K. pneumoniae,* ultimately providing a foundation for future work to continue investigation into the use of polyamine synthesis as a therapeutic target.

Acknowledgements

I would first like to thank my supervisor Dr Laura Hobley for supervising and supporting me throughout my PhD. I thank Professor Andrew Lovering at The University of Birmingham for co-supervising me and providing support and guidance relating to protein structure and analysis. Thank you to Dr Phil Hill, my University of Nottingham co-supervisor, for his help and support.

I want to thank Professor Cath Rees, Dr David Scott, and Dr Jon Hobman for their invaluable suggestions and inputs throughout my PhD project. Thank you to Dr Patrick Moynihan and his PhD student Aaron Franklin at the University of Birmingham for conducting the HPLC analysis.

I want to thank the B-floor laboratory technical team for their role in maintaining the daily running of the laboratory.

I would also like to thank the Medical Research Council for funding this project and the Integrated Midlands Partnership for Biomedical Training (IMPACT) doctoral training program for its guidance and support.

Finally, I would like to thank my mum for her support not only during my PhD but also my entire academic career. I would not have made it this far without her support.

COVID-19 Impact statement

My research has been significantly impacted by the COVID-19 pandemic. It reduced my ability to collect experimental data. It severely limited access to the laboratory and resources and prevented some portions of the project from being carried out entirely.

I began laboratory work in January 2020. Before lockdown, I had made attempts at gene deletions and had begun constructing new deletion constructs for further attempts. Following the closure of university facilities in March 2020 I was unable to contribute to my PhD work, for the entirety of the lockdown, as at this stage of the project I did not have any data to analyse and as a lab group there was not a sufficient amount of data available from other sources for me to analyse to mitigate the effect of lockdown. I was able to return to the laboratory in early September 2020, having spent 6 months away from the laboratory. Despite being able to return it was only myself and other early-year PhD students, with academics required to work from home. It therefore made it difficult to communicate with my supervisor to discuss elements of the project and therefore impacting progression at this stage.

Regarding the work presented in Chapter 6, it was originally planned to express, purify, and solve the 3D structure of the 1, 3-diaminopropane synthesis enzymes, followed by the search for inhibitory compounds. This body of work was planned to be undertaken in the laboratory of Professor Andrew Lovering, at the University of Birmingham. However, due to the COVID-19 pandemic, I was unable to complete this section of my PhD project. Restrictions on movement and building capacity meant that I could not visit the laboratory of Professor Lovering at The University of Birmingham. Additionally, the pandemic severely slowed my progress at my home institution which meant that the majority of time spent in the laboratory went towards completing other aspects of my project, as the facilities were not available in my laboratory to purify the proteins of interest. This limited my ability to carry out this body of work and meant that it could not be completed as originally planned and

ultimately was abandoned due to the impact of the pandemic. To mitigate the impact of the pandemic, it was decided to carry out the work presented in Chapter 5 to assess the role of cadaverine in *K. pneumoniae* expanding the project beyond just looking at the roles of 1, 3-diaminopropane. Additionally, it was decided to carry out bioinformatic analysis of the 1, 3-diaminopropane synthesis enzymes, using *in silico* 3D predicted structures, as presented in Chapter 6.

Thus, this final thesis is the result of the altered project with the changes to project aims incorporated due to the effects of the pandemic.

Table of Contents

Chapter 1 Introduction 1

1.1 *Acinetobacter baumannii* and clinical relevance 1

1.1.1 Pathogenesis and virulence factors 1

1.1.2 Antibiotic resistance 4

1.2 *Klebsiella pneumoniae* and clinical relevance 5

1.2.1 Pathogenesis and virulence factors 6

1.2.2 Antibiotic resistance 8

1.3 Polyamines 10

1.3.1 Overview 10

1.3.2 Structure 10

1.3.3 Biosynthetic pathways 11

1.3.4 Transport of polyamines 22

1.3.5 The roles of polyamines in eukaryotes 24

1.3.6 The roles of polyamines in bacteria 26

1.3.7 Role in *A. baumannii* 36

1.3.8 Role in *K. pneumoniae* 39

1.3.9 Inhibition of polyamine synthesis as a treatment 41

1.3.10 Basis for utilising polyamine synthesis as a therapeutic target in *A. baumannii* and *K. pneumoniae* 42

1.4 Aims 44

Chapter 2 Materials and Methods 45

2.1 Growth media preparation 45

2.1.1 Lysogeny broth (Miller) and agar 45

2.1.2 100 mM MES buffered 1x M9-Glucose broth 45

2.1.3 1x M9-succinate broth 45

2.1.4 M9 agar 45

2.1.5 6 % (w/v) Sucrose agar 46

2.1.6 0.5 % (w/v) Motility agar 46

2.1.7 Lysine decarboxylase broth (Taylor Modification) 46

2.1.8 Mueller Hinton broth 46

2.1.9 Mueller Hinton Agar 46

2.1.10 Nutrient agar 46

2.1.11 Tryptone soya agar 46

2.1.12 Tryptone soya broth minimal media 46
2.1.13 Antibiotic stocks 47
2.2 Bacterial strains, primers, and plasmids 47
2.2.1 Bacterial strains used in this study 47
2.2.2 Primers used in this study 49
2.2.3 Plasmids used in this study 53
2.3 Bacterial growth and maintenance 55
2.3.1 Bacterial growth 55
2.3.2 Storage of bacterial strains 55
2.4 Cloning methods 55
2.4.1 Genomic DNA purification 55
2.4.2 Plasmid DNA purification 56
2.4.3 PCR amplification of DNA 56
2.4.4 Gel electrophoresis 57
2.4.5 DNA purification from agarose 57
2.4.6 PCR product purification 58
2.4.7 Quantification of nucleic acids 58
2.4.8 Restriction endonuclease digestion 58
2.4.9 Ligation of DNA fragments 59
2.4.10 Production of chemically competent *E. coli* 59
2.4.11 Heat shock transformation 59
2.4.12 Production of electrocompetent cells 60
2.4.13 Electroporation transformation 60
2.5 DNA sequencing 61
2.5.1 DNA sequencing of PCR products 61
2.5.2 DNA sequencing of plasmids 61
2.5.3 Whole genome sequencing 61
2.5.4 Analysis of whole genome sequencing data 62
2.6 Deletion of polyamine synthesis genes 63
2.6.1 Creation of deletion plasmids 63
2.6.2 Conjugation of *K. pneumoniae* and *A. baumannii* with *E. coli* β2163 containing the pGPI-SceI-2 deletion vectors 65
2.6.3 Conjugation of transformants with *E. coli* β2163 containing pDAI-SceI-SacB 66
2.6.4 Sucrose counterselection 67
2.7 Genetic complementation of *K. pneumoniae* 67

2.7.1 Primer design and amplification of polyamine synthesis genes 67
2.7.2 Insertion of synthesis genes into pGEM-T and transformation into *K. pneumoniae* deletion strains. 68
2.8 Bioinformatic analysis 68
2.8.1 DNA and protein sequences 68
2.8.2 Folded protein prediction 68
2.8.3 DNA, amino acids and 3D protein alignments 69
2.8.4 Prediction of promoters and terminators 69
2.8.5 Prediction of RNA secondary structure 69
2.8.6 Analysis of DNA curvature 69
2.8.7 Prediction of protein features, domains, and conserved residues 70
2.8.8 Predicting the effect of missense mutation on folded protein 70
2.9 Analysis of polyamine synthesis gene expression 70
2.9.1 Purification of total RNA 70
2.9.2 RT-PCR for analysis of gene expression 71
2.10 Analysis of polyamine content by HPLC 72
2.10.1 Preparation of reagents 72
2.10.2 Preparation of cellular extracts for HPLC analysis 73
2.10.3 Derivatization of polyamines for HPLC analysis 74
2.10.4 Reverse phase HPLC analysis 74
2.11 Analysis of lysine decarboxylase activity 75
2.12 Analysis of planktonic growth 75
2.12.1 Analysis of *K. pneumoniae* growth 75
2.12.2 Analysis of *A. baumannii* growth 75
2.12.3 Phase contrast microscopy 76
2.12.4 Microscopy image processing 76
2.12.5 Fluorescence microscopy 76
2.13 Analysis of capsule formation 77
2.14 Analysis of surface-associated motility 77
2.15 Stress assays 77
2.15.1 Oxidative stress 77
2.15.2 Nitrosative stress 78
2.16 Quantification of biofilm 79
2.16.1 Biofilm assay experimental preparation 79
2.16.2 Crystal violet staining of biofilms in M9 minimal media 79
2.16.3 Crystal violet staining of biofilms in LB media 80

2.17 Minimum inhibitory concentration assays 80
2.18 Analysis of *in vivo* virulence 81
2.18.1 Inoculum preparation 81
2.18.2 *G. mellonella* infection 82
2.19 Assessment of antimicrobial peptide activity in Haemolymph of *G. mellonella* 82
2.19.1 Pre-infection of *G. mellonella* 82
2.19.2 Haemolymph extraction 83
2.19.3 Antimicrobial peptide radial diffusion assay 84
2.20 Expression of Dat and Ddc enzymes from *K. pneumoniae* 52145 and *A. baumannii* 17978 85
2.20.1 Construction of pET28a and pET41c Dat and Ddc expression vectors 85
2.20.2 Expression of Dat and Ddc in *E. coli* BL21 87
2.20.3 Protein extraction and SDS-PAGE 88
2.20.4 Purification of HIS-tagged proteins 89
2.21 Analysis of protein: protein interactions with Bacterial two-hybrid system 90
2.21.1 Creation of BACTH vectors 90
2.21.2 Measurement of protein interaction by ONPG β-galactosidase assay 91
2.22 Statistical analysis 93
Chapter 3 Role of 1, 3-diaminopropane in *Acinetobacter baumannii* 95
3.1 Chapter introduction 95
3.2 Research aims 95
3.3 Chapter results 96
3.3.1 The genomic location, size, and structure of 1, 3-diaminopropane synthesis genes in *A. baumannii* 17978 96
3.3.2 Expression of 1, 3-diaminopropane synthesis genes 96
3.3.3 Deletion of 1, 3-diaminopropane synthesis genes in *A. baumannii* 17978 99
3.3.4 Identification of potential genotype variants of *A. baumannii* 17978 107
3.3.5 Deletion of the *ddc* gene abolishes 1, 3-diaminopropane synthesis. 109
3.3.6 Deletion of *ddc* alters colony morphology and growth kinetics of *A. baumannii* 17978 111
3.3.7 Deletion of *ddc* impacts cell division and morphology of cells 113
3.3.8 Cells within chains have defined septa 117

3.3.9 Planktonic growth kinetics are not complemented with other polyamines 117
3.3.10 Deletion of *ddc* abolishes *A. baumannii* 17978 surface-associated motility 120
3.3.11 Complementation with exogenous 1, 3-diaminopropane restores surface-associated motility 121
3.3.12 Complementation with polyamines other than 1, 3-diaminopropane does not restore surface-associated motility 122
3.3.13 Growth defects are complemented with exogenous 1, 3-diaminopropane 124
3.3.14 Complementation with β-alanine does not restore surface-associated motility 127
3.3.15 Deletion of the *ddc* gene reduces biofilm formation of *A. baumannii* 17978 128
3.3.16 Complementation with exogenous 1, 3-diaminopropane results in overproduction of biofilm in the Δ*ddc* but not in the wild type 130
3.3.17 Deletion of the *ddc* gene does not alter the susceptibility of *A. baumannii* 17978 to oxidative stress 131
3.3.18 The deletion of the *ddc* gene alters susceptibility to aminoglycosides 132
3.3.19 Deletion of *ddc* attenuates the virulence of *A. baumannii* 17978 in *Galleria mellonella* 133
3.3.20 The attenuated virulence of the Δ*ddc* strain is possibly a result of increased antimicrobial peptide susceptibility 135
3.4 Chapter discussion 138
3.4.1 Loss of 1, 3-diaminopropane results in significant growth defect and alters cell morphology 138
3.4.2 Loss of 1, 3-diaminopropane decreases biofilm formation 139
3.4.3 Loss of 1, 3-diaminopropane alters susceptibility to aminoglycosides 140
3.4.4 Loss of 1, 3-diaminopropane increases susceptibility to host immune system factors 141
3.4.5 Limitations 142
3.4.6 Conclusion 143
Chapter 4 Role of 1, 3-diaminopropane in *Klebsiella pneumoniae* 144
4.1 Chapter introduction 144
4.2 Research aims 145
4.3 Chapter results 145
4.3.1 The genomic location, size and structure of 1, 3-diaminopropane synthesis genes in *K. pneumoniae* 52145 145

4.3.2 Deletion of 1, 3-diaminopropane synthesis genes in *K. pneumoniae* 52145 146
4.3.3 Expression of 1, 3-diaminopropane synthesis genes..... 151
4.3.4 Analysis of the polyamines produced by *K. pneumoniae* 52145..... 154
4.3.5 Deletion of the *dat* or *ddc* genes does not alter *K. pneumoniae* hypermucoviscous phenotype..... 157
4.3.6 Deletion of *dat* or *ddc* does not affect the growth kinetics of *K. pneumoniae* 52145 159
4.3.7 Δ*dat* and Δ*ddc* exhibit altered biofilm formation of *K. pneumoniae* 52145 160
4.3.8 Loss of 1, 3-diaminopropane synthesis does not increase susceptibility to oxidative stress..... 162
4.3.9 Loss of 1, 3-diaminopropane synthesis does not significantly alter susceptibility to antibiotics..... 164
4.3.10 Deletion of *dat* or *ddc* does not alter *in vivo* virulence of *K. pneumoniae* in *Galleria mellonella* infection model..... 165
4.4 Chapter discussion..... 166
4.4.1 1, 3-diaminopropane contributes to biofilm formation in *K. pneumoniae* 52145 166
4.4.2 Synthesis of spermidine analogues from 1, 3-diaminopropane..... 167
4.4.3 Limitations 168
4.4.4 Conclusions..... 169
Chapter 5 Role of cadaverine in *Klebsiella pneumoniae* 170
5.1 Chapter introduction 170
5.2 Research aims..... 170
5.3 Chapter results..... 171
5.3.1 The genomic location, size, and structure of cadaverine synthesis genes in *K. pneumoniae* 171
5.3.2 Conservation of the cadaverine synthesis pathway..... 172
5.3.3 Expression of cadaverine synthesis genes in *K. pneumoniae* 52145. 186
5.3.4 Confirmation of the Δ*ldcC*, Δ*cadA,* and Δ*ldcC* Δ*cadA* deletions in *K. pneumoniae* 52145 189
5.3.5 Point mutations in *K. pneumoniae* 52145 wild type and Δ*ldcC*, Δ*cadA,* and Δ*ldcC* Δ*cadA* deletion strains. 191
5.3.6 Genetic complementation of cadaverine biosynthesis mutants..... 194
5.3.7 *K. pneumoniae* 52145 synthesises cadaverine 195
5.3.8 Deletion of *cadA* results in loss of acid-inducible cadaverine production..... 199

5.3.9 Genetic complementation with *cadA* does not restore lysine decarboxylase activity 200
5.3.10 Deletion of cadaverine synthesis genes does not alter *K. pneumoniae* hypermucoviscous phenotype 201
5.3.11 Cadaverine synthesis promotes growth in acidic conditions 202
5.3.12 Loss of cadaverine synthesis does not increase susceptibility to Oxidative stress 204
5.3.13 Deletion of *cadA* results in altered growth kinetics in the presence of nitrite 205
5.3.14 Deletion of cadaverine synthesis does not impact biofilm formation of *K. pneumoniae* 52145 210
5.3.15 Loss of cadaverine synthesis does not alter susceptibility to antibiotics 211
5.3.16 Deletion of cadaverine synthesis does not alter *in vivo* virulence of *K. pneumoniae* in *Galleria mellonella* infection model 212
5.4 Chapter discussion 214
5.4.1 Cadaverine contributes to acid tolerance in *K. pneumoniae* 52145 . 214
5.4.2 Synthesis of spermidine analogues from cadaverine 216
5.4.3 Cadaverine contributes to nitrosative stress resistance 216
5.4.4 Limitations 218
5.4.5 Conclusion 219
Chapter 6 Analysis of 1, 3-diaminopropane synthesis enzymes 220
6.1 Chapter introduction 220
6.2 Research aims 220
6.3 Chapter results 221
6.3.1 Expression and purification of *K. pneumoniae* and *A. baumannii* Dat and Ddc 221
6.3.2 Analysis of protein interactions with the bacterial two-hybrid system 227
6.3.3 *In silico* analysis of Dat and Ddc 233
6.3.4 Prediction of Dat 3D structure 243
6.3.5 Prediction of the Ddc 3D monomeric structure 248
6.3.6 Prediction of the 3D multimeric structure of Dat and Ddc 251
6.4 Chapter discussion 253
6.4.1 Conclusion 255
Chapter 7 Discussion 256
Chapter 8 References 258
Chapter 9 Appendix 279

Table of tables

Table 1.1 Residues required for the function of CadB in *E. coli* K12 17
Table 1.2 pH sensing residues of the periplasmic domain of CadC in *E. coli* K12..... 17
Table 1.3 DNA binding residues of the cytoplasm domain of CadC in *E. coli* K12..... 19
Table 2.1. Antibiotic stocks..... 47
Table 2.2 Strains used in this study 47
Table 2.3. Primers used in this study..... 49
Table 2.4 Plasmids used in this study 53
Table 2.5 PCR reaction mixtures..... 56
Table 2.6 PCR thermocycler conditions..... 57
Table 2.7 Reaction mixture for joining deletion fragments..... 64
Table 2.8 Thermocycler conditions for joining deletion construct fragments 64
Table 2.9: OneStep Reverse transcription PCR reaction mixture..... 72
Table 2.10: Onestep reverse transcription PCR thermocycler conditions 72
Table 3.1. SNPS unique to *A. baumannii* 17978 UN Δ*ddc* strain 105
Table 3.2. The MIC of antimicrobials determined for *A. baumannii* 17978 wild type and Δ*ddc* strains 133
Table 4.1. SNPS unique to *K. pneumoniae* 52145 Δ*dat* and Δ*ddc* strains 150
Table 4.2 Predicted intrinsic terminators upstream and downstream of the *dat* ORF..... 153
Table 4.3. Shared polyamine modulon features between *E. coli* K12 and *K. pneumoniae* 52145 162
Table 4.4 The MIC of antimicrobials determined for *K. pneumoniae* 52145 wild type, Δ*dat*, and Δ*ddc* strains..... 164
Table 5.1. Regions of CadC protein and corresponding residues. 175
Table 5.2. Regions of LysP protein and their corresponding residues 182
Table 5.3. Point mutations unique to the *K. pneumoniae* cadaverine deletion strains 192
Table 5.4 The MIC of antimicrobials determined for *K. pneumoniae* 52145 wild type, Δ*ldcC*, Δ*cadA* and Δ*ldcC* Δ*cadA* strains 212
Table 6.1 Comparison of the predicted 3D structure of Ddc with group II decarboxylases 250

Table 9.1. Growth rates and doubling times for *A. baumannii* 17978 wild type and Δ*ddc* strains.....279
Table 9.2. Growth rate and doubling times for *K. pneumoniae* 52145 wild type, Δ*dat* and Δ*ddc* strains.....281
Table 9.3. Growth rates and doubling times for the *K. pneumoniae* 52145 wild type, Δ*ldcC*, Δ*cadA* and Δ*ldcC* Δ*cadA* strains.....282
Table 9.4. Growth rates and doubling times for the *K. pneumoniae* 52145 wild type, Δ*ldcC*, Δ*cadA* and Δ*ldcC* Δ*cadA* strains when exposed to acidified nitrite, sodium nitroprusside and ferrocyanide.....282

Table of figures

Figure 1.1. The virulence factors of *A. baumannii*. 2
Figure 1.2. The virulence factors of *K. pneumoniae*. 7
Figure 1.3. The structure of the diamines 1, 3-diaminopropane, putrescine and cadaverine. 10
Figure 1.4. The structure of spermidine and structural analogues. 11
Figure 1.5. The structure of spermine and structural analogues. 11
Figure 1.6. Formation of a Schiff base between pyridoxal 5'-phosphate and the active site lysine residue. 12
Figure 1.7. Overview of the known 1, 3-diaminopropane biosynthesis pathway in *A. baumannii*. 13
Figure 1.8. Functional residues of the L-2, 4-diaminobutyrate aminotransferase (EctB) from *C. salexigens* DSM 3043. 14
Figure 1.9. Overview of the known putrescine synthesis pathway in *E. coli*. 15
Figure 1.10. Overview of the known cadaverine biosynthesis pathway in *E. coli*. 15
Figure 1.11. Overview of the acid-inducible Cad system in *E. coli*. 16
Figure 1.12. Representation of the role of the linker sequence within the CadC protein. 18
Figure 1.13. Overview of the genetic elements relating to the regulation of *cadBA* expression. 19
Figure 1.14. The role of H-NS in the regulation of *cadBA* expression. 20
Figure 1.15. Overview of the known spermidine synthesis pathway present in *E. coli*. 21
Figure 1.16. Examples of polyamine transporters identified in *E. coli*. 22
Figure 1.17. Diagram depicting the hypusination of eIF5A. 25
Figure 1.18. Proposed molecular mechanisms of polyamines modulating protein expression. 26
Figure 1.19. Mechanisms of polyamine modulation in *E. coli*. 29
Figure 1.20. The formation of ROS and RNS following phagocytosis. 30
Figure 1.21. Overview of the effect of polyamine modulation of SoxR, EmrR, GshA, and RpoS. 31
Figure 1.22. Diagram showing the proposed mechanism norspermidine promotes biofilm formation in *V. cholerae*. 35

Figure 1.23. The structure of baumannoferrin A and B. 37
Figure 1.24. The proposed synthesis pathway of spermidine analogues norspermidine and aminopropyl cadaverine in *K. pneumoniae* 52145. 40
Figure 1.25. The structure of ornithine and the fluorinated structural analogue α-difluoromethylornithine (DFMO). 41
Figure 3.1. The genomic organisation of the *dat* and *ddc* genes. 96
Figure 3.2. The *dat* and *ddc* genes of *A. baumannii* 17978 are expressed during exponential growth. 97
Figure 3.3. The *dat* ORF of *A. baumannii* 17978 does not have a dedicated intrinsic terminator. 98
Figure 3.4. The *dat* and *ddc* genes are co-expressed in *A. baumannii* 17978. 99
Figure 3.5. Overview of generating markerless gene deletions. 100
Figure 3.6. Confirmation of vectors for the deletion *dat* and *ddc* in *A. baumannii* 17978. 102
Figure 3.7. Confirmation of the deletion of the *ddc* gene of *A. baumannii* 17978. 103
Figure 3.8. The AbaAL44 accessory locus. 107
Figure 3.9. *A. baumannii* 17978 WT laboratory glycerol stock and the Δ*ddc* strain are of the UN genotype. 109
Figure 3.10. Retention times of 1, 3-diaminopropane, putrescine and 1, 7-diaminoheptane standards. 110
Figure 3.11. Deletion of the *ddc* gene abolishes 1, 3-diaminopropane synthesis. 111
Figure 3.12. Deletion of the *ddc* gene results in a growth deficiency as observed by reduced colony size in *A. baumannii* 17978. 112
Figure 3.13. Deletion of the *ddc* gene reduces the planktonic growth rate of *A. baumannii* 17978. 113
Figure 3.14 Deletion of the *ddc* gene results in a cell septation defect. 114
Figure 3.15. The Δ*ddc* strain forms chains throughout all growth phases. 116
Figure 3.16. Chaining cells have defined points of septation. 117
Figure 3.17. Polyamines other than 1, 3-diaminopropane are incapable of complementing the growth defect of the Δ*ddc* strain. 119
Figure 3.18. Diamines, triamines, and tetra-amines cannot be substituted for 1, 3-diaminopropane. 120

Figure 3.19. Deletion of the *ddc* gene abolishes the motility of *A. baumannii* 17978UN. 121
Figure 3.20. Exogenous 1, 3-diaminopropane complements the motility defect of the Δ*ddc* strain..... 122
Figure 3.21. Polyamines, other than 1, 3-diaminopropane, are incapable of restoring the surface-associated motility phenotype of *A. baumannii* 17978 Δ*ddc.* 123
Figure 3.22. Spermine is toxic to *A. baumannii* 17978 on motility agar. 124
Figure 3.23. Exogenous 1, 3-diaminopropane complements the growth defect of the Δ*ddc* strain..... 125
Figure 3.24. Exogenous 1, 3-diaminopropane complements the Δ*ddc* strains cell division defect. 127
Figure 3.25. β-alanine is incapable of complementing the surface motility defect of the Δ*ddc* strain. 128
Figure 3.26. Deletion of the *ddc* gene reduces the levels of biofilm formed by *A. baumannii* 17978 and complementation with exogenous 1, 3-diaminopropane results in overproduction of biofilm by the Δ*ddc* strain. 129
Figure 3.27. Deletion of the *ddc* gene does not change the susceptibility to hydrogen peroxide-induced in *A. baumannii* 17978. 132
Figure 3.28. Deletion of the *ddc* gene results in attenuated virulence of *A. baumannii* 17978. 135
Figure 3.29. Deletion of the *ddc* gene increases the susceptibility of *A. baumannii* 17978 to *G. mellonella* haemolymph. 136
Figure 3.30. Infection with Δ*ddc* does not alter the antimicrobial properties of *G. mellonella* haemolymph. 137
Figure 4.1. The genomic organisation of the *dat* and *ddc* genes. 145
Figure 4.2. Confirmation of vectors for single deletion of the *dat* and *ddc* genes in *K. pneumoniae* 52145. 147
Figure 4.3. Confirmation of the deletion of *dat* and *ddc* genes of *K. pneumoniae* 52145. 148
Figure 4.4. The *dat* and *ddc* genes of *K. pneumoniae* 52145 are expressed during exponential growth. 152
Figure 4.5. The *dat* ORF of *K. pneumoniae* 52145 does not have a dedicated intrinsic terminator. 153

Figure 4.6. The *dat* and *ddc* genes are co-expressed in *K. pneumoniae* 52145. 154
Figure 4.7. Retention times of 1, 3-diaminopropane, putrescine, 1, 7-diaminoheptane and spermidine polyamine standards.....155
Figure 4.8. 1, 3-diaminopropane is synthesised by *K. pneumoniae* 52145. 157
Figure 4.9. Deletion of the *dat* and *ddc* genes does not impact capsule formation or the hypermucoviscous phenotype of *K. pneumoniae* 52145. 158
Figure 4.10. Deletion of the *dat* and *ddc* genes does not affect the growth kinetics of *K. pneumoniae* 52145.....160
Figure 4.11. Deletion of the *dat* and *ddc* genes reduces the levels of biofilm formed by *K. pneumoniae* 52145 in MES-buffered M9 minimal salt media (pH 6.5).....161
Figure 4.12. Loss of 1, 3-diaminopropane synthesis does not increase the susceptibility of *K. pneumoniae* 52145 to oxidative stress caused by hydrogen peroxide.....164
Figure 4.13. 1, 3-diaminopropane is not required for the virulence of *K. pneumoniae* 52145.....166
Figure 5.1. The genomic organisation of the *ldcC* gene and the *cadCBA* operon. 172
Figure 5.2. Functional residues of LdcC and CadA are highly conserved between *E. coli* K12 and *K. pneumoniae* 52145.....174
Figure 5.3. Amino acid sequence of CadB is highly conserved between *E. coli* K12 and *K. pneumoniae* 52145.....176
Figure 5.4. Several residues required for pH sensing are not conserved between the CadC of *E. coli* K12 and *K. pneumoniae* 52145.....178
Figure 5.5. 266Q, G284, E468 and P499 of *E. coli* K12 CadC are not completely conserved in *Klebsiella* species.....180
Figure 5.6. The amino acid sequence of LysP is highly conserved between *E. coli* K12 and *K. pneumoniae* 52145.....183
Figure 5.7. Regulatory elements with the *cadBA* promoter region are partially conserved. 184
Figure 5.8. The 3' end of cadC ORF and the intergenic region between *cadC* and *cadB* in *K. pneumoniae* 52145 have intrinsic curvature. 185
Figure 5.9. *ldcC* and *cadA* genes of *K. pneumoniae* 52145 are expressed at neutral and acidic pH.....187
Figure 5.10. The *cadBA* genes are co-expressed in *K. pneumoniae* 52145. 189

Figure 5.11. Confirmation of the deletion of *ldcC* and *cadA* genes of *K. pneumoniae* 52145. 190
Figure 5.12. Confirmation of vectors for genetic complementation of Δ*ldcC*, Δ*cadA*, and Δ*ldcC* Δ*cadA*. 194
Figure 5.13. Retention times of 1, 3-diaminopropane, putrescine, cadaverine, 1, 7-diaminoheptane and spermidine polyamine standards. 195
Figure 5.14. Putrescine and spermidine are synthesised at pH 6.5 and stationary phase in *K. pneumoniae* 52145. 196
Figure 5.15. Cadaverine is synthesised at pH 5.5 and stationary phase in *K. pneumoniae* 52145. 197
Figure 5.16. Cadaverine is synthesised at pH 6.5 and stationary in *K. pneumoniae* 52145 and is possibly converted into aminopropylcadaverine. 198
Figure 5.17. Deletion of the *cadA* gene results in the loss of acid-inducible lysine decarboxylase activity. 199
Figure 5.18. The loss of inducible lysine decarboxylase activity cannot be genetically complemented. 201
Figure 5.19. Deletion of the *ldcC* and *cadA* genes does not impact capsule formation or the hypermucoviscous phenotype of *K. pneumoniae* 52145. 202
Figure 5.20. The *cadA* gene promotes growth at pH 4. 204
Figure 5.21. Cadaverine does not protect against oxidative stress induced by H_2O_2. 205
Figure 5.22. Deletion of the Δ*cadA* gene impacts growth kinetics in the presence of acidified sodium nitrite. 207
Figure 5.23. Deletion of the Δ*cadA* gene impacts growth kinetics in the presence of sodium nitroprusside at pH 5.5. 208
Figure 5.24. Preliminary data suggests that exogenous cadaverine is unable to alleviate the effect of acidified nitrite on *K. pneumoniae* 52145. 210
Figure 5.25. Deletion of the *ldcC* and *cadA* genes does not affect the biofilm formation of *K. pneumoniae* 52145 in MES-buffered M9 minimal salt media (pH 6.5). 211
Figure 5.26. Cadaverine synthesis is not required for the virulence of *K. pneumoniae* 52145. 213
Figure 6.1. Confirmation of the pET28a and pET41c expression vectors. 223
Figure 6.2. The *K. pneumoniae* Dat can be expressed in *E. coli* BL21. 224

Figure 6.3. The *A. baumannii* Dat can be expressed in *E. coli* BL21. 225
Figure 6.4. The Ddc from *K. pneumoniae* and *A. baumannii* can be expressed in *E. coli* BL21. 226
Figure 6.5. SDS-PAGE of 1, 3-diaminopropane synthesis enzymes following affinity chromatography. 227
Figure 6.6. Diagram of BACTH vector MCS sequences. 228
Figure 6.7. Confirmation of the BACTH vectors. 229
Figure 6.8. Dat and Ddc form homomultimeric structures but do not form heteromultimeric structures. 231
Figure 6.9. Dat and Ddc interact to form homomultimeric structures. 232
Figure 6.10. The predicted domains and features of the Dat protein in *A. baumannii* 17978. 233
Figure 6.11. The predicted domains and features of the Ddc protein in *A. baumannii* 17978. 234
Figure 6.12. Residues involved in PLP-binding and substrate binding pocket are conserved between EctB of *C. salexigens* and *A. baumannii*. 236
Figure 6.13. The -S(N, T)-X-H-K tetrapeptide sequence is not completely conserved in Ddc of *A. baumannii* 17978 and *K. pneumoniae* 52145. 238
Figure 6.14. The predicted domains and features of the Dat protein in *K. pneumoniae* 52145. 239
Figure 6.15. The predicted domains and features of the Ddc protein in *K. pneumoniae* 52145. 240
Figure 6.16. Residues involved in PLP-binding and the substrate-binding pocket are conserved between EctB of *C. salexigens* and *K. pneumoniae*. 242
Figure 6.17. The predicted monomeric structure of Dat from *K. pneumoniae* 52145. 244
Figure 6.18. The predicted monomeric structure of Dat from *A. baumannii* 17978. 245
Figure 6.19. Alignment of the ColabFold predicted 3D structures of Dat from *K. pneumoniae* 52145 and *A. baumannii* 17978. 246
Figure 6.20. Alignment of the ColabFold predicted 3D structures of L-2, 4-diaminobutyrate:2-ketoglutarate 4-aminotransferase from *K. pneumoniae* 52145 and *A. baumannii* 17978 with the 3D structure of EctB (6RL5) from *C. salexigens* DSM 3034. 247

Figure 6.21. The predicted monomeric structure of Ddc from *K. pneumoniae* 52145. 248
Figure 6.22. The predicted monomeric structure of Ddc from *A. baumannii* 17978. 249
Figure 6.23. Alignment of the ColabFold predicted 3D structures of Ddc from *K. pneumoniae* 52145 and *A. baumannii* 17978. 249
Figure 6.24. Dat forms a tetrameric structure. 252
Figure 6.25. Ddc forms dimeric structure. 253
Figure 9.1. The Δ*ddc* strain has a septation defect and forms chains in planktonic culture. 280
Figure 9.2. 1, 3-diaminopropane complements the septation defect of the Δ*ddc* strain. 281

Table of equations

Equation 2.1. Miller equation 93
Equation 3.1. The Fenton reaction 131
Equation 5.1. The formation of reactive nitrogen species from nitrite in the presence of hydrogen ions. 206

List of abbreviations

%	percentage
<	less than
=	equals
>	greater than
±	plus or minus
≤	less than or equal to
≥	greater than or equal to
°C	degrees Celsius
µF	microfarad
µg	microgram
µl	microlitre
µm	micrometre
µM	micromolar
16S	rRNA component of the 30S ribosomal subunit
3'	3 prime hydroxyl end of DNA or RNA
30S	30S ribosomal subunit
5'	5 prime hydroxyl end of DNA or RNA
Å	angstrom
Ab	*A. baumannii*
Abs	absorbance
Acb complex	*Acinetobacter calcoaceticus* - *baumannii* complex
Ala	alanine
Amp	ampicillin
Arg	arginine
ASN	acidified sodium nitrite
ATP	adenosine triphosphate
ATPase	ATP hydrolase
BACTH	bacterial adenylate cyclase-based two-hybrid system
BLAST	basic local alignment search tool
BLASTn	Nucleotide BLAST
BLASTp	protein BLAST
bp	base pair

CAUTIs	catheter-associated urinary tract infection
CFU	colony forming units
CFU/ml	colony forming units per ml
CLSI	clinical and laboratory standards institute
CPS	capsule polysaccharide
Dat	L-2, 4-diaminobuyrate: 2-ketoglutarate aminotransferase
dat	gene encoding L-2, 4-diaminobutyrate: 2-ketoglutarate aminotransferase
Ddc	L-2, 4-diaminobuyrate decarboxylase
ddc	gene encoding L-2, 4-diaminobuyrate decarboxylase
DFMA	difluoromethylarginine
DFML	difluoromethyllysine
DFMO	DL-alpha-difluoromethylornithine
DNA	deoxyribonucleic acid
dNTPS	deoxynucleotide triphosphates
eIF5A	Eukaryotic initiation factor 5A
Em	emission
Ex	excitation
g	grams
GFP	green fluorescent protein
Gln	glutamine
Glu	glutamic acid
Gly	glycine
H_2O_2	hydrogen peroxide
His	histidine
H-NS	histone-like nucleoid-structuring protein
HPLC	high-performance liquid chromatography
IPTG	Isopropyl β- d-1-thiogalactopyranoside
Kbp	Kilobase pair
kDa	kilodalton
kg	kilogram
Kp	*K. pneumoniae*
kV	kilovolts
l	litres
LC-MS	Liquid chromatography–mass spectrometry

LDC	lysine decarboxylase
LDDT	local distance difference test
Leu	leucine
LOS	Lipooligosaccharide
LPS	lipopolysaccharide
Lys	lysine
M	molar
MCS	multiple cloning site
MFML	monofluoromethyllysine
mg	milligram
MGBG	methylglyoxal bis(guanylhydrazone)
MIC	minimum inhibitory concentration
min	minute
ml	millilitre
mM	millimolar
ms	milliseconds
NADPH	nicotinamide adenine dinucleotide phosphate
NCBI	National Centre for Biotechnology Information
nm	nanometres
NO	nitric oxide
OD	optical density
Omp	outer membrane protein
ONPG	2-Nitrophenyl β-D-galactopyranoside
ORF	open reading frame
PAE	predicted aligned error score
PBP	penicillin binding protein
PDB	protein data bank
pLDDT	predicted local distance difference test
PLP	pyroxidal 5-phosphate
PMF	proton motive force
r	resistance
Rf	retardation factor
RMSD	root mean square deviation
RNA	ribonucleic acid

RNS	reactive nitrogen species
ROS	reactive oxygen species
rpm	revolutions per minute
rRNA	ribosomal RNA
s	seconds
SDS	sodium dodecyl sulphate
SDS-PAGE	sodium dodecyl sulphate polyacrylamide gel electrophoresis
SEC	size exclusion chromatography
SFC	sodium ferrocyanide
SMART	simple modular architecture research tool
SNP(s)	single nucleotide polymorphism(s)
SNP	sodium nitroprusside
Tet	tetracycline
Thr	threonine
Tmp	trimethoprim
TM-score	template modelling score
tRNA	transfer ribonucleic acid
$tRNA^{supE}$	suppressor tRNA
UTI	urinary tract infection
UV	ultraviolet
v/v	volume by volume
Val	valine
w/v	weight by volume
WGS	whole genome sequencing
WHO	world health organisation
x g	relative centrifugal force
XDR	extensive drug resistance
X-Gal	5-bromo-4-chloro-3-indolyl-beta-D-galacto-pyranoside
α	alpha
β	beta
γ	gamma
Δ	delta (deletion)
ε	epsilon
Ω	ohms

Chapter 1 Introduction

1.1 *Acinetobacter baumannii* and clinical relevance

Acinetobacter baumannii is a Gram-negative, pleomorphic, strictly aerobic bacterium often referred to as an opportunistic pathogen that primarily causes nosocomial infection. The estimated annual incidence of *A. baumannii* infection is one million cases, globally (Spellberg and Rex, 2013). One of the most common infections is ventilator-associated pneumonia found to have a mortality rate between 30-80 % (Inchai et al., 2015; Özgür et al., 2014). *A. baumannii* is also responsible for a significant number of bloodstream infections, with mortality rates reported to be close to 40 % (Wisplinghoff et al., 2012). Nosocomial meningitis caused by *A. baumannii* is of increasing concern. Primarily associated with neurosurgery, the mortality rate has been reported as high as 73 % (Tuon et al., 2010). Less commonly *A. baumannii* is capable of causing urinary tract infections with these often being catheter-associated (Moubareck and Halat, 2020). *A. baumannii* is also known to infect skin, soft tissue, and bone. Incidences have been associated with trauma victims in warzones and following natural disasters, with examples being the Iraq (Scott et al., 2007) and Syrian (Rafei et al., 2014) conflicts and the Turkish/Syrian and Wenchuan earthquakes of 2023 and 2008, respectively (Eryilmaz-Erem et al., 2023; Xie et al., 2010). During the COVID-19 pandemic *A. baumannii* was responsible for increased incidences of secondary infection, and an increased mortality rate (Iacovelli et al., 2023).

1.1.1 Pathogenesis and virulence factors

Several virulence factors have been identified in *A. baumannii.* These provide fitness advantages that allow for survival and persistence within the environment and contribute to pathogenesis in the host.

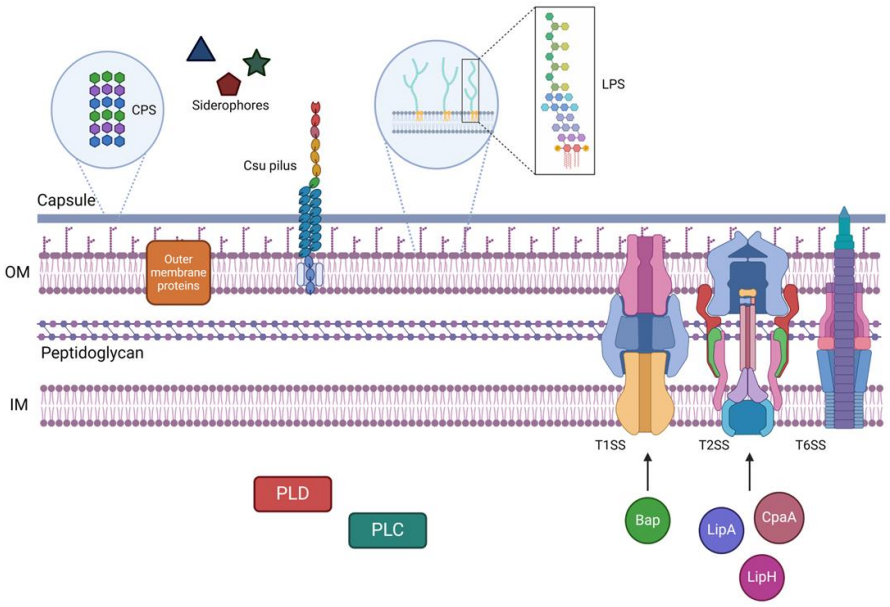

Figure 1.1. The virulence factors of *A. baumannii*. An overview of some of the virulence factors employed by *A. baumannii* including capsule polysaccharide (CPS), phospholipase C and D (PLC/D), biofilm-associated protein (Bap), Lipases (LipA/H), metallopeptidase (CpaA), type one secretion system (T1SS), type two secretion system (T2SS), type six secretion system (T6SS), chaperone usher pilus (Csu pilus) and lipopolysaccharide (LPS). The outer membrane protein is representative of OmpA, Omp33, and CarO. OM: outer membrane. IM: inner membrane. Figure was made using BioRender.

Like many Gram-negative bacteria, a major component of the outer membrane of *A. baumannii* is Lipopolysaccharide (LPS) (Figure 1.1) (Bertani and Ruiz, 2018). The outer membrane can also feature lipooligosaccharide (LOS), which does not contain the O antigen. Instead, it has an extended core of oligosaccharides (Bertani and Ruiz, 2018). *A. baumannii* is capable of Lipid A modification, carried out by LpxL and LpxM lipid A acetylate transferases that add lauryl acyl groups to lipid A. The modification carried out by $LpxM_{Ab}$ is found to increase resistance to antimicrobial peptides (AMPs) and desiccation and is required for virulence (Boll et al., 2015). *A. baumannii* is also capable of producing a capsule (Figure 1.1). This protects against disinfectants and desiccation (Tipton et al., 2018). This allows for persistence and survival, a major problem with *A. baumannii* in healthcare settings. Capsule also allows growth in human serum by protecting against host complement (Russo et al.,

2010). This is primarily due to the capsule creating an impassible barrier preventing interaction with the cell surface.

A. baumannii is capable of several different types of lifestyles. One example of this is biofilm. This describes a population of bacteria that are adhered to biotic or abiotic surfaces and are surrounded by an extracellular matrix comprised of exopolysaccharides, proteins, and extracellular DNA (Flemming et al., 2016). Biofilm is a key element in *A. baumannii* infection and contributes to the pathogen's ability to persist and overcome the environment. Several biofilm-related components have been identified such as chaperone/usher (Csu) pili (Figure 1.1), biofilm-associated protein (Bap) (Figure 1.1) and poly-β-(1-6)-N-acetylglucosamine (PNAG) the predominant polysaccharide present in *A. baumannii* biofilm (Brossard and Campagnari, 2012; Loehfelm et al., 2008; Tomaras et al., 2003). In addition to adhesion and biofilm formation, motility is a key element of *A. baumannii* virulence. There are two distinct motility phenotypes the first is twitching motility mediated by the type IV pilus (Harding et al., 2013). The second is a less understood mechanism of "surface-associated motility". This motility is similar in appearance to swarming motility however it does not rely on flagella. What is known is that it is not type IV pilus-dependent (Clemmer et al., 2011) and the loss of 1, 3-diaminopropane synthesis completely abolishes motility (Skiebe et al., 2012). It is regulated by quorum sensing and influenced by blue light (López-Martín et al., 2021; Mussi et al., 2010) with the latter directly modulating the quorum-sensing network (Perez Mora et al., 2023; Tuttobene et al., 2021). This makes motility an interesting target for possible future therapeutic endeavours.

A diverse secretome contributes to the virulence and success of *A. baumannii*. Several systems are utilised for secretion for example the type I secretion system exports the previously discussed Bap protein (Harding et al., 2017), while the type II secretion system (T2SS) secretes several effectors including lipases such as LipH and LipA (Figure 1.1) and the protease CpaA (Figure 1.1) with these contributing to bacterial fitness and host colonisation (Harding et al., 2016). The T2SS is also capable of secreting phospholipase C and D (Figure

1.1). The former is toxic to epithelial cells (Camarena et al., 2010), while the latter has been associated with *in vivo* virulence, serum resistance, and invasion (Jacobs et al., 2010; Stahl et al., 2015). Secretion of an invasin-like adhesin by the T2SS contributes to adhesion to bladder and epithelial kidney cells and is required for virulence in a catheter-associated UTI model (Jackson-Litteken et al., 2022). *A. baumannii* can also utilise the type VI secretion system (Figure 1.1). There are conflicting reports however of the role of the system. In the ATCC 17978 strain it does not contribute to virulence, interbacterial competition, or biofilm formation (Weber et al., 2013). While in other strains it contributes to surface motility and serum resistance (Corral et al., 2021; Dong et al., 2022; Repizo et al., 2015). Along with secretion systems membrane vesicles can mediate the transport of virulence factors. Outer membrane proteins (Omp) are commonly associated with virulence and are transported by vesicles. OmpA aids in invasion and induces apoptosis (Choi et al., 2008) and Omp33 modulates autophagy, induces apoptosis, and contributes to intracellular survival (Rumbo et al., 2014; Smani et al., 2013). Iron is an important nutrient for bacterial growth, to counter this the host significantly limits the availability of iron to bacterial pathogens. *A. baumannii* employs iron chelators known as siderophores (Figure 1.1). *A. baumannii* is known to utilise acinetobactin, fimsbactin, and baumannoferrin (Sheldon and Skaar, 2020). With many of these factors providing benefits to fitness within the host targeting them could provide a novel anti-virulence therapeutic approach in the future.

1.1.2 Antibiotic resistance

A. baumannii is an ESKAPE pathogen. This group are recognised for their prevalence of causing nosocomial infection and high potential to exhibit multidrug resistance (Rice, 2008). Carbapenems are a common treatment for infection. Additionally, fluoroquinolones, aminoglycosides, trimethoprim, tetracyclines, and polymyxins are all used to treat infection (Kanafani and Kanj, 2024). The increasing prevalence of carbapenem resistance significantly complicates *A. baumannii* treatment. Carbapenemases are of significant

concern as they allow for resistance to carbapenems and most β-lactams. This significantly complicates the treatment of infection. The highest rates of carbapenem resistance have been reported as high as 90 % (Ma and McClean, 2021). Results from the SMART surveillance program indicated the incidence of multidrug resistance ranges from 47 % in North America to >93 % in Europe and the Middle East (Lob et al., 2016). Analysis of members of the *A. calcoaceticus–A. baumannii* (Acb) complex taken from the SENTRY antimicrobial surveillance program indicated an increase in the occurrence of extensive multidrug resistance (XDR) (Gales et al., 2019). Exemplifying the concern surrounding carbapenemase-producing *A. baumannii* is that the World Health Organization deeming these isolates as of critical concern for the investigation of new antimicrobials to treat infection (Tacconelli et al., 2018). Concerning other antimicrobial classes the European Antimicrobial Resistance Surveillance Network (EARS-Net) shows that approximately 43 % and 40 % of *A. baumannii* isolates tested are resistant to fluoroquinolones and aminoglycosides, respectively (Europen Centre for Disease Prevention and Control, 2023). Second-line antibiotic polymyxins have been utilised to treat *A. baumannii* resistant infection (Kanafani and Kanj, 2024). Polymyxin resistance varies greatly between geographical locations, with rates being as high as 17.5 % in Lebanon and as low as 0.2 % in Germany (Pormohammad et al., 2020). Polymyxin resistance is commonly conferred by lipid A modification as a result of genetic mutation (Novović and Jovčić, 2023). Plasmids harbouring the *mcr-1* and *mcr-4.3* genes, encoding lipid A modifying enzymes, have now been identified in *Acinetobacter* (Hameed et al., 2019; Martins-Sorenson et al., 2020) significantly increasing the concern about this type of resistance. Resistance to polymyxins is extremely concerning as they are regarded as a last-line antibiotic used to treat multidrug resistant isolates.

1.2 *Klebsiella pneumoniae* and clinical relevance

Klebsiella pneumoniae is a Gram-negative, facultative anaerobe, an opportunistic pathogen, commonly associated with nosocomial infections.

There are two distinct pathotypes of *K. pneumoniae* these being classical and hypervirulent. Classical isolates primarily cause nosocomial infection in the immunocompromised or patients with underlying comorbid conditions. Typically, *K. pneumoniae* is associated with pneumonia and urinary tract infection but can infect the blood and soft tissue (Paczosa and Mecsas, 2016). Hypervirulence was first reported in Taiwan in 1986 (Liu et al., 1986). These isolates are capable of causing serious infections such as pyogenic liver abscess, endophthalmitis, and meningitis (Choby et al., 2019). In addition to this, they have also been associated with community-acquired infections (Russo and Marr, 2019). This increased virulence is associated with the acquisition of 200-220 Kbp virulence plasmids, that can encode several elements that increase pathogenic capabilities (Choby et al., 2020). Currently, several characteristics are used to differentiate hypervirulent isolates from classical isolates. These are the ability to cause severe illness in healthy individuals, the ability to spread to additional anatomical sites of the host, and the common observation that hypervirulent strains tend to present a hypermucoviscous phenotype. More recently the *peg-344*, *iroB, iucA,* $_{p}$*rmpA*, and $_{p}$*rmpA2* genes have been suggested as biomarkers for hypervirulent *K. pneumoniae* (Russo et al., 2018).

1.2.1 Pathogenesis and virulence factors

The primary strategy of *K. pneumoniae* during infection is defence against the external environment and survival within the host and it uses several approaches to achieve this (Figure 1.2).

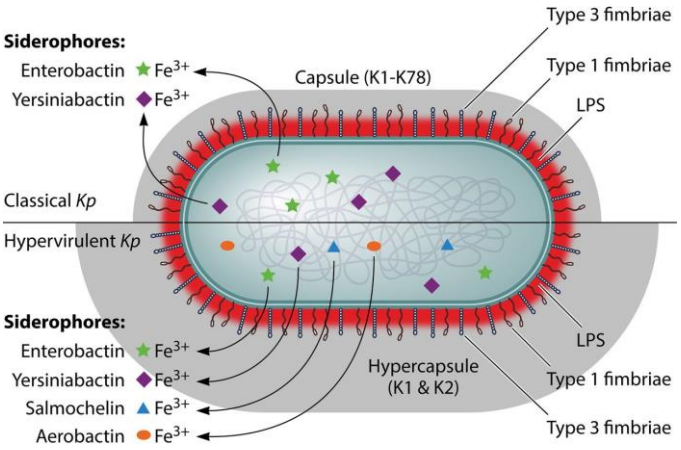

Figure 1.2. The virulence factors of *K. pneumoniae*. Top: virulence factors commonly observed in classical isolates. Bottom: virulence factors frequently observed in hypervirulent isolates. Figure adapted from Paczosa and Mecsas (2016).

Capsule formation is a key element of *K. pneumoniae* virulence with synthesis being encoded by the *cps* operon (Karampatakis et al., 2023). While classical strains of *K. pneumoniae* produce capsule hypervirulent strains that exhibit hypercapsulation. Several factors contribute to this, the first being the transcriptional regulators RmpA and RmpA2 that directly increase expression of the *cps* operon (Cheng et al., 2010). The *magA* gene, now renamed *wzy_K1*, encoding O-antigen polymerase also contributes to hypercapsulation (Fang et al., 2010). Capsule provides significant protection to several host factors such as complement, AMPs, and neutrophils (Álvarez et al., 2000; Campos et al., 2004; Pomakova et al., 2012) and seemingly increases virulence, as demonstrated in several infection models (Insua et al., 2013; March et al., 2013). In addition to CPS the LPS is a key element of the *K. pneumoniae* cell surface. Like CPS the LPS also protects against the host complement demonstrated by resistance to serum (Merino et al., 1992) with the O antigen preventing interaction of complement with the cell surface.

Fimbriae are another important virulence factor being the mediators of adhesion *K. pneumoniae* encodes both type 1 and 3 fimbriae, with the *fimBEAICDFGH* and *mrkABCD* operons, respectively (Paczosa and Mecsas, 2016). Type 1 contributes to colonisation of the urinary tract (Struve et al., 2008). While type 3 fimbriae mediate binding to epithelial and urinary bladder

cells (Tarkkanen et al., 1997) but are not required for urinary tract infection (Struve et al., 2009). Investigation with a murine-based CAUTI model revealed that both type 1 and 3 fimbriae are an important factor in biofilm linked CAUTIs (Murphy et al., 2013), and type 3 fimbriae strongly enhance biofilm formation and adherence to abiotic surfaces (Di Martino et al., 2003).

Like many bacterial pathogens, *K. pneumoniae* utilises iron acquisition systems during infection. These vary depending on the pathotype in question. Both classical and hypervirulent strains synthesise enterobactin, which is the primary iron uptake system of *K. pneumoniae,* and yersiniabactin (Bach et al., 2000; Lawlor et al., 2007). Enterobactin's contribution *in vivo* is limited due to it being bound by the immune protein Lipocalin-2 (LCN2) (Bachman et al., 2011; Goetz et al., 2002). Yersiniabactin appears to contribute to respiratory infection but does not support growth in serum (Bachman et al., 2011). This may be due to the inability of yersiniabactin to strip iron from host factors such as transferrin in serum. Hypervirulent isolates have an expanded repertoire of siderophores (Figure 1.2). The first is salmochelin which is structurally similar to enterobactin but is c-glycosylated. The second is aerobactin which is often associated with hypercapsule due to *rmpA* and the aerobactin locus frequently carried on the same virulence plasmids. Aerobactin contributes to virulence in both subcutaneous and pneumonia models (Russo et al., 2015, 2014) while salmochelin supports nasopharynx colonisation (Bachman et al., 2009; Fischbach et al., 2006). The success of hypervirulent isolates is somewhat dependent on these siderophores with their ability to subvert the activity of LCN2 being a major contributing factor. The connection between hypervirulence and these factors highlights several possible avenues for the future development of therapeutics.

1.2.2 Antibiotic resistance

Treatment of *K. pneumoniae* infection uses a range of antimicrobials including cephalosporins, carbapenems, aminoglycosides, polymyxins, Fosfomycin and tetracyclines (Ashurst and Dawson, 2023). There is significant concern

surrounding *K. pneumoniae* and antimicrobial resistance with this species also being a member of the ESKAPE pathogens (Rice, 2008). Of particular concern are extended-spectrum β-lactamase and carbapenemase-producing strains, similar to *A. baumannii* (Section 1.1.2). This is exemplified by the World Health organisation listing the development of new antimicrobials as of critical concern (Tacconelli et al., 2018). Concerning other antimicrobials, according to EARS-Net the prevalence of aminoglycoside resistance in Europe is 23 % (Europen Centre for Disease Prevention and Control, 2023). Fluoroquinolone resistance has been recorded as high as 32 % (Europen Centre for Disease Prevention and Control, 2023). polymyxins are often used to treat carbapenem-resistant *K. pneumoniae*. Analysis revealed that 2.95 % of isolates from bloodstream infections between 2016 and 2019 were resistant to colistin, increasing to 12.9 % from 2020 onwards (Uzairue et al., 2022). Similar to *A. baumannii* resistance is conferred by mutation however plasmid-borne resistance in the form of the *mcr-1* gene and its variants have been observed worldwide (Mendes et al., 2018). While antibiotic resistance in classical isolates is a concern, this is compounded by the convergence of hypervirulence with carbapenem resistance. Three different scenarios have been described for this. The first is the acquisition of plasmids encoding resistance genes by hypervirulent strains. The second is the transfer of hypervirulence plasmids into resistant classical strains, with the acquisition of these plasmids dramatically increasing virulence (Zhou et al., 2020). The third is the acquisition of a hybrid plasmid that encodes the virulence factors associated with hypervirulence and antibiotic resistance. An example is in China where a novel plasmid was identified encoding the *iroBCDN*, *iucABCD iutA*, and *rmpA2* virulence genes and carbapenemase gene (Jin et al., 2021). Carbapenem-resistant hypervirulent *K. pneumoniae* isolates have been identified globally (Han et al., 2022). This demonstrates an ever-growing problem that requires sufficient surveillance but further investigation to potentially provide a novel therapeutic solution to infection by these isolates.

1.3 Polyamines

1.3.1 Overview

Polyamines are polycationic organic compounds, that feature two or more amine groups within their structure and are positively charged at physiological pH.

1.3.2 Structure

1.3.2.1 Diamines

Diamines feature two amine groups. Three diamines have been described in nature these being 1, 3-diaminopropane [$H_2N(CH_2)_3NH_2$], putrescine [$NH_2(CH_2)_4NH_2$], and cadaverine [$NH_2(CH_2)_5NH_2$] (Figure 1.3).

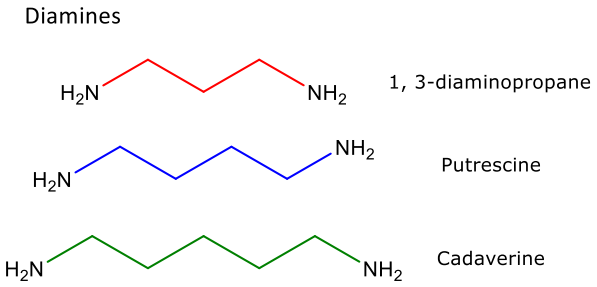

Figure 1.3. The structure of the diamines 1, 3-diaminopropane, putrescine and cadaverine. Figure generated in ChemDraw 22.2.

1.3.2.2 Triamines

Triamines contain three amine groups. The most common triamine, found across all domains of life is spermidine [$NH_2(CH_2)_3NH(CH_2)_4NH_2$] (Figure 1.4). Several analogues of spermidine have been described these being norspermidine [$NH_2(CH_2)_3NH(CH_2)_3NH_2$], aminopropylcadaverine [$NH_2(CH_2)_3NH(CH_2)_5NH_2$], and homospermidine [$NH_2(CH_2)_4NH(CH_2)_4NH_2$] (Figure 1.4).

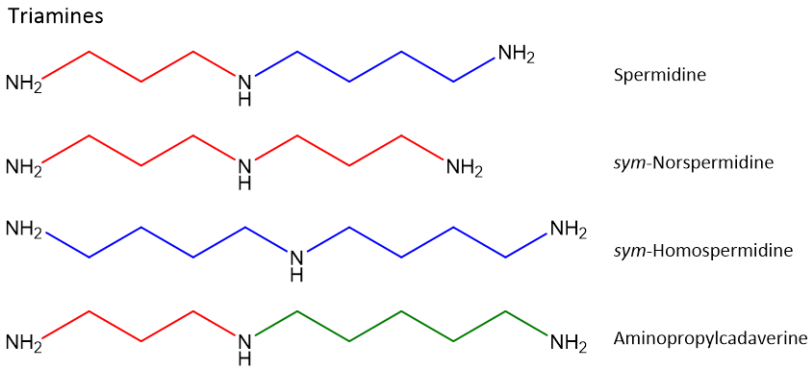

Figure 1.4. The structure of spermidine and structural analogues. Red: Aminopropyl group. Blue: aminobutyl group. Green: aminopentyl group. Figure generated in ChemDraw 22.2.

1.3.2.3 Tetramines

Tetramines feature four amino groups within their structure. The most common described is spermine [$NH_2(CH_2)_3NH(CH_2)_4NH(CH_2)_3NH_2$] (Figure 1.5). Several analogues of spermine have also been described these being thermospermine [$NH_2(CH_2)_3NH(CH_2)_3NH(CH_2)_4NH_2$], and norspermine [$NH_2(CH_2)_3NH(CH_2)_3NH(CH_2)_3NH_2$], also referred to as thermine (Figure 1.5).

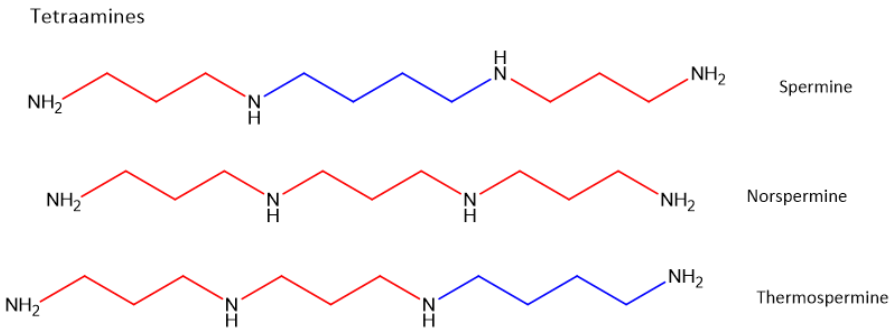

Figure 1.5. The structure of spermine and structural analogues. Red: Aminopropyl group. Blue: aminobutyl group. Figure generated in ChemDraw 22.2.

1.3.3 Biosynthetic pathways

1.3.3.1 pyridoxal 5'-phosphate-dependent enzymes

Several enzymes involved in polyamine synthesis are pyridoxal 5'-phosphate (PLP) dependent. PLP is a coenzyme required for catalysis. It acts as the coenzyme for aminotransferase, decarboxylation and deamination reactions. PLP-dependent enzymes feature a conserved residue for PLP interaction. The

aldehyde group of PLP forms a Schiff-base linkage with the ε-amino group of a specific lysine residue within the active site (Liang et al., 2019) (Figure 1.6). When the substrate binds in the active site its' α-amino group displaces the lysine ε-amino group and a new Schiff-base is formed between the substrate and the aldehyde group of PLP (Liang et al., 2019). Once this stage is complete the following decarboxylation, aminotransferase, or deamination can occur.

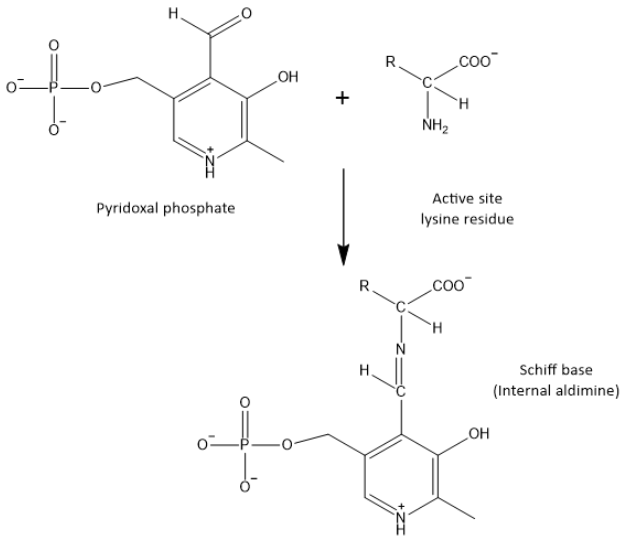

Figure 1.6. Formation of a Schiff base between pyridoxal 5'-phosphate and the active site lysine residue. Figure generated in ChemDraw 22.2.

1.3.3.2 1, 3-diaminopropane synthesis

The synthesis of 1, 3-diaminopropane is less widespread than other polyamine synthesis pathways. Being described as the major polyamine of the *Acinetobacter* genus, this synthesis pathway has also been identified in several other bacteria including *Haemophilus influenzae* and the *Vibrio* genus (Hamana and Matsuzaki, 1992; Ikai and Yamamoto, 1998; Lee et al., 2009). L-aspartate β-semialdehyde and L-glutamate are used to synthesise the intermediate L-2, 4-diaminobutyrate and 2-oxoglutarate, with the reversible reaction being catalysed by PLP-dependent L-2, 4-diaminobutyrate:2-ketoglutarate 4-aminotransferase (Dat) (Figure 1.7).

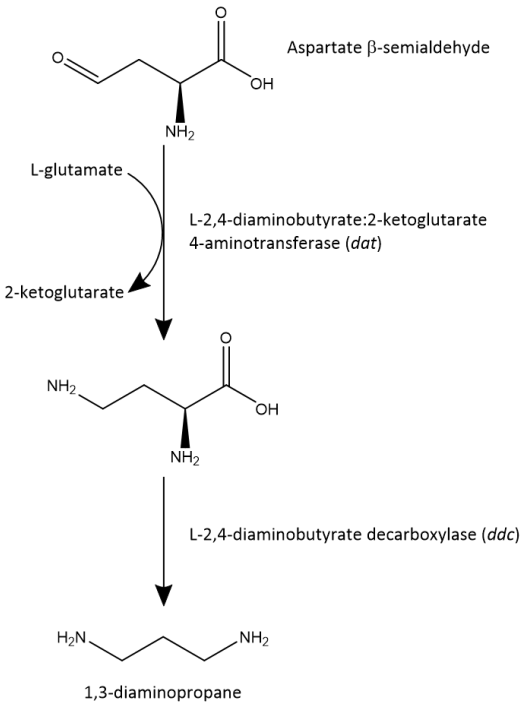

Figure 1.7. Overview of the known 1, 3-diaminopropane biosynthesis pathway in *A. baumannii*. Figure generated in ChemDraw 22.2.

The *dat* gene encoded by *A. baumannii* and its product were initially identified over twenty years ago. Bioinformatic analysis revealed the ORF in *A. baumannii* encodes a protein similar to several other aminotransferase enzymes and purification of the enzyme suggested it to be a tetramer (Ikai and Yamamoto, 1997). The purified Dat of *A. baumannii* showed significant activity for L-2, 4-diaminobutyrate, and 2-ketoglutarate generating L-glutamate and L-aspartate β-semialdehyde, demonstrating the capability of Dat to carry out this reversible reaction. When *A. baumannii* was incubated with radiolabelled aspartic acid a radioactive 1, 3-diaminopropane was produced (Ikai and Yamamoto, 1997). While L-2,4-diaminobutyrate is the intermediate for 1, 3-diaminopropane synthesis it alternatively can be utilised in the synthesis of the osmolyte ectoine and the siderophore pyoverdine, a process catalysed by EctB in *Halomonas elongata* and PvdH in *Pseudomonas aeruginosa*, respectively (Michael, 2016). The only solved structure of a Dat enzyme homolog is that of EctB from *Chromohalobacter salexigens* (Hillier et al., 2020). The EctB enzyme was found to be a tetramer of two functional dimers and characterisation determined important functional and structural residues (Figure 1.8).

Figure 1.8. Functional residues of the L-2, 4-diaminobutyrate aminotransferase (EctB) from *C. salexigens* DSM 3043. The small domain (blue) is formed from the N and C termini, while the large domain (grey) comprises the central part of the polypeptide chain. Residues that stabilise the tetramer (red) and PLP-interacting residues (yellow). Residues involved in substrate specificity (green) and dimer association (pink). Figure adapted from Hillier et al (2020).

Following the production of L-2, 4-diaminobutyrate, this intermediate undergoes a decarboxylation reaction, carried out by the PLP-dependent L-2, 4-diaminobutyrate decarboxylase, resulting in the synthesis of 1, 3-diaminopropane (Figure 1.7). There are currently no crystal structures available for the Ddc enzyme. Some characterisation has been carried out on the Ddc from the *Acinetobacter* genus. Expression and purification revealed it to form homodimers. The Ddc of *A. baumannii* has been cloned into *E. coli*, resulting in significant production of 1, 3-diaminopropane (Ikai and Yamamoto, 1994).

1.3.3.3 Putrescine synthesis

There are two putrescine synthesis pathways described in *E. coli*. The first utilises arginine as a starting point for synthesis which is decarboxylated by arginine decarboxylase, encoded by the *speA* gene, yielding agmatine (Morris and Pardee, 1966) (Figure 1.9). The pathway can diverge at this point either agmatine is converted directly into putrescine by agmatine ureohydrolase, often referred to as agmatinase, and encoded by *speB* (Figure 1.9) or it can be synthesised indirectly through the intermediate N-carbamoylputrescine

through the activities of deiminase/iminohydrolase and N-carbamoyl putrescine amidase/amidohydrolase (Nakada and Itoh, 2003). The second pathway synthesises putrescine directly from ornithine this is catalysed by ornithine decarboxylase, encoded by the *speC* gene (Morris and Pardee, 1966) (Figure 1.9).

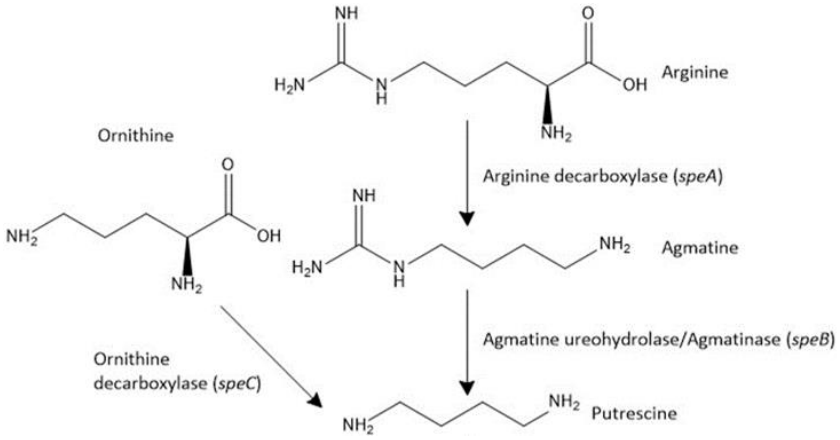

Figure 1.9. Overview of the known putrescine synthesis pathway in *E. coli*. Figure generated in ChemDraw 22.2.

1.3.3.4 Cadaverine synthesis

The diamine cadaverine is synthesised by the decarboxylation of lysine, catalysed by PLP-dependent lysine decarboxylase (LDC) (Figure 1.10). This occurs via two known pathways. The first is the constitutively expressed pathway, with the lysine decarboxylase encoded by the *ldcC* gene in *E. coli* and *K. pneumoniae*.

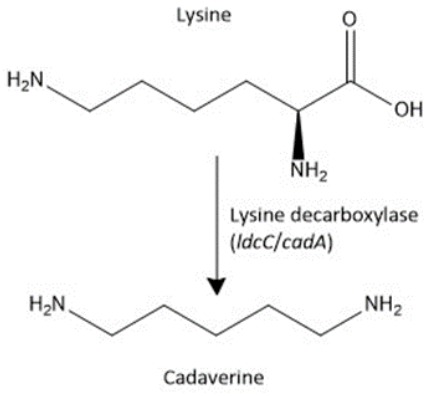

Figure 1.10. Overview of the known cadaverine biosynthesis pathway in *E. coli*. Figure generated in ChemDraw 22.2.

The second is referred to as the acid-inducible pathway involving the *cadCBA* operon, which is comprised of the constitutively expressed *cadC* gene, encoding the ToxR-like membrane-associated transcriptional regulator CadC, the *cadB* gene encoding the cadaverine/lysine antiporter, CadB and the *cadA* gene encoding the inducible lysine decarboxylase, CadA. The synthesis of cadaverine via this pathway is induced in low pH and high lysine conditions in *E. coli*. To summarise the CadC transcriptional regulator senses low pH within the periplasm. Along with this the co-sensor lysine permease, LysP, senses external lysine (Figure 1.11). In low lysine conditions, LysP interacts with the transmembrane domain of CadC inhibiting its activity (Figure 1.11). When lysine is abundant LysP transduces the availability of extracellular lysine to the CadC protein (Figure 1.11C). The sensing of low pH by CadC and high lysine concentrations by LysP ultimately results in a conformational change in CadC that allows for the interaction of the CadC cytoplasmic domain with the promoter sequence of the *cadBA* genes (Figure 1.11C).

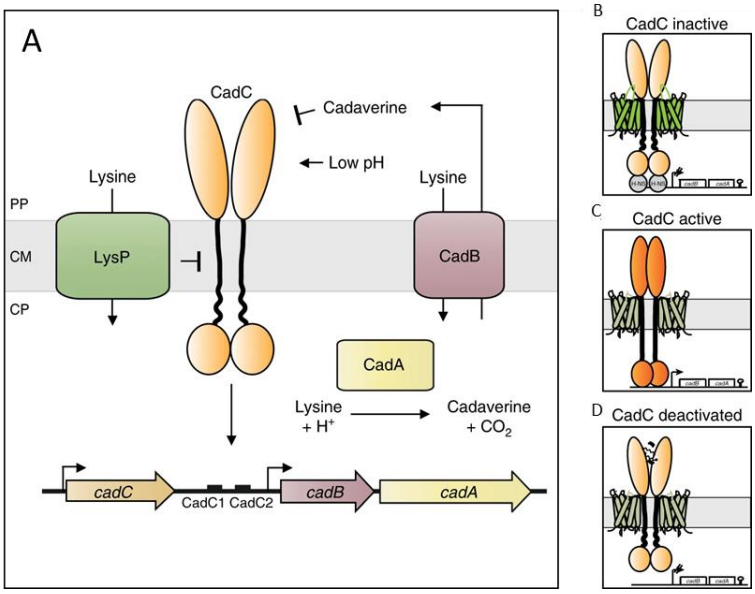

Figure 1.11. Overview of the acid-inducible Cad system in *E. coli*. (A) At low pH and high lysine concentration expression of *cadBA* is induced by CadC by binding to the CadC1 and C2 promoter sites. CadA decarboxylates lysine to generate cadaverine. The CadB antiporter uptakes lysine and exports cadaverine. Exported cadaverine increases extracellular pH **(B)** Under non-inducing conditions CadC and LysP are inactive; H-NS binds to the cadBA promoter. **(C)** CadC and LysP are activated by low pH and lysine, respectively. **(D)** CadC is inhibited by cadaverine. CP: cytoplasm. CM: cell membrane. PP: periplasm. Figure adapted from Brameyer et al (2019).

The *E. coli* LdcC and CadA feature three domains. These are the N-terminal domain, the lysine decarboxylase major domain, and the C-terminal domain. Monomers of LdcC and CadA come together to form homodecamers. Despite LdcC and CadA being lysine decarboxylases the former differs from the latter in that it is weakly expressed, less thermostable, is capable of activity over a broad range of pH and has a higher optimum pH. The cadaverine synthesised by CadA is transported to the periplasm by the inner membrane transporter, CadB. Several residues have been identified as being required for function (Table 1.1).

Table 1.1 Residues required for the function of CadB in *E. coli* K12

Amino acid residue	Effect of mutation	Reference
W43, Y57, Y107, W41, Y174, D185 Y366, Y368, E408	Impaired cadaverine uptake	(Soksawatmaekhin et al., 2006)
R299	Impaired cadaverine excretion	
Y55, Y89, Y90, Y235, Y246, Y310, C370, Y423	Impaired uptake and excretion	

Table 1.2 pH sensing residues of the periplasmic domain of CadC in *E. coli* K12

Amino acid residue	Effect of mutation	References
G170, C208, C272, N263, Q266	Confers pH and lysine-independent *cadBA* expression	(Dell et al., 1994; Haneburger et al., 2011; Tetsch et al., 2011)
D198, D200, H240, K458, Y460, E468, D471	Abolishes *cadBA* induction	
K242, G284, E461, D471, L474, T475, L479, P499	Confers pH-independent *cadBA* expression	

CadC is the primary regulator of *cadBA* expression. Located in the inner membrane, this ToxR-like protein is comprised of 512 amino acids and is made up of three distinct domains. The periplasmic domain is responsible for pH sensing. Several residues have been identified as being required for function (Table 1.2). The other two domains are the transmembrane and cytoplasmic. A disordered linker sequence connects the two (Figure 1.12). It is hypothesised that this linker is involved in transducing the signal of the periplasmic sensory

domain into a structural rearrangement of the CadC cytoplasmic DNA binding domain (Buchner et al., 2015).

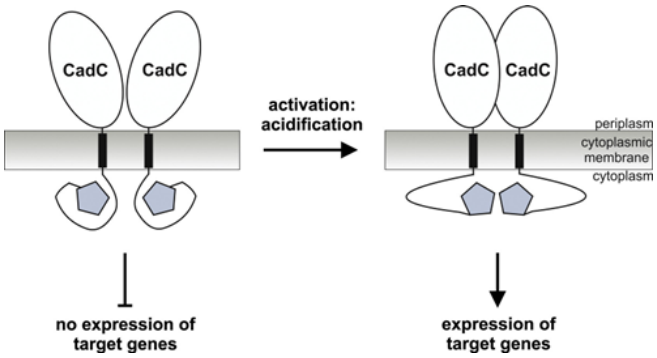

Figure 1.12. Representation of the role of the linker sequence within the CadC protein. Upon inducing conditions, conformational change in the linker allows for the dimerisation of the CadC cytoplasmic domains and interaction with the *cadBA* promoter. Figure adapted from Buchner et al (2015).

The cytoplasmic domain interacts directly with the promoter of the *cadBA* genes, to promote gene expression (Küper and Jung, 2005). CadC binds upstream of the transcriptional start site of the *cadBA* promoter region at two sites deemed cadC1 and C2. Initially, it was hypothesised that the quasi-palindromic repeat of C1 (Figure 1.13A) was somehow involved in the interaction (Küper and Jung, 2005). In *E. coli* the specific amino acid and nucleotide interaction has now been mapped to the consensus sequence 5'-T-T-A-x-x-x-x-T-3' (Schlundt et al., 2017) (Figure 1.13B).

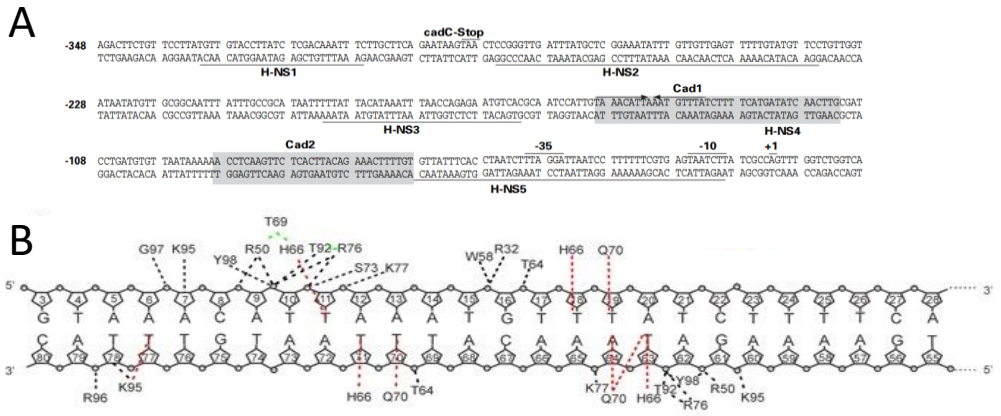

Figure 1.13. Overview of the genetic elements relating to the regulation of *cadBA* expression. (A) The genomic sequence of *E. coli* depicting the 3' end of the cadC gene and the intergenic region upstream of cadB. H-NS 1-5: The predicted H-NS binding sites. Cad1/2: The predicted binding sites of the CadC cytoplasmic domain. Arrows: depict quasi-palindromic sequence believed to be involved in CadC binding. The predicted positions of the -35, -10 and transcriptional start site are depicted. **(B)** Interactions that the CadC cytoplasmic domain has with the cadC1 sequence. Red lines: Sequence specific interactions between protein side chains and DNA bases. Black lines: contacts with the DNA backbone. Green lines: Sequence specific protein: protein interactions. **(A)** Adapted from Küper and Jung (2005). **(B)** Adapted from Schlundt et al 2017.

Only the side chains of K95, H66, and Q70 have specific contact with residues of the C1 site (Figure 1.13B). Much of the interaction with the DNA is non-specific and occurs with the phosphate or the sugar groups within the DNA backbone (Schlundt et al., 2017) (Figure 1.13B). Several residues of the CadC cytoplasmic domain have been identified as being required for function (Table 1.3). Despite this investigation, the role of the C2 site is yet to be fully understood.

Table 1.3 DNA binding residues of the cytoplasm domain of CadC in *E. coli* K12

Amino acid residue	Effect of mutation	Reference
E30	Enhances binding affinity inducing constitutive expression of *cadBA*	(Schlundt et al., 2017)
R32, R50, R60, V63, T64, H66, T69, Q70, S73, R76, K95, R96	Limits DNA binding affinity abolishing activation of *cadBA* expression under all conditions	

Expression of *cadBA* is indirectly controlled by external lysine through the lysine permease, LysP (Rauschmeier et al., 2014). Under non-inducing

concentrations, LysP interacts with the transmembrane domain of CadC and prevents the induction of the *cadBA* genes (Rauschmeier et al., 2014). Under elevated lysine concentration, LysP mediates uptake and dissociates from CadC. If under acidic conditions this allows the CadC to undergo a conformational change that allows for the expression of the *cadBA* genes (Rauschmeier et al., 2014). In the absence of lysine repression of *cadBA* still occurs even in the presence of acid. In addition to regulation by CadC and LysP, expression of the *cadBA* genes is also regulated by H-NS binding to the *cadBA* promoter region. Several sites have been predicted for this interaction (Figure 1.14). Under non-inducing conditions, it is hypothesised that H-NS establishes a repressor complex by binding to four sites (Küper and Jung, 2005) (Figure 1.14). This binding results in the looping of the DNA and occupation of the *cadBA* promoter sequence, preventing expression (Figure 1.14). Upon inducing conditions, the CadC regulator binds to the cadC1 site. This binding dissolves the repressor complex, exposing the *cadBA* promoter and allowing gene expression (Figure 1.14).

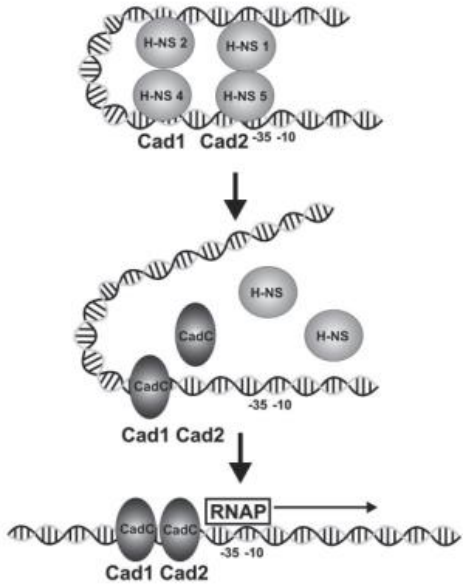

Figure 1.14. The role of H-NS in the regulation of *cadBA* expression. Under non-inducing conditions, H-NS binds at four sites establishing a repressor complex blocking the promoter of *cadBA*. Under inducing conditions, CadC binding to C1 causes dissociation of the complex allowing for expression. Figure adapted from Küper and Jung (2005).

1.3.3.5 Synthesis of spermidine and its analogues

The synthesis of spermidine is one of the most well-characterized polyamine synthesis pathways, distributed across all three domains of life. This pathway begins with putrescine and S-adenosylmethionine (Michael, 2016). The latter is decarboxylated by S-adenosylmethionine decarboxylase, generating decarboxylated S-adenosylmethionine that in turn is used to aminopropylate putrescine to yield spermidine and S-methyl-5'-thioadenosine, a process that is catalysed by Spermidine synthase (Michael, 2016) (Figure 1.15).

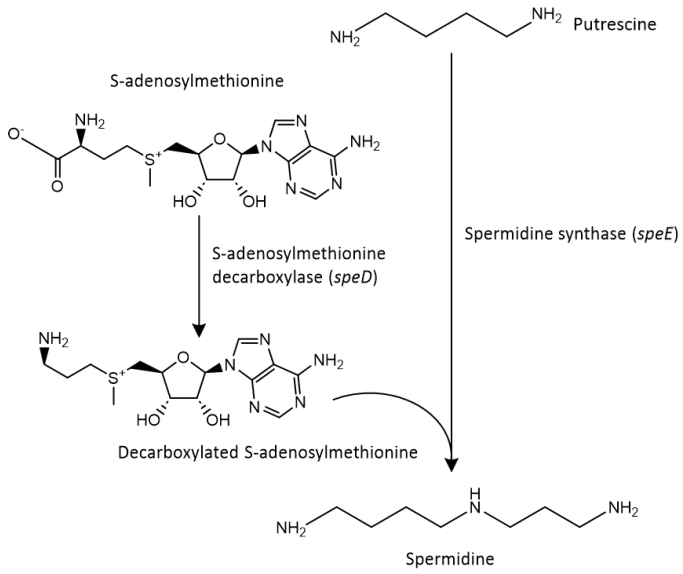

Figure 1.15. Overview of the known spermidine synthesis pathway present in *E. coli*. Figure generated in ChemDraw 22.2.

An alternate pathway for spermidine synthesis has been described. This utilises aspartate β-semialdehyde instead of decarboxylated by S-adenosylmethionine. In this pathway carboxyspermidine synthase aminopropylates putrescine, using aspartate β-semialdehyde, to generate carboxyspermidine. This is then decarboxylated, by carboxyspermidine decarboxylase, generating spermidine (Hanfrey et al., 2011). A similar pathway exists in *Vibrio cholerae*, for the synthesis of norspermidine. This pathway aminopropylates 1, 3-diaminopropane instead of putrescine, generating norspermidine (Lee et al., 2009). Spermidine synthase is also capable of synthesising aminopropylcadaverine. This process is identical to spermidine synthesis but

involves the aminopropylation of cadaverine (Bowman et al., 1973). Homospermidine is less commonly occurring and is largely found in plants and some bacteria (Böttcher et al., 1994).

1.3.3.6 Spermine synthesis

Spermine is the most widely distributed tetraamine found throughout metazoans, yeast, and plants. Spermine is synthesised by the aminopropylation of spermidine, a process catalysed by spermine synthase, using decarboxylated S-adenosylmethionine as the aminopropyl donor (Michael, 2016).

1.3.4 Transport of polyamines

Several dedicated polyamine transport systems have been described two well-established examples are the ATP-dependent PotABCD and PotFGHI (Figure 1.16). These transporters are comprised of the polyamine binding proteins, PotD/F; the ATP binding proteins, PotA/G; and the transmembrane channels, PotBC/HI (Igarashi and Kashiwagi, 2010). PotABCD was found to be spermidine preferential (Igarashi and Kashiwagi, 2010). While PotFGHI is only capable of putrescine transporter (Pistocchi et al., 1993). As for the biological significance, PotABCD was found to contribute to biofilm formation in *E. coli* (Thongbhubate et al., 2021) making it a possible target for the development of biofilm inhibitors. While PotFGHI is responsible for putrescine uptake in the presence of glucose (Terui et al., 2014) suggesting it helps maintain optimal intracellular polyamine concentration.

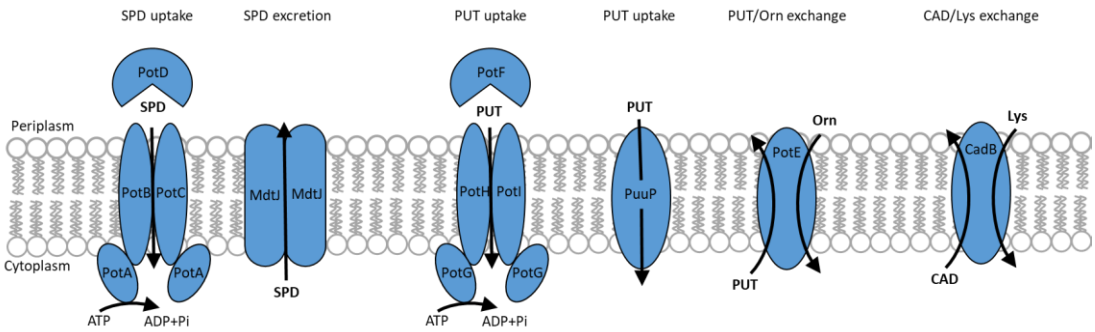

Figure 1.16. Examples of polyamine transporters identified in *E. coli*. PUT: Putrescine. Orn: Ornithine. CAD: Cadaverine. Lys: Lysine. SPD: Spermidine. Figure based on Igarashi and Kashiwagi (2010).

While several transport systems dedicated to putrescine and spermidine have been identified (Figure 1.16), none are described for 1, 3-diaminopropane. This lack of discovery may be due to this diamine being less widespread than other polyamines. Recently, it has been determined that 1, 3-diaminopropane is acetylated (Armalytė et al., 2023). The fate of acetylated 1, 3-diaminopropane is unknown. Polyamines tend to be acetylated and then secreted from the cell to maintain homeostasis, meaning this may be a method *A. baumannii* uses to alter intracellular levels of 1, 3-diaminopropane. In *E. coli* other dedicated polyamine transporters can transport this diamine. When the *dat* and *ddc* genes of *A. baumannii* were cloned into *E. coli*, to metabolically engineer *E. coli* to overproduce 1, 3-diaminopropane for use in chemical manufacturing, 1, 3-diaminopropane accumulated within the culture medium with this being attributed to PotE or CadB (Chae et al., 2015). The transport of polyamines from the cell also allows intracellular polyamine homeostasis. This is important as elevated levels can become detrimental to fitness. Non-specific transporters, such as multidrug efflux pumps, can mediate this type of transport. Several examples have now been described such as MdtJI, AceI and AmvA. These are discussed further in later sections 1.3.7 and 1.3.8. It is not surprising that MDR pumps also transport polyamines as it is well-documented that these systems, transport a variety of toxic substrates (Blanco et al., 2016). While they have been shown to contribute to growth and survival under experimentally induced polyamine stress (Higashi et al., 2008; Short et al., 2021). There is also evidence they are involved in homeostasis in the presence of biologically relevant concentrations with one example being within polymicrobial biofilms (Semenec et al., 2023). This suggests these efflux pumps may contribute to polyamine homeostasis within the environment or a host during infection. Polyamine transporters also promote growth and survival under stress conditions, such as low pH. Two examples are the CadB transporter and the PotE putrescine/ornithine antiporter system, both are discussed later (Section 1.3.6.3.3). Uptake can also be utilised to allow polyamines to be used as carbon/nitrogen sources. Two examples of this have been identified in *E. coli* these being the putrescine transporters PuuP and YdcSTUV, being part of the

glutamylation catabolism pathway (Putrescine degradation II) (Kurihara et al., 2009b) and the putrescine degradation I pathway, respectively (Schneider and Reitzer, 2012).

1.3.5 The roles of polyamines in eukaryotes

Polyamines are important metabolites across the Eukarya domain. The most important role of polyamines in eukaryotes is the hypusination of eukaryote initiation factor 5A (eIF5A). This is a two-step enzymatic process, whereby spermidine is utilised to donate a 4-aminobutyl group to the ε-amino group of one specific lysine residue (Figure 1.17B and C). The second reaction sees the addition of a hydroxyl group to the deoxyhypusine residue (Park et al., 2022) (Figure 1.17C). Hypusine (Figure 1.17A) was discovered in 1971 within the Bovine brain (Shiba et al., 1971). Hypusination of eIF5A is critical for viability as disruption of eIF5A is lethal (Nishimura et al., 2012). During translation, certain amino acids such as proline or glycine are considered less efficient in forming peptide bonds resulting in ribosomal stalling. Initially, it was believed that eIF5A was responsible for stimulating the translation of polyproline repeats (Gutierrez et al., 2013). More recently, it has been determined that eIF5A is capable of carrying out this function at many non-proline-specific sites (Pelechano and Alepuz, 2017; Schuller et al., 2017). Hypusination also dictates eIF5A subcellular location, promoting nuclear export to the cytoplasm for its involvement in protein synthesis (Lee et al., 2009).

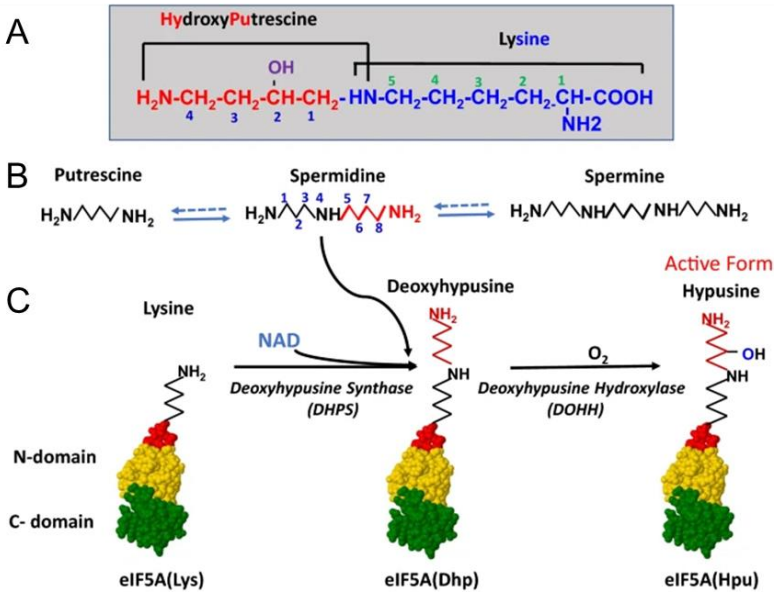

Figure 1.17. Diagram depicting the hypusination of eIF5A. (A) structure of hypusine. Red: Putrescine. Purple: Hydroxyl group. Blue: lysine. **(B)** synthesis of polyamines in mammalian cells. Red: aminobutyl group of spermidine that is utilised for hypusination. **(C)** Hypusine modification of eIF5A was carried out by deoxyhypusine synthase and deoxyhypusine hydroxylase. Green: C-terminal domain. Yellow: N-terminal domain. Red: Conserved loop containing the modified lysine residue. Figure adapted from Park et al (2022).

In addition to hypusination, polyamines have many additional roles in eukaryote cells. Several reports suggest that polyamines are key to cell proliferation being elevated in rapidly dividing cells (Pegg et al., 1970; Russell and Snyder, 1968), and disruption of synthesis arrests cell proliferation (Fredlund et al., 1995; Yamashita et al., 2013). A possible explanation for this is the influence polyamines have on protein expression. Eleven different proteins are part of the Eukaryote polyamine modulon, with seven different mechanisms having been described (Igarashi and Kashiwagi, 2021) (Figure 1.18). Many of the proteins affected by polyamines have significant downstream roles within the cell this highlights the far-reaching effect polyamines have on eukaryotic cells. Several additional roles have been linked to polyamines including macrophage polarisation, influencing of protein channels, and chromosomal condensation to name a few (Latour et al., 2020; Pegg, 2016).

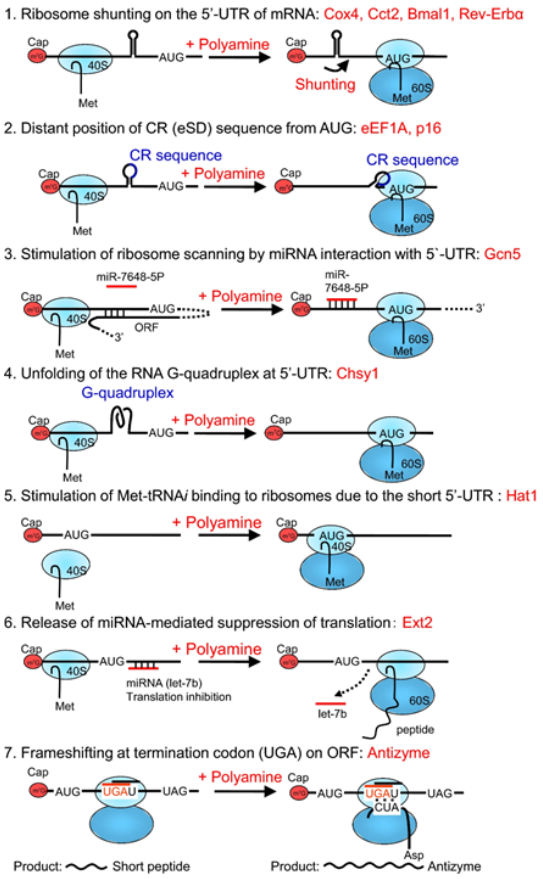

Figure 1.18. Proposed molecular mechanisms of polyamines modulating protein expression. 1-5: Polyamine modulation at initiation of translation. 6 and 7: Polyamine modulation at the level of elongation. Figure adapted from Igarashi and Kashiwagi (2021).

1.3.6 The roles of polyamines in bacteria

In bacteria, polyamines do not have a conserved function across all species. This is demonstrated by the variability in the synthesis pathways in a given species and the varying effects and roles of polyamines discovered between species and genera.

1.3.6.1 Cell growth

The effect of polyamines on the growth of bacteria was initially documented in *Haemophilus parainfluenzae*, where putrescine and to a lesser extent spermidine, spermine, and agmatine all promote growth (Herbst and Snell, 1949). It is unclear what role polyamines have in *H. parainfluenzae* that contributes to growth. With polyamines contributing to gene expression, acting

as carbon/nitrogen sources and as intermediates for downstream metabolites, any of these is a plausible candidate but is yet to be fully elucidated. Since then, the role of polyamines in bacterial growth has been investigated in a wide variety of species. One of the most well-characterised organisms concerning polyamine synthesis is *E. coli*. It is known that *E. coli* synthesises putrescine, cadaverine, and spermidine, however, none are essential for growth under aerobic conditions with a polyamine auxotroph showing a growth rate of 40 % that of the wild type (Chattopadhyay et al., 2009). *E. coli* was shown to grow in 95 % O_2, while this could be considered biologically irrelevant as *E. coli* does not naturally encounter these conditions, it was used to induce oxidative stress on the polyamine auxotrophic *E. coli*. This demonstrated that polyamine synthesis is required for growth in 95 % O_2 (Chattopadhyay et al., 2003). A possible explanation is that either polyamines act solely as antioxidant molecules or modulate oxidative stress responses in *E. coli* with the latter now being shown to be the case (Sakamoto et al., 2015). Interestingly, the triamines norspermidine, homospermidine, and aminopropylcadaverine support the growth of a putrescine/spermidine auxotrophic *E. coli* (Yoshida et al., 2016). Suggesting that the exact structure and symmetry are not critical for function but perhaps suggests the overall physicochemical attributes such as charge distribution over a flexible backbone are more important. In contrast, spermidine was found to be essential for the growth of *Campylobacter jejuni* and in *P. aeruginosa* deletion of ornithine and arginine-dependent putrescine pathways leads to severely impaired growth (Hanfrey et al., 2011; Nakada and Itoh, 2003). Unlike other species of bacteria, *Staphylococcus aureus* lacks *de novo* polyamine synthesis but grows well in their absence. Given the range of biological roles polyamines have, this independence could be considered a remarkable feat. *S. aureus* demonstrates hypersensitivity to exogenous spermidine and spermine (Joshi et al., 2011). The methicillin-resistant community-acquired USA300 clones circumvent this by utilising a spermidine/spermine acetyltransferase, found in the ACME island (Joshi et al., 2011). It has been suggested that the rapid emergence and spread of the USA300 clones is due to the decreased susceptibility to host polyamines (Joshi

et al., 2011; Thurlow et al., 2013). While this explains the specific case of USA300 clones it does not explain how resistance is conferred in non-USA300 *S. aureus.*

1.3.6.2 Gene expression

Analysis of polyamine distribution in *E. coli* has shown that approximately 90 % of spermidine and 48 % of putrescine are bound to RNA. While 5.1 % and 9.3 % are bound to DNA, respectively (Miyamoto et al., 1993) suggesting a possible role in gene regulation and protein expression. In *E. coli* polyamines primarily influence translation. Genes whose expression is stimulated by polyamines are referred to as the polyamine modulon. There are three proposed mechanisms for this all of which occur at translation. The first occurs when there is an obscure or distant Shine Dalgarno sequence from the initiation codon. Polyamines cause a conformational in the Shine Dalgarno and initiation codon region, promoting initiation complex formation (Figure 1.19A). This has been observed for RpoN (σ^{54}), FecI (σ^{18}), RpoE (σ^{24}), and H-NS/StpA (Terui et al., 2009, 2007; Yoshida et al., 2004). Polyamines may influence the translation of many more transcriptional regulators in this manner, as approximately 15 % of known transcription factors of *E. coli* have a non-consensus Shine Dalgarno sequence (Yoshida et al., 2004). This stimulation has also been observed in *Yersinia pestis*, where polyamines modulate the translation of HmsT a diguanylate cyclase involved in biofilm formation (Wortham et al., 2010). The second mechanism occurs when an inefficient initiation codon is present with polyamines increasing the binding affinity of the fMet-tRNA to the mRNA/ribosome complex (Figure 1.19B). This stimulation is associated with Cra, a transcriptional regulator for genes involved in glycolysis and gluconeogenesis, and Cya, an adenylate cyclase. Influencing the expression of these two proteins would ultimately carbon metabolism and downstream intracellular signalling, respectively. The third mechanism involves the read-through of premature stop codons with two examples described (Figure 1.19C). The first is the readthrough of the UAG codon, found at position 33 of RpoS mRNA, by Gln-tRNA^{supE} (Yoshida et al., 2002) (Figure 1.19C). The second action

is the enhancement of +1 frameshift (Figure 1.19C), found at the 26th UGA codon of Polypeptide Release Factor 2 to allow a read-through of the second open reading frame (ORF) (Higashi et al., 2006). Modulation of RpoS is important for cell viability during the stationary phase with overcoming the point mutation at position 33 granting increased bacterial fitness. Stimulation of RF2 would influence protein expression efficiency during the logarithmic phase. With many of the proteins of the *E. coli* polyamine modulon being regulatory proteins, this demonstrates the far-reaching effects polyamines have on cellular processes and with the widespread nature of polyamine synthesis, their propensity to interact with DNA and RNA and the discovery of modulation in the Bacteria and the Eukarya domains it can be easily speculated that polyamines may be responsible for modulating protein synthesis in a large number of bacterial species with this influence being yet to be uncovered.

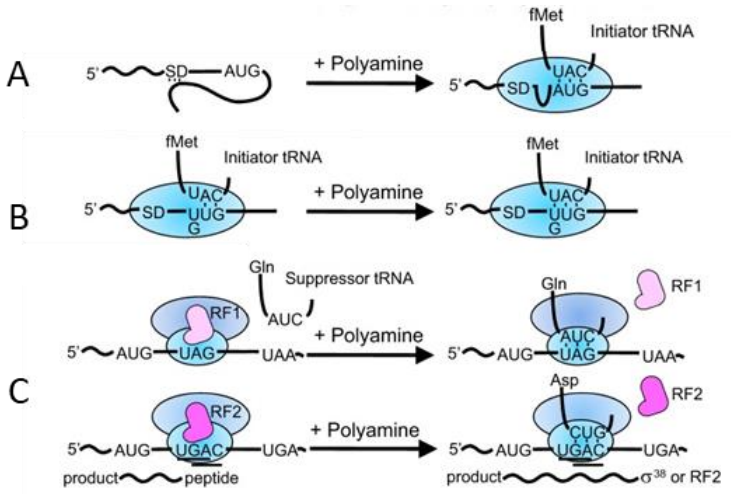

Figure 1.19. Mechanisms of polyamine modulation in *E. coli*. Polyamines modulate the translation of proteins by three mechanisms. **(A)** polyamines cause structural changes in the SD and start codon region allowing for initiation complex formation when a distant SD sequence is present. **(B)** Increase binding efficiency of fMet-tRNA to mRNA initiation complex when an inefficient start codon is present. **(C)** Polyamines increase the binding affinity of Gln-tRNAsupE or they stimulate a +1 frameshift. Figure adapted from Igarashi and Kashiwagi (2018).

1.3.6.3 Protection from stress

Polyamines have demonstrated the ability to protect bacteria from different stress conditions including acidic pH, and oxidative and nitrosative stress.

1.3.6.3.1 Oxidative stress

Bacteria encounter several different stress conditions. One of these is oxidative stress, a result of reactive oxygen species (ROS) such as superoxide, hydrogen peroxide, and hydroxyl radicals. Oxidative stress is of particular concern as it can cause significant damage to nucleic acids, proteins, and lipids. Oxidative stress is a key element of the immune response with phagocytes producing superoxide (Figure 1.20), which in turn leads to the formation of additional ROS (Figure 1.20) in an attempt to kill engulfed bacteria (Al-Shehri, 2021).

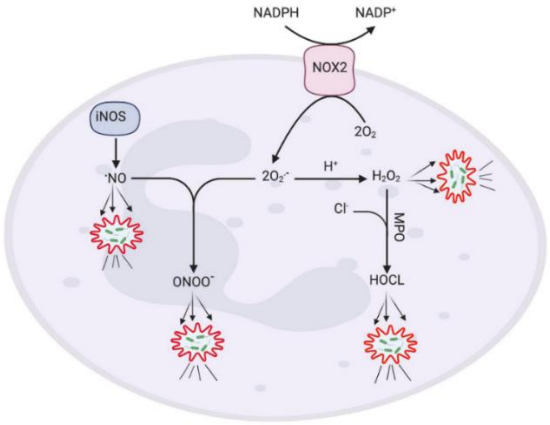

Figure 1.20. The formation of ROS and RNS following phagocytosis. NADPH oxidases (NOX2) form superoxide from NADPH and oxygen. Nitric oxide synthase (iNOS) produces nitric oxide (NO) from L-arginine. Superoxide and nitric oxide combine to form Peroxynitrite ($ONOO^-$). Two superoxide anions can generate hydrogen peroxide (H_2O_2), catalysed by superoxide dismutase. Myeloperoxidase (MPO) produces hypochlorous acid (HOCl) from H_2O_2 and chloride anions. Adapted from Al-Shehri (2021).

Polyamines play a role in resistance to oxidative stress. Polyamine auxotrophic *E. coli* have increased susceptibility to exogenous H_2O_2 and paraquat (Chattopadhyay et al., 2003; Minton et al., 1990). A similar, but less pronounced, observation was also made in *Salmonella enterica* serovar Typhimurium (Espinel et al., 2016). Polyamines themselves can act as antioxidants. Additionally, in *E. coli* several genes relating to oxidative stress resistance are modulated by polyamines these being SoxR, EmrR, and GshA (Figure 1.21) (Sakamoto et al., 2015). Cadaverine has been linked to oxidative stress resistance, protecting against ROS in *E. coli* and *V. vulnificus* (Akhova et al., 2021; Kang et al., 2007). It has been found that the acid-inducible genes of

V. vulnificus are induced by the oxidative stress response regulator, SoxR, and in *E. coli* by RpoS and SoxS (Akhova et al., 2021; Kim et al., 2006). With ROS being a part of the innate immune system polyamines influencing ROS resistance may benefit bacterial fitness during infection.

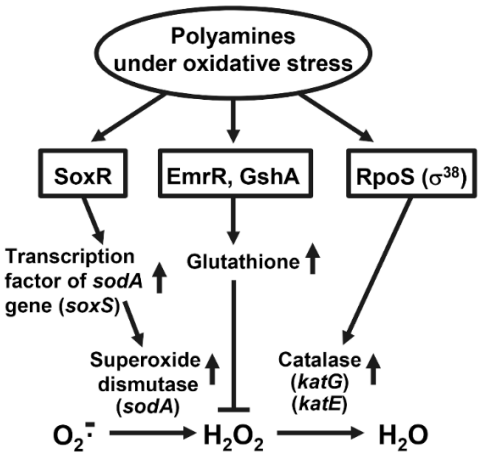

Figure 1.21. Overview of the effect of polyamine modulation of SoxR, EmrR, GshA, and RpoS. Adapted from Sakamoto et al (2015).

1.3.6.3.2 Nitrosative stress

It has been demonstrated that polyamines are involved in the protection from oxidative stress. They have also been shown to protect against nitrosative stress. Similar to oxidative stress nitrosative stress is a component of the immune response (Al-Shehri, 2021). Nitric oxide is a key element of nitrosative stress. It is generated by nitric oxide synthases and is employed by macrophages to kill pathogens (Al-Shehri, 2021). Nitric oxide reacts with superoxide to generate the highly oxidising peroxynitrite (Radi, 2013). Infection of the urinary tract is associated with reactive nitrogen species with nitrite and nitric oxide both increasing during infection (Svensson et al., 2018). The synthesis of polyamines has been tied to the susceptibility to nitrosative stress in *E. coli*. When exposed to acidified nitrite the *E. coli* UTI89 strain increases cadaverine production. The deletion of *cadCBA* operon, results in increased susceptibility to nitrosative stress (Bower and Mulvey, 2006). This resistance was also observed in other UPEC clinical isolates and it is believed that this resistance to nitrosative stress may promote colonisation of the urinary tract

(Bower et al., 2009). Spermidine also contributes to nitrosative stress resistance in *Salmonella enterica* serovar Typhimurium (Espinel et al., 2016). Similarly, *Streptococcus pneumoniae* exhibits increased susceptibility to S-Nitrosoglutathione, following *potABCD* and *speA* deletion (Nakamya et al., 2021b, 2021a). A possible explanation could be that loss of SpeA and subsequent decarboxylation affect intracellular buffering capacity. Similar to ROS, resistance to RNS mediated by polyamines may protect against the innate immune system during infection.

1.3.6.3.3 Acid stress

Another stress condition bacteria encounter is acidic environmental pH. The most significant example is within the stomach, which has a pH range of 1.5-3.0 resulting in extreme acid stress (Kanjee and Houry, 2013). In the gastrointestinal tract bacteria still face acidic stress in the form of fermentation. This results in the production of short-chain fatty acids (Kanjee and Houry, 2013). These cross the cell membrane in an uncharged state and dissociate within the cytoplasm lowering internal pH (Kanjee and Houry, 2013). Enteric bacteria have several systems to overcome acid stress. In *E. coli* there are four described amino acid-dependent acid resistance systems, each system has two specific components. A cytoplasmic PLP-dependent decarboxylase catalyses the decarboxylation of the amino acid substrate and an inner membrane substrate/product antiporter, that exchanges internal product for an external substrate. The first two systems in *E. coli* are glutamate and arginine-based. While glutamate is less relevant concerning polyamines. The arginine-based system uses the biodegradative form of arginine decarboxylase, AdiA. This produces agmatine, the intermediate in putrescine synthesis. This is then exported by AdiC. This system protects at pH <2.5 in *E. coli* (Iyer et al., 2003). The next system is the lysine/cadaverine-based system, encoded by the *cadCBA* operon, as previously discussed (Section 1.3.3.4). In *E. coli*, this system is most efficiently utilised under mildly acidic conditions. These differences allow *E. coli* to adapt to a wide range of conditions experienced within the GI tract. The former grants tolerance to weak organic acids, produced during

carbohydrate fermentation in the intestines. The latter two allow tolerance to conditions within the stomach. In contrast in *Salmonella,* the lysine/cadaverine system appears to provide significantly more protection to extreme acidic pH (Park et al., 1996). This maintains cytoplasmic pH in a range suitable for protein synthesis. This allows for acid-shock protein synthesis (Park et al., 1996). The final amino acid-based system is the ornithine/putrescine system, mediated by the inducible ornithine decarboxylase, SpeF, and the putrescine transporter PotE. The two genes are colocalised on the chromosome and it has been demonstrated that inducible ornithine decarboxylase activity occurs at pH 5.2 in *E. coli* (Kashiwagi et al., 1991). This suggests that PotE is responsible for tolerance to similar environments to the CadCBA system.

1.3.6.4 Motility

Polyamines are involved in several different forms of motility across several bacterial species. In *E. coli* spermidine contributes to swarming motility and disruption of synthesis and uptake by the PotABCD transporter resulting in severely reduced or inhibited motility on rich and minimal media, respectively (Kurihara et al., 2009a). Also in *E. coli* putrescine has been linked to type 1 pili-mediated surface motility with synthesis pathway and the YeeF transporter being indispensable for motility (Kurihara et al., 2011). In *Proteus mirabilis* putrescine is required for swarming motility (Sturgill and Rather, 2004). The putrescine importer, PlaP, is the species' primary uptake system and contributes to motility (Kurihara et al., 2013). With both synthesis and uptake being involved in all three cases this potentially indicates polyamines are utilised as a signalling molecule to orchestrate bacterial motility.

1.3.6.5 Antibiotic susceptibility

The effect exogenous polyamines have on antimicrobial susceptibility has been assessed in several organisms through several different mechanisms. Polyamines alter membrane permeability by interacting with OmpF and C in *E. coli* (Dela Vega and Delcour, 1996). Potencies were in the order of spermine > spermidine > cadaverine ≠ putrescine (Dela Vega and Delcour, 1996). This

interaction contributes to reduced antibiotic uptake in *E. coli* and *Mycobacterium bovis* (Sarathy et al., 2013; Tkachenko et al., 2006). Evidence suggests this is due to polyamines interacting with the porin channel impacting gating kinetics (Liu et al., 1997). Investigation in *P. aeruginosa* indicates spermidine and putrescine stabilise the outer membrane, reducing susceptibility to AMPs (Johnson et al., 2012). *In silico* simulation of membrane dynamics has visualised this interaction showing electrostatic interaction and hydrogen bonding between spermidine and membrane phosphate groups (Li et al., 2020). This interaction is ultimately what protects the outer membrane from attack by AMPs. In addition to these abilities, polyamines also protect against antimicrobial-mediated ROS. For example, in *Burkholderia cenocepacia*, both exogenous and endogenous putrescine reduce the ROS induced by antibiotic treatment (El-Halfawy and Valvano, 2014), and similar observations have been made in *E. coli* (Tkachenko et al., 2012). Additionally, exposure of *E. coli* to both β-lactams and fluoroquinolones increases cadaverine synthesis, which is not surprising as oxidative stress is known to promote expression of the *ldcC* and *cadBA* genes, via SoxS and RpoS (Akhova et al., 2021).

1.3.6.6 Biofilm formation

Polyamines are involved in biofilm formation in several bacterial species. In *Bacillus subtilis* spermidine is required for colony biofilm formation and structural analogues of spermidine be substituted in its place (Hobley et al., 2017, 2014). While spermidine's mechanism of influencing *B. subtilis* biofilm is not fully understood, it is known that spermidine influences the expression of exopolysaccharide and the TasA protein, two major components in biofilm formation, through the SlrR regulatory protein (Hobley et al., 2017). Whether spermidine directly impacts *slrR* expression or whether its effect is exerted upstream in the regulatory network is unknown. In *E. coli* spermidine is required for biofilm formation with genes of the polyamine modulon directly contributing to this (Sakamoto et al., 2012; Thongbhubate et al., 2021). Transmission of the zoonotic pathogen, *Yersinia pestis*, requires biofilm

formation within the flea. Deletion of the putrescine synthesis genes results in a complete inability to form biofilm (Patel et al., 2006). This was attributed to decreased expression of the HmsT and HmsR proteins, as previously discussed (section 1.3.6.2). One of the most well-characterised occurrences of polyamines influencing biofilm is that in *Vibrio cholerae*. Deletions made in its norspermidine synthesis pathway, result in an inability to form biofilm (Lee et al., 2009). Polyamine-mediated biofilm formation in *Vibrio* is tied to a polyamine sensor, NspS, and the membrane-spanning protein, MbaA. Deletion of *nspS* results in a decrease in biofilm formation (Karatan et al., 2005). It is believed that NspS binds norspermidine and interacts with the periplasmic domain of MbaA, inhibiting phosphodiesterase activity, increasing cyclic di-GMP in turn promoting biofilm formation (Figure 1.22) (Bridges and Bassler, 2021). Sensing extracellular stimuli likely allows a transition between a planktonic and biofilm lifestyle when *V. cholerae* moves between specific environments.

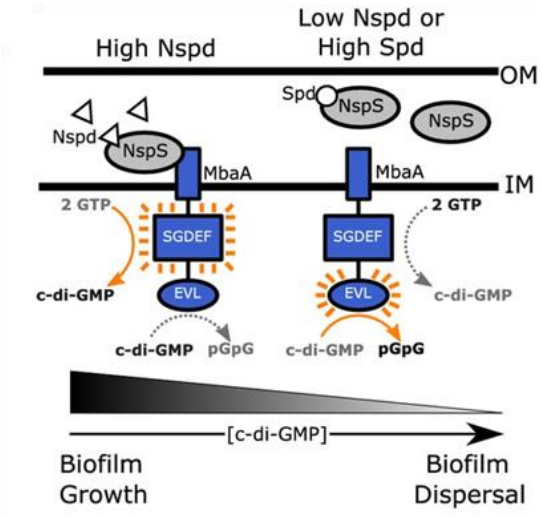

Figure 1.22. Diagram showing the proposed mechanism norspermidine promotes biofilm formation in *V. cholerae.* High Nspd: Norspermidine binds NspS which is followed by interaction with MbaA. This inhibits the phosphodiesterase activity of MbaA and induces diguanylate cyclase activity and c-di-GMP synthesis, resulting in increased biofilm formation. Low Nspd or High Spd: In the presence of Spd or low Nspd NspS does not interact with MbaA and fails to inhibit phosphodiesterase activity resulting in c-di-GMP hydrolysis and ultimately dispersal of biofilm. Nspd: norspermidine. NspS: norspermidine sensor. MbaA: maintenance of biofilm architecture protein. SGDEF: diguanylate cyclase GGDEF domain. EVL: phosphodiesterase EAL domain. OM: outer membrane. IM: inner membrane. Figure adapted from Bridges and Bassler (2021).

1.3.6.7 Siderophores

Siderophores are small secondary metabolites that have a high affinity for iron. Their secretion allows them to chelate iron within the surrounding environment allowing for its uptake and utilisation by bacterial cells. A large number of siderophores utilising di-, tri-, and tetramines as scaffolds have been described. This is not due to the ability of polyamines to sequester iron but their flexible structure and distribution of positive charges across their backbone to which hydroxamate, catechol, or polycarboxylate groups are added. A large number of polyamine-based siderophores are covered in the excellent and expansive review by Long et al. (2023). Polyamine-based siderophores have been identified in a range of pathogenic and non-pathogenic species from soil to marine environments. This highlights the diversity and expanse of polyamine synthesis and the versatility of polyamines as precursors for other metabolites. Due to the expansive nature of this topic, more specific examples relating to *A. baumannii* will be discussed later (Section 1.3.7).

1.3.7 Role in *A. baumannii*

1, 3-diaminopropane was determined as being the major polyamine of the *Acinetobacter* genus over 30 years ago (Hamana and Matsuzaki, 1992). Some characterisation of the two enzymes has been conducted, as previously discussed (Section 1.3.3.2). Since then, investigation into the role of 1, 3-diaminopropane in *A. baumannii* has established that the diamine plays a role in surface-associated motility, biofilm formation, and virulence. Transposon insertion into the *dat* and *ddc* genes initially discovered a potential linkage between 1, 3-diaminopropane and the virulence of *A. baumannii*. This loss of 1, 3-diaminopropane completely abolishes the surface-associated motility of *A. baumannii* (Skiebe et al., 2012). Loss of synthesis also significantly reduces planktonic growth, and biofilm formation and attenuates virulence in the *G. mellonella* (Blaschke et al., 2021; Skiebe et al., 2012). The mechanism by which 1, 3-diaminopropane influences these factors remains unknown. These

findings led to the suggestion that 1, 3-diaminopropane synthesis could potentially be utilised as a therapeutic target in treating A. *baumannii* infection. 1, 3-diaminopropane is also a precursor to the hydroxamate siderophores, baumannoferrin A and B (Penwell et al., 2015) (Figure 1.23). *A. baumannii* 17978 utilises acinetobactin, baumannoferrin and fimsbactin with functional redundancy being observed. Acinetobactin is the only siderophore of the three that is indispensable for survival within the host (Sheldon and Skaar, 2020). Putrescine is used to synthesise fimsbactin. While not essential for virulence this siderophore can support the growth of *A. baumannii* in serum (Sheldon and Skaar, 2020).

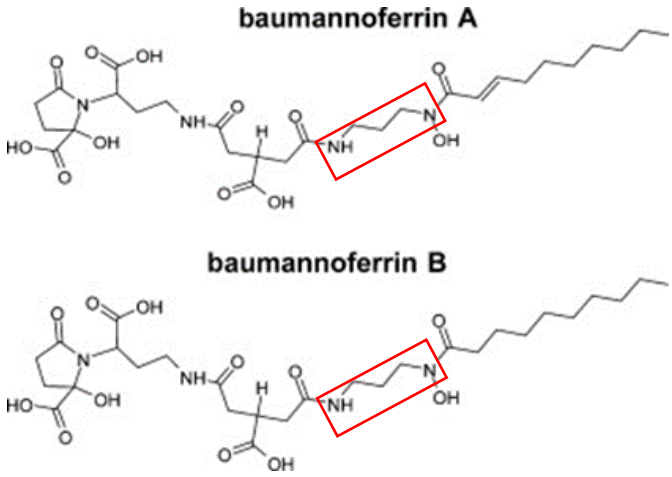

Figure 1.23. The structure of baumannoferrin A and B. Red boxes: 1, 3-diaminopropane moieties. Figure adapted from Penwell et al (2015).

Recently it was established that *A. baumannii* encodes a unique 1, 3-diaminopropane acetyltransferase (Dpa). Deletion of Dpa results in increased and decreased surface motility and biofilm formation, respectively. *dpa* expression is also elevated in stationary phase, biofilm cells, and cells adhered to eukaryotic epithelial cells (Armalytė et al., 2023). There are two possible scenarios for these effects. The first is that acetylation reduces intracellular 1, 3-diaminopropane shutting down the motility regulon allowing a shift to an adherent state. Alternatively, the acetylated product may directly modulate biofilm formation. Significant investigation is needed to understand the intricacies of 1, 3-diaminopropane's role in *A. baumannii*. While many polyamine-specific transporters have been identified, none have been

identified in *A. baumannii.* However, it has been demonstrated that the multidrug efflux pumps AceI and AmvA are capable of cadaverine and spermidine export, respectively and their deletion leads to increased intracellular polyamines accumulation during polyamine shock (Hassan et al., 2019; Short et al., 2021). The AdeABC efflux pump encoded by *A. baumannii* is also upregulated in response to polyamine stress with intracellular accumulation occurring following deletion (Short et al., 2021). AmvA appears highly conserved across the species, suggesting a rooted role in *A. baumannii* biology. While these investigations provide insight into polyamine homeostasis the degree to which these transporters were involved during *in vivo* homeostasis at the time was unknown. However, it has been recently determined that AceI and AmvA are both significantly expressed when *A. baumannii* and *K. pneumoniae* are co-cultured (Semenec et al., 2023), providing evidence of how these two systems may contribute to homeostasis *in vivo*. As previously mentioned, *E. coli* encoding the *dat* and *ddc* of *A. baumannii* are capable of 1, 3-diaminopropane excretion attributed to CadB and PotE (Chae et al., 2015). Little is known about synthesis pathways relating to 1, 3-diaminopropane. Recently it has been shown in *Acinetobacter baylyi* that 1, 3-diaminopropane can be acted upon by promiscuous enzymes to generate β-alanine (Perchat et al., 2022). This investigation suggests that this pathway contributes to significant β-alanine production. This somewhat challenges the accepted assumption that these promiscuous background reactions do not have a significant impact on wild type backgrounds. *A. baumannii* also encodes homologues of these enzymes and therefore may utilise the same β-alanine salvage pathway. The presence of Dat and Ddc in other species and the promiscuity of the enzymes involved suggests that this pathway could be widely utilised across a diverse range of species. So far investigation into 1, 3-diaminopropane in *A. baumannii* has shown it to be involved in several diverse roles. Its association with virulence is of particular interest as it could be used as a novel therapeutic target going forward, similar to other pathways discussed later (Section 1.3.9).

1.3.8 Role in *K. pneumoniae*

The role of polyamines in *K. pneumoniae* is poorly understood. Encoding the genes for the synthesis of 1, 3-diaminopropane, putrescine, cadaverine, and spermidine (Morris, 2017) all along with acetylspermidine have been detected within several species of *Klebsiella* (Hamana, 1996). There is some evidence for the roles of putrescine, cadaverine and spermidine in *K. pneumoniae* however very little is known about 1, 3-diaminopropane or acetylspermidine. Investigation of polyamines in *K. pneumoniae* primarily focused on putrescine and spermidine. Deletion of the *speE* gene in *K. pneumoniae* 52145 reduces the capsule synthesis suggesting spermidine may be involved in the capsule formation of *K. pneumoniae*, through an unknown mechanism (Morris, 2017). Interestingly deletion of the *speABC* genes did not affect the hypermucoviscous capsule phenotype. This taken with the observations made with the *speE* strain suggests that it may not be an absence of spermidine but an overaccumulation of putrescine contributing to the phenotype. Alternatively, it has been hypothesised (pers. comm. Dr L Hobley, University of Nottingham) that the explanation for the Δ*speABC* strains not phenocopying the Δ*speE* strain may be that the SpeE enzyme is acting upon other diamines such as cadaverine and/or 1, 3-diaminopropane to generate aminopropylcadaverine and norspermidine (Figure 1.24). These analogues are then acting as substitutes for the role of spermidine, however further investigation is needed to confirm this.

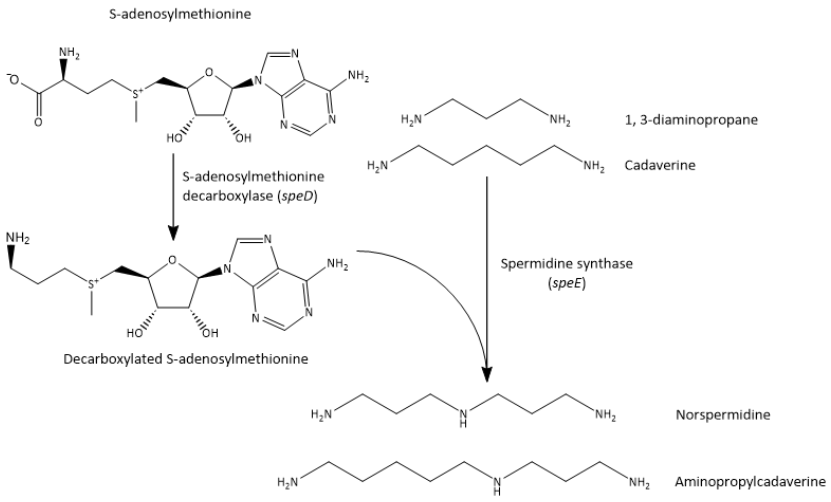

Figure 1.24. The proposed synthesis pathway of spermidine analogues norspermidine and aminopropyl cadaverine in *K. pneumoniae* 52145. Figure generated in ChemDraw 22.2.

Some characterisation has been done concerning the LdcC and CadA enzymes encoded by *K. pneumoniae*. Both enzymes show near-exclusive specificity for lysine as a substrate and have an optimal temperature of 37 °C and a pH of 7 (J. H. Kim et al., 2016). Deletion of the *cadA* gene in *K. pneumoniae* NTUH-K2044, results in a loss in acidic inducible decarboxylase activity and shows the *cadCBA* operon to be essential for resistance to acid stress (Hsieh et al., 2010). In addition to this, the transcriptional regulator CadC, may play a role in the adaptation and survival of bile stress (Hsieh et al., 2010). While the role in acid tolerance is to be expected, the resistance to bile stress highlights a novel role for the *cad* loci in the adaptation to gastrointestinal stress and colonisation. As previously mentioned, multidrug efflux pumps are capable of polyamine efflux. Investigation in *K. pneumoniae* showed that exposure to lung surfactant upregulates the MdtJI efflux pump, a known polyamine transporter in *E. coli* (Higashi et al., 2008) and deletion of MdtJI reduces virulence in a murine pneumonia model (Willsey et al., 2018). This suggests it may play a role in regulating polyamine homeostasis in the host environment. As previously mentioned, the co-culture of *K. pneumoniae* with *A. baumannii* results in the increased expression of AmvA and AceI in *A. baumannii*. It was also observed that the putrescine transporter SapB, in *K. pneumoniae* was significantly upregulated (Semenec et al., 2023), supporting the argument that the two

transporters in *A. baumannii* are upregulated as a response to *K. pneumoniae* excreting polyamines. Demonstrating a potential cross-talk between bacterial species, something that would be relevant to polymicrobial biofilms and infection.

1.3.9 Inhibition of polyamine synthesis as a treatment

With polyamines being important metabolites in humans and many species of pathogenic bacteria their synthesis has been identified as a possible therapeutic target. The most successful polyamine synthesis inhibitor is DL-alpha-difluoromethylornithine (Figure 1.25) a potent inhibitor of ornithine decarboxylase.

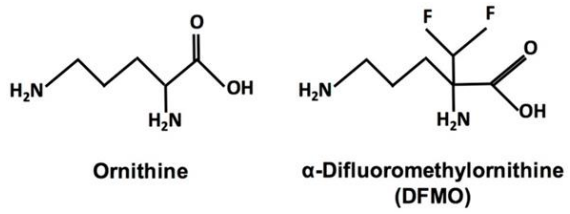

Figure 1.25. The structure of ornithine and the fluorinated structural analogue α-difluoromethylornithine (DFMO). Figure Adapted from LoGiudice et al (2018).

DFMO is an irreversible inhibitor of ornithine decarboxylase. Decarboxylation of DFMO results in it becoming covalently bound within the active site (Poulin et al., 1992). DFMO is primarily used to treat African sleeping sickness caused by *Trypanosoma brucei*. It has also been tested on several bacterial species. *Helicobacter pylori* is susceptible to DFMO independent of polyamine synthesis (Barry et al., 2011). Treatment was found to reduce *cagA* expression, a key virulence factor of *H. pylori* and alter host polyamine synthesis resulting in increased bacterial clearance (Barry et al., 2011). DFMO also limits the growth and inhibits capsule expression of *S. pneumoniae* (Ayoola et al., 2022). The success of DFMO as an antibacterial therapeutic suggests that this may be a plausible approach for both species moving forward. The inhibition of LDC activity has also been explored with α-difluoromethyl lysine (DFML) and α-monofluoromethyl lysine (MFML). A patent for the use of these inhibitors in treating periodontal diseases, such as gingivitis, has been filed in the US

(Levine, 2001). However, experimental evidence suggests that DFML does not cause adequate LDC inhibition (Lohinai et al., 2015) limiting the viability of its usage. Triamine synthesis inhibition has also been investigated with methylglyoxal bis(guanylhydrazone) (MGBG) and SAM486A, both targeting S-adenosylmethionine decarboxylase. Their usage has primarily been as cancer therapeutics. MGBG is abandoned with a driving factor being that it causes mitochondrial damage (Pathak et al., 1977). SAM486A appears to be a more potent inhibitor than MGBG, having a pronounced inhibitory effect on cell proliferation (Regenass et al., 1994; Stanek et al., 1993). Several SAM486a human clinical trials were conducted in the early 2000s (Millward et al., 2005; Paridaens et al., 2000). These however have only been constricted to phase I and II due to inadequate results. While polyamine synthesis inhibition appears to be a promising target, there have been few cases where it has been successful let alone widely applied. This is due to the unsuccessful results and unforeseen side effects. The diverse range of roles polyamines potentially have in Eukaryotes makes it challenging to utilise polyamine synthesis/transport as a therapeutic target.

1.3.10 Basis for utilising polyamine synthesis as a therapeutic target in *A. baumannii* and *K. pneumoniae*

Several components support the rationale for developing polyamine synthesis inhibitors as novel antimicrobials to treat bacterial infections. The first is significant evidence that polyamines play a role in the virulence of several bacterial pathogens. There is clear evidence to suggest that 1, 3-diaminopropane is involved in the virulence of *A. baumannii* (Armalytė et al., 2023; Blaschke et al., 2021; Skiebe et al., 2012). While the evidence for 1, 3-diaminopropane is non-existent in *K. pneumoniae*, polyamines have been linked to biofilm formation (Morris, 2017). The most attractive reason for targeting 1, 3-diaminopropane is that mammalian cells do not synthesise it. While it does exist in eukaryotes, as a byproduct of hypusination, there is no evidence of a role for this polyamine in humans. Therefore, targeting the pathway in *A. baumannii* and *K. pneumoniae* would avoid the off-target effects

of targeting putrescine or spermidine synthesis. Use of a novel inhibitor would not be limited to *A. baumannii* or *K. pneumoniae* species, as the synthesis of 1, 3-diaminopropane is ubiquitous across the *Acinetobacter* genus (Hamana and Matsuzaki, 1992) and therefore, could be utilised on other pathogenic species of *Acinetobacte*r and *Klebsiella* (Hamana, 1996). Additionally, this pathway is also found in several other organisms such as the *Vibrio* genus*, Haemophilus influenzae,* and several *Enterobacteriaceae* (Hamana, 1996; Ikai and Yamamoto, 1998; Yamamoto et al., 1986). Additionally, a homolog of the L-2, 4-Diaminobutyrate aminotransferase is present in *P. aeruginosa* and is required for pyoverdine synthesis. This demonstrates that targeting 1, 3-diaminopropane would not be limited to *K. pneumoniae* and *A. baumannii*.

1.4 Aims

The overall aim of this project was to investigate the role of polyamines in the virulence of *K. pneumoniae* and *A. baumannii*. It sought to determine possible phenotypes of polyamine synthesis disruption to elucidate the viability of polyamine synthesis being used as a therapeutic target.

Chapter 3 Role of 1, 3-diaminopropane in *Acinetobacter baumannii*

The chapter investigates the role of 1, 3-diaminopropane in the virulence of *A. baumannii* 17978. It attempts to discern possible reasons for the attenuated virulence following the loss of 1, 3-diaminopropane synthesis.

Chapter 4 Role of 1, 3-diaminopropane in *Klebsiella pneumoniae*

This chapter investigates the synthesis and possible roles of 1, 3-diaminopropane in *K. pneumoniae* 52145 to determine a possible link between 1, 3-diaminopropane and virulence to determine its viability as a therapeutic target.

Chapter 5 Role of cadaverine in *Klebsiella pneumoniae*

This chapter investigates the synthesis and role of cadaverine in *K. pneumoniae* 52145. With a specific focus on its role in resistance to stress conditions, encountered during infection and its possible contribution to virulence.

Chapter 6 Analysis of 1, 3-diaminopropane synthesis enzymes

This chapter investigates the conservation of the 1, 3-diaminopropane synthesis enzymes and the possible 3D monomeric and multimeric structures formed by each enzyme. Additionally, it attempts to find and optimise suitable conditions for the expression and purification of the 1, 3-diaminopropane biosynthesis enzymes from *K. pneumoniae* and *A. baumannii*.

Chapter 2 Materials and Methods

2.1 Growth media preparation

All growth media was prepared using MilliQ H_2O and to the manufacturer's specifications unless otherwise stated. Media was sterilised by autoclaving at 121 °C and at 15 psi for 15 minutes unless otherwise stated.

2.1.1 Lysogeny broth (Miller) and agar

25 g/l Miller LB broth. For LB agar 15 g/l agar was added to broth before sterilisation. Where indicated antibiotics and supplements were added to LB broth and agar. When required the pH of LB was altered with 2M HCl (Sigma) or 2M NaOH (Sigma) before autoclaving.

2.1.2 100 mM MES buffered 1x M9-Glucose broth

128 g/l M9 minimal salts (Difco), 9.524 g/l MES hydrate (Sigma) were dissolved in MilliQ H_2O and altered to a pH of 6.5 with 2 M KOH (Sigma) or a pH of 5.5 with HCl. Following sterilisation media was supplemented with a final concentration of 2 mM $MgSO_4$ (Fisher), 3 µM thiamine (Sigma), and 2 % (w/v) glucose (Sigma) (Kidd et al., 2017).

2.1.3 1x M9-succinate broth

11.28 g/l M9 minimal salts. Following sterilisation media was supplemented with a final concentration of 2 mM $MgSO_4$, 100 µM $CaCl_2$ (Fisher) 0.4 % (w/v) sodium succinate (Sigma) (Nagy et al., 2019).

2.1.4 M9 agar

56.4 g/l M9 minimal salts (5x stock solution) were added to molten 1.5 % (w/v) agar, following sterilisation of both components. For growth of *K. pneumoniae* 52145, M9 agar was supplemented with a final concentration of 2 mM $MgSO_4$, 3 µM thiamine, and 2 % (w/v) glucose. For growth of *A. baumannii* 17978 M9

agar was supplemented with a final concentration of 0.4 % (w/v) sodium succinate, 2 mM $MgSO_4$, and 100 µM $CaCl_2$.

2.1.5 6 % (w/v) Sucrose agar

60 g/l sucrose (Sigma), 5 g/l yeast extract (Difco), 10 g/l tryptone (Difco) and 1.5 % (w/v) agar (Morris, 2017).

2.1.6 0.5 % (w/v) Motility agar

5 g/l tryptone, 2.5 g/l NaCl (Fisher), 5g/l agarose (Sigma) (Skiebe et al., 2012). Agar was made fresh each day and used immediately after sterilisation.

2.1.7 Lysine decarboxylase broth (Taylor Modification)

One lysine decarboxylase tablet (Oxoid) was added per 5 ml of MilliQ H_2O.

2.1.8 Mueller Hinton broth

21 g/l Mueller Hinton broth (Sigma).

2.1.9 Mueller Hinton Agar

38 g/l Mueller Hinton agar (Sigma).

2.1.10 Nutrient agar

28 g/l nutrient agar (Oxoid).

2.1.11 Tryptone soya agar

60 g/l tryptone soy broth (Oxoid) and 10 g/l agarose.

2.1.12 Tryptone soya broth minimal media

Initially, a solution of HEPES (Sigma) buffer was made by dissolving 4.76 g/l in MilliQ H_2O and altered to pH 7.5 with 2 M NaOH and sterilised by filtration through a 0.22 µM filter. For the TSB minimal media 10 ml/l sterile tryptone soy broth, 100 ml/l 20 mM HEPES (pH 7.2), and 10 g/l agarose (Lehrer et al., 1991; Llobet et al., 2008).

2.1.13 Antibiotic stocks

Where appropriate antibiotics were supplemented into agar and broth. Antibiotic stock concentrations are presented in Table 2.1. Stocks were filter sterilised through a 0.22 µM filter.

Table 2.1. Antibiotic stocks

Antibiotic	Solvent	Stock concentration (mg/ml)
Trimethoprim	DMSO	50
		128
Tetracycline hydrochloride	70 % (v/v) ethanol	25
		16
Carbenicillin sodium	H_2O	50
Kanamycin sulphate		50
Gentamicin sulphate		16
Colistin sulphate		16
Meropenem		8
Streptomycin sulphate		16
Apramycin sulphate		16

2.2 Bacterial strains, primers, and plasmids

2.2.1 Bacterial strains used in this study

Table 2.2 Strains used in this study

Strain	Genotype/description	Source/Reference
E. coli C600	*thi thr leuB tonA lacY supE*	Appleyard (1954)
E. coli GT115	F^- *mcrA* Δ(*mrr-hsdRMS-mcrBC*) ϕ80Δ*lacZ*ΔM15 Δ*lacX74 recA1 rp sL* (*StrA*) *endA1* Δ*dcm uidA(ΔmluI) ::pir-116 ΔsbcC-sbcD*	InvivoGen
E. coli β2163	(F^-) RP4-2-Tc::Mu Δ*dapA*::(*erm-pir*) [Km^R Em^R]	Demarre et al. (2005)
E. coli BTH101	*F^-, cya-99, araD139, galE15, galK16, rpsL1, hsdR2, mcrA1, mcrB1*	Euromedex

E. coli BTH101 pUT18C-Zip pKT25-Zip	BTH101 strain containing the pUT18C-Zip and pKT25-Zip vectors	Euromedex
E. coli DH5α	F^- ϕ80*lac*ZΔM15 Δ(*lac*ZYA-*arg*F) U169 *rec*A1 *end*A1 *hsd*R17(r_K^-, m_K^+) *pho*A *sup*E44 λ^- *thi*-1 *gyr*A96 *rel*A1	Hanahan (1983)
E. coli K12 MG1655	F- lambda- *ilvG- rfb-50 rph-1*	Blattner et al. (1997)
E. coli BL21(DE3) pLysS	F–, *ompT*, *hsdSB* (rB–, mB–), *dcm*, *gal*, l(DE3), pLysS, Cm^R	Promega
K. pneumoniae 52145	Serotype O1: K2; Sequence type ST66	Lery et al. (2014)
A. baumannii 17978	Wild type strain	American Type Culture Collection
A. baumannii 17978 (UN)	Wild type strain, confirmed UN variant	American Type Culture Collection
K. pneumoniae 52145 Δ*dat*	52145 with in-frame deletion of the *dat* gene	This work
K. pneumoniae 52145 Δ*ddc*	52145 with in-frame deletion of the *ddc* gene	This work
K. pneumoniae 52145 Δ*ldcC*	52145 with in-frame deletion of the *ldcC* gene	Xuedi Liu, Hobley Group
K. pneumoniae 52145 Δ*cadA*	52145 with in-frame deletion of the *cadA* gene	Xuedi Liu, Hobley Group
K. pneumoniae 52145 Δ*ldcC* Δ*cadA*	52145 *ΔldcC* with in-frame deletion of the *cadA* gene	Xuedi Liu, Hobley Group
K. pneumoniae 52145 Δ*speE*	52145 with in-frame deletion of the *speE* gene	Morris (2017) (Hobley Group)
K. pneumoniae 52145 Δ*manC*	52145 with in-frame deletion of the *manC* gene	Kidd et al. (2017)
K. pneumoniae 52145 Δ*ompA*	52145 with in-frame deletion of the *ompA* gene	Llobet et al. (2009)
A. baumannii 17978 (UN) *Δddc*	17978 (UN) with in-frame deletion of the *ddc* gene	This work

2.2.2 Primers used in this study

Table 2.3. Primers used in this study

Primers	Role/description and amplicon size	Primer sequence 5' -> 3' *	Tm **
Primers used for gene deletion in *K. pneumoniae* 52145			
Kp_datddc_UpF1	*K. pneumoniae dat ddc* deletion and screening amplifies. Pair amplifies 713 bp "up fragment"	gcattctagagcaggagctgaaactgcagg	76
Kp_datddc_UpR1		GGATCCcatcatatcactcccacaac	71
Kp_datddc_DwnF1	*K. pneumoniae dat ddc* deletion. Pair amplifies 551 bp "down fragment"	GGATCCctgctggcgcaataacctgc	79
Kp_datddc_DwnR1		gcatTCTAGActtcctgcataccaaggtgg	73
Kp_datddc_DwnF2	*K. pneumoniae dat* deletion. With the Kp_datddc_DwnR1 the pair amplifies the 2042 bp "Δ*dat* fragment"	GGATCCgtaaaaccggtctgagtgga	74
Kp_datddc_upR2	*K. pneumoniae ddc* deletion. With the Kp_datddc_UpF1 pair amplifies 2108 bp "Δ*ddc* fragment"	GGATCCggtcacttactccactcaga	71
Kp_datddc_scF	*K. pneumoniae dat ddc* deletion screening. Pair amplifies 3372, 1986, and 1890 bp products in the WT, Δ*dat,* and Δ*ddc* strains	agggttatagtgacagagcg	58
Kp_datddc_scR		gaaactgccgcactccatgc	70
Kp_datddc_outF	*K. pneumoniae dat ddc* deletion confirmation. Amplifies 4614, 3228, and 3132 bp products in WT, Δ*dat* and Δ*ddc* strains	ggtgcacttctttgctgacg	66
Kp_datddc_outR		ccagcagagcgcgaatatcc	69
Primers used for gene deletion in *A. baumannii* 17978			
Ab_datddc_UpF1	*A. baumannii dat ddc* deletion and screening. Pair amplifies 826 bp "up fragment"	tctagacgaatttccgcgcg	69
Ab_datddc_UpR1		GGATCCgctcatatcggattaccatc	71
Ab_datddc_DwnF1	*A. baumannii dat ddc* deletion Pair amplifies 941 bp "down fragment"	GGATCCccaccaatcgactaattgag	71
Ab_datddc_DwnR1		TCTAGAaatgcttcaccaatctcacc	67
Ab_datddc_DwnF2	*A. baumannii dat* deletion. With the Ab_datddc_DwnR1 the pair amplifies the 2476 bp "Δ*dat* fragment"	GGATCCgtgcgaggcgcgtaagtatg	78
Ab_datddc_UpR2	*A. baumannii ddc* deletion. With the Ab_datddc_UpF1 the pair amplifies the 2202 bp "Δ*ddc* fragment"	GGATCCcaccatacttacgcgcctcg	77
Ab_datddc_outF	*A. baumannii*	gagtcaacatttgcgcacgc	69

Ab_datddc_outR	*ddc* deletion confirmation. Amplifies a 4876 and 3343 bp products in the WT and Δ*ddc* strains	ccagccataatgtgctgacc	65
Primers used for the confirmation of Δ*ldcC*, Δ*cadA* and Δ*ldcC* Δ*cadA*			
Kp_ldcC_UpF1	*K. pneumoniae* 52145 *ldcC* deletion confirmation. Amplifies a 3940 and 1786 bp products in the WT and Δ*ldcC* strains	atcgacgaagaagtgcatcg	65
Kp_ldcC_DwnR1		ttgagcgtatcctgaaaggc	64
Kp_cadA_UpF1	*K. pneumoniae* 52145 *cadA* deletion confirmation. Amplifies 4033 and 1879 bp products in the WT and Δ*cadA* strains	tattccggtagtcatgaccg	62
Kp_cadA_DwnR1		aaacaggctaatcgagctcc	62
Primers used for the creation of complementation vectors			
Kp_ldcC_comp_F	Amplifies a 2896 bp product including the *ldcC* gene of *K. pneumoniae* 52145 and predicted promoter with additional EcoRI sites for restriction cloning	gcatGAATTCccaccagaaaggtcgtgaaacc	79
Kp_ldcC_comp_R		GAATTCttattaacgcgcaagcctttcg	72
Kp_cadA_comp_F	Amplifies a 3078 bp product including the *cadA* gene of *K. pneumoniae* 52145 and predicted promoter with additional SalI sites for restriction cloning	gcatGTCGACTgatgtcgctacctatcagg	75
Kp_cadA_comp_R		GTCGACttattacttgttattctcttctttcagc	67
Primers used for the confirmation of the deletion of *speE* gene in *K. pneumoniae* 52145			
Kp52_speE/D_UpF1	*K. pneumoniae* 52145 *speE* deletion screening. Amplifies a 3226 and 2365 bp products in the wild type and Δ*speE* deletion strains	aatcgaactgctgagaacgc	64
Kp52_speE/D_DwnR1		ccgttatctgaacttcaacc	59
Primers used for UN/VU screening of *A. baumannii* 17978			
17978UN_cls_F	Amplifies a 2347 bp product from within the *clsC2* of AbaAL44 to confirm UN genotype	tctttctggctggttgcttactcagc	71
17978UN_cls_R		ccgcagctttctgattgagacaggc	74
17978VU_junction_F	Amplifies a 483 bp product from across junction where AbaAL44 is inserted into the genome to confirm VU genotype	aaacgctacgtgccagaggc	69
17978VU_junction_R		acggcttcaatcattggcggtg	74
Primers used for the construction of Dat and Ddc expression vectors			
Kp_dat28_F	Amplifies a 1443 bp product consisting of the *dat* gene of *K. pneumoniae* 52145 with overhangs complimentary to pET28a for restriction-free cloning	GCAGCGGCCTGGTGCCGCGCGGCAGCCatatgatgacggataaagtccgtattgata	94
Kp_dat28_R		CTCAGTGGTGGTGGTGGTGGTGCTCGAGTTagaccggttttacgccggcggcc	94
Kp_ddc28_F	Amplifies a 1539 bp product consisting of the *ddc* gene of *K. pneumoniae* 52145 with overhangs complimentary to pET28a for restriction-free cloning	GCAGCGGCCTGGTGCCGCGCGGCAGCCATatgaccgccatgttccacattgaatccga	99
Kp_ddc28_R		CTCAGTGGTGGTGGTGGTGGTGCTCGAgttattgcgccagcagctcctgagcg	94

Kp_dat41_F	Amplifies a 1436 bp product consisting of the *dat* gene of *K. pneumoniae* 52145 with overhangs complimentary to pET41c for restriction-free cloning	GTTTAACTTTAAGAAGGAGATATACatatgatgacggataaagtccgtattg	75
Kp_dat41_R		GCTGCACTACCGCGTGGCACAAGCTTgaccggttttacgccggcggccag	96
Kp_ddc41_F	Amplifies a 1496 bp product consisting of the *ddc* gene of *K. pneumoniae* 52145 with additional NdeI and XhoI sites for restriction cloning into pET41c	GCATCATATGaccgccatgtccacattgaatcc	80
Kp_ddc41_R		GCATCTCGAGttgcgccagcagctcctgagc	85
Ab_dat28_F	Amplifies a 1431 bp product consisting of the *dat* gene of *A. baumannii* 17978 with overhangs complimentary to pET28a for restriction-free cloning	GCAGCGGCCTGGTGCCGCGCGGCAGCCatatgagcgttacttctgtcaaccctgcca	98
Ab_dat28_R		CTCAGTGGTGGTGGTGGTGGTGCTCGAGttacgcgcctcgcactgcaaccaat	94
Ab_ddc28_F	Amplifies a 1589 bp product consisting of the *ddc* gene of *A. baumannii* 17978 with overhangs complimentary to pET28a for restriction-free cloning	GCAGCGGCCTGGTGCCGCGCGGCAGCCAtatggtggattttgcagaacatcgtaaag	96
Ab_ddc28_R		CTCAGTGGTGGTGGTGGTGGTGCTCGAGttagtcgattggtggtacgtagtta	87
Ab_dat41_F	Amplifies a 1388 bp product consisting of the *dat* gene of *A. baumannii* 17978 with additional NdeI and XhoI sites for restriction cloning into pET41c	gcatCATATGagcgttacttctgtcaaccc	73
Ab_dat41_R		GCATCTCGAGcgcgcctcgcactgcaacc	87
Ab_ddc41_F	Amplifies a 1547 bp product consisting of the *ddc* gene of *A. baumannii* 17978 with additional NdeI and XhoI sites for restriction cloning into pET41c	GCATCATATGgtggattttgcagaacatcg	75
Ab_ddc41_R		gcatCTCGAGgtcgattggtggtacgtagttacc	77
Primers used for the construction of BACTH vectors			
Kp_dat_B2H_F	Amplifies a 1410 bp product including the *dat* gene of *K. pneumoniae* 52145 and KpnI and XbaI sites for cloning into BACTH plasmid. Allowing fusion to C-terminal of T18/T25 fragments.	TCGACTCTAGAGatgatgacggataaagtccg	74
Kp_dat_B2H_R		CTTAGGTACCCGtcagaccggtttacgccgg	80
Kp_ddc_B2H_F	Amplifies a 1506 bp product including the *ddc* gene of *K. pneumoniae* 52145 and KpnI and XbaI for cloning into BACTH plasmid. Allowing fusion to C-terminal of T18/T25 fragments.	TCGACTCTAGAGgtgaccgccatgtccacattg	81
Kp_ddc_B2H_R		CTTAGGTACCCGttattgcgccagcagctcct	79
Ab_dat_B2H_F	Amplifies a 1398 bp product including the *dat* gene of *A. baumannii* 17978 and KpnI and XbaI for cloning into BACTH plasmid. Allowing fusion to C-terminal of T18/T25 fragments.	TCGACTCTAGAGatgagcgttacttctgtcaacc	74
Ab_dat_B2H_R		CTTAGGTACCCGttacgcgcctcgcactgcaacc	83
Ab_ddc_B2H_F	Amplifies a product of 1557 bp including the *ddc* gene of *A.*	TCGACTCTAGAGatggtggatttgcagaacatcg	78

Ab_ddc_B2H_R	*baumannii* 17978 and KpnI and XbaI for cloning into BACTH plasmid. Allowing fusion to the C-terminal of T18/T25 fragments.	CTTAGGTACCCGttagtcgattggtggtacgt	73
pUT18C_MCS_F	pUT18C insert screening and sequencing	agaaccgtgcatacggc	62
pUT18C_MCS_R	pUT18C insert screening and sequencing	acagcttgtctgtaagcg	57
pKT25_MCS_F	pKT25 insert screening and sequencing	caatgccgccggtatt	63
pKT25_MCS_R	pKT25 insert screening and sequencing	ttcaggctgcgaact	56
Primers used for investigation of polyamine synthesis gene expression			
Kp_rpoB_RTPCR_F	Amplifies 120 bp product internal to the *rpoB* gene of *K. pneumoniae* 52145	tcgtccacttcgcctttacc	66
Kp_rpoB_RTPCR_R		gttcaaccgttctctgctgc	65
Kp_dat_RTPCR_F	Amplifies 81 bp product internal to the *dat* gene of *K. pneumoniae* 52145	tccagttcatgccttacccg	67
Kp_dat_RTPCR_R		agtaggtcagggctttcacg	63
Kp_ddc_RTPCR	Amplifies 102 bp product internal to the *ddc* gene of *K. pneumoniae* 52145	ctgtggatgggtctggaagc	67
Kp_ddc_RTPCR_R		ctgcgacttcacgtactccg	66
Kp_ldcC_RTPCR_F	Amplifies 174 bp product internal to the *ldcC* gene of *K. pneumoniae* 52145	atcaaagaaccagccgtccg	68
Kp_ldcC_RTPCR_R		atgcatacctctacgtcgcc	64
Kp_cadA_RTPCR_F	Amplifies 152 bp product internal to the *cadA* gene of *K. pneumoniae* 52145	ccgtaactgccacaaatcgc	68
Kp_cadA_RTPCR_R		gtctctttcacacgcttggc	65
Ab_rpoB_RTPCR_F	Amplifies 146 bp product internal to the *rpoB* gene of *A. baumannii* 17978	gtctccaagccgcatttcg	68
Ab_rpoB_RTPCR_R		cattggtgccgcataagtcg	69
Ab_dat_RTPCR_F	Amplifies 139 bp product internal to the *dat* gene of *A. baumannii* 17978	agctggcttagttacaccgc	63
Ab_dat_RTPCR_R		gccaggcgtacaattcatgc	68
Ab_ddc_RTPCR_F	Amplifies 154 bp product internal to the *ddc* gene of *A. baumannii* 17978	tcacgagcaagcaatacaccc	67
Ab_ddc_RTPCR_F		tggactcatgggatcaaagcc	68
Primers used for investigation of co-transcription of polyamine synthesis genes			
Kp_dat/ddc_J_F	Amplifies 550 bp product spanning the 9 bp intergenic region between *K. pneumoniae* 52145 dat and *ddc* genes	gaagcgcaggatcacatgg	67

Kp_dat/ddc_J_R		taatcagcacttccgccgc	68
Kp_cadC/B_J_F	Amplifies 632 bp product spanning the 365 bp intergenic region between *K. pneumoniae* 52145 *cadC* and *cadB* genes	tacgtcctggcgaagatacc	64
Kp_cadC/B_J_R		aagccagagacatcgcacc	66
Kp_cadB/A_J_F	Amplifies a 484 bp product spanning the 76 bp intergenic region between *K. pneumoniae* 52145 *cadB* and *cadA* genes	taaagcctctgacctgttcgg	65
Kp_cadB/A_J_R		acaatacggaagtccaggcg	66
Kp_cadA/yjdL_J_F	Amplifies 450 bp product spanning the 59 bp intergenic region between *K. pneumoniae* 52145 *cadA* and *yjdL* genes	cgtcaacgccaacatgatcc	69
Kp_cadA/yjdL_J_R		aaccagagatgcgtaagcg	63
Kp_yjdL/lysS2_J_F	Amplifies 882 bp product spanning the 331 bp intergenic region between *K. pneumoniae* 52415 *yjdL* and *lysS2* genes	tgacggtcaggcctcaatgg	71
Kp_yjdL/lysS2_J_R		catcgttgtccttcgcatcg	69
Ab_dat/ddc_J_F	Amplifies 424 bp product spanning the 2 bp intergenic gap between *A. baumannii* 17978 *dat* and *ddc*	cgcaactctttaatgctaccgc	67
Ab_dat/ddc_J_R		ggccgcggtttaatgattgg	70
*Capital letters represent additional, non-annealing sequences (restriction endonuclease sequences, vector-specific overhangs) **Tm according to the manufacturer of oligonucleotides (Sigma)			

2.2.3 Plasmids used in this study

Table 2.4 Plasmids used in this study

Plasmids	Genotype / Description	Source / Reference
pGEM-T Easy	Cloning vector, F1 *ori*, Amp^R	Promega
pGPI-SceI-2	Suicide vector, R6K γ ori, I-SceI endonuclease recognition site, Tmp^R	Flannagan et al. (2008)
pDAI-SceI-SacB	pBBR1 ori, I-SceI endonuclease, *sacB*, Tet^R	Hamad et al. (2010)
pGEMT-Δ$datddc_{Kp}$	pGEM-T Easy containing Δ$datddc_{Kp}$ Amp^R	Laura Hobley
pGEMT-Δdat_{Kp}	pGEM-T Easy containing Δdat_{Kp} Amp^R	This Work
pGEMT-Δddc_{Kp}	pGEM-T Easy containing Δddc_{Kp} Amp^R	
pGEMT-Δ$datddc_{Ab}$	pGEM-T Easy containing Δ$datddc_{Ab}$ Amp^R	
pGEMT-Δdat_{Ab}	pGEM-T Easy containing Δdat_{Ab} Amp^R	
pGEMT-Δddc_{Ab}	pGEM-T Easy containing Δddc_{Ab} Amp^R	
pGPI-SceI-Δ$datddc_{Kp}$	pGPI-SceI-2 containing Δ$datddc_{Kp}$ Tmp^R	Laura Hobley

pGPI-SceI-Δ*dat*$_{Kp}$	pGPI-SceI-2 containing Δ*dat*$_{Kp}$ Tmp^R	This work
pGPI-SceI-Δ*ddc*$_{Kp}$	pGPI-SceI-2 containing Δ*ddc*$_{Kp}$ Tmp^R	
pGPI-SceI-Δ*datddc*$_{Ab}$	pGPI-SceI-2 containing Δ*datddc*$_{Ab}$ Tmp^R	
pGPI-SceI-Δ*dat*$_{Ab}$	pGPI-SceI-2 containing Δ*dat*$_{Ab}$ Tmp^R	
pGPI-SceI-Δ*ddc*$_{Ab}$	pGPI-SceI-2 containing Δ*ddc*$_{Ab}$ Tmp^R	
pUT18C	BACTH vector, ori ColE1, C-terminal fusion T18 fragment of cyaA, Amp^R	Euromedex
pKT25	BATCH vector, ori P15A, C-terminal fusion T25 fragment of cyaA, Kan^R	
pUT18C-zip	BATCH control vector encodes GCN4 leucine zipper fused in frame to T18 fragment	
pKT25-zip	BATCH control vector encodes GCN4 leucine zipper fused in frame to T25 fragment	
pUT18C-*dat*$_{Kp}$	pUT18C vector encoding *K. pneumoniae* 52145 *dat* gene, T18 C-terminal fusion	This work
pUT18C-*ddc*$_{Kp}$	pUT18C vector encoding *K. pneumoniae* 52145 *ddc gene*, T18 C-terminal fusion	
pUT18C-*dat*$_{Ab}$	pUT18C vector encoding *A. baumannii* 17978 *dat* gene, T18 C-terminal fusion	
pUT18C-*ddc*$_{Ab}$	pUT18C vector encoding *A. baumannii* 17978 *ddc gene*, T18 C-terminal fusion	
pKT25-*dat*$_{Kp}$	pKT25 vector encoding *K. pneumoniae* 52145 *dat* gene, T25 C-terminal fusion	
pKT25-*ddc*$_{Kp}$	pKT25 vector encoding *K. pneumoniae* 52145 *ddc* gene, T25 C-terminal fusion	
pKT25-*dat*$_{Ab}$	pKT25 vector encoding *A. baumannii* 17978 *dat* gene, T25 C-terminal fusion	
pKT25-*ddc*$_{Ab}$	pKT25 vector encoding *A. baumannii* 17978 *ddc* gene, T25 C-terminal fusion	
pET28a	Expression vector, pBR322 ori, His tag, Nterm thrombin cleavage site, Kan^R	Novagen
pET41c	Expression vector, pBR322 ori, His tag, Nterm thrombin cleavage site, Kan^R, modified to remove GST.	Lerner et al. (2012)
pET28a-*dat*$_{Kp}$	pET28a expressing the *dat* gene of *K. pneumoniae* 52145 (restriction free)	This work
pET28a-*ddc*$_{Kp}$	pET28a expressing the *ddc* gene of *K. pneumoniae* 52145 (restriction free)	
pET28a-*dat*$_{Ab}$	pET28a expressing the *dat* gene of *A. baumannii* 17978 (restriction free)	
pET28a-*ddc*$_{Ab}$	pET28a expressing the *ddc* gene of *A. baumannii* 17978 (restriction free)	
pET41c-*dat*$_{Kp}$	pET41c expressing the *dat* gene of *K. pneumoniae* 52145 (restriction free)	
pET41c-*ddc*$_{Kp}$	pET41c expressing the *ddc* gene of *K. pneumoniae* 52145 (restriction)	
pET41c-*dat*$_{Ab}$	pET41c expressing the *dat* gene of *A. baumannii* 17978 (restriction)	

pET41c-ddc_{Ab}	pET41c expressing the *ddc* gene of *A. baumannii* 17978 (restriction)	
pGEMT-$ldcC_{Kp}$	pGEM-T Easy encoding *K. pneumoniae* 52145 *ldcC* gene	
pGEMT-$cadA_{Kp}$	pGEM-T Easy encoding *K. pneumoniae* 52145 *cadA* gene	

2.3 Bacterial growth and maintenance

2.3.1 Bacterial growth

E. coli, K. pneumoniae and A. *baumannii* were quadrant streaked onto LB agar and incubated at 37 °C for 16 hours. A single colony was picked from an agar plate and added to the appropriate volume of LB broth. Cultures were incubated at 37 °C with shaking at 200 rpm for 16 hours. For growth in polyamine-free media a single colony of *K. pneumoniae* and *A. baumannii* were added to the appropriate volume of 100 mM MES buffered 1x M9-Glucose broth, *for K. pneumoniae* and 1x M9-succinate broth for *A. baumannii.* Cultures were incubated at 37 °C with shaking at 200 rpm for 16 hours.

2.3.2 Storage of bacterial strains

Frozen stocks were made by adding 750 µl of overnight culture to 750 µl of 50 % (v/v) sterile glycerol in 2 ml sterile screw-capped tubes. Glycerol stocks were stored at -80 °C.

2.4 Cloning methods

2.4.1 Genomic DNA purification

2 ml of bacterial culture was transferred to a 1.5 ml microfuge tube, in 1 ml aliquots and centrifuged at 13,000 x g for 2 minutes. Supernatants were removed. Genomic DNA was isolated using the PureLink™ Genomic DNA kit (Invitrogen) following the manufacturer's instructions. DNA was eluted using 50 µl of elution buffer.

2.4.2 Plasmid DNA purification

Following incubation whole cultures were centrifuged and the supernatants removed. For miniprep purification plasmid DNA was purified using the QIAprep Spin Miniprep Kit (Qiagen) following the manufacturer's instructions. For midiprep purification plasmid DNA was purified with the GenElute™ Plasmid Midiprep Kit (Sigma) following manufacturer's instructions. For minipreps, the DNA was eluted with 30 µl sterile MilliQ H_2O. For midipreps DNA was eluted using 500 µl of elution buffer, preheated to 55 °C.

2.4.3 PCR amplification of DNA

All PCR was carried out in a Biorad C1000 thermal cycler using several different polymerases and protocols depending on the planned application of the amplified DNA. DNA amplified for the construction of deletion vectors used *Taq* (NEB) and *Ex Taq* (Takara). DNA amplified for the creation of BACTH and expression vectors used Phusion (NEB) or *Pfu Ultra* (Agilent). All amplification of DNA for sequencing was done with Phusion. For routine PCR and standard screening of inserts and deletions *Taq* and *OneTaq* (NEB) were both used. Template DNA volume varied and for colony PCR the DNA template was replaced by a single colony, picked with a sterile 10 µl pipette tip and added directly to the PCR reaction mixture. All PCR reaction mixtures and conditions are shown in Table 2.5 and Table 2.6.

Table 2.5 PCR reaction mixtures

	Taq	***OneTaq* 2X Master Mix with Standard Buffer**	***TaKaRa Ex Taq***	**Phusion**	***Pfu ultra***
Reaction buffer (10x stock)	1 x	1 x	1 x	1 x	1 x
dNTPs	200 µM	-	200 µM	200 µM	200 µM
Primers	0.5 µM	0.5 µM	0.4 µM	0.5 µM	2-4 µl of PCR product
Template DNA	<1000 ng	<1000 ng	<500 ng	<250 ng	5-10 ng/ µl

DNA polymerase	0.125 µl	-	0.3 µl	0.5 µl	1 µl
Sterile MilliQ H_2O	Made up to 25 µl	Made up to 25 µl	Made up to 50 µl	Made up to 50 µl	Made up to 50 µl

Table 2.6 PCR thermocycler conditions

Step	Temperature (°C)	Duration	Cycles
Initial denaturation	94 (*OneTaq*) 95 (*Ex Taq*/*Taq*/*Pfu Ultra)* 98 (Phusion)	5 min (*Taq*/*OneTaq*/*Ex Taq*) 2 min (*Pfu Ultra*) 30 s (Phusion)	x 1
Denaturation	94 (*OneTaq*) 95 (*Ex taq*/*Taq*/*Pfu Ultra*) 98 (Phusion)	1 min (Taq/OneTaq) 45 s (Ex Taq) 30 s (*Pfu Ultra*) 10 s (Phusion)	x 30-35
Annealing	45-68 (*Taq*/*OneTaq*) 54 (*Ex taq*) 45-72 (Phusion) 55 (*Pfu ultra*)	1 min (Taq/OneTaq) 45 s (Ex Taq) 1 min (*Pfu Ultra*) 30 s (Phusion)	
Elongation	68 (*Taq*/*OneTaq*) 72 (*Ex taq*/Phusion/*Pfu Ultra*)	1 min/Kbp (*Taq*/*OneTaq*/*Ex taq/Pfu Ultra*) 30 s/Kbp (Phusion)	
Final Elongation	72 (All)	10 min (All)	x 1

2.4.4 Gel electrophoresis

DNA was separated by agarose gel electrophoresis. Agarose gel concentration varied between 0.8-2 % (w/v). Agarose was dissolved in 1x TAE buffer. Molten agarose was supplemented with ethidium bromide to a final 1 µg/ml concentration. 1 µL of 6x loading dye (NEB) was added to 5 µL of DNA Samples. Samples were loaded parallel to 1 Kbp DNA ladder (NEB). Electrophoresis was carried out in 1x TAE buffer at 90-100V for 60-90 minutes. DNA was visualised using ultraviolet light and imaged with a Gel Doc XR+ imaging system (Biorad).

2.4.5 DNA purification from agarose

50 µL PCR reaction mixtures were used for agarose gel purification. 10 µL of 6x loading dye was added to reaction mixtures and were loaded alongside a 1 Kbp DNA ladder. DNA was separated by gel electrophoresis (Section 2.4.4). Following electrophoresis, DNA fragments were visualised using a UV

transilluminator. DNA fragments were excised from the gel using a clean scalpel and placed into a sterile 1.5 ml microfuge tube. Gel slices were weighed ensuring that fragments were <400 mg. DNA was extracted from the agarose using the QIAquick Gel Extraction Kit (Qiagen), following the manufacturer's instructions. DNA fragments were eluted in 30 µL sterile milliQ H_2O.

2.4.6 PCR product purification

PCR products were purified with the QIAquick PCR Purification Kit (Qiagen) according to the manufacturer's instructions. DNA was eluted with 30 µl of sterile MilliQ H_2O.

2.4.7 Quantification of nucleic acids

The concentration and purity of purified DNA and RNA were quantified using a Nanodrop 1000 (Thermofisher). 1 µL of sterile MilliQ H_2O was used to initialise the spectrophotometer. The spectrophotometer was blanked with 1 µL of sterile MilliQ H_2O or elution buffer depending on the DNA suspension being quantified. 1-2 µl of DNA/RNA sample was loaded and the concentration and purity were measured.

2.4.8 Restriction endonuclease digestion

2.4.8.1 Preparation of insert fragments and vectors prior to ligation

PCR fragments and vectors were digested with the appropriate enzymes (NEB). Digested vectors were treated with calf intestinal phosphatase (NEB), to minimise self-ligation. Reaction mixtures were incubated at 37 °C for 3 hours.

2.4.8.2 Diagnostic digestion of vectors

Diagnostic restriction digests were used to confirm the correct insertion of DNA fragments into vectors. An appropriate concentration of vector (dependent on copy number) was digested with 1 µl of the relevant enzyme(s), 1 µl 10X rCutSmart Buffer, made up to a total volume of 10 µl with sterile MilliQ H2O, unless otherwise stated. All digests were incubated at 37 °C for 3 hours.

2.4.9 Ligation of DNA fragments

DNA fragments were ligated into an appropriate linearised and phosphatase-treated vector at a molar ratio of 1:3 or 1:7 vector to insert, depending on the application. Reaction mixtures comprised 2 µl of 10X T4 DNA Ligase Buffer (NEB) and 1 µl of T4 ligase (NEB). Total reaction volumes were made up to 20 µl with sterile MilliQ H_2O unless otherwise stated. All reactions were carried out alongside a self-ligation control. Ligations were incubated for a minimum of 3 hours at room temperature.

2.4.10 Production of chemically competent *E. coli*

Following incubation 600 ml of fresh LB was inoculated with 600 µl of liquid bacterial culture and incubated at 37 °C with shaking at 200 rpm until an OD_{600nm} of 0.2-0.3 was achieved. The culture was split into 50 ml aliquots in sterile 50 ml tubes and placed on ice for 30 minutes. Cells were centrifuged at 4000 x g for 10 minutes and the supernatant was discarded. Pelleted cells were carefully resuspended in 20 ml of cold 0.1 M $CaCl_2$ per tube. Cells were centrifuged at 4000 x g for 10 minutes and the supernatant was discarded. Cells were resuspended in 2 ml of cold 0.1 M $CaCl_2$ per tube. Resuspended cells were combined to give a final volume of 20 ml. Cells were incubated at 4 °C on ice for 16 hours. Following incubation 5 ml of 50 % (v/v) glycerol was added to the cells and mixed thoroughly. 400 µl aliquots were transferred to 1.5 ml sterile microfuge tubes. Tubes were stored at -80 °C until required.

2.4.11 Heat shock transformation

1.5 ml microfuge tubes containing 400 µl aliquots of *E. coli* $Cacl_2$ competent cells were defrosted on ice. 200 µl of cells were used for each transformation. Once defrosted, DNA was added directly to cell suspensions and left on ice for 30 minutes. Whole ligation reactions were added to defrosted cells. For purified plasmid DNA, an appropriate concentration was added to defrosted cells. For ligation reactions, the total reaction volume was added. All transformations were accompanied by negative control cells containing no DNA. Following incubation, cells were placed in a heat block at 42 °C for two

minutes. Once complete, microfuge tubes were placed immediately on ice for three minutes. Following heat shock, 1 ml of fresh sterile LB broth was added to each microfuge tube and incubated at 37 °C with shaking at 200 rpm for 1 hour. Following incubation 100 µl of each transformation was plated onto LB agar supplemented with the relevant antibiotic. The remaining transformation cells were centrifuged at 13,000 x g for two minutes. Supernatants were removed and pellets were resuspended in the residual media and plated onto LB agar supplemented with the relevant antibiotics. Plates were incubated at 37 °C for 16 hours.

2.4.12 Production of electrocompetent cells

Methodology adapted from Choi and Schweizer (2006). Following incubation, stationary phase cultures were split into 1.5 ml aliquots in microfuge tubes. Tubes were centrifuged at 13,000 x g for two minutes. Supernatants were removed and pellets were resuspended in 1 ml of 300 mM sucrose. Cell suspensions were centrifuged again at 13,000 x g for two minutes. Supernatants were removed and pellets were resuspended in 1 ml of 300 mM sucrose. Cell suspensions were centrifuged again at 13,000 x g for two minutes and pellets were resuspended in 200 µl of 300 mM sucrose ready for electroporation. Electrocompetent cells were freshly prepared when required.

2.4.13 Electroporation transformation

Methodology adapted from Choi and Schweizer (2006). 100 µl of electrocompetent cell suspension was transferred to a microfuge tube, along with the DNA to be electroporated. The mixture was mixed and transferred to a 0.2 cm Flowgen electroporation cuvette (SLS). Electroporation conditions were 2.5 kV, 200 Ω, 25 µF and a time constant of 5 ms. Following electroporation, 1 ml of room temperature Super Optimal broth with Catabolite repression (SOC; 2 % (w/v) tryptone, 0.5 % (w/v) yeast extract, 10 mM NaCl, 2.5 mM KCl, 10 mM $MgCl_2$, 10 mM $MgSO_4$, and 20 mM glucose) (Sigma) media was added directly to the electroporation cuvette. The cell suspension was transferred to a 1.5 ml microfuge tube and incubated at 37 °C

with shaking at 200 rpm for 1 hour. Following incubation, 100 µl of each transformation mix was plated onto LB agar supplemented with relevant antibiotics. The remaining transformation cells were centrifuged at 13,000 x g for two minutes. Supernatants were removed and the pellets were resuspended in the residual media and plated onto LB agar supplemented with the relevant antibiotics. Plates were incubated at 37 °C for 16 hours.

2.5 DNA sequencing

2.5.1 DNA sequencing of PCR products

PCR products were purified with the QIAquick PCR Purification Kit, following the manufacturer's instructions. DNA was bound to a silica spin column and purified through centrifugation. PCR products were eluted in 30 µL sterile milliQ H_2O. DNA concentration was measured using nanodrop 1000 (section 2.4.7). Sequencing of PCR products was carried out by Eurofins Scientific, using the Sanger sequencing Tubeseq services. A minimum of 15 µl of DNA samples at a concentration of 20 ng/µl were sent for sequence analysis.

2.5.2 DNA sequencing of plasmids

Plasmids were purified for sequencing using either the QIAprep Spin Miniprep Kit or the GenElute™ Plasmid Midiprep Kit (Section 2.4.2). Sequencing of plasmids was carried out by Eurofins Scientific, using the Sanger sequencing Tubeseq services. 20 µl of plasmid DNA, at a concentration of 50-100 ng/µl was sent for sequencing.

2.5.3 Whole genome sequencing

2.5.3.1 Sample preparation

Whole genome sequencing (WGS) was conducted on *K. pneumoniae* 52145 and *A. baumannii* 17978 wild type strains and all polyamine mutants by MicrobesNG. Whole cells were sent for DNA extraction and sequencing and were prepared according to MicrobesNG's directions. To prepare, strains were

freshly quadrant streaked, for single colonies, onto LB agar. Plates were incubated for 16 hours. Single colonies of each strain were inoculated into 10 ml of fresh sterile LB broth in a 50 ml sterile falcon tube. For *A. baumannii* 17978 *Δddc* a single colony was inoculated into 50 ml fresh sterile LB broth in a 250 ml sterile screw top conical flask. All cultures were incubated at 37 °C with shaking at 200 rpm for 18 hours. Following incubation 1 ml of culture was diluted in 9 ml of fresh sterile LB broth in a 50 ml falcon tube. For *A. baumannii* 17978 *Δddc* 5 ml of culture was diluted in 45 ml of fresh sterile LB broth in a 250 ml screw top conical flask. All cultures were incubated at 37 °C with shaking at 200 rpm for 2.5 hours. Following incubation cultures were diluted to an optical density that gave between 4 x 10^9 and 6 x 10^9 cells/ml. Cell suspensions were washed in PBS twice and resuspended in the provided DNA/RNA shield buffer. Samples were then sent to MicrobesNG for sequencing using their "Standard Service" which resulted in a minimum of 30x coverage of each chromosome by paired-end Illumina Sequencing.

2.5.4 Analysis of whole genome sequencing data

2.5.4.1 Mapping sequence data to reference genomes

Dr Hobley carried out the analysis of WGS data. The sequenced data was mapped to the genomic sequences of *K. pneumoniae* 52145 (Genbank ref: NZ_F0834906) and *A. baumannii* 17978 (UN) [Genbank ref: CP079931]. This was done in Galaxy, using the BWA-MEM2 program. This produced "binary bam alignment files". These were visualised with IGV viewer. This maps the reads of the sequencing to the known reference sequence.

2.5.4.2 SNP analysis

To determine the presence of SNPs, the snippy program was used in Galaxy, using the trimmed reads files from WGS and the reference sequences.

2.6 Deletion of polyamine synthesis genes

The markerless deletion of 1, 3-diaminopropane synthesis genes used a methodology based on that of Aubert et al (2014).

2.6.1 Creation of deletion plasmids

2.6.1.1 Primer design and creation of deletion constructs

Primers for mutagenesis were designed using the genome sequences of *A. baumannii* ATCC 17978 (Genbank ref: NZ_CP049363) and *K. pneumoniae* 52145 (Genbank ref: FO834906). The *dat* and *ddc* genes, including 1 Kbp upstream and downstream were used to design primers to amplify the flanking regions of the gene to be deleted. The gene sequences and the upstream and downstream regions were assessed for restriction endonuclease sites using NEBcutter. EcoRI was the endonuclease for cloning *A. baumannii* deletion constructs from pGEMT into pGPI-SceI-2. Due to the presence of EcoRI sites in the *K. pneumoniae* sequence, the Kp_datatddc_UF1 and DwnR1 primer pair had an additional XbaI and 4 nucleotides added to the 5' end of each primer (Table 2.3) to allow the addition of XbaI site onto the deletion construct, enabling downstream restriction cloning of the DNA fragment. The internal primers of each construct were designed to introduce BamHI overhangs to amplicons to allow fragments the upstream and downstream deletion fragments to be annealed together. Deletion construct fragments were amplified with appropriate primers (Table 2.3) using the standard Taq polymerase protocol (Section 2.4.3). Amplified deletion fragments were separated by gel electrophoresis (Section 2.4.4) and purified from agarose (Section 2.4.5). Purified upstream and downstream deletion fragments underwent two additional PCRs. The first utilised ExTaq to join the deletion fragments and polymerise a single product. Reaction mixture and conditions are shown in Table 2.7 and Table 2.8. The second 10 µl of the first reaction mixture was combined with appropriate primers (Table 2.3) and the full constructs were amplified using ExTaq (Section 2.4.3). Amplified deletion

constructs were verified and separated by gel electrophoresis (Section 2.4.4) and were purified from agarose using the QIAquick Gel Extraction Kit (Section 2.4.5).

Table 2.7 Reaction mixture for joining deletion fragments

Reagent	Volume (µl)
10X ExTaq buffer	5
2.5 mM dNTPs	4
ExTaq Polymerase	0.5
'Up deletion fragment'	1-3
'Down deletion fragment'	1-3
MilliQ H_2O	Made up to 50 µl

Table 2.8 Thermocycler conditions for joining deletion construct fragments

Temperature (°C)	Duration	Cycles
95	5 min	x 1
95	45 s	x 30
55	90 s	
72	90 s	
72	10 min	x 1

2.6.1.2 Insertion of deletion construct into pGEM-T-Easy vector

DNA amplification of the deletion fragments introduced 3' adenosine overhangs to the amplified products. This allowed purified deletion constructs to be TA-ligated into the linearised pGEM-T, as part of the pGEM®-T Easy Vector Systems kit (Promega). Ligation reactions were in a molar ratio of 1:3 vector to insert. Mixtures consisted of 5 µl of 2X Rapid Ligation Buffer, 50 ng linearised pGEMT-Easy, 1 µl T4 ligase made, a variable volume of deletion fragment made up to a final volume of 10 µl with sterile MilliQ H_2O. Following ligation, reaction mixtures were heat shock transformed into *E. coli* C600 (Section 2.4.11). Following incubation of plates, colonies were patch plated with a sterile toothpick, onto LB agar and LB agar supplemented with appropriate antibiotics.

Five patches were inoculated into 5 ml of LB broth and were grown under standard conditions. Following incubation plasmids were purified (Section 2.4.2) and inserts were verified by a diagnostic digest of purified plasmid DNA (Section 2.4.8.2). PCR was also used to confirm the presence of deletion constructs.

2.6.1.3 Insertion of deletion constructs into pGPI-SceI-2 suicide vector

pGEM-T containing deletion constructs and empty pGPI-SceI-2 suicide vector were digested with appropriate enzymes (Section 2.4.8.1) and gel purified (Section 2.4.5). Digested deletion constructs were ligated into pGPI-SceI-2 (Section 2.4.9). Following ligation whole reaction mixtures were heat shock transformed into $CaCl_2$ chemically competent *E. coli* GT115. Following incubation of plates, colonies were patch-plated onto LB agar and LB agar supplemented with appropriate antibiotics. Colonies were PCR screened (Section 2.4.3) and *E. coli* GT115 containing pGPI-SceI-2 deletion vectors were inoculated into 5 ml of LB broth in a sterile plastic universal and were grown under standard conditions. Following incubation, deletion vectors were purified (Section 2.4.2).

2.6.1.4 Creation of *E. coli* β2163 donor strains

Purified pGPI-SceI-2 deletion vectors were heat shock transformed into $CaCl_2$ chemically competent *E. coli* β2163 (Section 2.4.11) and were confirmed by PCR and diagnostic digest.

2.6.2 Conjugation of *K. pneumoniae* and *A. baumannii* with *E. coli* β2163 containing the pGPI-SceI-2 deletion vectors

K. pneumoniae 52145 and *A. baumannii* 17978 wild type strains were inoculated into 5 ml sterile LB broth in 30 ml plastic sterile universal tubes and incubated at 37 °C for 16 hours. Donor strains of *E. coli* β2163, containing pGPI-SceI-2 deletion vectors, were inoculated into 5 ml sterile LB broth in 15 ml plastic sterile falcon tubes and incubated statically at 37 °C for 18 hours. Donor strains were supplemented with 0.3 mM diaminopimelic acid and 100 µg/ml

trimethoprim. Following incubation, recipient strains were diluted and regrown to the exponential phase. 500 µL of culture was inoculated into 4.5 ml of fresh sterile LB broth in a 30 ml sterile plastic universal tube. Cultures were incubated at 37 °C with shaking at 200 rpm for 2.5 hours. Following incubation donor and recipient cultures were centrifuged at 4000 x g for 10 minutes. Supernatants were discarded and pellets were resuspended in 5 ml of sterile 10 mM $MgSO_4$. Cell suspensions were centrifuged at 4000 x g for 10 minutes. Supernatants were discarded and pellets were resuspended in 500 µl of sterile 10 mM $MgSO_4$. 100 µl of the donor and recipient cell suspensions were combined in a sterile 1.5 ml microfuge tube. The mixture was placed onto an LB agar supplemented with 0.3 mM diaminopimelic acid and incubated at 37 °C for 18 hours. Following incubation, 1.5 ml of sterile LB broth was pipetted onto the agar plate and a sterile plastic L-shaped spreader was used to recover the bacterial growth. The cell suspension was transferred to a sterile 1.5 ml microfuge tube and serially diluted. Dilutions were spread and plated onto LB agar supplemented with appropriate antibiotics. Plates were incubated under standard conditions. Exconjugants were selected for and maintained by patch plating onto LB supplemented with appropriate antibiotics.

2.6.3 Conjugation of transformants with *E. coli* β2163 containing pDAI-SceI-SacB

A second conjugation that introduced the pDAI-SceI-SacB plasmid was carried out on previous transformants. Five patched transconjugants, from the previous transformation, were selected and inoculated individually into 5 ml of sterile LB broth supplemented with 100 µg/ml trimethoprim in a 30 ml sterile plastic universal and incubated at 37 °C for 16 hours with shaking at 200 rpm. A single colony of *E. coli* β2163 containing pDAI-SceI-SacB was inoculated into 5 ml sterile LB broth, supplemented with 12.5 µg/ml tetracycline and 0.3 mM diaminopimelic acid, in a 15 ml plastic sterile falcon tubes and incubated statically at 37 °C for 18 hours. Conjugation was carried out as previously described. Once bacterial growth was recovered from the agar plate, cell suspensions were serially diluted in fresh sterile LB broth. 100 µL of each

dilution were spread plated onto LB agar supplemented with appropriate antibiotic. Resistant colonies were replica patch plated onto LB and LB with appropriate antibiotics.

2.6.4 Sucrose counterselection

Single colonies of presumptive mutants of *K. pneumoniae* and *A. baumannii* were individually inoculated into 5 ml sterile LB broth in a sterile 30 ml plastic universal tube and incubated at 37 °C with shaking at 200 rpm for 16 hours. Following incubation 100 µL of culture was inoculated into 10 ml of fresh sterile LB broth in a 30 ml sterile plastic universal. Cultures were incubated at 37 °C with shaking at 200 rpm until an optical density of 0.3-0.4 at 600 nm was obtained. Following incubation, cultures were serially diluted in fresh sterile LB broth. 100 µL of each dilution were plated onto 6 % (w/v) sucrose agar and plates were incubated at 30 °C for 24 hours. Following incubation, surviving colonies were screened for tetracycline resistance.

2.7 Genetic complementation of *K. pneumoniae*

2.7.1 Primer design and amplification of polyamine synthesis genes

Primers were designed using the gene sequences and up to 1 Kbp upstream of the start codon, to amplify the polyamine biosynthesis genes and potential promoters of each gene. Promoters were predicted using BProm. The gene sequences and upstream regions were assessed for the presence of restriction endonuclease sites using NEBcutter. Restriction endonuclease sites, that were absent from the gene sequence and upstream regions, were added to the 5' end of each primer, to allow for the insertion of fragments into digested pGEMT (Table 2.3). Sequences were amplified using the standard Phusion polymerase protocol (Section 2.4.3). Amplified DNA was separated by gel electrophoresis (Section 2.4.4) and was purified (Section 2.4.5).

2.7.2 Insertion of synthesis genes into pGEM-T and transformation into *K. pneumoniae* deletion strains.

Purified PCR fragments and pGEM-T-Easy were digested with appropriate enzymes (Section 2.4.8.1) and gel purified (Section 2.4.5). DNA concentration was quantified using Nanodrop 1000 (Section 2.4.7) and fragments were ligated into digested pGEM-T-Easy (Section 2.4.9). Following ligation, reaction mixtures were transformed into electro-competent *K. pneumoniae* 52145 polyamine deletion strains (Section 2.4.13). Following incubation, colonies were selected and patch-plated onto LB with the appropriate antibiotic. Transformants underwent colony PCR, using appropriate primers (Table 2.3) and the standard Taq polymerase protocol (Section 2.4.3). Patches containing vectors harbouring the correct gene insert were inoculated into 5 ml of LB broth in a sterile plastic universal and were incubated at 37 °C with shaking at 200 rpm for 16 hours. Plasmid DNA was purified (Section 2.4.2). Purified complementation vectors were screened for correct insert by diagnostic digest. Once the presence of vectors was confirmed in *K. pneumoniae* 52145 strains were glycerol stocked and stored at - 80 °C (Section 2.3.2).

2.8 Bioinformatic analysis

2.8.1 DNA and protein sequences

Genomic DNA sequences were acquired from NCBI nucleotide. Amino acid sequences were acquired from UniprotKB (Bateman et al., 2023) or taken from the relevant Genbank files.

2.8.2 Folded protein prediction

Predicted folded protein structures were acquired from the Alphafold database (Jumper et al., 2021; Varadi et al., 2022). Where structures were unavailable the open-source software Colabfold V1.5.5 was employed. This was done using the notebook “ColabFold: AlphaFold2 using MMseqs2” via the Google Collaboratory platform (Mirdita et al., 2022). Settings for ColabFold were

standard. Crystalised protein structures were acquired for the protein databank (Berman et al., 2003, 2000). 3D structures were visualised using pyMOL V2.5.

2.8.3 DNA, amino acids and 3D protein alignments

DNA and Protein sequences were compared to sequences found in the relevant NCBI databases using BLASTN and BLASTP, for nucleotide and amino acid sequences, respectively (Altschul et al., 1990). Specific DNA and amino acid sequences were aligned using EMBL-EBI tools EMBOSS NEEDLE (Pairwise) (Needleman and Wunsch, 1970) and Clustal Omega (Multiple) (Sievers et al., 2011). Amino acid sequence alignments were visualised using ESPript3 (Robert and Gouet, 2014). Where appropriate DNA alignments were coloured using Boxshade. Alignment of 3D protein structures was carried out using PDB pairwise structure alignment (Prlić et al., 2010). Alignment used the TM-Align method.

2.8.4 Prediction of promoters and terminators

Promoters were predicted with Bprom (Solovyev and Salamov, 2011). Rho-independent terminators were predicted with TransTermHP and Rho-dependent terminators were predicted with RhoTermPred (Di Salvo et al., 2019; Kingsford et al., 2007). Both tools are available at Galaxy EU.

2.8.5 Prediction of RNA secondary structure

RNA secondary structure was predicted using the MXfold2 webserver (Sato et al., 2021).

2.8.6 Analysis of DNA curvature

DNA curvature was predicted using the Bend.it webserver (Vlahoviček et al., 2003). Prediction used default settings, except for smoothing which was set to simple.

2.8.7 Prediction of protein features, domains, and conserved residues

Protein domains and features were predicted using the InterPro databases (Paysan-Lafosse et al., 2023) and SMART (Letunic et al., 2021).

2.8.8 Predicting the effect of missense mutation on folded protein

Missense3D (Ittisoponpisan et al., 2019) was used to predict the structural impact of missense mutations using the AlphaFold or ColabFold predictions of folded proteins. To determine the impact missense mutations potentially have on polar contacts within the protein structure the PyMOL mutagenesis tool was used to mutate single amino acid residues of the polypeptide sequence.

2.9 Analysis of polyamine synthesis gene expression

2.9.1 Purification of total RNA

2.9.1.1 Culture preparation

Stationary phase bacterial cultures were diluted and regrown to obtain exponentially growing cells. Cultures were diluted 1:50 in fresh sterile LB broth in a 30 ml sterile plastic universal tube. For *A. baumannii* Δ*ddc* cultures were diluted 1:10. Cultures were incubated at 37 °C with shaking at 200 rpm for 2 hours.

2.9.1.2 Total RNA extraction

Following incubation, 1 ml of culture was transferred to a sterile 2 ml microfuge tube and centrifuged at 13,000 x g for 2 minutes and supernatants were removed. Cell pellets were resuspended in 1 mg/ml lysozyme solution and incubated at room temperature for 5 minutes. Total RNA was extracted using the SV total RNA isolation system (Promega). RNA was bound to a silica membrane through centrifugation. RNA samples were DNase I treated, on the

spin column, as part of the purification process. RNA was eluted in 100 µl RNase-free H_2O, provided with the kit. Purified RNA samples were frozen at -20 °C until further Dnase I treatment.

2.9.1.3 Additional Dnase I treatment of total RNA samples

Following purification, all total RNA samples underwent a secondary Dnase I treatment to remove any remaining gDNA, using the DNA-free kit (Invitrogen). DNase I treatment was carried out on RNA samples with a maximum concentration of 200 µg/ml. If total RNA initially exceeded this samples were diluted with Rnase-free H_2O to the appropriate concentration in a total volume of 50 µl. Dnase I treatments were carried out on a total volume of 50 µl of RNA sample. 5 µl of 10X Dnase I buffer was added to RNA samples. Initially, 1 µl of Dnase I was added to the reaction mixture and incubated at 37 °C for 30 minutes. Following incubation, 1 µl was added and reaction mixtures were incubated for 30 minutes at 37 °C. Following incubation, reaction mixtures were transferred to a 2 ml sterile microfuge tube and 10 µl of DNase I inactivation reagent was added, gently mixed, and incubated at room temperature for 2 minutes. Reaction mixtures were centrifuged at 12,000 x g for 2 minutes to separate the inactivation reagent and RNA sample, into two distinct layers, with RNA remaining in the top aqueous layer. RNA samples were recovered and aliquoted into new sterile 0.2 ml PCR tubes. Dnase I treated RNA samples were stored at -20 °C.

2.9.2 RT-PCR for analysis of gene expression

A. baumannii 17978 and *K. pneumoniae* 52145 gDNA were used as positive PCR controls and RNase-free water was used as a negative RT-PCR control. RT-PCR reaction mixtures and thermocycling conditions are shown in Table 2.9 and Table 2.10, respectively. RT-PCR products were visualised on a 2 % (w/v) TAE agarose gel, parallel to a 100 bp ladder (NEB). RT-PCR was carried out in duplicate on two independently extracted RNA samples.

Table 2.9: OneStep Reverse transcription PCR reaction mixture

Reagent	Volume (µl)
5X reaction buffer	5
Q-solution	5
dNTP mix	1
Forward Primer	1.5
Reverse primer	1.5
Enzyme mix	1
RNA template	0.5
Rnase-free H2O	Made up to 25 µl

Table 2.10: Onestep reverse transcription PCR thermocycler conditions

Step	Temperature	Duration	Cycles
Reverse transcription	50	30 min	x 1
Initial denaturation	94	15 min	x 1
Denaturation	94	30 s	x 35
Annealing	53	30 s	
Elongation	72	1 min	
Final Elongation	72	10 min	x 1

2.10 Analysis of polyamine content by HPLC

2.10.1 Preparation of reagents

2.10.1.1 Saturated sodium carbonate

Initially, 22 g of Na_2CO_3 was dissolved in 100 ml analytical grade H_2O. Additional sodium carbonate was added to the solution until crystals precipitated out of the solution indicating saturation.

2.10.1.2 H_2O saturated ethyl acetate

80 ml of ethyl acetate (Sigma) was combined with 10 ml of analytical grade H_2O. The mixture was shaken to disperse the water throughout the ethyl acetate. The mixture was allowed to settle for 10 minutes, this mixing was repeated two additional times. Once both layers had settled only the top ethyl acetate layer was used.

2.10.1.3 10 mM HCl

HCl solution (Sigma) was purchased at a concentration of 37 %, which was equivalent to 12 M. 8.3 ml of 12 M HCl was diluted in 91.7 ml of analytical grade H_2O. A 10 mM HCl solution was made by diluting 1 ml of 1 M HCl in 99 ml of analytical grade H_2O.

2.10.1.4 10 % (v/v) TCA solution

10 ml 6.1 N TCA solution (Sigma) was diluted in 90 ml 10 mM HCl solution.

2.10.1.5 25 % (w/v) L-Proline

5 g of L-proline (Sigma) was dissolved in 20 ml of analytical grade H_2O and sterilised by filtration through a 0.22 µM filter. Solutions were aliquoted and stored at -20 °C until use.

2.10.1.6 1, 7-diaminoheptane

For a 1 M stock 5 g of 1, 7-diaminoheptane (Sigma) was dissolved in 38.4 ml of analytical grade H_2O. Aliquots were stored at stored at -20 °C until use. For a 400 µM stock solution, 40 µl 1 M 1, 7-diaminoheptane was diluted in 960 µl analytical grade H_2O, giving a 40 mM stock solution. For 400 µM this was diluted 1:10 in analytical grade H_2O.

2.10.1.7 10 mg/ml Dansyl chloride

100 mg of dansyl chloride was dissolved in acetone (Sigma), and tubes were wrapped in foil and kept on ice. Dansyl chloride solution was made fresh when required.

2.10.2 Preparation of cellular extracts for HPLC analysis

For analysis of polyamine content cellular extracts were prepared as previously described (Hobley et al., 2014). Following incubation, the optical density at 600 nm was determined for each sample. Cells were centrifuged at 4000 x g for 10 minutes. The volume of cells centrifuged was equal to the cell density required for 1 ml of cell suspension at an OD_{600nm} of 1.0. Cell pellets were resuspended

in 500 µl analytical grade H_2O. 15 µl of 0.4 mM 1,7-diaminoheptane to each sample, as an internal standard. 500 µl of 10 % (v/v) tri-chloroacetic acid HCl solution was added to each sample and left on ice for 30 minutes to precipitate proteins. Following incubation, samples were centrifuged at 4 °C for 10 minutes to pellet the proteins. Following centrifugation supernatants were transferred to a fresh 2 ml microcentrifuge tube. The supernatant was extracted five times with water-saturated ethyl acetate. This was achieved by the addition of 1 ml of water-saturated ethyl acetate to each sample, followed by mixing by inversion. The two layers were allowed to settle, with polyamines remaining in the bottom layer. The top ethyl acetate layer was removed by pipetting and repeated four additional times. Samples were freeze-dried overnight to remove all remaining liquid.

2.10.3 Derivatization of polyamines for HPLC analysis

Polyamines were derivatised by dansylation as previously described (Hobley et al., 2014). Following freeze drying, residual material was reconstituted in 50 µl 10 mM HCl. 200 µl of saturated Na_2CO_3 solution was added to each sample, followed by 200 µl dansyl chloride solution. Samples were mixed by inversion for 10 seconds and were then incubated at 70 °C for 10 minutes. Following incubation, samples were allowed to return to room temperature. 100 µl of 25 % (w/v) L-proline solution was added to remove excess dansyl chloride. Samples were mixed thoroughly by inversion and were centrifuged at 13,000 x g for 2 minutes. Following centrifugation, the top acetone layer of each sample was retained and stored at -20 °C until HPLC was carried out.

2.10.4 Reverse phase HPLC analysis

HPLC analysis was carried out at The University of Birmingham in Dr Patrick Moynihan's laboratory by his PhD student Aaron Franklin. Derivatised polyamines were analysed by HPLC using Phenomenex 00F-4475-AN reverse phase chromatography column. Derivatised samples were detected by fluorescence detection (Ex = 340 nm / Em = 535 nm). 5 µl of sample was injected. Elution was performed with HPLC-grade methanol at a flow rate =

0.175 ml/min with a 25-minute run time. Methanol concentration was altered throughout the run time: 0-10 minutes, 0.5 %; 10-17 minutes, 100 %; 17-25 minutes, 0.5 %.

2.11 Analysis of lysine decarboxylase activity

A single colony of each strain was picked from an LB agar plate and added to the 5 ml of LDC broth. 2 ml of sterile mineral oil was overlaid on top of the broth to create an anaerobic environment. Universals were incubated statically at 37 °C for 24 hours. Following incubation, the colour of the media was observed, and images were taken.

2.12 Analysis of planktonic growth

2.12.1 Analysis of *K. pneumoniae* growth

Following incubation 30 ml of each stationary phase culture was centrifuged at 4000 x g for 10 minutes. Supernatants were removed and pellets were resuspended in 30 ml of fresh sterile LB broth at pH 7.5, 5.5, 4, and 3. Cultures were diluted to an OD_{600nm} of 0.2, in a volume of 15 ml of fresh sterile LB at the same pH as the LB used for initial pellet resuspension. 100 µL of each altered culture was serially diluted in PBS. 10 µL of each dilution was plated on LB agar, in triplicate, to allow determination of initial CFU/ml. Agar plates were incubated at 37 °C for 16 hours. Cultures were then incubated at 37 °C with shaking at 200 rpm. Optical density at 600 nm was measured every hour over 8 hours. Experiments were carried out as three independent replicates.

2.12.2 Analysis of *A. baumannii* growth

Following incubation stationary phase cultures were diluted to an OD_{600nm} of 0.1 in a volume of 50 ml of fresh sterile LB broth in a sterile 250 ml screw top conical flask. 100 µL of each altered culture was serially diluted in PBS. 10 µL of each dilution was plated on LB agar, in triplicate, to allow determination of initial CFU/ml. Agar plates were incubated at 37 °C for 16 hours. Cultures were

then incubated at 37 °C with shaking at 200 rpm. Optical density at 600 nm was measured every hour for 9 hours. At every time point, enumeration was carried out. Additionally, phase contrast microscopy was used to analyse cell morphology. Experiments were carried out as three independent replicates.

2.12.3 Phase contrast microscopy

To immobilise cells on the microscope slide 1 ml of 2.5 % (w/v) molten agarose was pipetted onto the slide. 10 µL of culture was pipetted onto the solidified agarose layer and a cover slip was placed on top. Cell morphology was examined under oil immersion using the x100 magnification lens on a Zeiss Axiovert 135 TV inverted Microscope. Images were captured using Zeiss Axiocam 105 colour and Zeiss Zen software.

2.12.4 Microscopy image processing

Captured images were processed using Fiji software. Cells were manually counted in each image using the cell counter plugin. To aid in counting conjoined cells the binary and watershed functions were used.

2.12.5 Fluorescence microscopy

To visualise the cell membrane cells were fluorescently stained and imaged by microscopy. Bacterial membranes were stained with lipophilic FM 1-43 dye (Thermofisher). 1 ml of stationary phase bacterial cultures was centrifuged at 13,000 x g for 2 minutes. Pellets were resuspended in 500 µL PBS. FM 1-43 was added to each microfuge tube of cells incubated on ice for 15 minutes. Following staining cells were centrifuged at 13, 000 x g for 2 minutes and pellets were washed with PBS three times to remove excess dye. 10 µL of cell suspension was pipetted onto an agarose pad microscope slide and a cover slip was placed on top. Cells were examined using the x100 magnification lens on a Zeiss Axiovert 135 TV inverted Microscope, with epifluorescence and filter set 62 HE, GFP filter (Ex: 474/28 Em: 527).

2.13 Analysis of capsule formation

Following incubation of agar plates, mucoviscosity was quantified by the string test (Fang et al., 2004). A sterile inoculation loop was placed onto a single colony, between 2–4 mm in diameter, and stretched vertically alongside a ruler**.** Ten measurements were taken for all strains per replicate and experiments were carried out as three independent replicates.

2.14 Analysis of surface-associated motility

Agar plate motility assays were used to assess the motility of *A. baumannii* 17978 using methodology adapted from Skiebe et al. (2012). Prior to the assay the wild type and 1, 3-diaminopropane mutant were freshly streaked onto LB agar. Motility assays utilised 0.5 % (w/v) agarose plates. For chemical complementation, media was supplemented with 125 µM of 1, 3-diaminopropane. Agarose plates were allowed to solidify and dry in a laminar flow for 30 minutes. A single colony was picked from LB agar with a 10 µL pipette tip. The motility agar surface was punctured with the pipette tip allowing inoculation through the media to the agarose and polystyrene petri dish interphase. Single colonies were only taken from LB agar plates streaked less than one week before motility assays were carried out. Motility plates were incubated upright, at 37 °C for 16 hours. Following incubation, the radius of motility was measured and motility areas were imaged. Experiments were carried out as three independent replicates.

2.15 Stress assays

2.15.1 Oxidative stress

Disc diffusion methodology was based on that of The European Committee on Antimicrobial Susceptibility Testing (2024). Stationary phase *K. pneumoniae* and the relevant deletion strain cultures were diluted to an OD_{600nm} of 0.2. For *A. baumannii* cultures were diluted to an OD_{600nm} of 0.5. Altered cultures were

swab-inoculated onto Mueller-Hinton agar. Plates were swabbed in three alternate directions to allow complete coverage of the plate surface. Once the plates were dry a single 2 mm paper disc was placed on the surface. Discs were impregnated with 3 %, 10 % or 30 % (v/v) H_2O_2 (Sigma). Agar plates were incubated at 37 °C for 16 hours. Following incubation, the diameter of the zones of inhibition was measured. Experiments were carried out as three independent replicates.

2.15.2 Nitrosative stress

2.15.2.1 Preparation of reagents

2.15.2.1.1 300 mM Sodium nitrite

207 mg sodium nitrite (Sigma) was dissolved in 10 ml of MilliQ H_2O and sterilised by filtration through a 0.22 µM filter.

2.15.2.1.2 300 mM Sodium ferrocyanide

1.452 g sodium ferrocyanide decahydrate (Sigma) was dissolved in 10 ml of MilliQ H_2O and sterilised by filtration through a 0.22 µM filter.

2.15.2.1.3 300 mM Sodium nitroprusside

845.85 mg sodium nitroprusside dihydrate (Sigma) was dissolved in 10 ml of MilliQ H_2O and sterilised by filtration through a 0.22 µM filter.

2.15.2.2 Nitrosative stress induced by acidified sodium nitrite

Methodology adapted from Bower and Mulvey (2006). Following incubation, stationary phase cultures were centrifuged at 4000 x g for 10 minutes. Supernatants were removed and pellets were resuspended in 30 ml of fresh sterile 100 mM MES-buffered LB broth at pH 5.5. Cultures were diluted to an OD_{600nm} of 0.2. Altered cultures were supplemented with 300 mM sodium nitrite to a final concentration of 3 mM. 100 µL of each culture was serially diluted in PBS. 100 µL of each dilution was plated on LB agar, in triplicate, to allow determination of initial CFU/ml. Agar plates were incubated at 37 °C for

16 hours. Cultures were incubated at 37 °C with shaking at 200 rpm and the optical density at 600 nm was measured every hour over 8 hours. Experiments were carried out as three independent replicates.

2.15.2.3 Nitrosative stress induced by sodium nitroprusside

Sodium nitroprusside was also used to induce nitrosative stress, as previously described (Srinivasan et al., 2012). Following incubation, stationary phase cultures were centrifuged at 4000 x g for 10 minutes. Supernatants were removed and pellets were resuspended in 30 ml of fresh sterile LB broth at pH 5.5 and 7.5. Cultures were diluted to an OD_{600nm} of 0.2. Altered cultures were supplemented with 300 mM sodium nitroprusside and sodium ferrocyanide, at a final concentration of 3 mM for each. Cultures were incubated at 37 °C with shaking at 200 rpm and the optical density at 600 nm was measured every hour over 8 hours. Experiments were carried out as three independent replicates.

2.16 Quantification of biofilm

2.16.1 Biofilm assay experimental preparation

Biofilm assay methodology was adapted from Kidd et al. (2017). Stationary phase cultures of *K. pneumoniae* were diluted to an approximate OD_{600nm} of 0.02 in freshly prepared sterile M9-glucose media. For *A. baumannii* the wild type was diluted to an approximate OD_{600nm} of 0.01 and the *Δddc* mutant to an OD_{600nm} of 0.015 in freshly prepared sterile M9-succinate or LB broth. For chemical complementation of 1, 3-diaminopropane synthesis mutants 1, 3-diaminopropane was added to altered cell suspensions at a final concentration of 125 µM. 100 µl of each diluted strain was added to 2 columns (12 internal wells) of a polystyrene U-bottomed 96-well plate (Greiner bio-one, 650161), across triplicate plates. Plates were incubated statically at 37 °C for 24 hours.

2.16.2 Crystal violet staining of biofilms in M9 minimal media

Following incubation, 25 µl of freshly prepared 0.5 % (v/v) crystal violet (Sigma), diluted in sterile MilliQ H_2O, was added directly to each well. Plates were

incubated at room temperature for 1 hour. Following staining, the crystal violet was discarded and plates were washed by submersion in distilled H_2O and dried. 150 µl of 95 % (v/v) Ethanol was added to all wells and incubated at room temperature for 1 hour. Crystal violet staining of biofilm biomass was then quantified by measuring the absorbance at 595 nm of each well in a microplate reader. Three independent cultures of each strain were tested per day, across a minimum of three independent days.

2.16.3 Crystal violet staining of biofilms in LB media

Following incubation, the LB broth was removed from all wells and washed with 150 µl of sterile PBS. The PBS was removed and 125 µl of freshly prepared 0.1 % (v/v) crystal violet, diluted in sterile MilliQ H_2O, was added to all wells. Plates were incubated at room temperature for 30 minutes. Following incubation, the crystal violet was discarded, and plates were washed by submersion in distilled H_2O and dried. 125 µl of 95 % (v/v) Ethanol was added to all wells and incubated at room temperature for 30 minutes. Crystal violet staining of biofilm biomass was then quantified by measuring the absorbance at 595 nm of each well in a microplate reader. Three independent cultures of each strain were tested per day, across a minimum of three independent days.

2.17 Minimum inhibitory concentration assays

MICs of antimicrobials were determined by 96-well broth microdilution, adapted from the CLSI methodology. single colonies of *K. pneumoniae* and *A. baumannii* strains were inoculated into 5 ml sterile Mueller Hinton broth in a sterile 30 ml plastic universal tube and incubated at 37 °C for 16 hours. Following incubation, optical densities were diluted to a CFU/ml equivalent to 10^8 CFU/ml. This was diluted 1:100 in MHB to give 10^6 CFU/ml bacterial suspension. Following alterations, 100 µL aliquots were serially diluted and spread plated onto LB agar to determine the correct inoculum was achieved. 50 µL of sterile MHB was added to columns 2-11 of a U-bottom polystyrene 96-well plate. 100 µL was added to column 12 as a sterility control. 100 µL of each

antibiotic was added to separate wells of column 1. Antibiotic suspensions were serially diluted down to column 10. 50 µL was removed from column 10 after dilution. 50 µL of altered bacterial suspensions were added to columns 1-11 to give a final inoculum of 5 x 10^5 CFU/ml per well. Plates were incubated at 37 °C for 24 hours. Following incubation, the growth in wells was observed. For tetracycline, pinpoint growth was disregarded. For trimethoprim, MICs were read as the lowest concentration that inhibited >80 % of bacterial growth compared to the growth control. MICs for bactericidal antibiotics were determined as the lowest concentration that completely inhibited growth. Experiments were carried out as three independent replicates.

2.18 Analysis of *in vivo* virulence

The role of polyamines in the virulence of *K. pneumoniae* 52145 and *A. baumannii* 17978 was assessed using a *Galleria mellonella* infection model. The methodology was adapted from Insua et al. (2013) and Bartholomew et al. (2019).

2.18.1 Inoculum preparation

Single colonies of wild type *K. pneumoniae* and polyamine deletion mutants were inoculated into 5 ml sterile LB broth in a sterile 30 ml plastic universal tube. For *A. baumannii* and polyamine, deletion mutants were inoculated into 50 ml sterile LB broth in a sterile 250 ml screw top conical flask. Both were incubated at 37 °C with shaking at 200 rpm for 16 hours. Following incubation 500 µL of culture was inoculated into 4.5 ml of fresh sterile LB broth in a 50 ml falcon tube. Cultures were incubated at 37 °C with shaking at 200 rpm for 2.5 hours. Following incubation cultures were centrifuged at 4000 x g for 10 minutes. The supernatant was removed, and pellets were resuspended in 5 ml sterile PBS. Resuspended cells were centrifuged at 4000 x g for 10 minutes and resuspended in 5 ml sterile PBS. *K. pneumoniae* cell suspensions were diluted to an OD_{600nm} of 0.2, the equivalent of 1 x 10^8 CFU/ml. Altered cell suspensions were further diluted 1:10 to yield 1 x 10^7 CFU/ml. For *A. baumannii* cell

suspensions were diluted to an OD_{600nm} of 0.005 and 0.05 for the wild type and *Δddc* mutant, respectively, to yield 5 x 10^6 CFU/ml for each. Suspensions were further diluted 1:10 to yield 5 x 10^5 CFU/ml. Cell suspensions were enumerated by serially diluting and plating dilutions onto LB agar. Plates were incubated at 37 °C for 16 hours.

2.18.2 *G. mellonella* infection

Galleria mellonella were obtained from UK Waxworms Ltd. Upon receipt organisms were stored at 15 °C. For analysis of *in vivo* virulence larvae were weighed and only those that were between 250-350 mg and appeared healthy without lesions or melanisation were selected. Larvae were used within 7 days of receipt. For injection, the surface of the larvae was sterilised by wiping it with 70 % (v/v) ethanol. 10 µL of each bacterial suspension was injected with a Hamilton syringe and 30-gauge needle below the last right proleg. Injection of 10 µL of each suspension of *K. pneumoniae* gave inoculums of 1 x 10^6 and 1 x 10^5 CFU. Injection of 10 µL of each suspension of *A. baumannii* gave inoculums of 5 x 10^4 CFU and 5 x 10^3 CFU. Following injection, larvae were placed into a petri dish and incubated statically, in the dark, at 37 °C. Survival was recorded every 24 hours for 5 days. Larvae were considered dead when unresponsive to physical stimuli. For each replicate, 10 larvae were injected for each strain and inoculum concentration. An additional 10 larvae were injected with PBS control as a vehicle and trauma control. Experiments were carried out as three independent replicates.

2.19 Assessment of antimicrobial peptide activity in Haemolymph of *G. mellonella*

2.19.1 Pre-infection of *G. mellonella*

To elicit the production of antimicrobial factors larvae were pre-infected before haemolymph extraction (Insua et al., 2013). Following incubation 500 µL of stationary phase culture was inoculated into 4.5 ml of fresh sterile LB broth in

a 50 ml falcon tube. Cultures were incubated at 37 °C with shaking at 200 rpm for 2.5 hours. Following incubation cultures were centrifuged at 4000 x g for 10 minutes. The supernatant was removed, and pellets were resuspended in 5 ml sterile PBS. Resuspended cells were centrifuged at 4000 x g for 10 minutes and resuspended in 5 ml sterile PBS. *E. coli* was diluted to an optical density equivalent to 1 x 10^8 CFU/ml in PBS. Following alteration *E. coli* were heat-killed, 1 ml aliquots of the bacterial suspension were transferred to a plastic microfuge tube and incubated at 65 °C for 20 minutes. For *A. baumannii*, cultures were diluted to an optical density equivalent to 5 x 10^6 CFU/ml in PBS and diluted 1:10 to yield 5 x 10^5 CFU/ml (Section 2.18.1). 10 µl of heat-killed *E. coli* or *A. baumannii* strain were injected into larvae equating to an inoculum of 1 x 10^6 CFU of *E. coli* and 5 x 10^3 for *A. baumannii*. A group were injected with PBS as a control for antimicrobial peptide activity in the haemolymph. Following injection larvae were incubated at 37 °C for 24 hours. All cell suspensions were serially diluted in sterile PBS. 100 µL of each dilution was spread plated onto LB agar to determine the correct CFU/ml was obtained.

2.19.2 Haemolymph extraction

For haemolymph, the extraction methodology was adapted from Insua et al. (2013). Following incubation three infected larvae were randomly selected and placed into a 50 ml plastic falcon tube. Larvae were placed on ice for a minimum of 10 minutes to anaesthetise them. Deceased larvae were discarded. Before haemolymph extraction 10 µl of 1 mg/ml N-phenylthiourea was dispensed into pre-chilled microfuge tubes and were kept on ice until used. Following the 10-minute incubation larvae were placed into a petri dish and their surface was sterilised with 70 % (v/v) ethanol. To extract the haemolymph larvae were cut at the last metamere with a sterile scalpel and the outpouring of haemolymph was collected in the pre-chilled microfuge containing 10 µl of 1 mg/ml N-phenylthiourea. Haemolymph from three larvae were pooled in one microfuge tube. Following haemolymph collection, the microfuge tubes were centrifuged at 4000 x g at 4 °C for 10 minutes to remove cellular debris.

2.19.3 Antimicrobial peptide radial diffusion assay

Antimicrobial peptide susceptibility was assessed using radial diffusion assay with the methodology adapted from Llobet et al. (2008) and Lehrer et al. (1991). Following incubation, 500 µL of stationary phase culture was diluted in 4.5 ml of fresh sterile LB broth in a 50 ml falcon tube. Cultures were incubated at 37 °C with shaking at 200 rpm for 2.5 hours. Following incubation cultures were centrifuged at 4000 x g for 10 minutes. The supernatant was removed and pellets were resuspended in 5 ml of sterile PBS. Resuspended cells were centrifuged at 4000 x g for 10 minutes and resuspended in 5 ml sterile PBS. Bacterial cell suspensions were diluted to OD_{540nm} of 0.3 in PBS. Following alteration 43 ml of TSB minimal agar (Section 2.1.12) was poured into a 50 ml sterile plastic falcon tube and 260 µL of each bacterial suspension was added, mixed and poured into a sterile square 12 x 12 cm petri dish. Once solidified the end of a sterile 200 µl pipette tip was cut off and wells were bored into the set media. 10 µl of haemolymph suspension was added to wells in triplicate. N-phenylthiourea and PBS were used as two negative controls. Agarose plates were incubated at room temperature for 3 hours to allow diffusion of antimicrobial peptides into the media. Following incubation 43 ml of TSB agar was poured on top of the minimal media, to allow for the growth of bacteria in the underlying layer. Plates were allowed to set and were incubated at 37 °C for 18 hours. Following incubation, the diameter of the inhibitory zones was measured for each inoculated well. Experiments were carried out as three independent replicates.

2.20 Expression of Dat and Ddc enzymes from *K. pneumoniae* 52145 and *A. baumannii* 17978

2.20.1 Construction of pET28a and pET41c Dat and Ddc expression vectors

2.20.1.1 Restriction-free cloning

Restriction-free cloning methodology was adapted from Van Den Ent and Löwe. (2006).

2.20.1.1.1 Primer design

Forward primers were designed to be complementary to the first 25 base pairs after the start codon of the gene of interest (Table 2.3). An overhang complementary to 32 base pairs of the pET28a vector was added to the 5' end (Table 2.3). The reverse primer was designed to be complementary to the final 25 base pairs, including the stop codon (Table 2.3), of the target gene. An overhang complementary to 28 base pairs of the pET28a vector was added to the 5' end (Table 2.3).

2.20.1.1.2 Amplification of synthesis genes

Amplification of the *dat* and *ddc* genes of *K. pneumoniae* and *A. baumannii* was carried out, using the gDNA of both strains as a template and the appropriate primer pairs (Table 2.3). Amplification generated a PCR product that comprises the gene of interest with the 28 base pair overhang, complementary to the expression vector. Amplicons were separated by gel electrophoresis (Section 2.4.4). DNA was excised from the gel and purified (Section 2.4.5).

2.20.1.1.3 Incorporation of gene sequence into pET28a

Purified DNA fragments were used as a "megaprimer" in a PCR using *pfu ultra* (Section 2.4.3). Following PCR 1 µl of DpnI was added directly to the reaction mixture to remove the methylated "parent" plasmid. The reaction mixture was

incubated for 3 hours at 37 °C. Following incubation, the plasmid DNA was purified (Section 2.4.6). Purified plasmid DNA was heat shock transformed into $CaCl_2$ chemically competent *E. coli* DH5α (Section 2.4.11).

2.20.1.2 Restriction cloning

2.20.1.2.1 Primer design

Gene sequences were checked for the presence of NdeI and XhoI restriction sites using NEBcutter2 before primer design. If present synthesis genes were cloned into pET41c with the restriction-free method (Section 2.20.1.1). Primers were designed to be complementary to the first 20 base pairs after the start codon of the target gene (Table 2.3). An overhang was added to the 5' end which included 4 base pairs, to allow efficient binding of the restriction enzyme, followed by an XbaI restriction site sequence (Table 2.3). The reverse primers were designed to be complementary to the last 20 base pairs, excluding the stop codon, of the target gene (Table 2.3). An overhang was added to the 5' end which included 4 base pairs followed by an XhoI restriction site sequence (Table 2.3).

2.20.1.2.2 Insertion of gene sequence into pET41c

PCR was carried out using the relevant primer pairs (Table 2.3) and Phusion polymerase (Section 2.4.3). PCR products were separated by gel electrophoresis (Section 2.4.4). DNA fragments were excised from the gel and purified (Section 2.4.5). Purified PCR products and the pET41c vector were digested with NdeI and XhoI (Section 2.4.8.1). Following digestion, DNA was separated by gel electrophoresis, was excised from the gel and purified (Section 2.4.5). DNA fragments were ligated into suitably digested pET41c in a molar ratio of 1:3 vector to insert. Following ligation, the total reaction mixture was heat shocked transformed into $CaCl_2$ chemically competent *E. coli* DH5α (Section 2.4.11).

2.20.2 Expression of Dat and Ddc in *E. coli* BL21

The creation of expression strains and subsequent protein expression and purification was carried out by MSc students supervised by Dr David Scott, with the methodology below being adapted from their submitted MSc project reports. All expression vectors were purified using Monarch plasmid miniprep kit (NEB). The following miniprep plasmids were verified by restriction digests and sequencing of the insertion region. Following final confirmation, vectors were heat shocked and transformed into chemically competent *E. coli* BL21(DE3) pLysS cells.

2.20.2.1 Small scale expression

A single colony of transformed *E. coli* BL21 harbouring the expression plasmids was inoculated into 10 ml LB broth supplemented with 30 µg/ml of kanamycin and 34 µg/ml chloramphenicol. Cultures were incubated for 18 hours at 37 °C with shaking at 180 rpm. Following incubation, 500 µl of each culture was inoculated into 50 ml of fresh LB broth supplemented with kanamycin and chloramphenicol, as previously. Cultures were incubated at 37 °C until OD_{600nm} of 0.8 was reached. Following incubation, 100 µl aliquots of each culture were taken and frozen at -20 °C. Cultures were then supplemented with 1 mM IPTG, to induce expression. The expression-induced cultures were incubated for 18 hours at 25 °C with shaking at 180 rpm. For expression of the *A. baumannii* Dat induced cultures were incubated for 3 hours at 37 °C. Following incubation, another 100 µl aliquot was taken and frozen. Cultures were then centrifuged at 3200 x g for 40 minutes at 20 °C and pellets were frozen at -20 °C.

2.20.2.2 Larger scale expression

Larger scale expression was carried out once the optimum conditions were determined. 10 ml of stationary phase *E. coli* BL21 culture was inoculated into 1 litre of fresh LB broth. Growth and induction were carried out in the same manner as small-scale expression.

2.20.3 Protein extraction and SDS-PAGE

2.20.3.1 Extraction following small-scale expression

Frozen pellets were thawed at room temperature and resuspended in 2.5-5 ml BugBuster Master Mix (Sigma). The cell suspensions were placed on an MX-T6S tube roller (DLAB) at 4 °C to allow for sufficient lysis. Following, incubation lysates were centrifuged at 17,000 x g for 45 minutes. The supernatant and pellets were collected for downstream application.

2.20.3.2 Extraction following large-scale expression

Following the scale-up of expression, the protein extraction method varied. Pellets of centrifuged cells were resuspended in an appropriate volume of PBS. 10 mg/ml Lysozyme solution was prepared with Tris-PEG buffer. Lysozyme solution was added to the suspension at a final concentration of 1 mg/ml and incubated at room temperature. Following incubation, suspensions were sonicated at 16.2 amplitude for 6 cycles. Following lysis, samples were centrifuged at 17, 000 x g for 45 minutes at 4 °C.

2.20.3.3 SDS-PAGE

10x SDS running buffer was prepared by dissolving 30 g Tris base (Sigma), 144 g glycine (Sigma) and 10 g of SDS (Sigma) in 1 Litre of H_2O. A 1x working stock was made by combining 100 ml of 10X stock in 1 Litre of H_2O. 30 µl of prepared sample was combined with 10 µl of laemmli buffer (Bio-Rad) and heated at 95 °C for 5 minutes. 15 µl of each sample were loaded into Mini-PROTEAN TGX Gel (Bio-Rad), alongside 5 µl of Dual colour Precision Plus Protein™ standards (Bio-Rad). Electrophoresis was carried out at 180 volts for 40 minutes. Following electrophoresis, gels were stained with Quick Coomassie stain (Protein Ark limited). Staining was carried out overnight, with gentle shaking. Gels were imaged and the migrated distance of the proteins and dye fronts was measured, and the retardation factor (Rf) was calculated. The same was done for the molecular weight ladders, and a standard curve was generated. From this, the molecular weight of the protein of interest was determined.

2.20.4 Purification of HIS-tagged proteins

2 ml of HisPur cobalt resin (Thermo Scientific) was dispensed into an affinity column. The resin was washed with 6 ml of MilliQ H_2O and repeated with PBS. Following this, the samples for purification were loaded onto the column and allowed to flow through with this being collected in a clean falcon tube. 6 ml of 0.1 mM imidazole was loaded onto the resin and the flowthrough was again collected. This step was carried out a total of three times. Following this, 6 ml of 0.5 mM imidazole was added to the column to elute bound protein, with three washes being carried out, as previously. All collected flowthrough was placed on ice immediately. For the purification of Dat from *K. pneumoniae* samples were put through a Ni-NTA affinity chromatography column, according to the manufacturer's instruction. Protein was eluted in the same 0.5 mM imidazole. Following elution, dialysis was carried out to remove residual buffer components. The protein suspension was aliquoted into a dialysis bag (Thermofisher). The dialysis bag was immersed in 500 ml sterile H_2O, in a glass beaker. The contents of the beaker were stirred overnight at 4 °C. Following incubation, the contents of the dialysis bag were transferred to a fresh falcon tube. The concentration and purity of the treated protein were determined by nanodrop. The *K. pneumoniae* Ddc protein was further purified by size exclusion chromatography. The eluted dialysed protein was added to the concentration column. The column was centrifuged at 4000 x g at 4 °C for 5 minutes. The protein was resuspended and added to the equilibrated SEC column and allowed to run for 1 hour.

2.21 Analysis of protein: protein interactions with Bacterial two-hybrid system

2.21.1 Creation of BACTH vectors

2.21.1.1 Primer design for cloning polyamine synthesis genes into BACTH vectors

Forward primers were designed to be complementary to the first 20 base pairs of the target gene (Table 2.3). An overhang complementary to the pUT18C and pKT25 vectors was added to the 5' end which included 5 base pairs toward the 5' end of the primer sequence followed by an XbaI restriction site sequence, followed by a single base at the 3' end (Table 2.3). Reverse primers were designed to be complementary to the last 20 base pairs of the target gene, including the stop codon (Table 2.3). An overhang complementary to the pUT18C vector was added to the 5' end, which included 4 base pairs toward the 5' end of the primer sequence, followed by a KpnI restriction site sequence and then two base pairs at the 3' end (Table 2.3). The overhang sequences were designed to ensure the gene sequence remained in frame with the T18/T25 fragments of pUT18C and pKT25, respectively. The additional bases of the reverse primer were complementary to the pKT25 plasmid only, as this sequence is only required to maintain the reading frame and to allow efficient binding for the KpnI restriction enzyme.

2.21.1.2 Amplification of gene sequences

Amplification used gDNA from wild type *K. pneumoniae* and *A. baumannii*, relevant primer pairs (Table 2.3) and the standard Phusion polymerase protocol (Section 2.4.3). DNA fragments were separated by Gel electrophoresis (Section 2.4.4). DNA was excised from the agarose gel and purified (Section 2.4.5).

2.21.1.3 Insertion of sequences and transformation into *E. coli* DH5α

Restriction digests with XbaI and KpnI were carried out on the purified PCR products, and the pUT18C and pKT25 vectors (Section 2.4.8.1). Following digestion of pUT18C and pKT25 linearised plasmid DNA was separated by gel electrophoresis (Section 2.4.4). DNA bands were excised from the agarose gel and purified (Section 2.4.5). Digested PCR products were purified (Section 2.4.6). DNA concentration was quantified using Nanodrop 1000 (Section 2.4.7). DNA fragments were ligated into pUT18C and pKT25 vectors (Section 2.4.9). The total reaction mixture underwent heat shock transformation into $CaCl_2$ chemically competent *E. coli* DH5α (Section 2.4.11). 1 µl of empty pUT18C and pKT25 were transformed as controls.

2.21.1.4 Analysis of BACTH interactions

To analyse bacterial-two interactions each strain was inoculated, from glycerol stock, into 5 ml of LB broth supplemented with 50 µg/ml carbenicillin and 25 µg/ml kanamycin in a 30 ml sterile plastic universal and incubated at 29 °C for 18 hours. Following incubation, 5 µl of each strain was spotted onto nutrient agar supplemented with 40 µg/ml X-gal (Novagen), 50 µg/ml carbenicillin and 25 µg/ml kanamycin and incubated at 29 °C for 48 hours, with images taken of agar plates every 24 hours. *E. coli* BTH101 containing pUT18C and pKT25 empty vectors and the vectors encoding the isoleucine zippers were used as negative and positive controls, respectively.

2.21.2 Measurement of protein interaction by ONPG β-galactosidase assay

2.21.2.1 Preparation of reagents

2.21.2.1.1 Z-buffer

8.348 g/l Na_2HPO_4 (anhydrous) (Sigma), 5.6 g/l $NaH_2PO_4.H_2O$ (Sigma), 5 ml/l 2 M KCl (Sigma), 1 ml/l 1 M $MgSO_4$. The solution was altered to pH 7 using 2 M NaOH. Z-buffer was sterilised by filtration through a 0.22 µM filter and stored

at 4 °C until required. Before use, the Z-buffer was supplemented with 2.7 ml/l β-mercaptoethanol (Sigma).

2.21.2.1.2 0.1M Phosphate buffer

8.5 g/l Na_2HPO_4 (anhydrous), 5.50 g/l $NaH_2PO_4.H_2O$. Volume was adjusted to 1 L. pH was adjusted to 7.0 using 2 M NaOH and was sterilised by filtration through a 0.22 µM filter.

2.21.2.1.3 4 mg/ml ONPG solution

4 mg/ml ONPG (Sigma) dissolved in 0.1 M phosphate buffer (pH 7), sterilised by filtration through a 0.22 µM filter. ONPG solution was made fresh daily.

2.21.2.1.4 0.1 % (w/v) SDS solution

100 mg of SDS pellets was dissolved in 100 ml MilliQ H_2O

2.21.2.2 Preparation of bacterial cultures

Single colonies of *E. coli* BTH101 co-transformed with different combinations of pUT18C and pKT25 encoding enzymes of the 1, 3-diaminopropane synthesis pathway were inoculated into 5 ml sterile LB broth supplemented with 50 µg/ml carbenicillin and 25 µg/ml kanamycin in a sterile 5 ml plastic universal tube and incubated at 29 °C with shaking at 200 rpm for 16 hours. *E. coli* BTH101 transformed with pUT18C-Zip and pKT25-Zip encoding leucine zippers as positive controls. *E. coli* BTH101, containing the empty pUT18C and pKT25 vectors, were used as the negative control.

2.21.2.3 ONPG assay

BACTH interaction was further assessed using the ONPG β-galactosidase activity assay (Miller, 1972). Following incubation, 1 ml of stationary phase culture of each strain was transferred to a new sterile 15 ml plastic tube. Cultures were centrifuged at 4400 x g at 4 °C. Following centrifugation, supernatants were discarded and pellets were resuspended in 2 ml of Z-buffer supplemented with β-mercaptoethanol. 0.5 ml of each cell suspension was

diluted in 0.5 ml of Z-buffer. Cells were permeabilised with the addition of 100 µl of 0.1 % (w/v) SDS solution and 100 µl of chloroform. Reaction mixtures were vigorously mixed and incubated at 29 °C with shaking at 200 rpm for 20 minutes. The optical density at 600 nm of the remaining 1.5 ml cell suspension was measured. 0.2 ml ONPG solution was added to each reaction mixture and the time of addition was recorded. Following addition, reactions were incubated at 29 °C with shaking at 200 rpm and following sufficient colour development reactions were quenched with 0.5 ml 0.1 M Na_2CO_3. The exact time of quenching was recorded. After the reactions were complete 1.2 ml was transferred to a microfuge tube and centrifuged at 16,000 x g for 1 minute to pellet cell debris and separate the chloroform present. 1 ml of the reaction mixture was transferred to a plastic cuvette and the optical density was measured at 420 nm and 550 nm. Where relevant samples were diluted 1:10 in a Z-buffer to allow accurate optical density measurement. The enzymatic activity of β-galactosidase is presented as Miller units and was calculated using Equation 2.1, OD_{420} is the optical density measurements of o-nitrophenol at 420 nm, following quenching. OD_{550} is the optical density measurement from cell debris, when multiplied by 1.75 approximates the scatter observed at $OD_{420.}$ T is the time of reaction in minutes. V is the volume of cell suspension used in the assay present in ml. OD_{600} is the optical density measurement of washed cell suspension. Experiments were carried out as three independent replicates.

Equation 2.1. Miller equation

$$\text{Miller Units} = 1000 \times [(\text{OD420} - 1.75 \times \text{OD550})] \div (\text{T} \times \text{V} \times \text{OD600})$$

2.22 Statistical analysis

All raw data was processed using Microsoft Excel or GraphPad Prism version 9/10 for Windows 10. All statistical analysis was carried out using GraphPad Prism 9/10. Where appropriate data was tested for normality. The relevant

tests were selected depending on the distribution. T-tests and Mann-Whitney U tests were used for normally, and non-normally distributed non-parametric datasets, respectively. Kaplan Meier survival curves were analysed using the Logrank (Mantel-Cox), and Gehan-Breslow-Wilcoxon tests.

Chapter 3 Role of 1, 3-diaminopropane in *Acinetobacter baumannii*

3.1 Chapter introduction

The diamine, 1, 3-diaminopropane, is the major polyamine of the *Acinetobacter* genus (Hamana and Matsuzaki, 1992). In *A. baumannii* it has been established that 1, 3-diaminopropane is essential for the surface-associated motility of and loss of synthesis attenuates virulence and decreases biofilm formation (Blaschke et al., 2021; Skiebe et al., 2012). This was the first instance polyamine synthesis had been implicated in the virulence of *A. baumannii*. More recently 1, 3-diaminopropane is required for the synthesis of the hydroxamate siderophores, Baumannoferrin A and B (Penwell et al., 2015). These findings support the belief that the synthesis of 1, 3-diaminopropane, in *A. baumannii*, could be a viable target for therapeutic development. In addition to this 1, 3-diaminopropane is not actively synthesised by humans. Therefore, this would possibly rule out any off-target effects caused by the use of a therapeutic targeting the L-2, 4-diaminobutyrate:2-ketoglutarate 4-aminotransferase and L-2, 4-diaminobutyrate decarboxylase enzymes, a problem that would potentially be encountered targeting pathways that are conserved in humans.

3.2 Research aims

- To generate markerless deletions of the *dat* and *ddc* genes in *Acinetobacter baumannii* 17978 and investigate and confirm previously described phenotypes of *dat* and *ddc* deletion.
- Further characterise the phenotypes of the deletion strains to expand the understanding of the role 1, 3-diaminopropane has in *A. baumannii.*
- To chemically complement observed phenotypes.
- Determine the conservation of Dat and Ddc across other species.

3.3 Chapter results

3.3.1 The genomic location, size, and structure of 1, 3-diaminopropane synthesis genes in *A. baumannii* 17978

Sequencing and annotation of the *A. baumannii* 17978 genome (Smith et al., 2007) identified the *dat* gene (A1S_2454) is 1374 bp in length and encodes the pyridoxal 5 phosphate (PLP) dependent L-2, 4-diaminobutyrate: 2-ketoglutarate aminotransferase. The annotated *ddc* gene (A1S_2453) is 1533 bp in length and encodes the PLP-dependent L-2, 4-diaminobutyrate decarboxylase. The upstream gene A1S_2455 encodes a Putative signal peptide. The downstream gene A1S_2452 encodes an NAD-dependent aldehyde dehydrogenase.

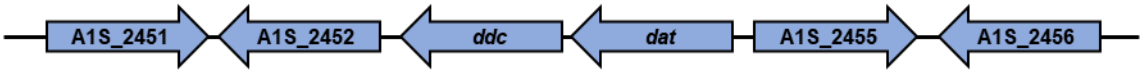

Figure 3.1. The genomic organisation of the *dat* and *ddc* genes. 7.3 Kbp region of the *A. baumannii* 17978 reference genome showing the location of the *dat* and *ddc* genes and the upstream and downstream genes within the region.

3.3.2 Expression of 1, 3-diaminopropane synthesis genes

3.3.2.1 Expression of the *dat* and *ddc* genes

The connection between 1, 3-diaminopropane synthesis disruption and loss of motility (Blaschke et al., 2021; Skiebe et al., 2012) suggests it is highly likely the *dat* and *ddc* genes of the *A. baumannii* 17978 are expressed. To confirm this RT-PCR was carried out on total RNA extracted from exponentially growing *A. baumannii* 17978. Primers were designed to amplify 139 bp and 154 bp products for the *dat* and *ddc* genes, respectively (Figure 3.2A). The *rpoB* gene was used as an RT-PCR positive expression control, and primers for *rpoB* were designed to amplify a 146 bp product. RT-PCR produced the expected 139 bp and 154 bp products for the *dat* and *ddc* genes, respectively (Figure 3.2B). This confirms the expression of each gene in *A. baumannii* 17978 during exponential growth in LB broth. RT-PCR of RNA extracted from the Δ*ddc* mutant, resulted

in the absence of product for the *ddc* gene, confirming the deletion of *ddc* completely removes expression. The *dat* gene was also expressed in the Δ*ddc* mutant strain, and the wild type and deletion strain showed the expected expression of the *rpoB* gene.

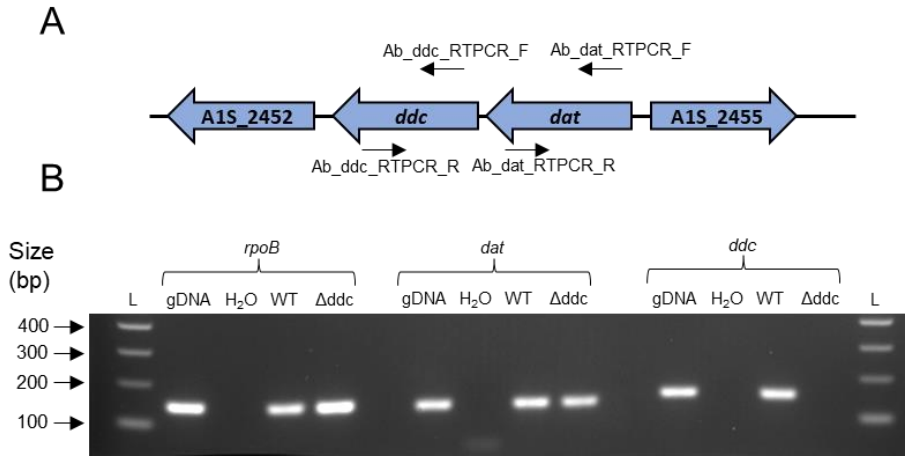

Figure 3.2. The *dat* and *ddc* genes of *A. baumannii* 17978 are expressed during exponential growth. (A) Diagram of the predicted amplification within the *dat* and *ddc* genes of *A. baumannii* 17978, indicating the primer pair used and annealing sites. **(B)** Reverse transcriptase PCR was performed on RNA isolated from exponentially growing *A. baumannii* 17978 wild type and Δ*ddc* strains. Primers internally amplified the *rpoB*, *dat,* and *ddc* genes. The Ab_rpoB_RTPCR_F and Ab_rpoB_RTPCR_R pair were used for the *rpoB* gene amplifying a product of 146 bp. The Ab_dat_RTPCR_F and Ab_dat_RTPCR_R pair were used for the *dat* gene amplifying a product of 139 bp. The Ab_ddc_RTPCR_F and Ab_ddc_RTPCR_R pair were used for the *ddc* gene amplifying a product of 154 bp. L: 100 bp ladder. gDNA: Wild type DNA positive control. H_2O: negative control. WT: RNA extracted from wild type strain. Δ*ddc:* RNA extracted from Δ*ddc* strain. RT-PCR is representative of two independent repeats.

3.3.2.2 Co-transcription of the *dat* and *ddc* genes

The *dat* and *ddc* genes of *A. baumannii* 17978 are located together, with two base pairs separating each ORF. It was previously reported there is a lack of a discernible terminator sequence found within the 5' end of the *dat* gene (Ikai and Yamamoto, 1997). This evidence suggests that both genes are expressed as a single transcriptional unit.

3.3.2.2.1 Identification of possible terminator sequences

To begin investigating the transcriptional units of the *dat* and *ddc* genes transcriptional terminators were predicted within the *A. baumannii* 17978 UN

genome sequence. This used TransTermHP and RhoTermPredict that predict Rho-independent and dependent terminators, respectively. Neither predicted a terminator sequence following the *dat* ORF. TransTermHP predicted a possible intrinsic terminator following *ddc* (Figure 3.3). Therefore, it is probable that both genes are expressed as a single transcriptional unit, being expressed from a single promoter upstream of the *dat* gene.

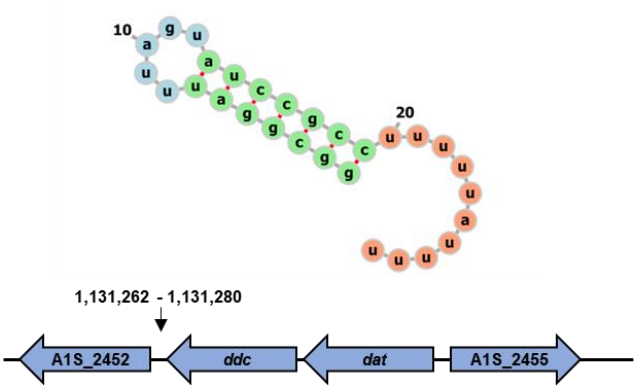

Figure 3.3. The *dat* ORF of *A. baumannii* 17978 does not have a dedicated intrinsic terminator. The predicted intrinsic terminator sequence for the *dat* and *ddc* ORF within the *A. baumannii* 17978 reference genome and the predicted RNA secondary structure formed by the predicted sequence. Intrinsic terminators were predicted TransTermHP and RNA secondary structure predicted with MXfold2 webserver.

3.3.2.2.2 Co-transcription of the *dat* and *ddc* genes

To assess whether *dat* and *ddc* in *A. baumannii* 17978 are co-expressed, primers were designed to amplify across the intergenic gap between the two genes, generating a 424 bp product if both genes were transcribed as a bicistronic mRNA transcript (Figure 3.4A). RT-PCR of total RNA extracted from *A. baumannii* 17978 generated the expected 424 bp product (Figure 3.4B). This shows that *dat* and *ddc* in *A. baumannii* 17978 are expressed as a single transcriptional unit.

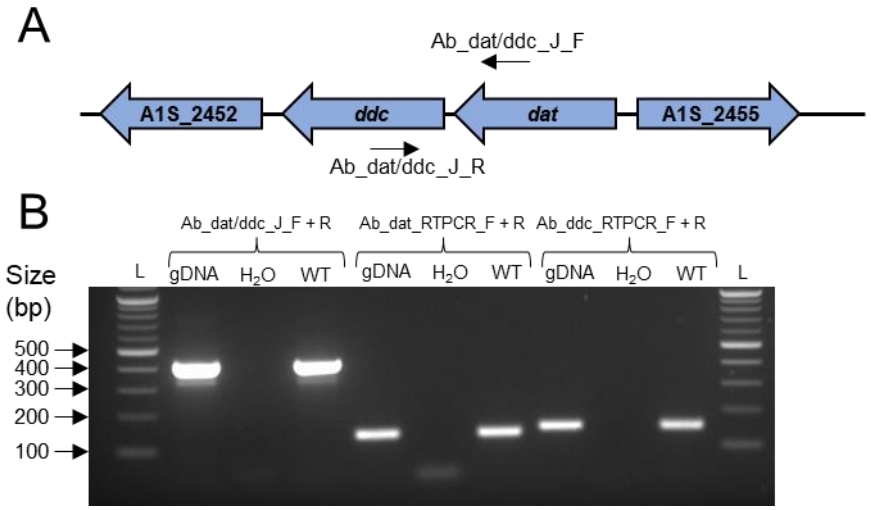

Figure 3.4. The *dat* and *ddc* genes are co-expressed in *A. baumannii* 17978.
(A) Diagram of the predicted amplification across the intergenic region between the *dat* and *ddc* genes of *A. baumannii* 17978, indicating the primer pair used and their annealing site. **(B)** Reverse transcriptase PCR performed on RNA isolated from exponentially growing *A. baumannii* 17978 wild type, using Ab_dat/ddc_J_F and Ab_dat/ddc_J_R primer pair to amplify across the intergenic region between *dat* and *ddc* genes with the expected amplified product being 424 bp. Additional RT-PCR was carried out with Ab_dat_RTPCR_F and Ab_dat_RTPCR_R pair, amplifying a product of 139 bp, and Ab_ddc_RTPCR_F and Ab_ddc_RTPCR_R pair, amplifying a product of 154 bp, to confirm the expression of the *dat* and *ddc* genes, respectively. L: 100 bp ladder. gDNA: Wild type genomic DNA positive control. H_2O: negative nucleic acid control. WT: RNA extracted from wild type strain. RT-PCR is representative of two independent repeats.

3.3.3 Deletion of 1, 3-diaminopropane synthesis genes in *A. baumannii* 17978

1, 3-diaminopropane has been identified as the only polyamine to be synthesised by *A. baumannii* (Hamana and Matsuzaki, 1992). Previously, Skiebe et al (2012) disrupted the *dat* and *ddc* synthesis genes through transposon mutagenesis. To further investigate the role of 1, 3-diaminopropane and complement the investigation of enzyme 3D structure and search for novel inhibitors markerless deletion of the *dat* and *ddc* genes was attempted.

3.3.3.1 Construction and confirmation of *A. baumannii* 1, 3-diaminopropane synthesis deletion vectors and *E. coli* donor strains

For deletion of the *dat* and *ddc* genes deletion constructs were made by amplifying the regions upstream and downstream of the gene to be deleted,

with the amplified products being joined together and inserted into the final pGPI-SceI-2 suicide vectors.

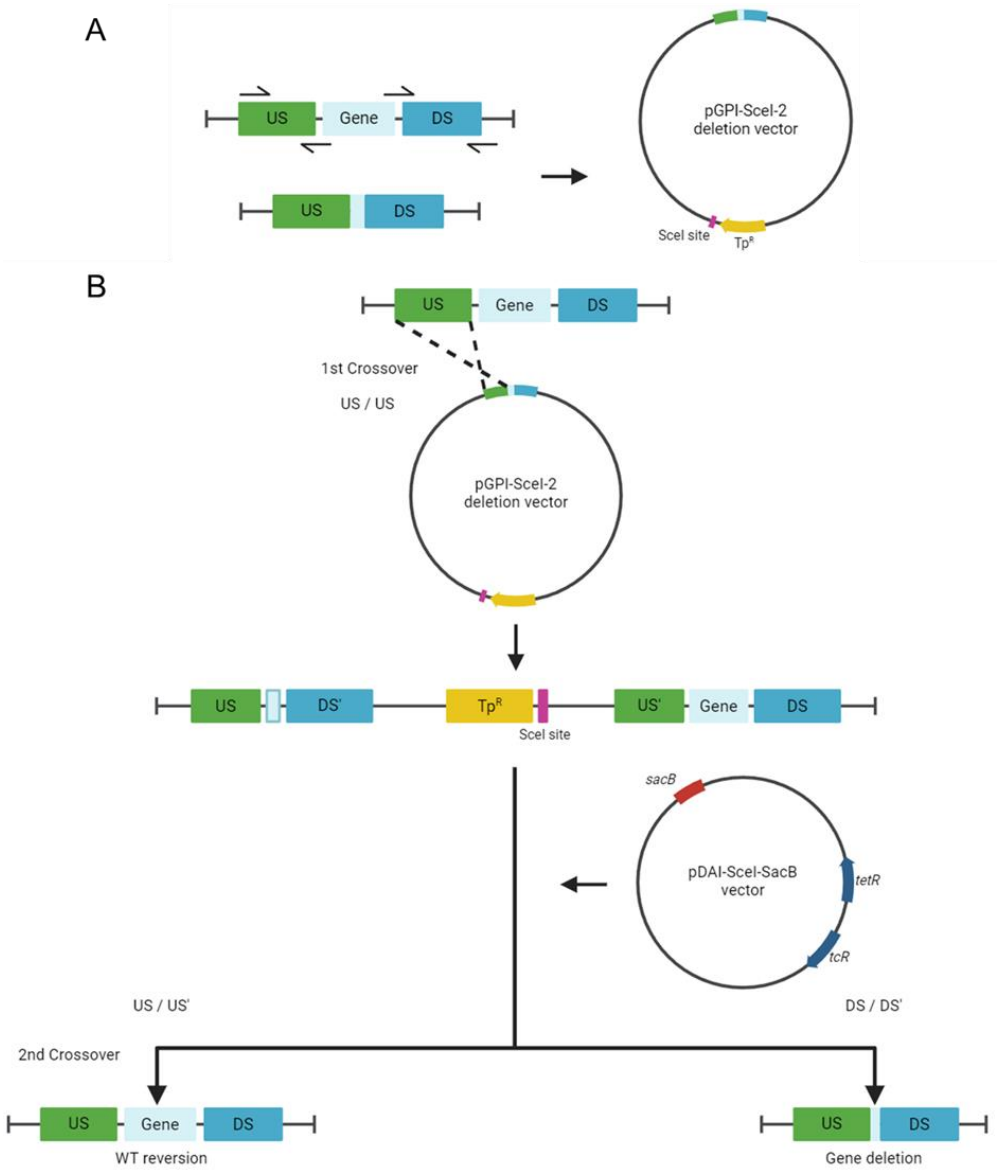

Figure 3.5. Overview of generating markerless gene deletions. (A) up to 1 Kbp upstream (US) and downstream (DS) of the gene to be deleted is amplified and cloned into the pGPI-SceI-2 suicide vector. **(B)** The pGPI-SceI-2 deletion vectors are conjugated into recipient strains. Being unable to replicate pGPI-SceI-2 incorporates into the chromosome (1st crossover event). The upstream/upstream (US/US') event is depicted but can also occur in the downstream region (DS/DS'). The pDAI-SceI-SacB vector is conjugated into exconjugants. The SceI endonuclease targets the SceI site in the pGPI-SceI-2 backbone inducing a double-strand break and 2nd crossover event. If this occurs in the same region as the previous event there is a reversion to wild type genotype. If this occurs in the opposite region, in this case, DS/DS', then the gene of interest is deleted. Figure made with Biorender and based on that of Aubert et al (2014).

Before conjugations, vectors were introduced into *E. coli* β2163 with heat shock transformation. The presence of suicide vectors was confirmed by PCR of the vectors purified from *E. coli* β2163. Two pGPI-SceI-Δ*datddc*, pGPI-SceI-Δ*dat,* and pGPI-SceI-Δ*ddc* vectors were selected for confirmation. PCR amplified the full deletion constructs, in all vectors, using the Ab_datddc_UpF1 and Ab_datddc_DwnR1 primer pair (Figure 3.6A). The Ab_datddc_UpF1 and Ab_datddc_UpR1 primer pair were used to amplify the upstream fragment of pGPI-SceI-Δ*datddc* and pGPI-SceI-Δ*dat* (Figure 3.6A). The Ab_datddc_DwnF1 and Ab_datddc_DwnR1 pair were used to amplify the downstream fragment of pGPI-SceI-Δ*datddc and* pGPI-SceI-Δ*ddc* (Figure 3.6A). The downstream fragment of pGPI-SceI-Δ*dat* and the upstream of pGPI-SceI-Δ*ddc* were amplified with the Ab_datddc_DwnF2 and Ab_datddc_DwnR1 and Ab_datddc_UpF1 and Ab_datddc_UpR2, respectively, (Figure 3.6A). All vectors analysed were positive for the correct insertion of the deletion constructs. The pGPI-SceI-Δ*datddc* produced amplicons of 1.7 Kbp for the full construct, 0.8 Kbp for the upstream fragment and 0.9 Kbp for the downstream fragment (Figure 3.6B). The pGPI-SceI-Δ*dat* produced amplicons of 3.2 Kbp for the full construct, 0.8 Kbp for the upstream fragment and 2.4 Kbp for the downstream (Figure 3.6B). The pGPI-SceI-Δ*ddc* produced amplicons of 3 Kbp for the full construct, 2.1 Kbp for the upstream and 0.9 Kbp for the downstream (Figure 3.6B).

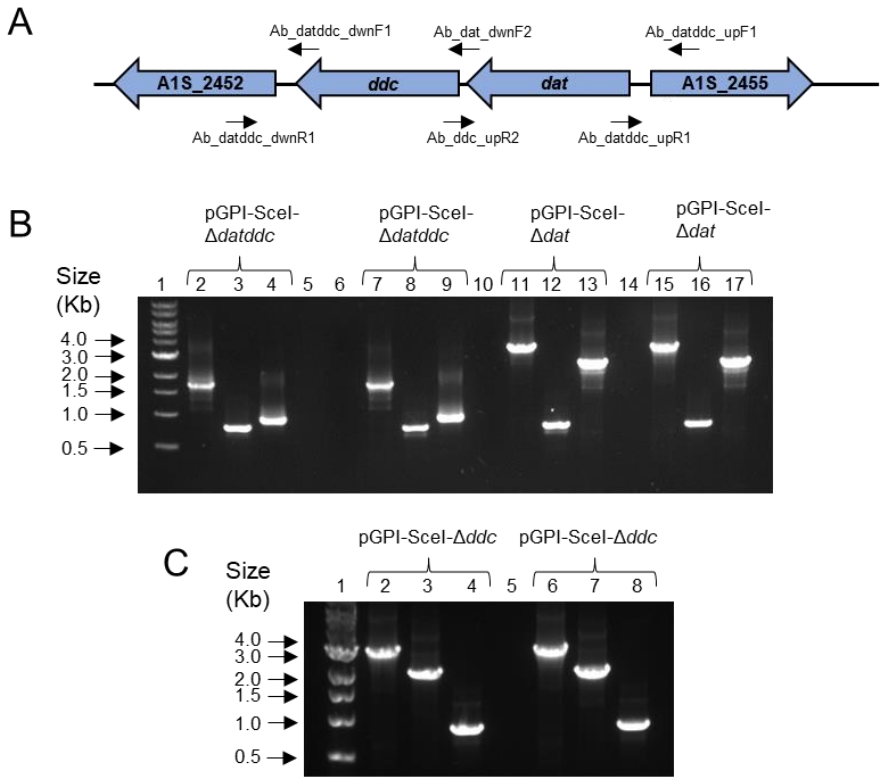

Figure 3.6. Confirmation of vectors for the deletion *dat* and *ddc* in *A. baumannii* 17978. (A) Diagram of the predicted amplification of the full deletion constructs and their constituent upstream and downstream fragments. The Ab_datddc_UpF1 and Ab_datddc_UpR1 primer pair were used to amplify the upstream fragment of pGPI-SceI-Δ*datddc* and pGPI-SceI-Δ*dat*. The Ab_datddc_DwnF1 and Ab_datddc_DwnR1 pair were used to amplify the downstream fragment of pGPI-SceI-Δdatddc and pGPI-SceI-Δ*ddc*. The downstream fragment of pGPI-SceI-Δ*dat* and the upstream of pGPI-SceI-Δ*ddc* were amplified with the Ab_datddc_DwnF2 and Ab_datddc_DwnR1 and Ab_datddc_UpF1 and Ab_datddc_UpR2, respectively. **(B)** PCR confirmation of two separate pGPI-SceI-Δ*datddc* and pGPI-SceI-Δ*dat* vectors for the double deletion of the dat and ddc genes and single deletion of the dat gene in *A. baumannii* 17978. Lane 1: 1 Kbp ladder. Lane 2/7: Amplification of the full Δ*datddc* construct. Lane 3/8: Amplification of the up-fragment portion of the Δ*datddc* construct. Lane 4/9: Amplification of the down fragment portion of the Δ*datddc* construct. Lane: 11/15: Amplification of the Δ*dat* full construct. Lane 12/16: Amplification of the up fragment portion of the Δ*dat* construct. Lane 13/17: Amplification of the down fragment portion Δ*dat* construct. **(C)** PCR confirmation of two separate pGPI-SceI-Δ*ddc* vectors for deletion of the *ddc* gene in A*. baumannii* 17978 Lane 1: 1Kbp ladder. Lane 2/6: Amplification of the full Δ*ddc* construct. Lane 3/7: Amplification of the up-fragment portion of the Δ*ddc* construct. Lane 4/8: Amplification of the down fragment portion of the Δ*ddc* construct.

3.3.3.2 Confirmation of Δ*ddc* deletion in *A. baumannii* 17978

Following conjugations presumptive gene deletions were screened for trimethoprim susceptibility and then confirmed by PCR, using the

Ab_datddc_outF and Ab_datddc_outR primer pair, that bind outside of the deletion region amplifying inwards toward the deleted gene (Figure 3.7A). Amplification of the *dat* and *ddc* loci from wild type genomic DNA results in a product of 4.8 Kbp (Figure 3.7B). pGPI-SceI-Δ*ddc* vectors produced several nonspecific products. Amplification of the same loci in the Δ*ddc* produced a product of 3.2 Kbp (Figure 3.7B). This confirms the successful deletion of the *ddc* gene. Sanger sequencing (Section 2.5.1) confirmed the deletion of the *ddc* gene. In addition, the Δ*ddc* strain underwent WGS (Section 2.5.3). This showed a complete absence of the *ddc* gene, thus confirming the Δ*ddc* mutant. Successful deletion of the *ddc* gene indicates that 1, 3-diaminopropane is not essential for *A. baumannii* 17978 growth in agreement with the findings of Skiebe et al (2012).

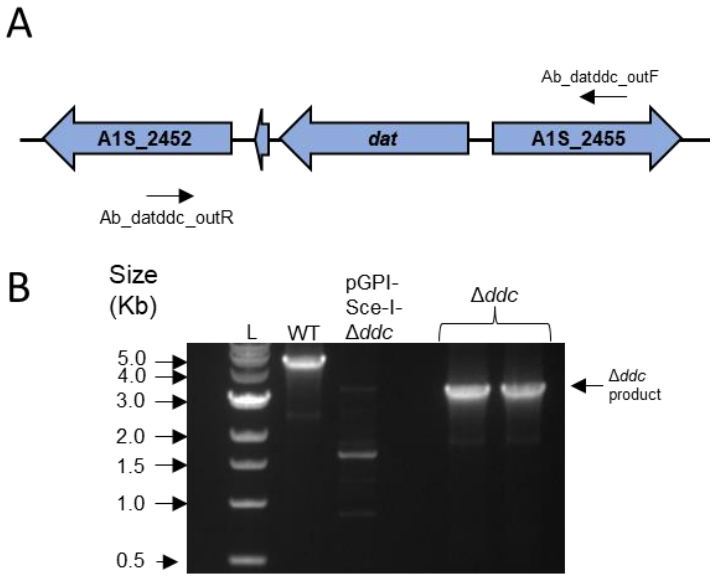

Figure 3.7. Confirmation of the deletion of the *ddc* gene of *A. baumannii* 17978. (A) Diagram of the predicted amplification across the chromosomal region containing the *dat* and *ddc* genes showing the primers used to confirm the deletion of the *ddc* gene. **(B)** PCR screen and subsequent gel electrophoresis confirming the successful deletion of the *ddc* gene of *A. baumannii* 17978, with the Ab_datddc_outF and R primer pair, indicated by the amplified 3.2 Kbp product compared to the 4.8 Kbp product from the wild type strain. L: 1 Kbp ladder. WT: Genomic DNA extracted from *A. baumannii* 17978 wild type strain. pGPI-SceI-Δ*ddc*: Purified suicide vector DNA used for the deletion of the ddc gene. Δ*ddc*: Genomic DNA extracted from presumptive *A. baumannii* Δ*ddc* strains.

3.3.3.3 Point mutations present in the Δ*ddc* deletion strain

Sequencing revealed the presence of point mutations within the deletion region of the Δ*ddc* strain and WGS confirmed this. Sequencing of the Δ*ddc* strain and comparison to the reference genome (GenBank Accession: CP079931.1) shows Eighteen SNPs in the Δ*ddc* genome, four were shared with the wild type. Of the remaining fourteen, ten are found within ORFs with the remaining four occurring in intergenic regions. Of particular importance are mutations that have arisen from *ddc* deletion. There was one mutation possibly arising from this deletion. This is a synonymous mutation located in the *dat* gene. This being a synonymous mutation poses no concern. Analysis of the effects of the additional mutations, with Missense3D, revealed that only two are predicted to cause structural damage to the 3D protein structure. The first occurs in KZA74_04045, an ORF predicted to encode a putative Na+/H+ antiporter. The mutation results in the replacement of a buried hydrophobic leucine with hydrophilic charged histidine (Table 3.1). The second occurs in KZA74_08790, encoding Acyl-CoA dehydrogenase (Table 3.1). S414A results in a significant loss of hydrogen bonding by the buried serine residue resulting in possible structural damage (Table 3.1). As for the impact on the cell Na+/H+ antiporters commonly play a role in pH and sodium homeostasis and contribute to growth in alkaline and high-salinity environments (Patiño-Ruiz et al., 2022) suggesting this mutation may impact bacterial fitness under certain conditions. Acyl-CoA dehydrogenases are involved in fatty acid catabolism, suggesting this mutation may impact β-oxidation (Swigoňová et al., 2009). Neither of these phenotypes was assessed as part of this study as they are beyond the scope of the work conducted. Therefore, further investigation is needed to understand their impact. The chemical complementation presented later in this investigation suggests that these mutations do not contribute to the phenotypes observed in the Δ*ddc* strain.

Table 3.1. SNPS unique to *A. baumannii* 17978 UN Δ*ddc* strain

Nucleotide position	Allele in 17978UN reference genome (amino acid residue)	Allele in Δ*ddc* (amino acid residue)	Gene	Description	Possible effect on the structure of the protein
140188	T	A	Intergenic	Downstream of *parE* (KZA74_00630), encoding DNA topoisomerase IV subunit B, and upstream of KZA74_00635 a gene predicted to encode ureidoglycolate lyase	
160424	G (E184)	A (K184)	KZA74_00740 (*gshB*)	glutathione synthase	E184K disrupts the H-bonding with G180 and E188, while the interaction with L189 is still maintained
301093	A (V163)	G (A163)	KZA74_01435	hypothetical protein	
836703	T (L249)	A (H249)	KZA74_04045	cation:proton antiporter	Maintains H-bonds with T245 and A253. Possible structural damage due to replacing buried hydrophobic/uncharged residue with a buried/charged/hydrophilic residue.
1042197	T	G	Intergenic	Downstream of *tmk* (KZA74_04935) encoding dTMP kinase and upstream of KZA74_04940 predicted to encode PaaI family thioesterase	
1127683	T (L351)	C (L351)	KZA74_05330	L-2, 4-diaminobuyrate: 2-ketoglutarate aminotransferase	Synonymous mutation

1456831	G	A	Intergenic	Downstream of KZA74_06830, predicted to encode type 1 glutamine amidotransferase domain-containing protein and upstream *prfA* (KZA74_06835) encoding peptide chain release factor 1	
1850938	T (S414)	G (A414)	KZA74_08790	acyl-CoA dehydrogenase	S414A results in loss of H-bond with V410 in Acyl-CoA dehydrogenase resulting in possible structural damage
2213388	T (N2)	A (Y2)	KZA74_10625	phosphotransferase	N2Y results in the loss of H-bond with Q4. No predicted structural damage
2213439	A	T	Intergenic	Upstream of KZA74_10625, predicted to encode a phosphotransferase and upstream of KZA74_10630, predicted to encode LPS-assembly protein LptD	
2737088	A (Y118)	C (Stop codon)	KZA74_13160	DUF4265 domain-containing protein	Nonsense mutation
2775143	G (A20)	T (E20)	KZA74_13285	putative Ig domain-containing protein	
2911996	G (G465)	A (G465)	KZA74_13900	aldehyde dehydrogenase	Synonymous mutation
2986892	T (Q396)	A (H396)	KZA74_14255	phosphomannomutase/phosphoglucomutase	No predicted structural damage

3.3.4 Identification of potential genotype variants of *A. baumannii* 17978

The presence of two variants of *A. baumannii* ATCC 17978 with distinct genotypes and phenotypes was first reported in 2021 (Wijers et al., 2021). The variants are referred to as 17978 UN or VU. The major difference between the two is that the UN variant contains a 44-Kbp accessory locus referred to as AbaAL44 (Figure 3.8). Several genes of AbaAL44 are predicted to enhance the pathogenesis of the UN variant most notably *smf-1*, *yadV*, *htrE* and *mrkD*, which are predicted to encode components related to type-1 pilus or fimbriae; KZA74_09300, which is a putative catalase; and *clsC2*, which is a putative cardiolipin synthase.

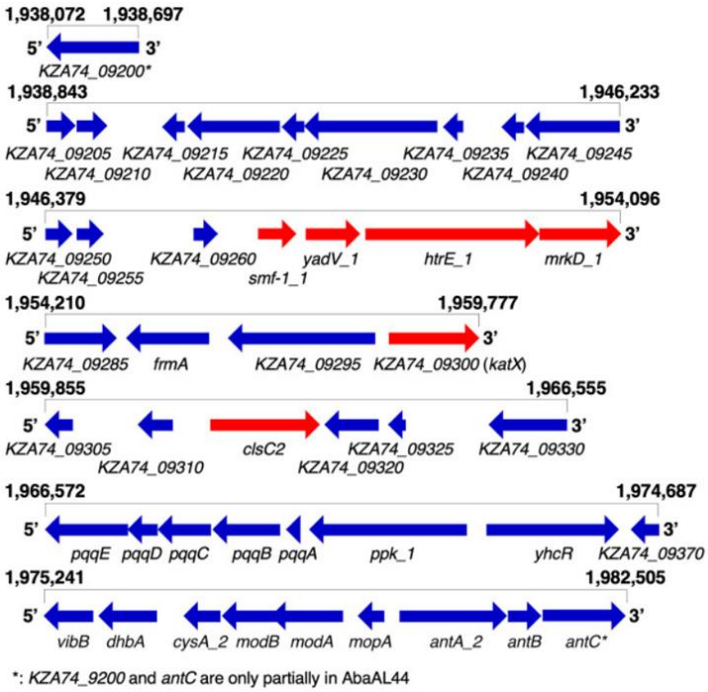

Figure 3.8. The AbaAL44 accessory locus. Genes present within the AbaAL44 accessory locus in the *A. baumannii* 17978 (UN) reference genome (CP079931). Relative position in the genome (base pairs) is indicated above each row. Locus tags refer to CP079931. Arrows: transcriptional direction. Red genes: putative virulence genes. Figure adapted from Wijers et al (2021).

To screen for the UN/VU genotypes in our laboratory strain collection Eric Skaar (Vanderbilt University; pers. comm.) provided sequences for the UN/VU screening primers. The UN primers anneal within the *clsC2* gene sequence,

unique to AbaAL44. The presence of a 2347 bp product is used to confirm the UN or VU genotype variants, respectively. The VU primers amplify across the junction of the 44-Kbp Island insert. In the VU genotype, this generates a 483 bp product. There is an absence of a product in the UN variant. It was hypothesised that the 17978 strain within the laboratory strain collection would be of one genotype as stocks were previously made from a streak-purified single colony. Colony PCR was carried out to screen for variants. 58 colonies were selected and then purified through restreaking and all were screened with primer pairs (Table 2.3). All 58 were found to be of the UN genotype (Figure 3.9A and B). This suggests that the entire collection of *A. baumannii* 17978 in the laboratory strain collection is of the UN genotype or that the population is mixed. The VU variant could be present at a far lower frequency than the UN, a result previously seen by Wijers et al. (2021). For all subsequent work after this, the wild type strain was taken from one of these purified isolates that were glycerol stocked and used as the laboratory wild type. Once the wild type strain genotype was established the next step was to determine the background genotype Δ*ddc* strain was derived from. Colony PCR established that the Δ*ddc* was derived from the UN variant (Figure 3.9C and D). The *A. baumannii* 17978 UN strain and Δ*ddc* were both whole genome sequenced. This confirmed the presence of the AbaAL44 accessory locus in both strains.

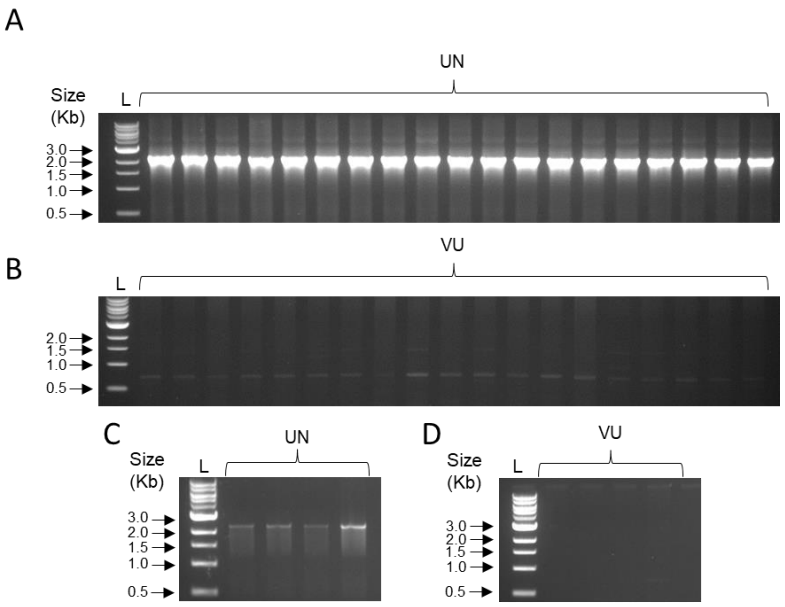

Figure 3.9. *A. baumannii* 17978 WT laboratory glycerol stock and the Δ*ddc* strain are of the UN genotype. Colony PCR was performed on streak-purified single colonies of *A. baumannii* 17978 (**A**) wild type and the (**C**) Δ*ddc* strains using the 17978UN_cls_R/F pair amplifying a product of 2.3 Kbp if of the UN genotype. PCR was performed on the same colonies of the wild type (**B**) and (**D**) Δ*ddc* strains using the 17978VU_junction_F/R primer pairs amplifying a product of 483 bp if of the VU genotype**.** L: 100 bp ladder.

3.3.5 Deletion of the *ddc* gene abolishes 1, 3-diaminopropane synthesis

Deletion of the *ddc* gene would result in an inability to produce 1, 3-diaminopropane. To confirm this HPLC analysis was carried out. *A. baumannii* 17978 wild type and the Δ*ddc* strains were initially grown on/in M9 succinate minimal media devoid of polyamines, to allow for the detection of only endogenous polyamines. Polyamines were extracted from stationary phase cultures and then derivatised using dansyl chloride (Section 2.10). 1, 7-diaminoheptane was added to all samples, before extraction and derivatisation, as an internal standard. HPLC analysis was carried out by Aaron Franklin in Dr Patrick Moynihan's laboratory (University of Birmingham).

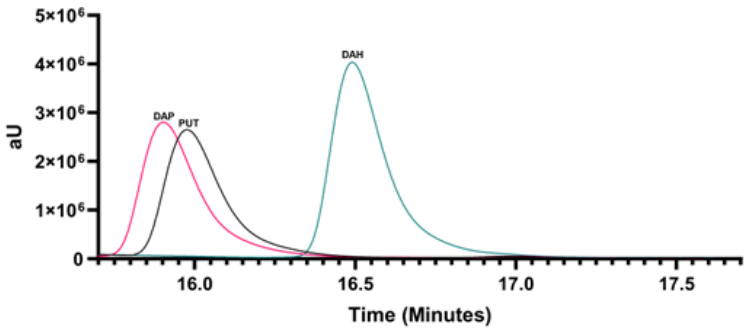

Figure 3.10. Retention times of 1, 3-diaminopropane, putrescine and 1, 7-diaminoheptane standards. Separation of polyamines standards and the corresponding retention times of 1, 3-diaminopropane, DAP; putrescine, PUT; 1, 7-diaminoheptane, DAH.

The chromatogram in Figure 3.10, represents the retention time for known polyamine standards used for analysis. 1, 3-diaminopropane was detected at approximately 15.9 minutes, putrescine at 16 minutes, and the internal standard 1, 7-diaminoheptane at 16.5 minutes. The added internal standard 1, 7-diaminoheptane was detected in both the wild type and Δ*ddc* samples, indicated by the distinct peak, corresponding to the relevant retention time (Figure 3.11). Analysis of polyamines in extracts from the wild type strain confirmed the presence of 1, 3-diaminopropane (Figure 3.11A). The deletion of the *ddc* gene should result in the inability of *A. baumannii* to decarboxylate L-2, 4-diaminobutyrate to synthesise 1, 3-diaminopropane. This is reflected in Figure 3.11B, where there is a complete absence of detectable 1, 3-diaminopropane, in the Δ*ddc* derived extract. Unexpectedly appears to be another polyamine detected in the Δ*ddc* derived sample (Figure 3.11B). This corresponds to the putrescine retention time. This was initially unexpected as 1, 3-diaminopropane is widely regarded as the major polyamine of this species. *A. baumannii* 17978 is known to synthesise fimsbactin, a putrescine-based siderophore, and encodes an ornithine decarboxylase as part of the fimsbactin pathway (Yang and Wencewicz, 2022). Therefore, putrescine identified by HPLC could be due to the synthesis of fimsbactin. It is worth noting that all strains were grown in a minimal medium devoid of all polyamines ruling out uptake as a possible source.

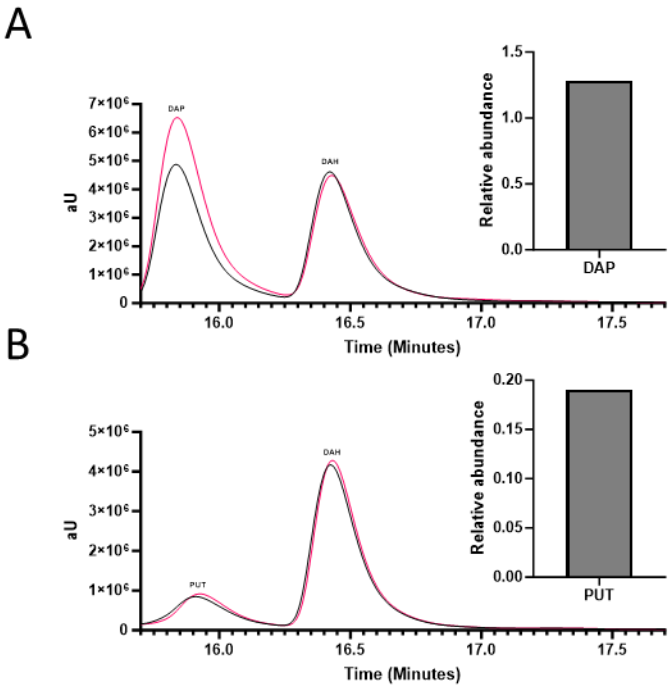

Figure 3.11. Deletion of the *ddc* gene abolishes 1, 3-diaminopropane synthesis. Comparison of the detection of polyamines synthesised by the *A. baumannii* wild type **(A)** and Δ*ddc* strains **(B)** by HPLC and their relative abundance, when grown at pH 6.5. Cells were grown in M9 minimal media, devoid of exogenous polyamines. 15 µl of 0.4 mM 1,7-diaminoheptane was added to each sample before extraction and derivatisation as an internal standard. Polyamines were extracted with trichloroacetic acid: HCl extraction and derivatised with dansyl chloride. DAP, 1, 3-aminopropane; PUT, putrescine; DAH, 1, 7-diaminoheptane. The data presented represent two biological repeats.

3.3.6 Deletion of *ddc* alters colony morphology and growth kinetics of *A. baumannii* 17978

3.3.6.1 *A. baumannii* Δ*ddc* exhibits altered colony morphology

During the deletion process, it was observed that the presumptive Δ*ddc* strain had an altered colony morphology. However, it was thought this may have been due to antibiotic selection. After the deletion was confirmed and the strain later streaked onto media devoid of antibiotics the same phenotype was present. Δ*ddc* colonies on LB agar appear smaller, with a punctiform appearance compared to the larger circular colonies of the wild type strain, after the same length of incubation (Figure 3.12). Supplementation of the LB media with 1, 3-diaminopropane was found to restore the growth defect of the

Δ*ddc* to some extent but not to that of the wild type (Figure 3.12). Supplementation does not increase the growth of the wild type strain compared to growth on non-supplemented agar (Figure 3.12).

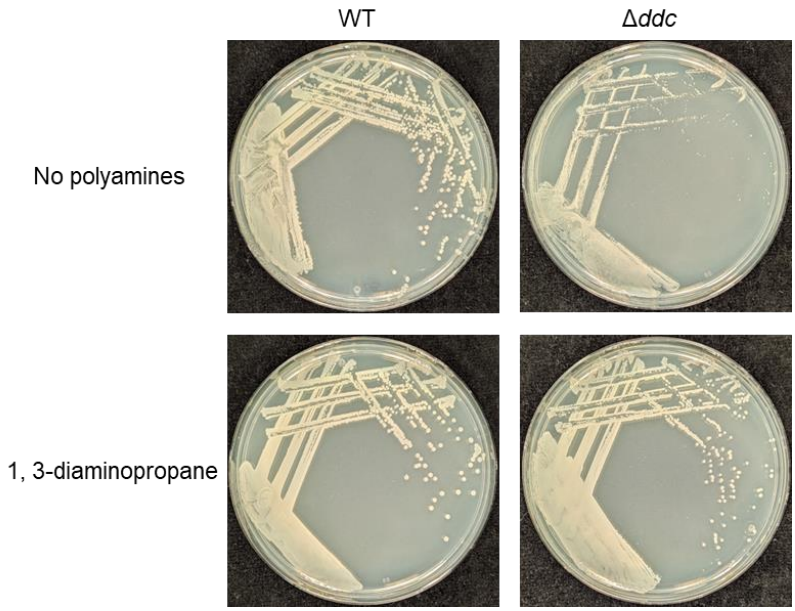

Figure 3.12. Deletion of the *ddc* gene results in a growth deficiency as observed by reduced colony size in *A. baumannii* 17978. Comparison of growth of *A. baumannii* 17978 wild type and Δ*ddc* strains on LB agar and the effect of supplementation with 125 µM 1, 3-diaminopropane has on the wild type and Δ*ddc* strains. The images presented are representative of two biological repeats.

3.3.6.2 Deletion of *ddc* alters planktonic growth kinetics

Skiebe et al (2012) previously showed that disruption of the *dat* and *ddc* genes results in an alteration in the growth kinetics of *A. baumannii* compared to the wild type strain. To assess whether the growth kinetics of the *Δddc* generated in this study were altered planktonic growth was analysed. Briefly, stationary phase cultures were diluted into fresh LB broth at 0.1 OD_{600nm}. Optical density measurements and enumeration were carried out every hour for 8 hours, with a final time point being carried out at 24 hours. Figure 3.13 shows the growth curves of *A. baumannii* 17978 wild type and Δ*ddc* in LB broth. Deletion of the Δ*ddc* gene results in an alteration of growth kinetics when compared to the wild type strain (Figure 3.13). The Δ*ddc* strain reaches a lower optical density at every time point compared to the wild type (Figure 3.13). At approximately 4 hours the growth of the wild type strain slows, occurring later with the Δ*ddc*

strain, at approximately 5 hours (Figure 3.13). The growth rate and doubling time (Table 9.1) of the Δ*ddc* strain are significantly less than that of the wild type strain (P = 0.0002 and 0.0003). By 24 hours the Δ*ddc* mutant reached a marginally lower final optical density than the wild type, with the wild type and ddc strains reaching 6.01 and 5.06 OD_{600nm}, respectively (Figure 3.13). Alongside optical density measurements, both strains were enumerated at each time point, with the Δ*ddc* never reaching the CFU/ml of the wild type strain, indicative of the differences in optical density throughout the experiment (data not shown).

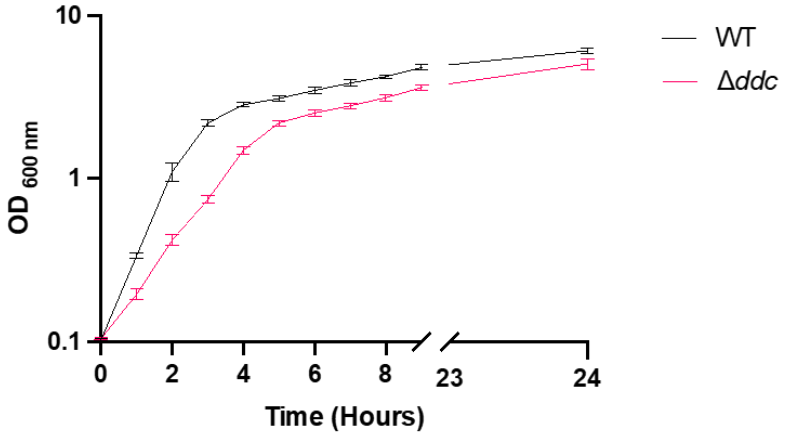

Figure 3.13. Deletion of the *ddc* gene reduces the planktonic growth rate of *A. baumannii* 17978. Comparison of the planktonic growth of *A. baumannii* wild type and the Δ*ddc* strains in LB broth. OD_{600nm} measurements were taken every hour for 8 hours, with a final measurement at 24 hours. The values presented represent the mean and SEM of three independent experiments.

3.3.7 Deletion of *ddc* impacts cell division and morphology of cells

Acinetobacter baumannii is a coccobacilli and under exponential conditions, cells tend to have a more bacilli-like appearance. Under nutrient-limiting conditions, cells have a more distinct coccoid shape. When attempting to match OD to a known CFU/ml it was observed that the CFU/ml of the wild type and the Δ*ddc* could not be matched to the same OD suggesting that there may have been alterations in cell growth or morphology. Phase contrast microscopy was carried out on the wild type and Δ*ddc* strains. It was found that the Δ*ddc*

strain forms long chains that vary greatly in length While there were some shorter chains present in the wild type, they were far more numerous in the Δ*ddc* culture and were of far greater lengths. The cells of the Δ*ddc* strain also appear larger than the wild type strain. This led to the hypothesis that deletion of 1, 3-diaminopropane synthesis may result in altered cell division and morphology.

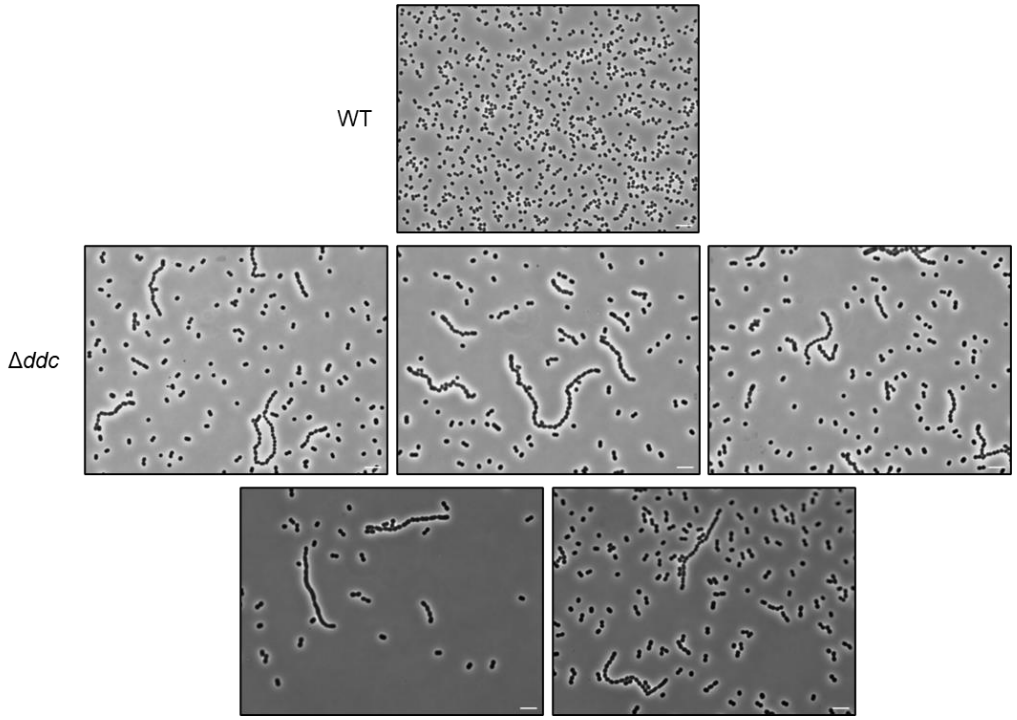

Figure 3.14 Deletion of the *ddc* gene results in a cell septation defect. Phase contrast microscopy of *A. baumannii* Δ*ddc* stationary phase cultures, showing the chaining phenotype of the Δ*ddc* strain. Scale bar: 5 µm. Images are representative of two biological repeats.

To analyse cell morphology and to assess the percentage difference of cell morphologies present within the population phase contrast microscopy was carried out. Images were taken at each time point and were processed using ImageJ. The number of single cells, dividing cells and chains present at each time point were recorded. Chains were deemed as cells that were conjoined and had ≥2 septa. Filamentous cells with no discernible septa were also counted and were combined with the chained counts. The total number of cells counted was always >500. This was due to all cells being counted in a given image. As opposed to selectively counting cells present until n=500 was met.

The data presented in Figure 3.15 is the combined counts from all three biological repeats. Appendix Figure 9.1 shows the individual data for each repeat. Before incubation, the stationary phase cultures used for the experimental setup were assessed. There appeared to be an abundance of single cells, primarily cocobacilli in shape, in both the wild type and Δ*ddc* cultures, which in the case of *A. baumannii* is indicative of a stationary phase. Over 65 % of the total cells counted appeared to be single cells, in the wild type culture (Figure 3.15A). While, in the Δ*ddc* culture there appears to be a greater percentage of doublets, at approximately 54 %, and fewer singular cells at 40 %, of the total cells counted (Figure 3.15B). The remainder is comprised of chaining cells with chains being comprised of varying numbers of segments.

Following incubation, the abundance of double or dividing cells increases and the proportion of single cells decreases (Figure 3.15), in both the wild type and the Δ*ddc* strain. Both strains approach a plateau in optical density (Figure 3.13). The wild type strain does this following four hours of incubation, while the onset is delayed for the Δ*ddc* strain, occurring at approximately six hours (Figure 3.13). This plateau indicates a slowing growth and an approach to a stationary phase. This is signified in both strains, with an increase in the percentage of single cells following four hours of incubation for the wild type and six hours for the Δ*ddc* strain (Figure 3.15). Across all time points, there are few chaining cells within the wild type culture (Figure 3.15A). At two hours the lowest percentage was observed at 0.062 % (Figure 3.15A). While the highest percentage was observed at 4 hours at 0.543 % (Figure 3.15A). By contrast, there is a significant presence of chaining cells in the Δ*ddc* culture across all time points (Figure 3.15B), indicating that chaining is not isolated to a specific growth phase as chains can be seen throughout logarithmic and stationary phases. The lowest percentage of chains was observed after two hours of incubation at 5.57 % of the total cells counted (Figure 3.15B). This then increased to 11.03 %, the highest percentage observed, following four hours of incubation (Figure 3.15B). The chains formed by the Δ*ddc* strain were not limited to planktonic growth either. Cells from colonies grown on agar and

those scraped from the surface of polystyrene plates, grown as biofilms, also exhibit the same morphology. It was proposed that the phenotype may be due to increased capsule production, which prevents the cells from fully separating. To test this, an aliquot of bacterial culture of the Δ*ddc* strain was vortexed for over ten minutes. When visualised by microscopy there was still an abundance of chaining cells. The significant and consistent presence of chaining cells in the Δ*ddc* cultures suggests that this phenotype has arisen from deletion of the *ddc* gene and that the loss of 1, 3-diaminopropane synthesis results in a disruption to cell septation, suggesting a possible role for 1, 3-diaminopropane in cell growth and division.

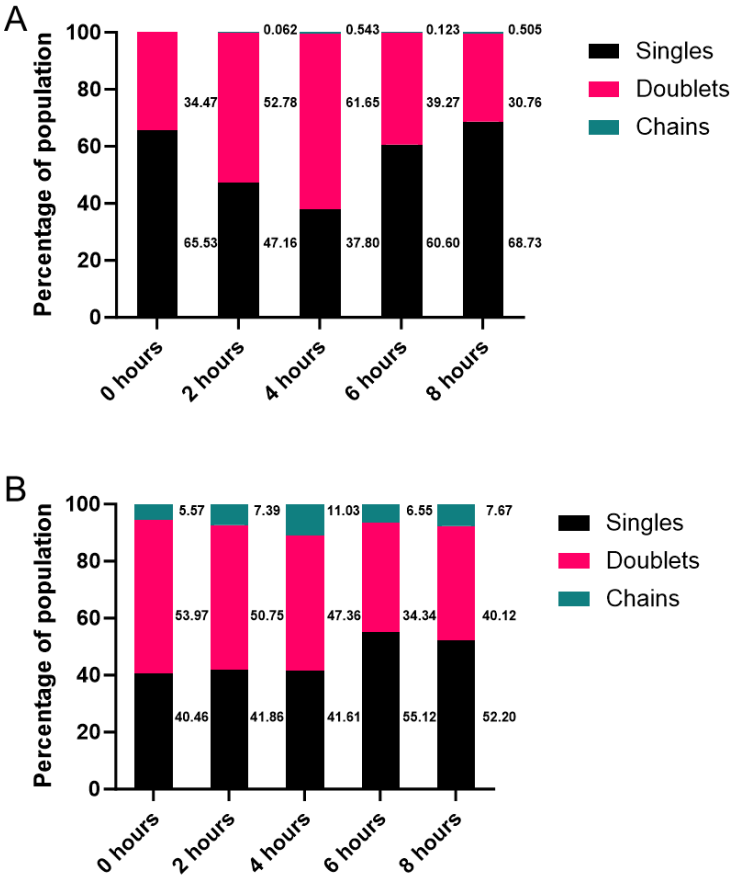

Figure 3.15. The Δ*ddc* strain forms chains throughout all growth phases. Comparison of the cell types present within wild type planktonic culture **(A)** and a Δ*ddc* planktonic culture **(B)** grown for 8 hours. Cultures were observed by phase contrast microscopy every 2 hours. Imaged cells were counted at every timepoint (N=>500) and reported as a percentage of the whole. The data presented is the combined counts of three biological repeats.

3.3.8 Cells within chains have defined septa

With the observation that deletion of the *ddc* results in cell chaining, possibly arising from disrupted cell replication or septation, it was unknown at what stage cell division had potentially stalled. Only preliminary staining and images could be generated, and while of poor quality, they do further expand on the understanding of this phenotype (Figure 3.16). Cells were stained with the lipophilic stain FM 1-43 which was selected for its ability to embed in the outer membrane. This determined that each segment within a chain appears to have undergone septum constriction and potentially has separated cytoplasmic compartments (Figure 3.16). This suggests that the disruption in septation may occur within the late stages and could be linked to peptidoglycan synthesis or separation.

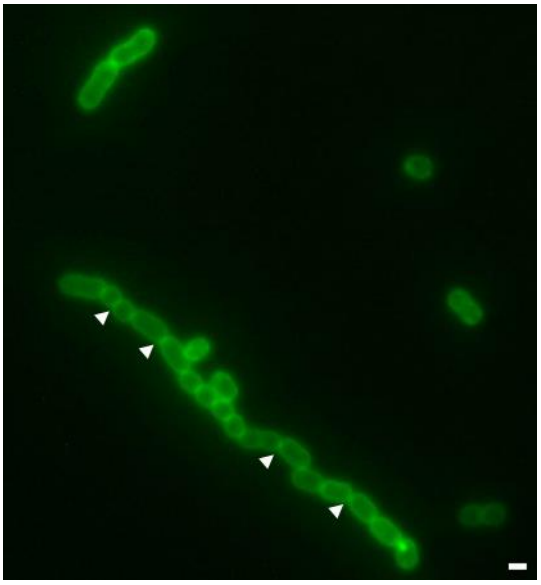

Figure 3.16. Chaining cells have defined points of septation. Fluorescence microscopy images of *A. baumannii* 17978 Δ*ddc* during stationary phase. Cells were stained with FM 1-43 and visualised with epifluorescence using a GFP filter (Ex: 474/28 Em: 527). White arrows: indicate midpoint membrane constriction. Scale bar: 5 µm. Images are representative of one biological repeat.

3.3.9 Planktonic growth kinetics are not complemented with other polyamines

Having shown that the growth defect of the Δ*ddc* strain can be complemented with 1, 3-diaminopropane, it was decided to assess whether other di-, tri, or

tetra-amines could also complement in the same manner. It has previously been demonstrated that some polyamines can be substituted for one another (Hobley et al., 2017). To assess this possibility growth analysis was carried out with 125 μM of spermine and spermidine to growth media (Figure 3.17B), with both being selected for 1, 3-diaminopropane moiety in their structure. For comparison, media was supplemented with polyamines that do not contain 1, 3-diaminopropane moiety in their structure, cadaverine and putrescine (Figure 3.17A). The wild type with and without additional polyamines grows exponentially until approximately two hours, with growth slowing after this and beginning to enter into a plateau following four hours of incubation (Figure 3.17). Supplementation did not result in any significant change in growth rate or doubling time of the wild type (Table 9.1) compared to the strain growing without supplementation. This suggests that exogenous polyamines do not promote or inhibit the growth of wild type *A. baumannii* 17978. The Δ*ddc* strain supplemented with spermidine, spermine, cadaverine, and putrescine appears identical to the Δ*ddc* strain grown without additional polyamines (Figure 3.17). Under all conditions, there is exponential growth until approximately five hours, when growth begins to slow and enter a plateau by the eighth hour (Figure 3.17). There was found to be no significant difference between any of the growth rates (Table 9.1) of the Δ*ddc* with and without these additional polyamines. All growth rates were significantly less than those of the wild type. This confirms that the four polyamines are incapable of complementing the Δ*ddc* growth defect.

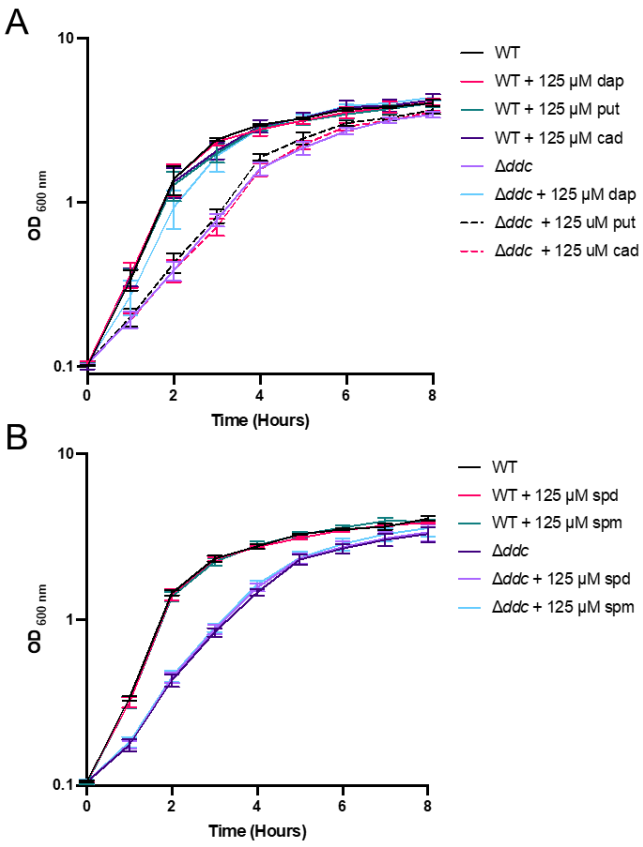

Figure 3.17. Polyamines other than 1, 3-diaminopropane are incapable of complementing the growth defect of the Δ*ddc* strain. (A) Comparison of the ability of 125 µM 1, 3-diaminopropane (dap), putrescine (put), and cadaverine (cad) to complement the growth deficiency of *A. baumannii* 17978 Δ*ddc*. **(B)** Comparison of the ability of 125 µM spermidine (spd) and spermine (spm) to complement the growth deficiency of *A. baumannii* 17978 Δ*ddc*. The OD_{600nm} was measured every hour across 8 hours. The values presented represent the mean and SEM of three independent experiments.

Similarly, to complementation with 1, 3-diaminopropane a sample of each culture was viewed under the microscope at four hours post incubation to assess the cell morphology and chaining phenotype. Viewing cells under the microscope revealed polyamines do not alter the cell morphology (Figure 3.18). In addition, none of the polyamines were capable of alleviating the chaining phenotype, with an abundance of chains being visible in all cultures of the Δ*ddc* strain (Figure 3.18). This supports the observations made in the growth analysis, where the addition of any di- or triamine, other than 1, 3-diaminopropane, is incapable of reverting the growth rate of the Δ*ddc* strain to a similar rate as the wild type. Taken together this confirms that only 1,3-diaminopropane is capable of chemically complementing the Δ*ddc* strain.

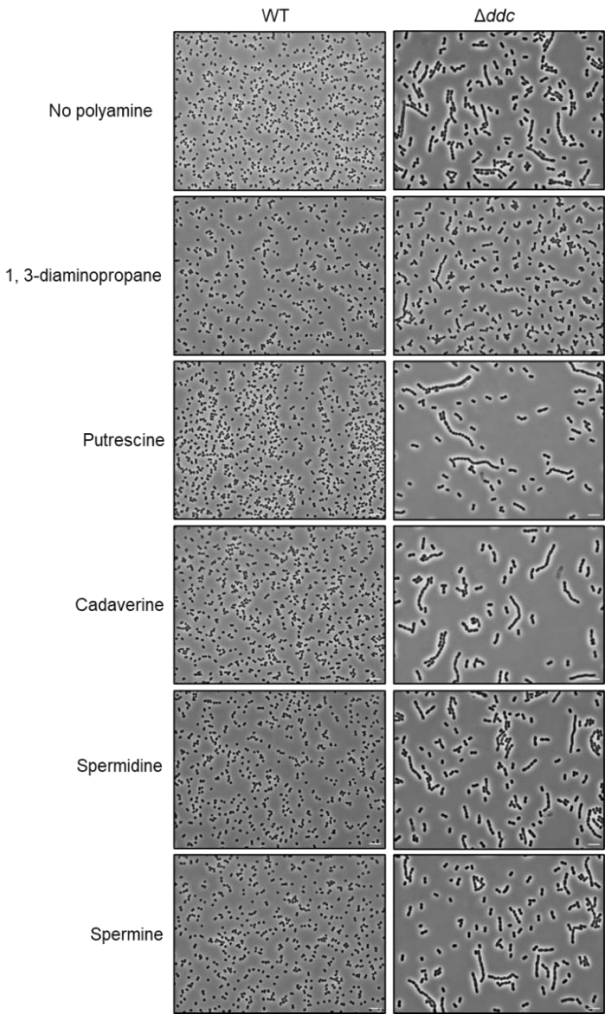

Figure 3.18. Diamines, triamines, and tetra-amines cannot be substituted for 1, 3-diaminopropane. Phase contrast microscopy of *A. baumannii* wild type and Δ*ddc* strains grown in the absence and presence of 1, 3-diaminopropane, putrescine, cadaverine, spermidine, and spermine. Images were taken 4 hours post incubation. Scale bar: 5 µm. Images are representative of three biological repeats.

3.3.10 Deletion of *ddc* abolishes *A. baumannii* 17978 surface-associated motility

A. baumannii 17978 exhibits two distinct motility phenotypes. These are twitching motility and the lesser-understood "surface-associated motility". 1, 3-diaminopropane is essential to *A. baumannii* motility (Skiebe et al., 2012). To assess the surface-associated motility of the 17978UN strain and the effect of the in-frame deletion of *ddc*. A single colony of wild type and Δ*ddc* strains were picked and stab inoculated through the surface of semi-solid motility agar; to allow for motility on the agar surface and to test for motility at the agar and

polystyrene petri dish interphase. The radius of motility was measured and the plates were imaged. Figure 3.19 confirms the *A. baumannii* 17978UN wild type is motile on the surface of semi-solid media. Motility was not observed through the agar or between the interface of the agar and polystyrene petri dish. Deletion of *ddc* completely abolished the motility phenotype, with growth only appearing at the inoculation site (Figure 3.19). These findings support the observation previously made that 1, 3-diaminopropane is essential for surface-associated motility (Skiebe et al., 2012).

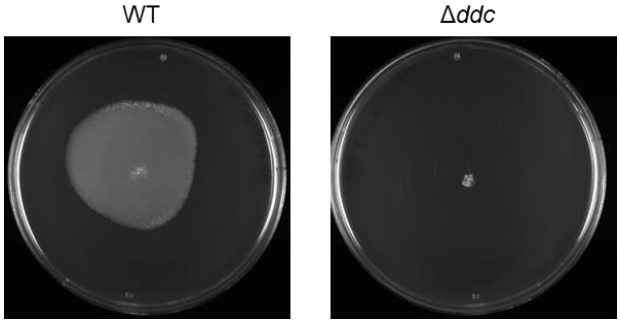

Figure 3.19. Deletion of the *ddc* gene abolishes the motility of *A. baumannii* 17978UN. Comparison of the motility of *A. baumannii* 17978UN wild type and Δ*ddc* strains. A single colony of each strain was stab inoculated through the surface of the agar to the underlying petri dish and plates were incubated for 16 hours. The images presented are representative of three biological repeats.

3.3.11 Complementation with exogenous 1, 3-diaminopropane restores surface-associated motility

To establish whether the Δ*ddc* motility defect could be chemically complemented, the motility agar was supplemented with 125 µM 1, 3-diaminopropane. Complementation with exogenous 1, 3-diaminopropane restores the motility of the Δ*ddc* strain (Figure 3.20) with there being no significant difference between the wild type strain and complemented Δ*ddc* strain indicating restoration of motility (Figure 3.20B). There was no significant difference between the motile zone of the wild type in the presence or absence of 1, 3-diaminopropane (Figure 3.20B). Showing that exogenous 1, 3-diaminopropane cannot increase surface migration.

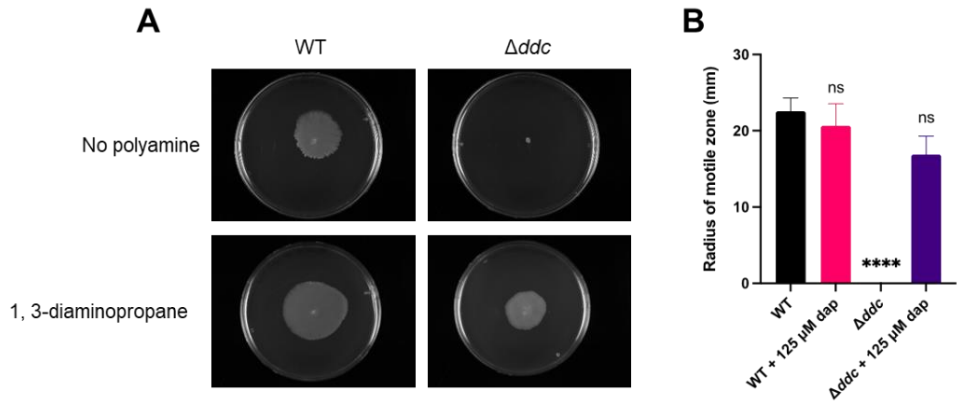

Figure 3.20. Exogenous 1, 3-diaminopropane complements the motility defect of the Δ*ddc* strain. (A) The surface-associated motility of *A. baumannii* 17978 wild type and Δ*ddc* strains and the effect supplementation with 125 µM 1, 3-diaminopropane has on the motility of each strain. A single colony of each strain was stab inoculated through the surface of the agar to the underlying petri dish and plates were incubated for 16 hours. The images presented are representative of three independent experiments. **(B)** Comparison of the distance migrated by *A. baumannii* 17978 wild type and Δ*ddc* strains and the effect supplementation with 125 µM 1, 3-diaminopropane has on the motility of each strain. Values presented represent the mean and SEM of three independent experiments **** = p-value <0.0001 (unpaired t-test with Welch's correction).

3.3.12 Complementation with polyamines other than 1, 3-diaminopropane does not restore surface-associated motility

With 1, 3-diaminopropane capable of complementing the loss of surface-associated motility it was decided to assess whether other polyamines could do the same. Spermidine and spermine were selected as they feature a 1, 3-diaminopropane moiety within their structures, and in some reports, polyamines with similar structures can be substituted for one another (Hobley et al., 2017; S. H. Kim et al., 2016). To test this hypothesis motility agar was supplemented with 125 µM of spermidine and spermine. Additionally, agar was supplemented with 125 µM of putrescine, cadaverine and agmatine. The wild type strain exhibited surface motility while the Δ*ddc* without exogenous 1, 3-diaminopropane was non-motile (Figure 3.21), and 1, 3-diaminopropane restored the motility of Δ*ddc* (Figure 3.21). Complementation with putrescine, cadaverine, spermidine, spermine and agmatine did not restore the motility of

Δ*ddc* (Figure 3.21). This suggests that the role mechanism by which 1, 3-diaminopropane is involved in motility is specific to this polyamine.

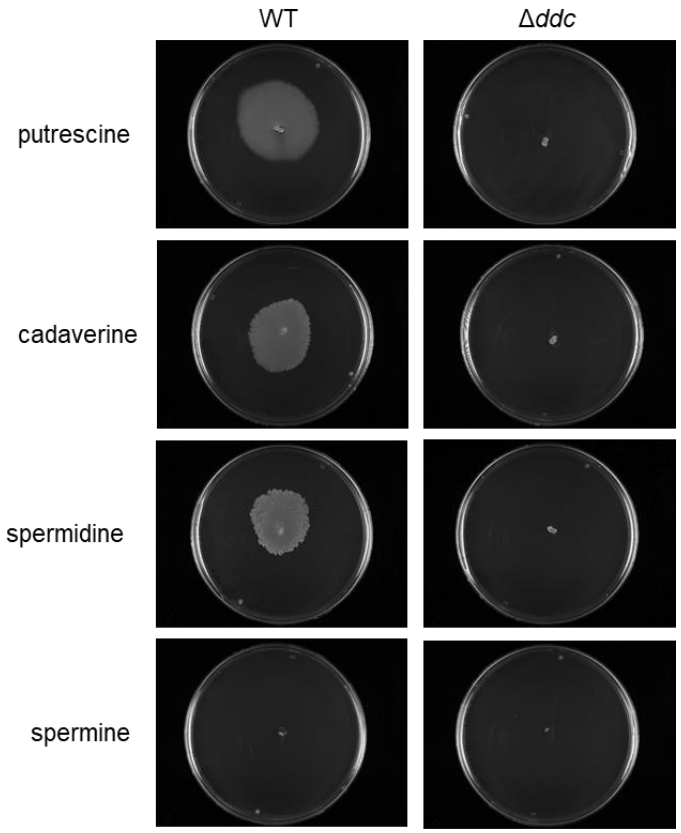

Figure 3.21. Polyamines, other than 1, 3-diaminopropane, are incapable of restoring the surface-associated motility phenotype of *A. baumannii* 17978 Δ*ddc.* Comparison of the ability of 125 µM of 1, 3-diaminopropane, putrescine, cadaverine, spermidine, and spermine to restore the motility deficiency of *A. baumannii* 17978 Δ*ddc*. A single colony of each strain was stab inoculated through the surface of the agar to the underlying petri dish and plates were incubated for 16 hours. The images presented are representative of three independent repeats.

It was observed that supplementation with 125 µM spermine led to a loss of motility of the wild type strain (Figure 3.21). Initially, this suggested that spermine can inhibit the motility of *A. baumannii* 17978. However, there was also a distinct lack of growth around the inoculation site on agar plates supplemented with 125 µM spermine (Figure 3.21). Additional motility assays were carried out using spermine at 25, 50, 75, and 125 µM (Figure 3.22). On agar lacking spermine, the wild type formed a large motile zone (Figure 3.22A). The addition of spermine reduced the size of this motile zone in a concentration-dependent manner (Figure 3.22B-D) and at 125 µM complete

inhibition was observed (Figure 3.22E), as previously seen. This suggests that spermine is toxic to *A. baumannii* 17978. It is worth noting that both the wild type and Δ*ddc* strains are capable of growth in LB broth supplemented with 125 µM of spermine (Figure 3.17). This suggests that this spermine toxicity is tied to the composition of the motility media used.

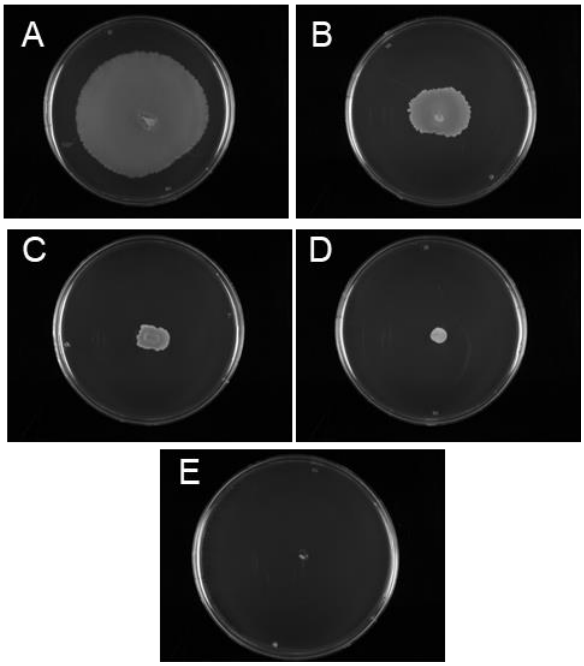

Figure 3.22. Spermine is toxic to *A. baumannii* 17978 on motility agar. The surface associated motility of *A. baumannii* 17978 **(A)** wild type and the effect that **(B)** 25 µM, **(C)** 50 µM, **(D)** 75 µM and **(E)** 125 µM of spermine has on growth and surface motility. A single colony of each strain was stab inoculated through the surface of the agar to the underlying petri dish and plates were incubated for 16 hours. The images presented are representative of two biological repeats.

3.3.13 Growth defects are complemented with exogenous 1, 3-diaminopropane

Following the observation that exogenous 1, 3-diaminopropane was able to chemically complement growth defects of colonies grown on agar (Section 3.3.6.1), it was hypothesised that it might also be able to complement the growth defect and altered morphology observed during planktonic growth. To assess LB broth was supplemented with 125 µM 1, 3-diaminopropane, and optical density measurements were carried out at every time point. Phase contrast microscopy was carried out every two hours. Complementation with

1, 3-diaminopropane fully restored the growth kinetics of the Δ*ddc* strain to wild type levels (Figure 3.23). Optical density values are marginally lower than those of the wild type until three hours when the optical density of the wild type and Δ*ddc* are similar (Figure 3.23). The exponential growth rate of the Δ*ddc* strain (Table 9.1) was significantly increased in the presence of exogenous 1, 3-diaminopropane, compared to the Δ*ddc* without complementation (P = 0.0001). There was also no significant difference between the complemented strain and the wild type, suggesting the growth rate had been restored, to that of the wild type. The Δ*ddc* strain maintained a growth rate significantly less than that of the wild type (P = 0.0226), as seen previously (Section 3.3.6.2). The addition of 1, 3-diaminopropane has no visible effect on the growth of the wild type strain (Figure 3.23). However, statistical analysis revealed a significant difference between the wild type strain's growth rate in the presence and absence of exogenous 1, 3-diaminopropane (P = 0.499). While there is a statistical significance, the p-value generated, suggests that the biological relevance of this significance may be negligible.

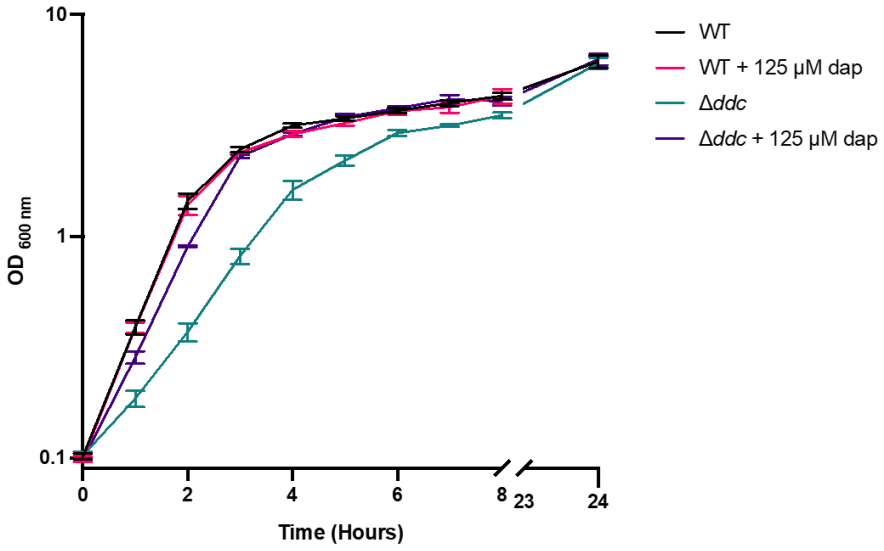

Figure 3.23. Exogenous 1, 3-diaminopropane complements the growth defect of the Δ*ddc* strain. The comparison of growth kinetics of *A. baumannii* 17978 wild type and Δ*ddc* grown in LB broth supplemented with and without 125 µM 1, 3-diaminopropane. The OD_{600nm} was measured every hour across an 8-hour period. Values represent the mean and SEM of three independent experiments.

Alongside optical density measurements, microscopy was again carried out to observe differences in cell morphology in the population in the presence and absence of 1, 3-diaminopropane. The results from individual replicates are presented in Appendix Figure 9.2. Similar to the results presented previously (Section 3.3.7), both the wild type and Δ*ddc* see an increase in doublet cells, during exponential growth and an increase in single cells as both cultures approach the stationary phase (Figure 3.24). Upon approaching the stationary phase the wild type was the expected coccobacilli shape and the addition of polyamines did not alter morphology compared to that observed in their absence (Figure 3.24C). For the wild type strain, the proportion of doublets was greater than the single cells after two hours of incubation, with the number of single cells overtaking the doublets at four hours post-inoculation (Figure 3.24A). The increased proportion of doublets appears to be present for longer in the Δ*ddc* culture. More doublets were observed at two and four hours post-incubation (Figure 3.24B). When the Δ*ddc* is supplemented with 1, 3-diaminopropane it appears that the fluctuation in the population mirrors that of the wild type. More doublets are observed at two hours post incubation, a greater proportion of single cells are observed four hours post incubation, and a greater proportion of single cells appear at six hours post inoculation (Figure 3.24D). This supports the observations made with the growth curve kinetics, where the Δ*ddc* strain has a slower growth rate reaching the beginning of a plateau by six hours, and that complementation with 1, 3-diaminopropane reverts the Δ*ddc* to a growth pattern similar to that of the wild type. As before, the Δ*ddc* culture appears to have a significant abundance of chaining cells. These were present across all time points, with abundance varying between 3-12 % of the total counted cells, throughout the time course (Figure 3.24B). As before, chaining cells were less numerous in the wild type culture, accounting for <1 % at each timepoint (Figure 3.24A). When chains were present in the wild type culture, they did not contain a similar number of septa as the Δ*ddc* chains, with only triplets and quadruplets observed. When 1, 3-diaminopropane was supplemented into the growth media of the Δ*ddc* strain there was a decline in chaining cells, with the average percentage ranging

between 0.8-1.4 % of the total population counted (Figure 3.24D). When comparison is made between conditions at each time point it was established that complementation results in a significant decrease in the presence of chaining cells. This shows that both the growth defect and the chaining phenotype can be chemically complemented with the addition of 1, 3-diaminopropane, thereby both phenotypes can be attributed to the deletion of the Δ*ddc* gene and loss of 1, 3-diaminopropane synthesis.

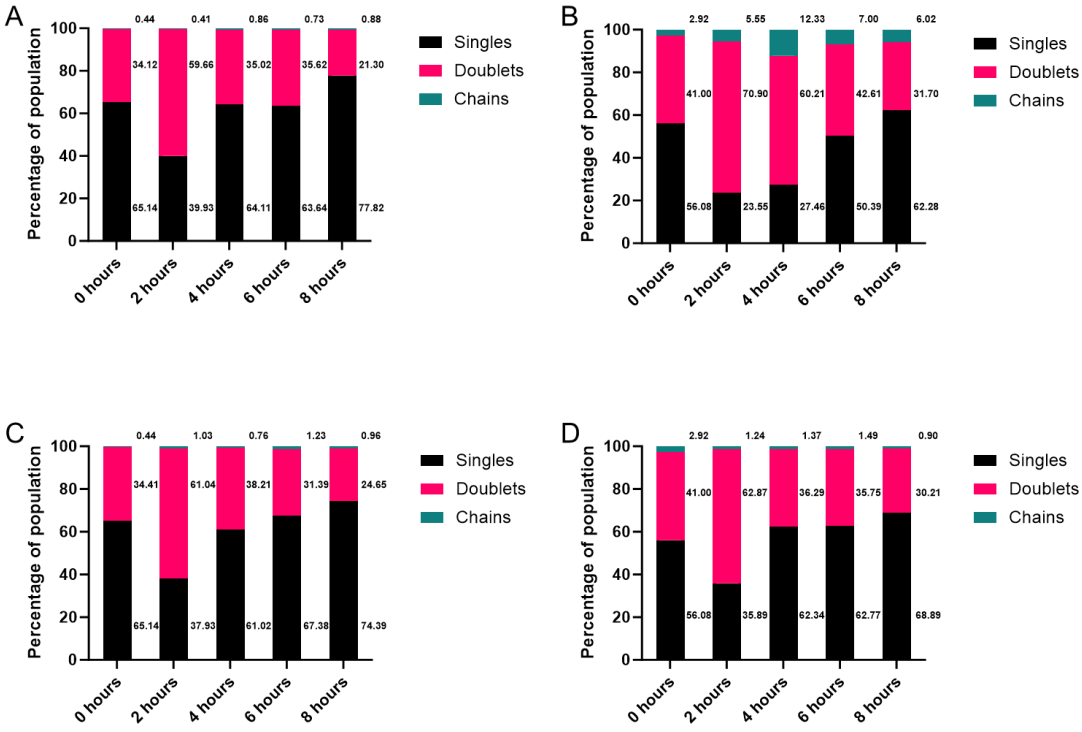

Figure 3.24. Exogenous 1, 3-diaminopropane complements the Δ*ddc* strains cell division defect. Comparison of the cell types present within **(A)** wild type and **(B)** Δ*ddc* planktonic culture and (C) wild type and (D) Δ*ddc* cultures supplemented with 125 µM 1, 3-diaminopropane grown for 8 hours. Cultures were observed by phase contrast microscopy every 2 hours. Imaged cells were counted at every timepoint (N=>500) and reported as a percentage of a whole. The data presented is the combined counts of three biological repeats.

3.3.14 Complementation with β-alanine does not restore surface-associated motility

It has been shown that 1, 3-diaminopropane can be used to synthesise β-alanine through a previously uncharacterised salvage pathway (Perchat et al., 2022). Deletion of the *ddc* gene would abolish the ability of *A. baumannii* to

use this hypothetical pathway. To assess whether the β-alanine salvage pathway plays a role in surface-associated motility of *A. baumannii*, motility agar was supplemented with 10, 100 and 200 µM β-alanine. Supplementation with β-alanine did not impact the motility of wild type *baumannii* 17978 and was unable to complement the motility deficiency of Δ*ddc* at any concentration (Figure 3.25). This suggests that, if present, the β-alanine salvage pathway utilising is not associated with the surface motility of *A. baumannii* 17978.

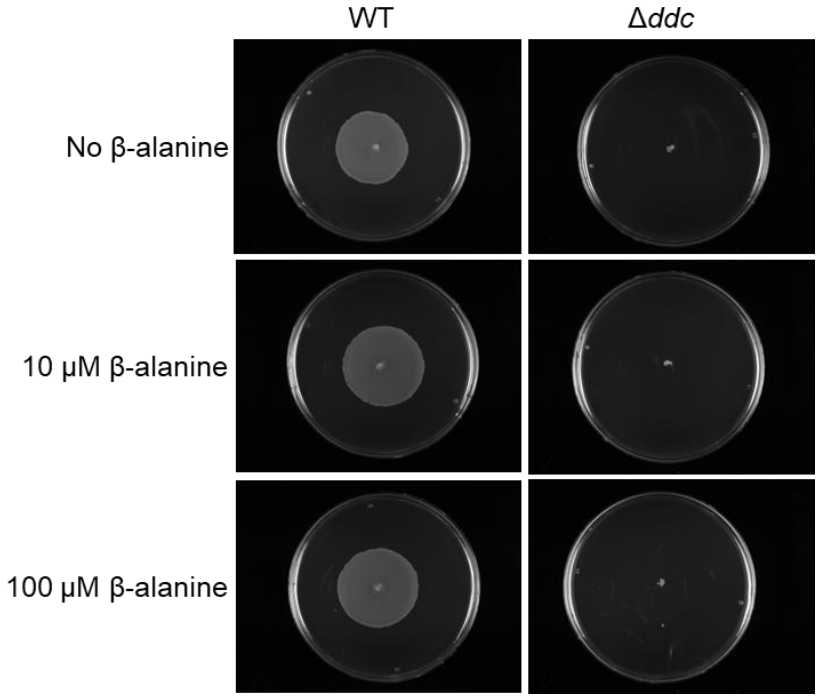

Figure 3.25. β-alanine is incapable of complementing the surface motility defect of the Δ*ddc* strain. Comparison of the ability of varying concentrations of β-alanine, to restore the motility deficiency of *A. baumannii* 17978 Δ*ddc*. A single colony of each strain was stab inoculated through the surface of the agar to the underlying petri dish and plates were incubated for 16 hours. The images presented are representative of two independent repeats.

3.3.15 Deletion of the *ddc* gene reduces biofilm formation of *A. baumannii* 17978

Investigation next sought to determine the effect of the deletion of *ddc* on the biofilm formation of *A. baumannii.* There have been several instances where polyamines have been reported to be involved in biofilm formation. Biofilm formation is a key element in *A. baumannii* infection (Ahmad et al., 2023). This

makes biofilm formation a desirable therapeutic target, with the targeting of polyamine synthesis being a possible approach. Analysis of biofilm utilised a 96-well crystal violet staining assay (Section 2.16). All strains were shown to produce less biofilm in M9 minimal media when compared to the nutrient-rich LB broth (Figure 3.26), indicating nutrient availability impacted biofilm formation. Deletion of the *ddc* gene resulted in a significant reduction in the biofilm formation of *A. baumannii* 17978 in nutrient-rich LB media (Figure 3.26A) (P = <0.0001) and the chemically defined M9 media (Figure 3.26B) compared to the wild type strain (P = <0.0294). However, in both cases, some biofilm biomass was observed in the Δ*ddc* strain (Figure 3.26). This indicates that 1, 3-diaminopropane is not essential for biofilm formation in *A. baumannii* 17978 but is required for wild type levels of biofilm formation.

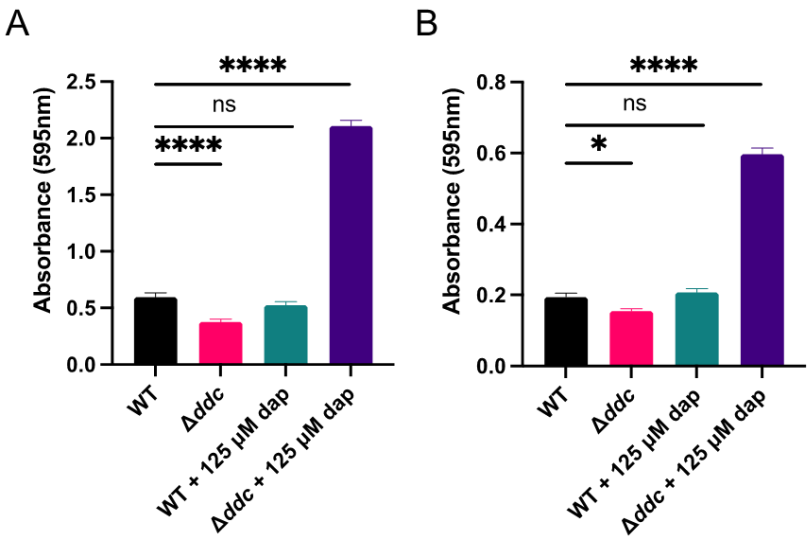

Figure 3.26. Deletion of the *ddc* gene reduces the levels of biofilm formed by *A. baumannii* 17978 and complementation with exogenous 1, 3-diaminopropane results in overproduction of biofilm by the Δ*ddc* strain. Comparison of biofilm formed by *A. baumannii wild* type and Δ*ddc* deletion strains and the effect of supplemented with 125 µM of 1, 3-diaminopropane, when grown in **(A)** LB broth and **(B)** M9-minimal media in a 96-well plate. Biofilm was quantified with crystal violet staining and absorbance measurement at 595 nm. The values presented represent the mean and SEM of three independent experiments. Each experiment was comprised of 36 wells per strain/condition across three technical replicates. **** = p-value ≤ 0.0001, * = p-value 0.0294 (Mann-Whitney).

3.3.16 Complementation with exogenous 1, 3-diaminopropane results in overproduction of biofilm in the Δ*ddc* but not in the wild type

Following the observation that the Δ*ddc* strain shows decreased biofilm formation and the effect chemical complementation has on other phenotypes, chemical complementation was carried out to determine if exogenous 1, 3-diaminopropane could reverse the biofilm deficiency phenotype. To assess whether the biofilm formation defect could be complemented 125 µM 1, 3-diaminopropane was supplemented into the LB and M9-succinate growth media prior to the experiment. Biofilm quantification was carried out as previously described. It was found that complementation with 125 µM 1, 3-diaminopropane does not significantly increase the biofilm produced by wild type *A. baumannii* 17978 in either growth medium (Figure 3.26). Unexpectedly, complementation with exogenous 1, 3-diaminopropane results in the Δ*ddc* strain forming significantly more biofilm when compared to *A. baumannii* 17978 wild type in both LB broth (Figure 3.26A) ($P = 0.0001$) and M9-minimal media (Figure 3.26B) ($P = <0.0001$). Following the observation that exogenous 1, 3-diaminopropane results in biofilm overproduction by the Δ*ddc* strain, complementation was carried out at varying concentrations of 1, 3-diaminopropane to determine whether the effect observed was dosage dependent. Initially a range of 10-125 µM of 1, 3-diaminopropane was administered, but there were high levels of biofilm staining, similar to those observed at the initial 125 µM concentration. Therefore, a lower range was selected, approximately ten times less than the initially tested concentrations. Preliminary data suggests that the overproduction of biofilm seen by the Δ*ddc* strain, in the presence of exogenous 1, 3-diaminopropane, may be dosage dependent. The complementation effect of exogenous 1, 3-diaminopropane does not occur at 0.25 µM and below and levels at 0.5, 0.75, and 1 µM 1, 3-diaminopropane are similar to that of the wild type, suggesting that these concentrations of 1, 3-diaminopropane potentially restore biofilm to the level of the wild type strain, and do not result in the overproduction. Taken together

this data suggests that elevated concentrations of exogenous 1, 3-diaminopropane result in the overproduction of biofilm, through an unknown mechanism, as a result of deletion of the *ddc* gene and that this overproduction can be reduced in a dosage-dependent manner.

3.3.17 Deletion of the *ddc* gene does not alter the susceptibility of *A. baumannii* 17978 to oxidative stress

Polyamines are known to protect against the detrimental effects of oxidative stress. (Chattopadhyay et al., 2009; Kang et al., 2007; Sakamoto et al., 2015). It was hypothesised that 1, 3-diaminopropane could fulfil this role in *A. baumannii*. Bacteria encounter ROS as part of the immune response. Therefore, this may provide a possible explanation for the attenuated virulence seen with the Δ*ddc* strain. To determine this *A. baumannii* was exposed to varying concentrations of hydrogen peroxide. H_2O_2 induces oxidative stress by interacting with Iron (II) ions, known as the Fenton reaction (Equation 3.1), this forms highly reactive, hydroxyl radicals, Iron (III) and hydroxide ions.

$$H_2O_2 + Fe^{2+} \rightarrow OH^- + OH\cdot + Fe^{3+}$$

Equation 3.1. The Fenton reaction

Susceptibility to H_2O_2 was assessed using a disc diffusion assay (Section 2.15.1). As expected, the size of the inhibitory zone was proportional to the concentration of hydrogen peroxide used, increasing as concentration increased (Figure 3.27). The diameter of inhibitory zones for wild type and Δ*ddc* at each concentration of H_2O_2 were comparable to one another at the same concentrations (Figure 3.27). This suggests that in *A. baumannii* 17978 1, 3-diaminopropane does not have a protective role against oxidative stress or at least that induced by hydrogen peroxide.

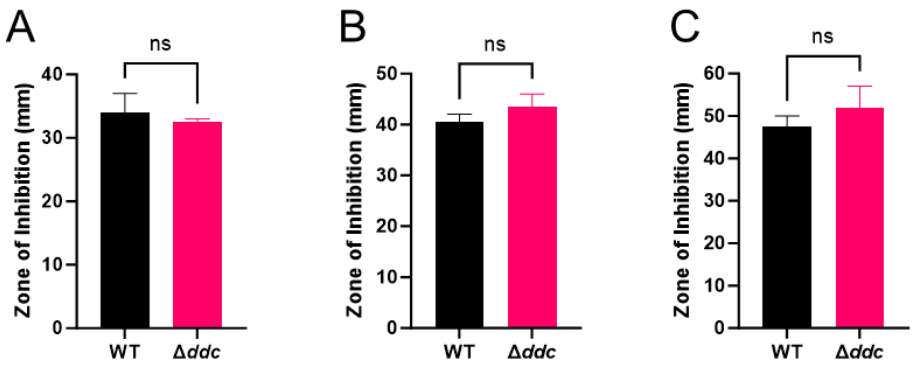

Figure 3.27. Deletion of the *ddc* gene does not change the susceptibility to hydrogen peroxide-induced in *A. baumannii* 17978. Comparison of survival of *A. baumannii* wild type and Δ*ddc* strains, in the presence of **(A)** 3 %, **(B)** 10 %, **(C)** 30 % (v/v) hydrogen peroxide. The inhibitory effect of hydrogen peroxide was assessed by disk diffusion assay. The values presented represent the mean and SEM of three independent experiments. Statistical analysis was measured using an unpaired T-test with Welch's correction.

3.3.18 The deletion of the *ddc* gene alters susceptibility to aminoglycosides

Polyamines have been linked to antimicrobial susceptibility in several microorganisms. (Dodds, 2017; El-Halfawy and Valvano, 2014; Sarathy et al., 2013). Therefore, it was decided to determine whether deletion of the *ddc* gene alters susceptibility to a range of antimicrobials in *A. baumannii* 17978. Alterations in antibiotic susceptibility are of interest as they could allow for 1, 3-diaminopropane synthesis inhibitor and antimicrobial combination therapy. MICs were determined by broth microdilution methodology (Section 2.17). Antibiotics were selected based on their previous links with polyamines and their usage in treating infection. The MICs of each antimicrobial are presented in Table 3.2. The MIC of trimethoprim and colistin were the same for the wild type and Δ*ddc* strain. The Δ*ddc* strain shows a decrease in MIC for ampicillin and tetracycline compared to the MICs determined for the wild type strain. The difference with tetracycline is within one doubling dilution and can therefore be disregarded.

Table 3.2. The MIC of antimicrobials determined for *A. baumannii* 17978 wild type and Δ*ddc* strains

Antibiotic	Antibiotic MIC (μg/ml)	
	WT	Δ*ddc*
Meropenem	0.25	0.25
Ampicillin	32	8
Gentamicin	2	>64
Colistin	0.5	0.25
Trimethoprim	32	32
Tetracycline	0.5	0.25
The values presented represent the MIC obtained from three independent experiments. MIC values were excluded if greater than one doubling dilution of the predominant value obtained according to the convention normally used in the published literature		

Originally the MIC assay for gentamicin was carried out with the highest concentration of the dilution series being 8 μg/ml. When reading the MICs it was initially believed that the MIC of gentamicin for the wild type strain and Δ*ddc* strain were identical at 2 μg/ml. However, when the 96-well plates were closely inspected the Δ*ddc* strain showed trailing growth at the elevated concentrations of gentamicin, with faint, pin-head-sized pellets forming at the bottom of the wells. The assay was repeated increasing the highest concentration to 64 μg/ml. There still appeared to be faint pellets at the bottom of the wells at this elevated concentration. Additional MIC assays were carried out using streptomycin, apramycin and kanamycin and a similar result was also observed for the Δ*ddc* strain. Small pinpoint pellets were observed at the higher concentrations of all tested aminoglycosides, indicating the presence of growth or persistence by the Δ*ddc* strain. This suggests that deletion of the *ddc* gene decreases susceptibility to aminoglycosides.

3.3.19 Deletion of *ddc* attenuates the virulence of *A. baumannii* 17978 in *Galleria mellonella*

To assess the *in vivo* virulence of *A. baumannii* 17978 wild type and the Δ*ddc* strains the *Galleria mellonella* infection model was selected. This was done because larvae have an immune system similar to the mammalian innate system and are easy to acquire, maintain, and infect. It was previously shown

that transposon insertion into the *dat* and *ddc* genes leads to attenuation in *A. baumannii* 17978 virulence (Skiebe et al., 2012). It was therefore hypothesised that the Δ*ddc* strain would also have an attenuated virulence *in vivo*. Strains were inoculated by injection of cell suspensions into the last right proleg of larvae to give an inoculum of 5 x 10^4 CFU and 5 x 10^3 CFU. PBS was injected as a mechanical and vehicle control. Survival was measured every 24 hours for five days. Figure 3.28A shows the survival of larvae over 72 hours after infection with 5 x 10^3 bacterial cells per larva. Injection with 5 x 10^3 CFU inoculum of *A. baumannii* 17978 wild type resulted in 20 % of larvae being killed within 24 hours post-infection (Figure 3.28A). Infection with Δ*ddc* resulted in no larvae death 24 hours post-infection (Figure 3.28A). By 72 hours a total of 30 % of larvae infected with the wild type had been killed (Figure 3.28A) while the Δ*ddc* killed 4 % of infected larvae (Figure 3.28A) showing a significant increase in larvae survival when infected with the Δ*ddc* at an inoculum of 5 x 10^3 (P = 0.0057). Larvae were also injected with 5 x 10^4 CFU of each strain. Figure 3.28B shows 24 hours post-infection 70 % of larvae infected with the wild type were killed, while infection with Δ*ddc* resulted in the killing of just 10 % (Figure 3.28B). By 72 hours post-infection the wild type strain had killed a total of 77 % of the larvae infected; of those infected with the Δ*ddc* strain a total of 27 % had been killed (Figure 3.28B). Injection with PBS resulted in the death of a single larva (Figure 3.28). The larvae in question did not appear to have any signs of physical trauma or melanisation suggesting the death may not be attributed to the injection of PBS. Statistical analysis established a significant increase in the survival of larvae when infected with the Δ*ddc* strain compared to infection with the wild type strain (P = <0.0001). The attenuation of virulence in the Δ*ddc* shows that the synthesis of 1, 3-diaminopropane is required for the full virulence of *A. baumannii* 17978.

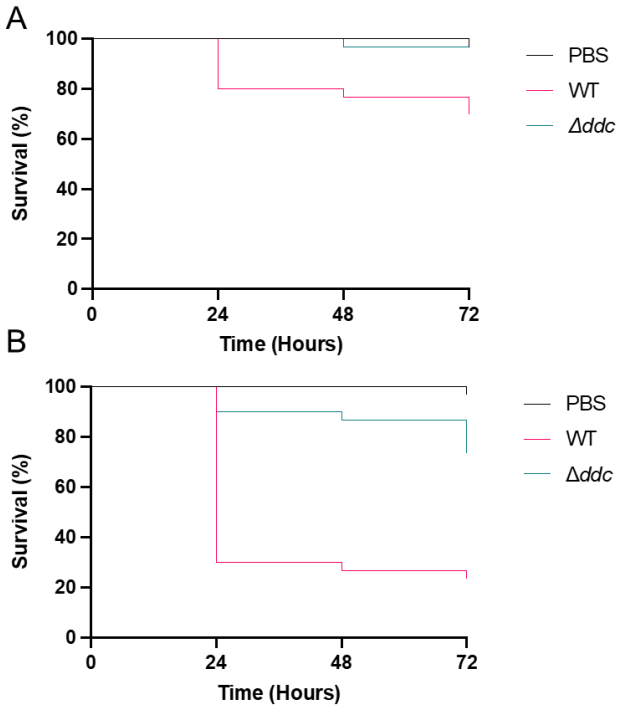

Figure 3.28. Deletion of the *ddc* gene results in attenuated virulence of *A. baumannii* 17978. Comparison of the percentage survival of *G. mellonella* 72 hours post-infection with an **(A)** $5x10^3$ and **(B)** $5x10^4$ CFU inoculum of *A. baumannii* 17978 wild type and Δ*ddc* strains. A vehicle and trauma control group were injected with PBS. A total of thirty larvae, across three groups of ten, were infected in each group. Statistical significance was determined using the log-rank Mantel-Cox test.

3.3.20 The attenuated virulence of the Δ*ddc* strain is possibly a result of increased antimicrobial peptide susceptibility

3.3.20.1 Deletion of *ddc* results in increased in vitro susceptibility to *Galleria mellonella* haemolymph

It was hypothesised that the attenuated virulence of the Δ*ddc* strain was possibly due to an increased susceptibility to antimicrobial peptides within the *G. mellonella* haemolymph. In brief, *G. mellonella* was inoculated with heat-killed *E. coli* MG1655. The haemolymph of inoculated larvae was extracted, and susceptibility was assessed by the radial diffusion method (Section 2.19). PBS and N-phenylthiourea were both used as negative controls. It was found that haemolymph extracted from larvae infected with heat-killed *E. coli* MG1655 showed an antimicrobial effect against the *A. baumannii* wild type and the Δ*ddc* strain (Figure 3.29). The Δ*ddc* strain showed marginally, but significantly, larger

zones of inhibition when compared to those of the wild type strain (P = 0.0021) (Figure 3.29). This shows that the Δ*ddc* strain may have increased susceptibility to antimicrobial peptides *in vivo* and may contribute to the attenuated virulence of the Δ*ddc* strain. However, it is worth noting the differences between inhibitory zones were marginal, suggesting that, despite the statistical significance, there may not be a biological difference *in vivo.* Therefore, further investigation would be needed to discern this.

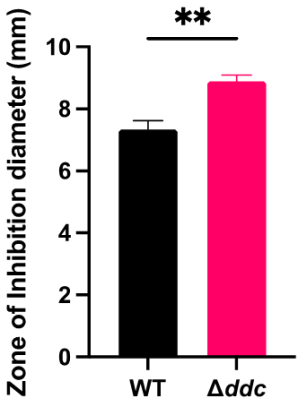

Figure 3.29. Deletion of the *ddc* gene increases the susceptibility of *A. baumannii 17978* to *G. mellonella* haemolymph. Comparison of the antimicrobial effect of haemolymph extracted from *G. mellonella*, 24 hours post-infection with heat-killed *E. coli* MG1655, against *A. baumannii* 17978 wild type and Δ*ddc*. Susceptibility was assessed using the radial diffusion method. *A. baumannii* wild type and Δ*ddc* strains were mixed with TSB minimal agar and poured into a 12 x 12 cm square petri dish. Once set holes were bored into the agar to create wells. Haemolymph extracted from larvae inoculated with heat-killed *E. coli* MG1655 was suspended in N-phenylthiourea and 10 µl of the suspension was dispensed into each well and allowed to diffuse into the agar for 3 hours. Plates were overlayed with TSB agar and incubated at 37 °C for 18 hours. Following incubation, the zone of inhibition diameter was measured. The values presented represent the mean and SEM of three independent experiments. ** = p-value 0.0021 (Mann-Whitney).

3.3.20.2 Infection with the Δ*ddc* strain does not alter the antimicrobial activity of *Galleria mellonella* haemolymph when compared to the wild type

It was also hypothesised that there may be differential antimicrobial peptide production when larvae are infected with the *A. baumannii* 17978 wild type and Δ*ddc*. In brief, larvae were infected with the wild type and Δ*ddc* strains.

Following 24-hour incubation, the haemolymph was extracted and the susceptibility of the wild type to the haemolymph was tested by radial diffusion method (Section 2.19). Haemolymph extracted from larvae infected with either the wild type or Δ*ddc* strain showed an antimicrobial effect against the wild type strain (Figure 3.30). The zones of inhibition were identical in diameter (Figure 3.30). There was no significant difference between the zone diameters indicating no detectable difference in antimicrobial peptide synthesis during infection with either strain. The haemolymph extracted from PBS-injected larvae showed minimal antimicrobial effect. This shows that injection with sterile PBS does not increase concentrations of antimicrobial peptides present in the larvae haemolymph to substantial levels.

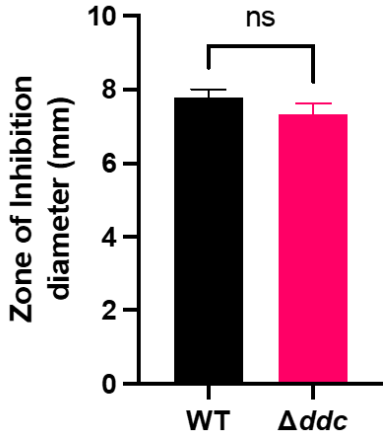

Figure 3.30. Infection with Δ*ddc* does not alter the antimicrobial properties of *G. mellonella* haemolymph. Comparison of the antimicrobial effect of haemolymph, on *A. baumannii* wild type, harvested from *G. mellonella* infected with either *A. baumannii* 17978 wild type or Δ*ddc*. Susceptibility was assessed using the radial diffusion method. *A. baumannii* wild type and Δ*ddc* strains were mixed with TSB minimal agar and poured into a 12 x 12 cm square petri dish. Once set holes were bored into the agar to create wells. Haemolymph extracted from larvae inoculated with heat-killed *E. coli* MG1655 was suspended in N-phenylthiourea and 10 µl of the suspension was dispensed into each well and allowed to diffuse into the agar for 3 hours. Plates were overlayed with TSB agar and incubated at 37 °C for 18 hours. Following incubation, the zone of inhibition diameter was measured. The values presented represent the mean and SEM of three independent experiments.

3.4 Chapter discussion

3.4.1 Loss of 1, 3-diaminopropane results in significant growth defect and alters cell morphology

Observation of the Δ*ddc* strain by microscopy resulted in the discovery of a cell division defect. This is the first documentation of the cell division and morphology defect following the loss of 1, 3-diaminopropane synthesis. It is worth noting that there is no reference to a similar defect in the 1, 3-diaminopropane transposon mutants previously investigated (Blaschke et al., 2021; Skiebe et al., 2012). While this seems unusual, microscopy of the deletion strains generated in this study was initially overlooked. It is possible observation of these mutant strains may have been neglected. It is difficult to comment on how the loss of 1, 3-diaminopropane synthesis affects cell division. I believe mutations discovered by WGS are not a contributing factor as the defect can be complemented by exogenous 1, 3-diaminopropane. With DNA being present within each cell in a chain (data not shown) it is clear that the chromosomes have been replicated and separated and that division is progressing due to visible membrane constriction (Figure 3.16). I believe this indicates that division is impacted toward the latter stages. Further investigation could begin with fluorescent membrane stains and amino acids to visualise membrane constriction and peptidoglycan synthesis. The major question posed by this observation is: why *A. baumannii* fails to septate following the loss of 1, 3-diaminopropane synthesis? I believe there are two possible explanations for this. The first is loss of 1, 3-diaminopropane may negatively affect the expression or function of proteins relating to cell division. The second possible explanation could be that loss of 1, 3-diaminopropane may directly alter metabolism or alter metabolism-related gene expression. There is precedent for this as in *S. pneumoniae* deletion of *cadA*, alters metabolic gene expression ultimately resulting in a reduction in peptidoglycan precursors (Ayoola et al., 2019). To investigate these possibilities several approaches could

be taken. RNA-Seq could be utilised for gene expression analysis. Ultra-performance liquid chromatography–high-resolution mass spectrometry (UPLC-HRMS) and mass spectrometry could be used for metabolomic and proteomic analysis. This investigation has highlighted a possible role for 1, 3-diaminopropane in cell division and suggests that 1, 3-diaminopropane may have a deeper role in *A. baumannii* 17978 biology beyond influencing virulence. Further investigation will develop an understanding of how *A. baumannii* utilises this important diamine for its cellular processes.

3.4.2 Loss of 1, 3-diaminopropane decreases biofilm formation

This chapter sought to investigate the role of 1, 3-diaminopropane in the virulence of *A. baumannii*. Deletion of the *ddc* gene significantly reduces biofilm formation (Figure 3.26) indicating a possible role for 1, 3-diaminopropane in biofilm regulation. While undertaking this investigation Blashcke et al (2021) also demonstrated that 1, 3-diaminopropane contributes to *A. baumannii* biofilm formation, corroborating the results generated here. This raises the question of how 1, 3-diaminopropane contributes to this process. Polyamines are known to influence the expression of proteins related to the regulation of biofilm-related genes (Sakamoto et al., 2012). Therefore, a similar function may be possible in *A. baumannii.* It is clear from the results presented in this study that 1, 3-diaminopropane is needed for motility but also contributes to biofilm formation. It seems unusual that this diamine would simultaneously regulate these vastly opposing phenotypes. A recent finding that sheds some light on this is the discovery of a 1, 3-diaminopropane acetyltransferase (Dpa) in *A. baumannii*. It has been determined that acetylation of 1, 3-diaminopropane promotes biofilm formation. The *dpa* gene is also upregulated in adhered cells, and deletion of *dpa* results in decreased biofilm formation but increased motility (Armalytė et al., 2023). This suggests two scenarios either 1, 3-diaminopropane acetylation shuts down the motility regulon promoting attachment, or the acetylated diamine activates biofilm formation. The results presented here show that motility and biofilm formation

rely on the synthesis and availability of 1, 3-diaminopropane. In light of the findings presented by Armalytė et al (2023), it is clear that alterations in the levels of 1, 3-diaminopropane through acetylation allow for changes in the lifestyle of *A. baumannii*. Further investigation is needed to fully understand the shift between 1, 3-diaminopropane and its acetylated form and how this potentially alters intracellular signalling and gene expression to enact this change. A possible approach for this could be assessing global gene expression using RNA-Seq. What is unexpected are the results following chemical complementation where exogenous 1, 3-diaminopropane induces biofilm overproduction in the Δ*ddc* strain (Figure 3.26). The possibility that 1, 3-diaminopropane affects crystal violet staining can be ruled out as the wild type strain is unaffected. Currently, it is difficult to comment on why there is an overproduction. It could be possible that the exogenous 1, 3-diaminopropane results in some form of dysregulation in the Δ*ddc* strain. However, further analysis is needed to understand this unexpected phenotype. The involvement of 1, 3-diaminopropane in biofilm formation poses a possible target for developing novel therapeutics to target the biofilm formation of this pathogen. Thus, further work should aim to investigate the role of 1, 3-diaminopropane in the lifestyles of *A. baumannii* and also in evaluating the role of this diamine in biofilm formation in environments more akin to those associated with infection such as medical devices and host tissue.

3.4.3 Loss of 1, 3-diaminopropane alters susceptibility to aminoglycosides

When conducting MIC assays with gentamicin small faint pellets were observed at the bottom of wells, suggesting possible growth or persistence of the Δ*ddc* strain. Aminoglycoside susceptibility has been linked to proton motive force (PMF) with altered PMF limiting uptake and effectiveness (Deng et al., 2020; Ribeiro et al., 2021; Webster et al., 2022). Therefore, I believe there is a link between the reduced growth rate and this potential persistence. Resistance to aminoglycosides can be conferred by mutation of the 16S rRNA gene (Garneau-

Tsodikova and Labby, 2016). However, these are rare as mutation of the 16S is often lethal. In the Δ*ddc* strain, none of the mutations identified are within the 16S rRNA gene. Of the mutations predicted to alter protein structure or be within intergenic regions, none have any known connection to aminoglycoside susceptibility within the literature. Therefore, I believe it is unlikely these mutations contribute to the results observed here. To further investigate this hypothesis genetic complementation of the Δ*ddc* strain followed by MIC assay could be carried out. With polyamines contributing to antimicrobial tolerance in some capacity in several organisms, an interesting possibility is a dual therapy using a novel therapeutic targeting Dat or Ddc and current antimicrobials. The results presented here show loss of 1, 3-diaminopropane does not alter antimicrobial susceptibility. This factor dramatically hinders the practicality of a dual polyamine inhibitor and antibiotic therapeutic approach to combat *A. baumannii*. This investigation has provided insight into how the loss of 1, 3-diaminopropane may further impact the cell, suggesting PMF could be altered following *ddc* deletion. It has also determined that 1, 3-diaminopropane does not contribute to antimicrobial tolerance as seen with polyamines in other bacterial species and suggests combination therapy may not have any added benefit in combating *A. baumannii*, ruling out this therapeutic strategy in the future.

3.4.4 Loss of 1, 3-diaminopropane increases susceptibility to host immune system factors

The virulence of the Δ*ddc* strain is attenuated in *G. mellonella* (Figure 3.28). As for an explanation for this, I believe several factors can be ruled out. Based on the exposure to H_2O_2 (Figure 3.27) I believe it is not related to susceptibility to host ROS. Secondly, I believe iron acquisition can also be ruled out as baumannoferrin, synthesised from 1, 3-diaminopropane, is not required for virulence (Sheldon and Skaar, 2020). The results suggest that attenuated virulence is linked to antimicrobial peptide susceptibility (Figure 3.29). It is difficult to speculate how the loss of 1, 3-diaminopropane may promote this

increased susceptibility. *G. mellonella* produces approximately twenty antimicrobial peptides (Ménard et al., 2021). AMPs commonly disrupt cell permeability. Polyamines interact with the cell surface, similar to divalent cations, and stabilise it against antimicrobial peptide action (Li et al., 2020). Loss of 1, 3-diaminopropane could therefore destabilise the outer membrane. This could be a possible explanation however the fact that the MIC of colistin is not decreased in the Δ*ddc* strain, suggests this may not be the case. If a lack of membrane stabilisation were responsible, the Δ*ddc* strain would likely be more susceptible to colistin. AMPs are capable of interacting with intracellular targets. Therefore, it could be possible that one or more of the AMPs within the haemolymph exert a greater effect on an intracellular target within the Δ*ddc* strain. To further investigate this hypothesis susceptibility assays could be done with purified or synthesised antimicrobial peptides (Andrejko et al., 2021; Correa et al., 2014). This investigation provides a potential reason for the attenuated virulence of the Δ*ddc* strain. Further investigation will determine how the loss of 1, 3-diaminopropane increases susceptibility to host AMPs and whether or not this applies to a mammalian host.

3.4.5 Limitations

There are several limitations to the investigation presented in this chapter. For division to occur membrane constriction and septal peptidoglycan synthesis and processing are required, and failure will result in septation defects. While the current fluorescent images show clear septal membrane constriction, they do not fully visualise the septum within these chains, meaning a full conclusion cannot be drawn at this stage. A limitation and oversight of the MIC assays conducted for all strains in this investigation is the lack of control strains used during testing. Control strains are used in MIC assays to confirm that the antibiotic stocks are working as intended with this being both concentration but also activity. The current data suggests that the antibiotics used functioning as expected, as the wild type and Δ*ddc* strains have equal MICs or MICs within one doubling dilution. However, there is still the need for control strains.

3.4.6 Conclusion

In this chapter, I aimed to investigate the role of 1, 3-diaminopropane in *A. baumannii.* This has provided new evidence that 1, 3-diaminopropane is involved in cell division through an unknown mechanism. This highlights a new understanding of the role of 1, 3-diaminopropane in *A. baumannii* biology. It has also been identified that 1, 3-diaminopropane contributes to biofilm formation an important element of *A. baumannii* virulence. The contribution of this diamine to biofilm formation provides the possibility that continued investigation may yield a novel anti-biofilm strategy to combat *A. baumannii* biofilm formation. In addition, it has provided a novel explanation for the attenuated virulence following the loss of 1, 3-diaminopropane synthesis. This expands the understanding of how *Acinetobacter* may utilise 1, 3-diaminopropane in its virulence and indicates how targeting of 1, 3-diaminopropane synthesis by a novel therapeutic may change interactions with the innate immune system. Complementation with other di- and triamines shows that *A. baumannii* has a specific requirement for 1, 3-diaminopropane. This is highly desirable as it shows that *A. baumannii* may not be capable of utilising host polyamines to replace 1, 3-diaminopropane and could mean the effects caused by a therapeutic of this nature would not be circumvented by polyamine replacement.

Chapter 4 Role of 1, 3-diaminopropane in *Klebsiella pneumoniae*

4.1 Chapter introduction

little is known about the roles of polyamines in *K. pneumoniae*. It is hypothesised that *K. pneumoniae* 52145 encodes the known pathways for 1, 3-diaminopropane, putrescine, cadaverine, and spermidine (Morris, 2017). Previously deletion of the Δ*SpeED* genes resulted in *K. pneumoniae* resulted in the reduction in capsule formation the loss of the distinct hypermucoviscous phenotype, and reduced biofilm formation (Morris, 2017). In addition to this, some investigation into the role of cadaverine produced in *K. pneumoniae* NTUH-K2044 has been conducted. This revealed that expression of the *cadCBA* operon promotes growth under acidic conditions (Hsieh et al., 2010). The polyamine transporter, MdtjI has also been identified in *K. pneumoniae*. Exposure of *K. pneumoniae* MGH 78578 to pulmonary surfactant was found to increase expression of the spermidine transporter (Willsey et al., 2018). This suggests a possible role of polyamines in the virulence and infection of *K. pneumoniae*. However, the knowledge surrounding 1, 3-diaminopropane synthesis and its role in the cell is limited. 1, 3-diaminopropane has previously been detected in the *Klebsiella* genus (Hamana, 1996), but has never been fully investigated. If 1, 3-diaminopropane is involved in the virulence of *K. pneumoniae* it would potentially make it a viable therapeutic target, similar to that in *A. baumannii.* With the additional benefit of a *de novo* 1, 3-diaminopropane synthesis absent in mammalian cells.

4.2 Research aims

- To generate markerless deletions of the *dat* and *ddc* genes in *Klebsiella pneumoniae* 52145
- Examine phenotypic differences due to *dat* and *ddc* deletion to further understand the role of 1, 3-diaminopropane in the virulence of *K. pneumoniae*
- To complement any observed phenotypes chemically or genetically
- Determine the conservation of *dat* and *ddc* across other species

4.3 Chapter results

4.3.1 The genomic location, size and structure of 1, 3-diaminopropane synthesis genes in *K. pneumoniae* 52145

Sequencing and annotation of the *K. pneumoniae* 52145 genome (Bialek-Davenet et al., 2014) indicates the *dat* gene (BN49_2899) is 1386 bp in length and encodes the PLP-dependent L-2, 4-diaminobuyrate: 2-ketoglutarate aminotransferase. Downstream of *dat* lies the *ddc* gene (BN49_2900) that is 1482 bp in length and encodes the PLP-dependent L-2, 4-diaminobutyrate decarboxylase. Upstream of *dat* and *ddc* lies BN49_ 2898 which encodes an unknown protein, thought to be similar to putative thiamine biosynthesis protein HI_0357 in *Haemophilus influenzae*. Downstream of *dat* and *ddc* lies the gene BN49_2901, which encodes an unknown protein, similar to a putative transcriptional regulator, from the LysR family from *Pectobacterium carotovorum*.

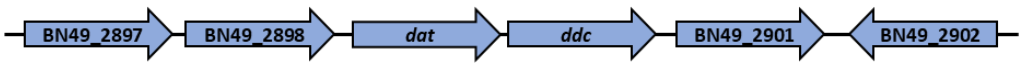

Figure 4.1. The genomic organisation of the *dat* and *ddc* genes. 7.5 Kb region of the *K. pneumoniae* 52145 reference genome showing the location of the *dat* and *ddc* genes and the upstream and downstream genes within the region.

4.3.2 Deletion of 1, 3-diaminopropane synthesis genes in *K. pneumoniae* 52145

4.3.2.1 Construction and confirmation of *K. pneumoniae* 1, 3-diaminopropane synthesis deletion vectors and *E. coli* donor strains

To generate markerless deletions in *K. pneumoniae,* deletion vectors were constructed using the same methodology used for deletion in *A. baumannii* (Figure 3.5). The presence of suicide vectors in *E. coli* β2163 was confirmed by PCR. The screening was carried out on a single pGPI-SceI-Δ*dat* and two pGPI-SceI-*Δddc* vectors. PCR amplified the full constructs using the Kp_datddc_UpF1 and Kp_datddc_DwnR1 primer pair (Figure 4.2A). Kp_datddc_UpF1 and Kp52_datddc_UpR1 primer pair were used to amplify the upstream fragment of pGPI-SceI-Δ*dat* and Kp_datddc_DwnF2 and Kp_datddc_DwnR1, for the downstream (Figure 4.2A). Kp_datddc_UpF1 and Kp_datddc_UpR2 were used for amplification of the upstream fragment of pGPI-SceI-*Δddc* and Kp_datddc_DwnF1 and Kp_datddc_DwnR1, for the downstream (Figure 4.2A). All vectors analysed were positive for the correct insertion of deletion constructs. The pGPI-SceI-Δ*dat* produced amplicons of 2.7 Kbp for the full construct (Figure 4.2B), 0.7 Kbp for the up fragment (Figure 4.2B). and 2 Kbp for the down fragment (Figure 4.2B). The pGPI-SceI-Δ*ddc* produced amplicons of 2.6 Kbp for the full construct (Figure 4.2B), 2.1 Kbp for the up fragment (Figure 4.2B) and 0.5 Kbp for the down fragment (Figure 4.2B). This confirms the presence of the correct deletion vectors in each *E. coli* β2163 strain.

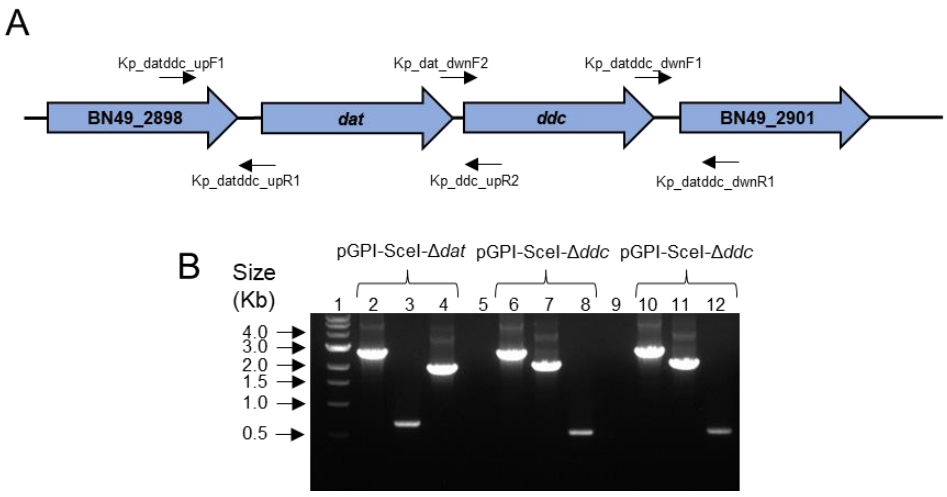

Figure 4.2. Confirmation of vectors for single deletion of the *dat* and *ddc* genes in *K. pneumoniae* 52145. (A) Diagram of the predicted amplification of the full deletion constructs and their constituent upstream and downstream fragments. The full constructs were amplified using the Kp_datddc_UpF1 and Kp_datddc_DwnR1 primer pair. Kp_datddc_UpF1 and Kp52_datddc_UpR1 primer pair were used to amplify the upstream fragment of pGPI-SceI-Δ*dat* and Kp_datddc_DwnF2 and Kp_datddc_UpR1, for the downstream. Kp_datddc_UpF1 and Kp_datddc_UpR2 were used for amplification of the upstream fragment of pGPI-SceI-Δddc and Kp_datddc_DwnF1 and Kp_datddc_DwnR1, for the downstream. **(B)** Lane 1: 1 Kbp ladder. Lane 2: Amplification of the full Δ*dat* construct. Lane 3: Amplification up fragment portion of the Δ*dat* construct. Lane 4: Amplification of the down fragment portion of the Δ*dat* construct. Lane 6/10: Amplification of the full Δ*ddc* construct. Lane 7/11: Amplification up fragment portion of the Δ*ddc* construct. Lane 8/11: Amplification of the down fragment portion of the Δ*ddc* construct.

4.3.2.2 Confirmation of the Δ*dat* and Δ*ddc* deletions in *K. pneumoniae* 52145

Previous members of the Hobley Lab had unsuccessfully attempted deletion of the *dat* and *ddc* genes simultaneously. Despite this, attempts were made as part of this body of work but again were unsuccessful. Single deletions of the *dat* and *ddc* genes were therefore attempted. Presumptive gene deletions were screened for trimethoprim susceptibility and were later confirmed by PCR, using the Kp_datddc_outF and Kp_datddc_outR primer pair, that bind outside of the deletion region amplifying inwards toward the deleted gene (Figure 4.3A). Amplification of the *dat* and *ddc* loci from the wild type genomic DNA results in a product of 4.6 Kbp (Figure 4.3B). The pGPI-SceI-Δ*dat* and pGPI-SceI-Δ*ddc* vectors were used as the negative controls for PCR, due to the

primers binding outside the region used in the deletion construct (Figure 4.3B). Amplification of the *dat* and *ddc* loci from genomic DNA from three presumptive Δ*dat* and Δ*ddc* deletion strains produced amplicons of approximately 3.2 Kbp and 3.1 Kbp, respectively (Figure 4.3B). This confirms the deletion of the *dat* and *ddc* genes in the respective strains. Final deletion confirmation used Sanger sequencing (Section 2.5.1) and whole genome sequencing (Section 2.5.3). Sequencing of the deletion regions found a complete absence of the *dat* and *ddc*, in the corresponding deletion strains. WGS further verified this, confirming the successful deletion of the 1, 3-diaminopropane synthesis genes. The successful deletion of the *dat* and *ddc* suggests that 1, 3-diaminopropane synthesis is not essential for the growth of *K. pneumoniae* 52145.

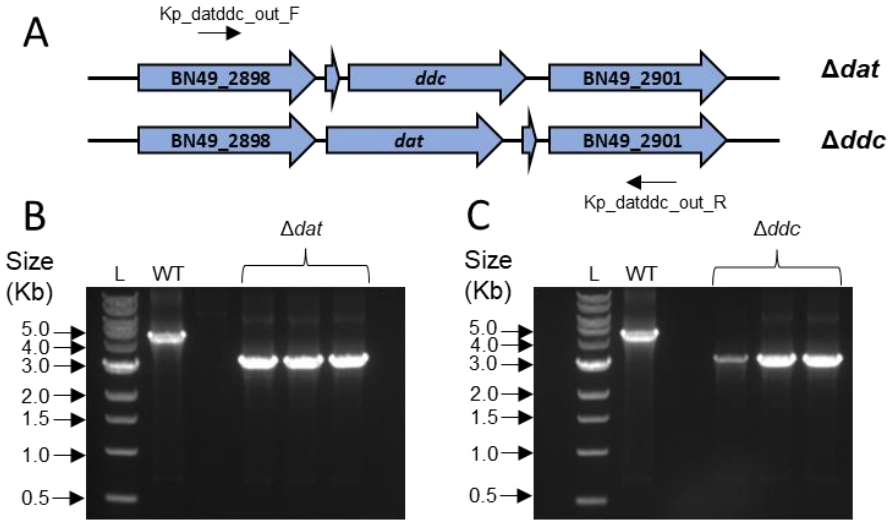

Figure 4.3. Confirmation of the deletion of *dat* and *ddc* genes of *K. pneumoniae* 52145. (A) Diagram of the amplification across the chromosomal region containing the *dat* and *ddc* genes showing the primers used to confirm the deletion of each gene. Agarose gel confirming the successful deletion of **(B)** *dat* and **(C)** *ddc* genes in *K. pneumoniae* 52145 using the Kp_datddc_outF and R primer pair amplifying a product of 4.6 Kbp for the wild type genes and products of 3.2 Kbp and 3.1 Kbp for the Δ*dat* and Δ*ddc*, respectively. L: 1 Kbp ladder. WT: Genomic DNA extracted from *K. pneumoniae* 52145. Δ*dat*: Genomic DNA extracted from presumptive Δ*dat* strains. Δ*ddc*: Genomic DNA extracted from presumptive Δ*ddc* strains.

4.3.2.3 Point mutations present in the Δ*dat* and Δ*ddc* deletion strains

Sequencing revealed the presence of point mutations within the deletion region of the Δ*dat* and Δ*ddc* strains and WGS further confirmed this. Sequencing of the Δ*dat* strain and comparison to the reference genome (GenBank Accession: FO834906.1) shows the presence of eleven SNPs and nine insertions. Of those SNPs, six occur in the wild type, while all the insertions are shared with the wild type strain. Of the unique SNPs, four were found within ORFs (Table 4.1). The Δ*ddc* strain features sixteen SNPs, ten insertions and one deletion when compared to the reference genome. Of those sixteen SNPs eleven occur in the wild type, while nine of the insertions are shared with the wild type. Of the additional SNPs, all five were found to be within ORFs. The additional insertion in Δ*ddc* and the deletion, not present in the wild type strain, were found to be within intergenic regions (Table 4.1). While mutations naturally occur there is a possibility that some could arise from genetic manipulation. Therefore, of particular importance are mutations that have potentially arisen from the deletion of the *dat* and *ddc* genes. In the Δ*dat* strain there are three point mutations present in the *ddc* gene (Table 4.1). The first two are synonymous mutations while the third is a missense mutation (Table 4.1). Missense3D suggests that this mutation does not cause structural damage (Table 4.1). Deletion of the *ddc* gene was found to have introduced four point mutations in the *dat* gene. The first is synonymous, while the second introduces a stop a premature stop codon in place of glutamine at position 250 of the amino acid sequence. This would result in the translation of a truncated protein (Table 4.1). The deletion also introduces a mutation in the upstream gene (BN49_2898) (Table 4.1). Analysis with Missense3D predicts that none of the SNPs in either strain result in structural damage to the proteins they affect.

Table 4.1. SNPS unique to *K. pneumoniae* 52145 Δ*dat* and Δ*ddc* strains

SNPS unique to *K. pneumoniae* 52145 Δ*dat*					
Nucleotide position	Allele in WT (amino acid residue)	Allele in mutant strain (amino acid residue)	Gene	Description	Possible effect on the structure of the protein
1222640	A	G	Intergenic	Downstream of *clpB*, encoding chaperone protein ClpB and upstream of the gene encoding small Subunit Ribosomal RNA	
3010594	A (E19)	G (E19)	BN49_RS16320 (*ddc*)	Aspartate aminotransferase family protein	Synonymous mutation
3011047	T (R170)	C (R170)			Synonymous mutation
3011825	G (A430)	A (T430)			No structural damage
5229800	T	A	BN49_RS26915	LuxR C-terminal-related transcriptional regulator	No structural damage
SNPS unique to *K. pneumoniae* 52145 Δ*ddc*					
348718	C	CT	Intergenic	Downstream of *asd*, predicted to encode an aspartate semialdehyde dehydrogenase and upstream of *glgB* gene, predicted to encode a 1, 4- alpha-glucan-branching enzyme	
3008700	A (Q267)	G (R267)	BN49_RS16310	ABC transporter substrate-binding protein	Q267R results in loss of H-bond with Q185 in a predicted thiamine biosynthesis protein. No structural damage
3009029	GT	G	Intergenic	Downstream of BN49_RS16310 and upstream of the *dat* gene	
3009724	T (Y194)	C (Y194)	BN49_RS16315 (*dat*)	L-2, 4-diaminobuyrate: 2-ketoglutarate aminotransferase	Synonymous mutation
3009890	C (Q250)	T (Stop codon)			Premature stop codon at position 250 results in truncated protein
3010029	C (A296)	T (V296)			No structural damage
3010112	T (F324)	C (L324)			No structural damage

4.3.3 Expression of 1, 3-diaminopropane synthesis genes

4.3.3.1 Expression of the *dat* and *ddc* genes

Little is known about the role of 1, 3-diaminopropane in *K. pneumoniae*, while there are genes encoding Dat and Ddc, it is unknown whether they are expressed. To assess this RT-PCR was carried out on total RNA extracted from exponentially growing *K. pneumoniae* 52145 wild type and the *Δdat* and Δ*ddc* strains. Primers were designed to anneal within the *dat* gene, amplifying a product of 81 bp and within the *ddc* gene, amplifying a product of 102 bp if each mRNA transcript was present (Figure 4.4A). The *rpoB* gene was used as an expression control, primers were designed to amplify a 120 bp product. RT-PCR produced the expected 81 bp and 102 bp products for the *dat* and *ddc* genes, respectively (Figure 4.4B). This confirms that the *dat* and *ddc* genes are expressed in *K. pneumoniae* 52145 under normal physiological conditions. There was a lack of RT-PCR product from the *dat* gene in the Δ*dat* strain and a lack of product from the ddc gene in the Δ*ddc* strain. This confirms that deletion of the *dat* and *ddc* genes abolishes their expression. RT-PCR was also carried out to assess the expression of the *ddc* gene in the ∆*dat* mutant and the *dat* gene in the ∆*ddc* mutant. RT-PCR showed a product for the *dat* gene in the Δ*ddc* mutant and the *ddc* gene in the Δ*dat* mutant. This indicates the expression of the downstream or upstream open reading frames is not impacted by the deletion of the *dat* and *ddc* genes (ORF).

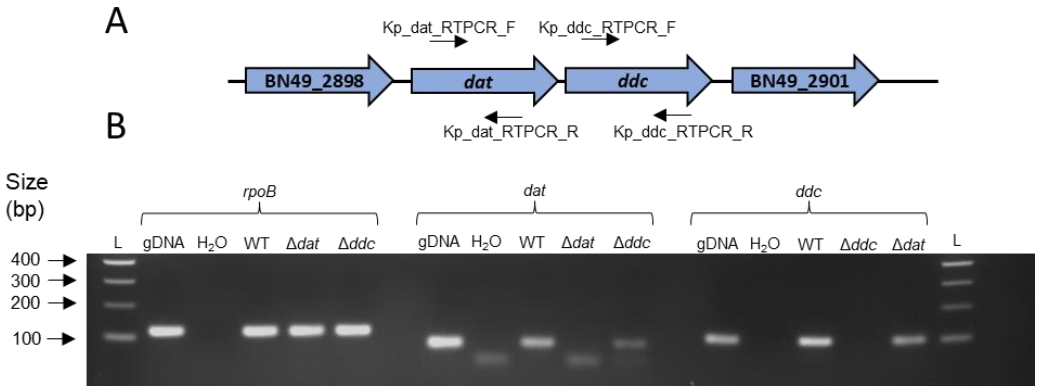

Figure 4.4. The *dat* and *ddc* genes of *K. pneumoniae* 52145 are expressed during exponential growth. (A) Diagram of the predicted amplification within the *dat* and *ddc* genes of *K. pneumoniae* 52145, indicating the primer pair used and annealing sites. **(B)** Reverse transcriptase PCR performed on RNA isolated from exponentially growing *K. pneumoniae* 52145 wild type, Δ*dat* and Δ*ddc* strains, using primers to amplify internally of the *rpoB*, *dat* and *ddc* genes. The Kp_rpoB_RTPCR_F and Kp_rpoB_RTPCR_R pair were used for the *rpoB* gene amplifying a product of 120 bp. The Kp_dat_RTPCR_F and Kp_dat_RTPCR_R pair were used for the *dat* gene amplifying a product of 81 bp. The Kp_ddc_RTPCR_F and Kp_ddc_RTPCR_R pair were used for the *ddc* gene amplifying a product of 102 bp. L: 100 bp ladder. gDNA: Wild type genomic DNA positive control. H_2O: negative nucleic acid control. WT: RNA extracted from wild type strain. Δ*dat*: RNA extracted from Δ*dat* strain. Δ*ddc*: RNA extracted from Δ*ddc* strain. RT-PCR is representative of two independent repeats.

4.3.3.2 Co-transcription of the *dat* and *ddc* genes

RT-PCR established that the *dat* and *ddc* of *A. baumannii* 17978 are expressed as a single transcriptional unit (Section 3.3.2.2). Therefore, it is reasonable to hypothesise that this is also the case in *K. pneumoniae* 52145.

4.3.3.2.1 Identification of possible terminator sequences

To begin investigating co-expressed of the *dat* and *ddc* genes transcriptional terminator sequences in the genome of *K. pneumoniae* 52145 were predicted. Analysis was first carried out with TransTermHP to predict intrinsic terminators. A predicted terminator was not found within the *ddc* ORF for *dat*. It was able to predict terminators for BN49_2898, upstream of the *dat* ORF and for the *ddc* ORF (Table 4.2 and Figure 4.5). Further analysis was carried out to determine the presence of Rho-dependent terminators using RhoTermPredict. This also suggested a lack of terminator sequence in the *ddc* ORF for *dat*. This lack of

either terminator suggests that the *dat* and *ddc* genes are co-expressed as a single transcriptional unit.

Table 4.2 Predicted intrinsic terminators upstream and downstream of the *dat* ORF

ORF	Terminator start	Terminator end	Sequence 5' – 3'
BN49_2898	3008847	3008872	cgctgacggaaggcattccgtcagcg
ddc	3012074	3012094	gccgataatgtccttatcggc

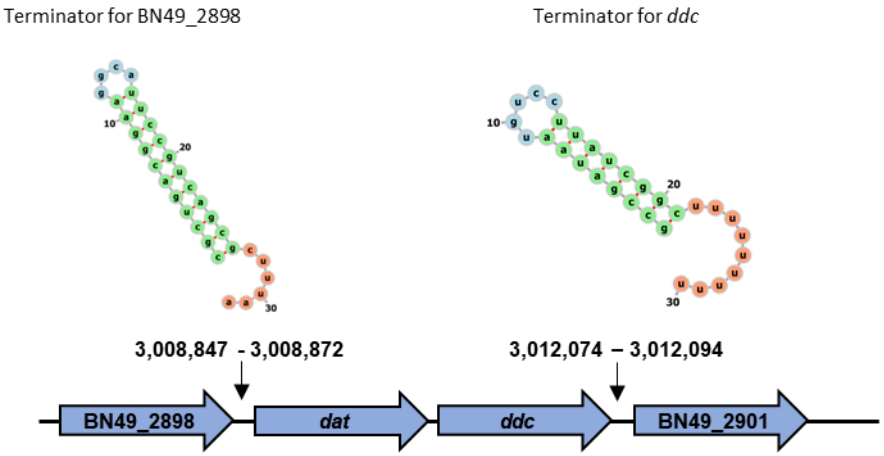

Figure 4.5. The *dat* ORF of *K. pneumoniae* 52145 does not have a dedicated intrinsic terminator. The predicted intrinsic terminators upstream and downstream of the dat ORF within the *k. pneumoniae* 52145 reference genome and the predicted RNA secondary structure formed by the predicted sequences. Intrinsic terminators were predicted TransTermHP and RNA secondary structure predicted with MXfold2 webserver.

4.3.3.2.2 Co-transcription of the *dat* and *ddc* genes

To assess co-transcription of the *dat* and *ddc* genes primers were designed to amplify across the 9 bp intergenic gap between the two genes producing an RT-PCR product of 550 bp with the product (Figure 4.6A). It appears RT-PCR did not produce the expected 550 bp product. However, upon closer inspection of the agarose gel, there appears to be a faint RT-PCR product for the co-expression of the two genes (Figure 4.6B). As a control, RT-PCR was carried out for the *dat* and *ddc* genes both produced the 81 and 102 bp products (Figure 4.6B) confirming the presence of a transcript of each gene. This evidence suggests that the *dat* and *ddc* of *K. pneumoniae* 52145 are co-expressed, the

same as their homologues in *A. baumannii*. The faint band produced for the suggests a possible issue within the RT-PCR. When analysed, the primers for co-transcriptional were predicted to be incapable of dimer and secondary structure formation, suggesting these may not be the reason for poor amplification. The presence of PCR products from the genomic DNA template indicates that the problem with the reaction lies with the mRNA and amplification across the intergenic region.

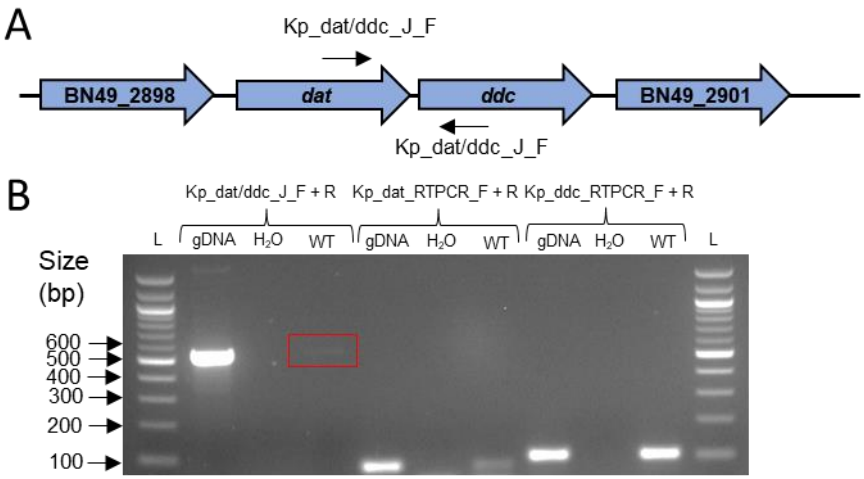

Figure 4.6. The *dat* and *ddc* genes are co-expressed in *K. pneumoniae 52145*. (A) Diagram of the predicted amplification across the intergenic region between the *dat* and *ddc* genes of *K. pneumoniae* 52145, indicating the primer pair used and their annealing site. **(B)** Reverse transcriptase PCR performed on RNA isolated from exponentially growing *K. pneumoniae* 52145 wild type strain, using Kp_dat/ddc_J_F and Kp_dat/ddc_J_R primer pair to amplify across the intergenic region between the *dat* and *ddc* genes with the expected amplified product being 550 bp. Additional RT-PCR was carried out with Kp_dat_RTPCR_F and Kp_dat_RTPCR_R pair, amplifying a product of 81 bp and Kp_ddc_RTPCR_F and Kp_ddc_RTPCR_R pair, amplifying a product of 102 bp to confirm the expression of the *dat* and *ddc* genes, respectively. L: 100 bp ladder. gDNA: Wild type DNA positive control. H_2O: negative control. WT: RNA extracted from wild type strain. RT-PCR is representative of two independent repeats.

4.3.4 Analysis of the polyamines produced by *K. pneumoniae* 52145

HPLC was carried out to determine the intracellular pool of polyamines in the wild type, Δ*dat* and Δ*ddc* strains (Section 2.10). Derivatised samples were analysed by Aaron Franklin in Dr Patrick Moynihan's laboratory, at The University of Birmingham. Alongside samples known polyamine standards

were assessed. The chromatogram presented in Figure 4.7, represents the retention times for each standard. 1, 3-diaminopropane is detected at approximately 15.9 minutes, putrescine is detected at 16 minutes, the added internal standard 1, 7-diaminoheptane is detected at 16.5 minutes and spermidine is detected at 17 minutes.

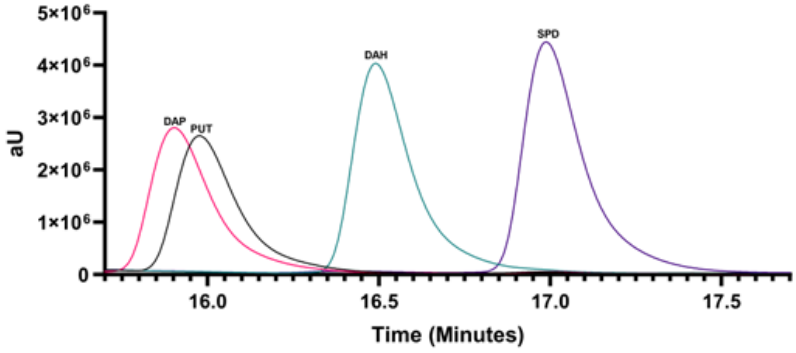

Figure 4.7. Retention times of 1, 3-diaminopropane, putrescine, 1, 7-diaminoheptane and spermidine polyamine standards. Separation of polyamines standards and the corresponding retention times of 1, 3-diaminopropane, DAP; putrescine, PUT; 1, 7-diaminoheptane, DAH; spermidine, SPD.

All samples analysed feature a peak corresponding to the retention time of the added internal standard 1, 7-diaminoheptane (Figure 4.8). This was used to determine the relative abundance of each polyamine in a given sample. Growth of the *K. pneumoniae* wild type strain in M9 minimal media altered to pH 6.5 produced detectable levels of putrescine and spermidine (Figure 4.8A). Putrescine shows a greater abundance when compared to spermidine (Figure 4.8A). Unexpectedly, there is not a detection of 1, 3-diaminopropane, in either sample. While this may imply that 1, 3-diaminopropane is not synthesised by *K. pneumoniae* 52145 it could be attributed to the vast abundance and detection of putrescine that obscures the ability to separate the diamine and 1, 3-diaminopropane. Analysis of the Δ*dat* and Δ*ddc* strains revealed that they produce putrescine and spermidine (Figure 4.8B and C) again with putrescine showing a greater relative abundance when compared to spermidine (Figure 4.8B and C). While it is highly probable that both strains do not produce 1, 3-diaminopropane, this cannot be confirmed when the separation issues are considered. Analysis of the Δ*speAB,* Δ*speABC* and Δ*speABCE* was also carried

out. Both strains lack putrescine synthesis and show detectable levels of 1, 3-diaminopropane (Figure 4.8E and F). This confirms that *K. pneumoniae* 52145 synthesises 1, 3-diaminopropane and deletion of the *speABCE* genes abolish putrescine and spermidine synthesis. The Δ*speAB* strain was found to synthesise putrescine, spermidine and cadaverine (Figure 4.8D). Interestingly the Δ*speABC* strain shows a peak for a polyamine, corresponding to the spermidine retention time (Figure 4.8D). With an inability to synthesise putrescine, in theory, this strain should be incapable of spermidine synthesis. It has previously been hypothesised (pers. comm. Dr L Hobley, University of Nottingham) that spermidine synthase, encoded by *speE*, may aminopropylate other diamines in addition to putrescine. Therefore, this product could be the spermidine analogue norspermidine, derived from 1, 3-diaminopropane. This analysis confirms that putrescine spermidine and 1, 3-diaminopropane are all synthesised by *K. pneumoniae* 52145, with putrescine appearing to be the major polyamine. The results observed with the *speABC* strain also support the hypothesis that SpeE of *K. pneumoniae* may synthesise additional spermidine analogues. However, further investigation is needed to determine this.

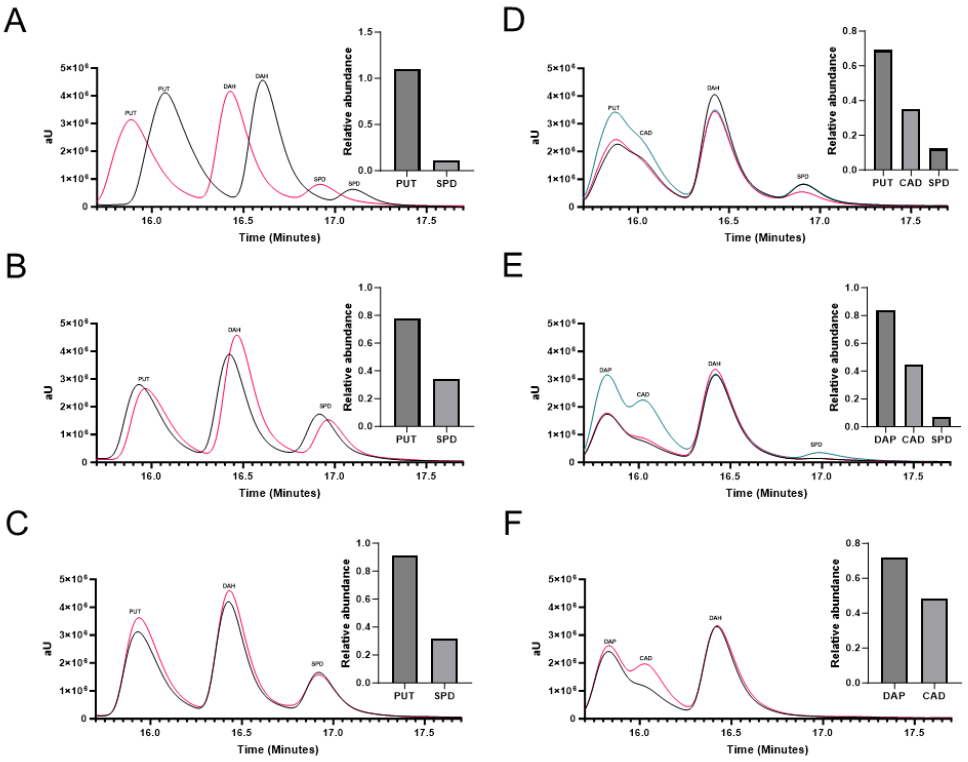

Figure 4.8. 1, 3-diaminopropane is synthesised by *K. pneumoniae* 52145. Comparison of the detection of polyamines produced by *K. pneumoniae* **(A)** wild type, **(B)** Δ*dat*, **(C)** Δ*ddc*, **(D)** Δ*speAB*, **(E)** Δ*speABC*, **(F)** Δ*speABCE* strains, when grown at pH 6.5, by HPLC and their relative abundance. Cells were grown in M9 minimal media, devoid of exogenous polyamines. 15 µl of 0.4 mM 1,7-diaminoheptane was added to each sample as an internal standard. Polyamines were extracted with trichloroacetic acid: HCl extraction and derivatised with dansyl chloride. DAP, 1, 3-aminopropane; PUT, putrescine; CAD, cadaverine; DAH, 1, 7-diaminoheptane; SPD, spermidine. Data presented for the wild type, Δ*dat*, Δ*ddc* and Δ*speABCE* strains represent two biological repeats. The data presented for the Δ*speAB* and Δ*speABC* strains are representative of three biological.

4.3.5 Deletion of the *dat* or *ddc* genes does not alter *K. pneumoniae* hypermucoviscous phenotype

The search for a detectable phenotype arising from the deletion of the *dat* and *ddc* began with the investigation of capsule production. Capsule production is a key element in *K. pneumoniae* virulence, and the loss of capsule synthesis attenuates virulence (Insua et al., 2013). If polyamines are linked to CPS expression targeting their synthesis would be a beneficial approach to treating *K. pneumoniae* infection. The Δ*dat* and Δ*ddc* strains did not appear to exhibit any growth defects. Colonies had the same mucoid appearance and when

centrifuged both demonstrated the same capsulated pellet as the wild type strain suggesting capsulation. The hypermucoviscous phenotype of the Δ*dat* and Δ*ddc* was assessed using the string test (Section 2.13). For comparison, the Δ*manC* was used as a capsule negative control. This acapsular strain features a deletion of the *manC* gene that encodes Mannose-1-phosphate guanylyltransferase, an enzyme involved in capsular polysaccharide production. The Δ*speE* strain was also included for comparison. When the string test was performed on colonies the length was comparable between the wild type, Δ*dat* and Δ*ddc* strains on both LB and M9 minimal agar (Figure 4.9) with no significant difference in string length between the wild type and either the Δ*dat* or Δ*ddc* strains. Growth of all three strains on M9 minimal agar increased the string length (Figure 4.9B), compared to those observed on LB agar (Figure 4.9A), indicating that nutrient availability impacts the capsule formation of *K. pneumoniae.* As expected, the Δ*manC* and Δ*speE* strains did not form strings on either agar (Figure 4.9). This shows that 1, 3-diaminopropane is not required for the capsule formation or the hypermucoviscous phenotype of *K. pneumoniae* 52145.

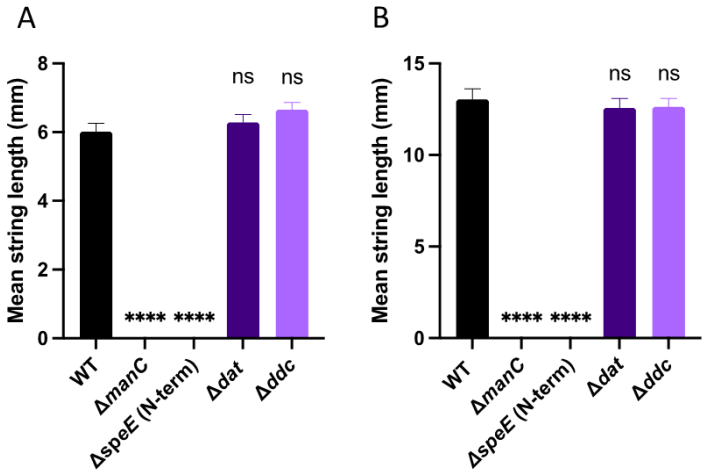

Figure 4.9. Deletion of the *dat* and *ddc* genes does not impact capsule formation or the hypermucoviscous phenotype of *K. pneumoniae* 52145. The mean string length produced when grown on **(A)** LB or **(B)** M9 minimal agar as an inoculation loop is moved vertically from a colony of 2-4 mm in diameter. Δ*manC* was used as a capsule negative control and Δ*speE* (N-term) was previously shown to have significantly reduced capsule expression. The values presented represent the mean and SEM of ten measurements of three independent experiments. **** = p-value ≤ 0.0001 (unpaired t-test with Welch's correction).

4.3.6 Deletion of *dat* or *ddc* does not affect the growth kinetics of *K. pneumoniae* 52145

Following the deletion of the *dat* and *ddc* genes investigation sought to determine the potential impact of the deletion on the growth of *K. pneumoniae*. Isolation of each mutant, planktonic growth and growth on agar all confirm that 1, 3-diaminopropane is not essential for the growth of *K. pneumoniae*. However, the possibility of each mutant having altered growth kinetics could not be ruled out. To test this stationary phase cultures were diluted in LB broth at pH 7.5, 5.5, 4 and 3 and growth kinetics were monitored by OD (Section 2.12.1). Growth of the Δ*dat* and Δ*ddc* strains revealed that both appear to phenocopy the wild type strain across all growth conditions (Figure 4.10). There was no significant difference between the Δ*dat* and Δ*ddc* growth rates (Table 9.2) when compared to the wild type strain across the pH range. At pH 7.5 and 5.5 growth begins to slow following 4 hours (Figure 4.10A and B) approaching a plateau in optical density at approximately 6 hours (Figure 4.10A and B). While at pH 4 growth slowly increases through the time course (Figure 4.10C) where it begins to slow at 7 hours and begins to plateau at 8 hours (Figure 4.10C). All three strains reach a comparative final optical density at pH 7.5, 5.5 and 4 (Figure 4.10). Subjecting all three strains to pH 3 results in little alteration in the optical density across the 8 hours (Figure 4.10D). When enumerated, following the final time point, very few viable cells were recovered. This suggests that, without prior adaptation to acidic pH, neither the wild type nor the Δ*dat* or Δ*ddc* are capable of prolonged survival at pH 3. Overall, the results observed at pH 7.5, 5.5 and 4 suggest that loss of 1, 3-diaminopropane synthesis does not alter the growth kinetics of *K. pneumoniae* in a nutrient-rich environment.

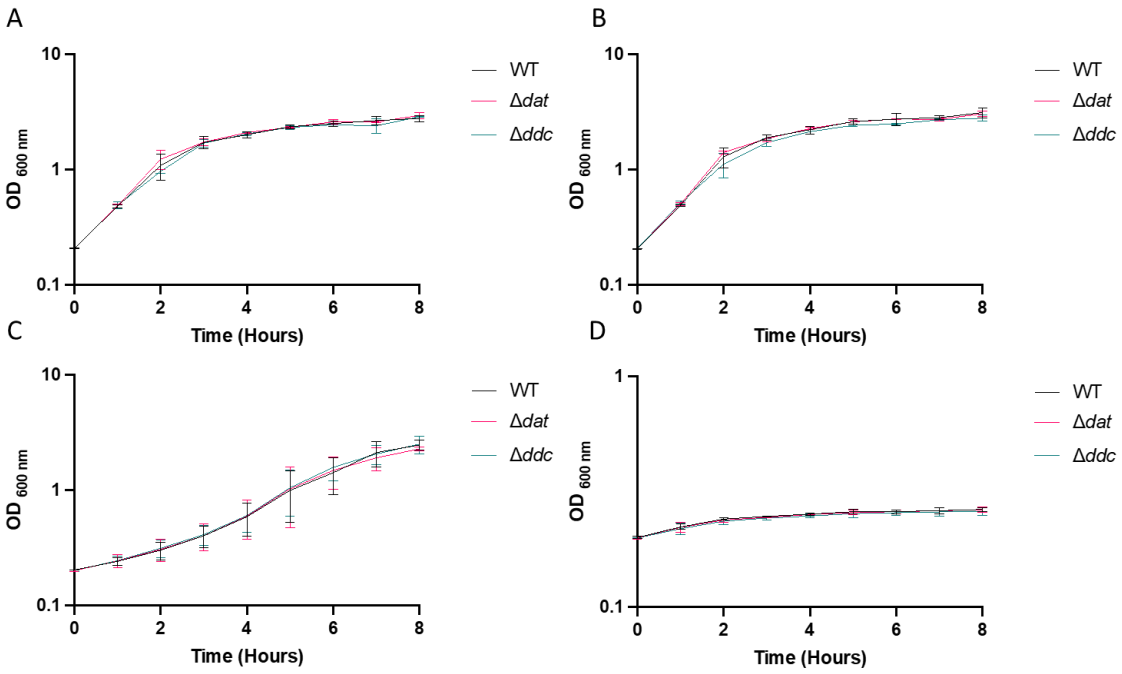

Figure 4.10. Deletion of the *dat* and *ddc* genes does not affect the growth kinetics of *K. pneumoniae* 52145. Comparison of the planktonic growth of K. *pneumoniae* wild type and the Δ*dat* and Δ*ddc* strains in LB broth at varying pH **(A)** 7.5, **(B)** 5.5, **(C)** 4 and **(D)** 3. The OD_{600nm} was measured every hour across and 8-hour period. Values represent the mean and SEM of three independent experiments.

4.3.7 Δ*dat* and Δ*ddc* exhibit altered biofilm formation of *K. pneumoniae* 52145

Due to the loss of 1, 3-diaminopropane synthesis reducing biofilm formation in *A. baumannii* 17978 (Section 3.3.15) and that biofilm formation is a key element in *K. pneumoniae* virulence the effect of the *dat* and *ddc* deletions on *K. pneumoniae* 52145 biofilm was investigated. Biofilm formation was assessed using a modified 96-well plate crystal violet staining assay (Section 2.16). The Δ*ompA* strain was used as a control strain as the deletion of *ompA* results in a significant decrease in biofilm formation. The *K. pneumoniae* wild type strain formed the greatest biofilm of the strains tested (Figure 4.11). The deletion of the *dat* and *ddc* genes resulted in significantly less biofilm formation when compared to the wild type strain (P = <0.0001 and P = 0.0002) (Figure 4.11). The Δ*ddc* strain formed more biofilm than the Δ*dat* (Figure 4.11). As expected, the Δ*ompA* control strain formed significantly less biofilm when compared with the wild type (P = <0.0001) and the least of all strains tested (Figure 4.11). The

ability of Δ*dat* and Δ*ddc* to form biofilm shows that 1, 3-diaminopropane is not essential for biofilm formation in *K. pneumoniae* but that it is required for wild type levels of biofilm formation and that targeting of 1, 3-diaminopropane could be a possible anti-biofilm strategy.

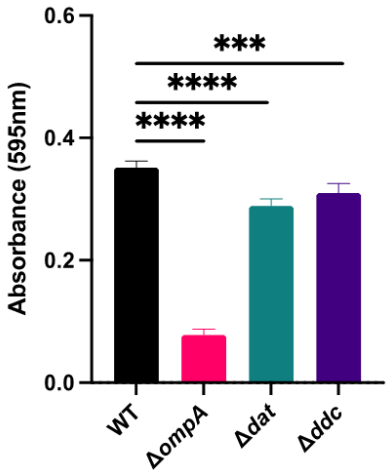

Figure 4.11. Deletion of the *dat* and *ddc* genes reduces the levels of biofilm formed by *K. pneumoniae* 52145 in MES-buffered M9 minimal salt media (pH 6.5). Comparison of biofilm formed by *K. pneumoniae* 52145 wild type and 1, 3-diaminopropane deletion strains in a 96-well plate. Biofilm was quantified with crystal violet staining and absorbance measurement at 595 nm. Δ*ompA* was used as a negative control. Deletion of the OmpA in *K. pneumoniae* significantly decreases biofilm formation. The values presented represent the mean and SEM of three independent experiments. Each experiment was comprised of 36 wells per strain/condition across three technical replicates in each experiment. **** = p-value ≤ 0.0001, *** = p-value 0.0002 (Mann-Whitney test).

Chemical complementation of the observed reduction in biofilm formation was attempted (Data not shown). Biofilm assays were carried out as previously described but with the addition of 125 µM of 1, 3-diaminopropane. Experimentation failed to generate a complete data set, due to a high degree of variability in crystal violet staining and subsequent absorbance measurements within and between biological repeats. Currently, the data suggests that supplementation with 1, 3-diaminopropane may complement the reduction in biofilm formation seen with the Δ*dat* and Δ*ddc* strains, however further investigation is needed to substantiate this.

4.3.7.1 Investigation of 1, 3-diaminopropane in biofilm formation

The polyamine modulon in *E. coli* involves modulating the translation of proteins that contribute to biofilm formation these being CpxR, UvrY, SpoT and RpoZ (Section 1.3.6.2). The DNA sequences of these genes were investigated in *K. pneumoniae* to determine any similarities between the two species that could explain 1, 3-diaminopropane's involvement in biofilm formation. It was found that *cpxR* had a distant Shine Dalgarno sequence, 10 bp from the initiation codon (Table 4.3). *uvrY* features the unusual start codon TTG, the same as *E. coli* (Table 4.3). *rpoZ* features a distal Shine Dalgarno sequence 11 bp from the start codon (Table 4.3). *spoT* features the unusual start codon TTG (Table 4.3). Taken together this suggests some genes relating to biofilm formation could be modulated at the translational level by acting on the mRNA in the Shine Dalgarno and the start codon region, inducing a conformational change promoting translational initiation or, in the case of the TTG start codon, by increasing the binding affinity of fMet-tRNA to the mRNA-ribosome complexes.

Table 4.3. Shared polyamine modulon features between *E. coli* K12 and *K. pneumoniae* 52145

Gene	Feature in *E. coli* K12 *	Feature in *K. pneumoniae* 52145
cpxR	cctc**ggagg**tatttaaacaatg	cctc**ggagg**tatttaaacaatg
spoT	gcccttgtatc	gcccttgtatc
rpoZ	ctg**tggag**ctttttaagtatg	ctgt**ggag**cattttaagtatg
uvrY	tcctttgatca	tcctttgatca
* Bold text indicates possible SD sequence; underlined text indicates start codon.		

4.3.8 Loss of 1, 3-diaminopropane synthesis does not increase susceptibility to oxidative stress

Polyamines protect cells from oxidative stress (Chattopadhyay et al., 2003; Minton et al., 1990). In *E. coli* they directly modulate the translation of proteins relating to oxidative stress (Sakamoto et al., 2015). Therefore, it was hypothesised that polyamines synthesised in *K. pneumoniae* may contribute to

oxidative stress resistance. The investigation began with the analysis of the annotated genome of *K. pneumoniae* 52145 to determine similarities between the sequences of the oxidative stress-related genes that are part of the polyamine modulon (*soxR*, *rpoS* and *gshA*) in *E. coli* and *K. pneumoniae*. As previously stated, modulation occurs through several mechanisms (section 1.3.6.2). Analysis of the genomic sequences found that the *rpoS* ORF of *K. pneumoniae* does not feature a premature stop codon. In *K. pneumoniae soxR* mRNA sequence was found to possibly have a distant Shine Dalgarno sequence at 11 bp from the start codon of the ORF, the same as that in *E. coli*. The *gshA* ORF was found to begin with the less common TTG start codon as opposed to AUG, again the same as that in *E. coli.* This provides evidence there may be a polyamine modulon in *K. pneumoniae* and that members of this contribute to oxidative stress resistance. Susceptibility to H_2O_2 was assessed using a disc diffusion assay (Section 2.15.1). As expected, the size of the inhibitory zone was proportional to the concentration of hydrogen peroxide used, increasing as concentration increased (Figure 4.12). The diameter of Inhibitory zones for Δ*dat* and Δ*ddc* at each concentration of H_2O_2 were identical to those of the wild type at the same concentrations (Figure 4.12) and therefore were not significantly different to the wild type across all hydrogen peroxide concentrations tested. This suggests that 1, 3-diaminopropane is not utilised as an antioxidant, to protect against ROS, in *K. pneumoniae*. It must be noted that this does not rule out the possibility that polyamines may protect against ROS. It is plausible to hypothesise any visible phenotype in Δ*dat* and Δ*ddc* is chemically complemented by native polyamine synthesis, the presence of exogenous polyamines or this function may be carried out by other polyamines within the cell as opposed to 1, 3-diaminopropane.

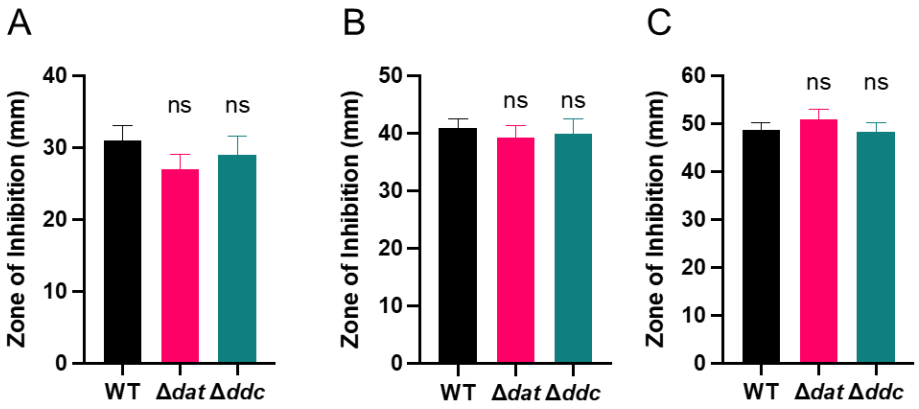

Figure 4.12. Loss of 1, 3-diaminopropane synthesis does not increase the susceptibility of *K. pneumoniae* 52145 to oxidative stress caused by hydrogen peroxide. Comparison of survival of *K. pneumoniae* wild type and Δ*dat* and Δ*ddc* strains, in the presence of **(A)** 3 %, **(B)** 10 % and **(C)** 30 % (v/v) hydrogen peroxide. The inhibitory effect of hydrogen peroxide was assessed by disk diffusion assay. The values presented represent the mean and SEM of three independent experiments. Statistical analysis was measured using an unpaired T-test with Welch's correction.

4.3.9 Loss of 1, 3-diaminopropane synthesis does not significantly alter susceptibility to antibiotics

Similar to *A. baumannii* (Section 3.3.18), the effect of the *dat* and *ddc* deletion on antimicrobial MICs was investigated. The MICs of all but gentamicin were the same between the wild type and deletion strains, with the *dat* strain showing a higher MIC than the wild type strain (Table 4.4). The MIC was within one doubling dilution of the wild type strain, suggesting is no difference between the two. These results indicate that loss of 1, 3-diaminopropane synthesis does not impact antimicrobial susceptibility and limits the possibility of an antibiotic/polyamine synthesis inhibitor combination therapy.

Table 4.4 The MIC of antimicrobials determined for *K. pneumoniae* 52145 wild type, Δ*dat,* and Δ*ddc* strains

Antibiotic	Antibiotic MIC (µg/ml)		
	WT	Δ*dat*	Δ*ddc*
Meropenem	1	1	1
Ampicillin	2	2	2
Gentamicin	1	2	1
Colistin	8	8	8
Trimethoprim	32	32	32
Tetracycline	1	1	1

The values presented represent the MIC obtained from three independent experiments. MIC values were excluded if greater than one doubling dilution of the predominant value obtained according to the convention normally used in the published literature

4.3.10 Deletion of *dat* or *ddc* does not alter *in vivo* virulence of *K. pneumoniae* in *Galleria mellonella* infection model

As with the *A. baumannii Δddc* strain the effect of the *dat* and *ddc* deletion on the virulence of *K. pneumoniae* 52145 was assessed using *G. mellonella* (Section 2.18). Infection with 1 x 10^5 CFU of the wild type strain resulted in the death of 20 % of infected larvae, 24 hours post-infection (Figure 4.13A). Infection with the Δ*dat* and Δ*ddc* resulted in the death of 30 % and 25 % of larvae, respectively, 24 hours post-infection (Figure 4.13A). By 72 hours post-infection, the wild type strain had killed a total of 43 % of infected larvae (Figure 4.13A), while infection with the Δ*dat* and Δ*ddc* strains resulted in a total of 40 % and 50 %, respectively (Figure 4.13A). There was no significant difference in bacterial killing of larvae when infected with 1 x 10^5 of the Δ*dat* or Δ*ddc* strains compared to the wild type. Larvae were also infected with 1 x 10^6 CFU of each strain (Figure 4.13B). Infection with the wild type resulted in the death of 60 % of infected larvae 24 hours post-infection (Figure 4.13B), while infection with the Δ*dat* and Δ*ddc* strains resulted in the death of 67.7 % and 46.7 % of larvae, respectively (Figure 4.13B). By 72 hours post-infection the wild type strain had killed a total of 90 % of the infected larvae (Figure 4.13B), while infection with Δ*dat* and Δ*ddc* strains resulted in the death of a total of 93 % and 76.7 %, respectively (Figure 4.13B). There was no significant difference in the survival of larvae when infected with the Δ*dat* strain compared to the wild type. There appears to be a slight attenuation of virulence of the Δ*ddc* strain (Figure 4.13B). Statistical analysis revealed there to be no difference when compared to the wild type strain. Injection with PBS did not result in the deaths of any larvae.

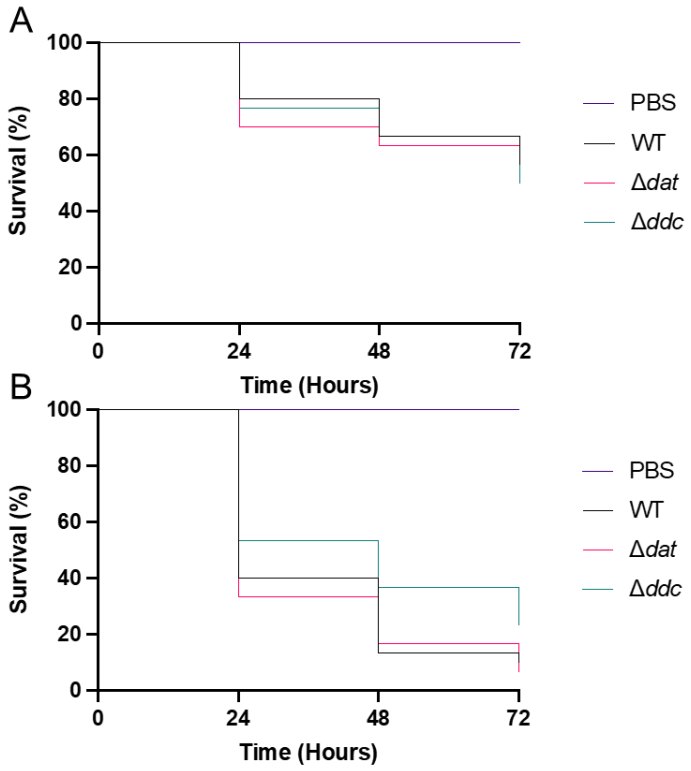

Figure 4.13. 1, 3-diaminopropane is not required for the virulence of *K. pneumoniae* 52145. Comparison of the percentage survival of *G. mellonella* 72 hours post-infection with an **(A)** 1 x 10^5 and **(B)** 1 x 10^6 CFU inoculum of *K. pneumoniae* 52145 wild type, Δ*dat,* and Δ*ddc* strains. A vehicle and trauma control group were injected with PBS. A total of thirty larvae, across three groups of ten, were infected in each group. Statistical significance was determined using the log-rank Mantel-Cox test.

4.4 Chapter discussion

4.4.1 1, 3-diaminopropane contributes to biofilm formation in *K. pneumoniae* 52145

This chapter sought to understand the role 1, 3-diaminopropane plays in *K. pneumoniae,* with a particular focus on virulence. This led to the investigation of 1, 3-diaminopropane in biofilm formation. Crystal violet staining of biofilm biomass established that the Δ*dat* and Δ*ddc* strains produce significantly less biofilm than the wild type strain (Figure 4.11). This is the first instance where 1, 3-diaminopropane has been implicated in the biofilm formation of *K. pneumoniae*. The current investigation does not indicate how 1, 3-

diaminopropane influences biofilm formation. It is clear from growth on agar and analysis of planktonic kinetics that 1, 3-diaminopropane is not needed to support growth and therefore compromised growth may not be a contributing factor. Several studies have associated polyamines and biofilm formation in other species (Bridges and Bassler, 2021; Thongbhubate et al., 2021; Wortham et al., 2010). The *E. coli* polyamine modulon contributes to biofilm formation (Sakamoto et al., 2012). Analysis of homologues of these genes in *K. pneumoniae* 52145 found that they feature the same hallmarks required for polyamine modulation in *E. coli* (Table 4.3). This suggests a possible link between biofilm and polyamine modulation in *K. pneumoniae* or at the very least modulation, in some capacity, in this species. Whether 1, 3-diaminopropane influences biofilm formation by modulating the same factors as in *E. coli* or not, based on the overwhelming evidence within the literature I believe that 1, 3-diaminopropane is likely to act upstream of biofilm-related genes influencing their regulatory elements, rather than modulating their expression directly. Further investigation is needed to determine the contribution of 1, 3-diaminopropane to *K. pneumoniae* biofilm formation. A potential route for this could be investigating the expression of genes relating to biofilm synthesis and regulation, using either RT-qPCR to study specific genes or RNAseq to study global gene expression to identify differentially expressed genes linked to biofilm formation. This investigation has provided evidence of a novel role for 1, 3-diaminopropane in *K. pneumoniae*. Further investigation will allow for a greater understanding of how this diamine contributes to biofilm formation with the possibility of developing a novel therapeutic to target 1, 3-diaminopropane synthesis as an anti-biofilm strategy.

4.4.2 Synthesis of spermidine analogues from 1, 3-diaminopropane

HPLC analysis of the *K. pneumoniae* 52145 wild type strain confirmed the synthesis of putrescine and spermidine (Figure 4.8). However, it could not confirm the synthesis of 1, 3-diaminopropane. This was confirmed by analysis

of the Δ*speABC* and Δ*speABCE* strains. Currently, I attribute this to the large quantity of putrescine within the wild type cell which masks the presence of other less prevalent diamines making it difficult to separate structurally similar diamines. Interestingly, this analysis revealed a possible synthesis of a spermidine analogue in *K. pneumoniae* 52145. This is the first instance where a triamine other than spermidine has been identified in *K. pneumoniae*. Previous investigation of the *E. coli* spermidine synthase revealed it is capable of utilising both spermidine and cadaverine as aminopropyl acceptors, while the human SpeE is capable of acting on 1, 3-diaminopropane, albeit with significantly reduced efficiency (Bowman et al., 1973; Wu et al., 2007). As for further investigation, LC-MS could be employed to determine the structure of this unknown triamine.

4.4.3 Limitations

The HPLC analysis is currently limited in what it has been able to determine. This is due to improper separation of the diamines within the wild type strain. Further optimisation is required to understand polyamine synthesis in *K. pneumoniae* 52145 fully. Another limitation is the crystal violet staining used for biofilm quantification. This method is an ideal starting point for quickly analysing biofilm formation and it was able to determine differences in biofilm formation between strains in this study. However, it was found to be highly susceptible to variation within and across replicates. Attempts were made to minimise this variation by increasing the number of technical replicates, but variation was still observed. Additionally, this method can only be used to infer an impact on biofilm biomass it cannot determine any effect on biofilm structure. Therefore, further investigation is needed to fully understand the role of 1, 3-diaminopropane in biofilm structure and formation. The method used for the construction of deletion constructs for all markerless deletions could be viewed as a limitation as it introduced several SNPs into the genome of *K. pneumoniae* and *A. baumannii* (Sections 4.3.2.3 and 5.3.5). While many of these are predicted as not affecting protein structure some are located within

intergenic regions which could influence gene expression if they disrupt regulatory elements. Others are frameshift mutations that will alter the translated amino acid sequences. These mutations were likely introduced by the Taq polymerase amplification step during vector construction. To avoid this a high-fidelity polymerase such as Phusion or *pfu* ultra could have been used for construction with an additional TA tailing step to allow for TA-cloning into pGEMT. Sequencing of the deletion vectors before conjugation would also allow for selection and usage of those that do not harbour mutations.

4.4.4 Conclusions

In this chapter, I aimed to investigate the role of 1, 3-diaminopropane in *K. pneumoniae* 52145. This has provided novel evidence for the involvement of 1, 3-diaminopropane in the biofilm formation of this species. Further investigation into gene expression may draw a link between the loss of 1, 3-diaminopropane and its effect on biofilm. This will further the understanding of how this diamine may regulate this lifestyle and its role in *K. pneumoniae* biology. This investigation has shown that several homologues of genes that are part of the *E. coli* polyamine modulon also share the same features required for modulation. For the first time, this raises the possibility that *K. pneumoniae* may also feature polyamine modulation. Additionally, it has ruled out a possible role in several phenotypes relating to *K. pneumoniae* virulence and infection narrowing down where a possible therapeutic could be applied. Overall, this investigation suggests that 1, 3-diaminopropane may be of limited use as a therapeutic target in treating *K. pneumoniae* infections but poses the possibility it could be targeted as an anti-biofilm strategy in the future.

Chapter 5 Role of cadaverine in *Klebsiella pneumoniae*

5.1 Chapter introduction

Cadaverine is known to be synthesised by two dedicated pathways. The first is the constitutively expressed pathway encoded by the *ldcC* gene and the second is the inducible pathway encoded by the *cadCBA* operon in *E. coli*. Its expression is induced under acidic conditions in the presence of lysine and anaerobic conditions and in *E. coli* it is one of the four acid resistance systems employed to overcome low external pH (Kanjee and Houry, 2013), also performing the same role in *V. cholerae* and *Salmonella* (Merrell and Camilli, 2000; Park et al., 1996). In addition to acidic stress, cadaverine has been shown to protect against oxidative stress in *E. coli* and species of *Vibrio* and nitrosative stress in uropathogenic *E. coli* and *Salmonella* (Bower and Mulvey, 2006; Mühlig et al., 2014). It also contributes to decreased susceptibility to several antibiotics in *E. coli.* The understanding of cadaverine in *K. pneumoniae* is less than other species. Genome annotation suggests that *K. pneumoniae* has both constitutive and acid-inducible lysine decarboxylases. Little is known about the constitutive LdcC in *K. pneumoniae*. As for the acid-inducible pathway, investigation with the NTUH-K2044 strain has revealed this strain has lysine decarboxylase activity and that cadaverine is synthesised in response to decreasing external pH (Hsieh et al., 2010). Additionally, this study also suggested that the *cadC* gene may contribute to bile tolerance (Hsieh et al., 2010).

5.2 Research aims

- Confirm the previously made *K. pneumoniae* Δ*ldcC*, Δ*cadA,* and Δ*ldcC* Δ*cadA* deletion strains.
- Investigate the expression of the *cadCBA* operon in *K. pneumoniae* 52145.

- Examine phenotypic differences arising from the deletion of cadaverine synthesis genes, to further understand the role of cadaverine in *K. pneumoniae* to infer whether cadaverine synthesis is a viable therapeutic target.
- Chemically or genetically complement any observed phenotypes.
- Determine the conservation of *ldcC* and *cadCBA* across other species.

5.3 Chapter results

5.3.1 The genomic location, size, and structure of cadaverine synthesis genes in *K. pneumoniae*

Sequencing and annotation of the *K. pneumoniae* 52145 genome (Bialek-Davenet et al., 2014) indicates this strain encodes the genes for two distinct cadaverine synthesis pathways. The first is a homologue of the biosynthetic constitutive pathway that is comprised solely of *ldcC* (BN49_4138) (Figure 5.1), a 2154 bp gene that encodes a putative PLP-dependent lysine decarboxylase. Upstream of *ldcC* lies *accA* (BN49_4135) (Figure 5.1), which encodes a putative acetyl-coenzyme A carboxylase carboxyl transferase subunit Alpha. Downstream of *ldcC* lies BN49_4137 (Figure 5.1), which encodes an unknown protein, which blast analysis shows to have similarity to a glyoxylase I family protein from *E. coli*. The second is homologous to the biodegradative acid-inducible pathway encoded by the *cadCBA* operon in *E. coli*. The *cad* operon is comprised of three genes (Figure 5.1). The *cadA* gene (BN49_1542) has a length of 2154 bp and encodes a putative PLP-dependent lysine decarboxylase. Upstream of *cadA* lies the *cadB* gene (BN49_1541) (Figure 5.1), which is 1335 bp in length and encodes the CadB lysine/cadaverine antiporter and upstream from *cadBA* lies the *cadC* gene (BN49_1540) (Figure 5.1), which is 1569 bp in length and encodes a ToxR-like transcriptional regulator, which in other *cad* operons directly responsible for the regulation of the *cadBA* genes (Küper and Jung, 2005). Downstream of *cadA* lies *yjdL* (BN49_1543) (Figure 5.1), a 1476 bp

gene encoding a putative di-tripeptide permease, and *lysS2* (BN49_1544) (Figure 5.1), a 1518 bp gene encoding a putative lysyl-tRNA synthetase.

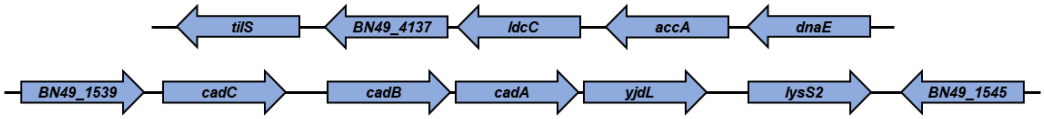

Figure 5.1. The genomic organisation of the *ldcC* gene and the *cadCBA* operon. Top: 8.5 Kbp region of the *K. pneumoniae* 52145 reference genome showing the location of the *ldcC* gene and the upstream and downstream genes within the region. **Bottom:** 10 Kbp region of the *K. pneumoniae* 52145 reference genome showing the location of the *cadCBA* operon and the downstream *yjdL* and *lysS2.*

5.3.2 Conservation of the cadaverine synthesis pathway

5.3.2.1 Analysis of the lysine decarboxylases LdcC and CadA

In *K. pneumoniae* 52145 the annotated ORF of *ldcC* encodes LdcC composed of 717 amino acids, with a calculated molecular mass of 81.3 kDa. Prediction of protein features with InterPro suggests it is comprised of three domains: the N-terminal domain predicted to be composed of residues 15-124, the lysine decarboxylase major domain predicted to span residues 130-544 and the C-terminal domain predicted to be composed of residues 570-700. The annotated ORF of *cadA* encodes CadA comprised of 717 amino acids, with a calculated molecular mass of 81.6 kDa. Similarly, to LdcC the CadA of *K. pneumoniae* 52145 consists of three domains: the N-terminal domain is predicted to be composed of residues 16-126 (Figure 5.2A), the lysine decarboxylase major domain is predicted to span residues 132-547 (Figure 5.2A) and the C-terminal domain is predicted to be made up of residues 572-702 (Figure 5.2A).

The amino acid sequences of CadA and LdcC were aligned with one another, which determined they share 69.1 % sequence identity and 84.1 % similarity (Figure 5.2B). Both sequences were compared to homologues found in other species of bacteria. The lysine decarboxylases of *E. coli* are the most well studied, a comparison of the LdcC and CadA from *K. pneumoniae* 52145 to those of *E. coli* K12, found the sequences to be highly similar. LdcC was found

to have an amino acid sequence identity of 88 % and a similarity of 93.6 % (Figure 5.2B). While CadA has a sequence identity of 94.7 % and a similarity of 98 % (Figure 5.2). Cadaverine synthesis has been described in several additional organisms, such as *Salmonella*, *V. vulnificus,* and *P. aeruginosa*. *Salmonella* is known to encode the constitutive and acid-inducible synthesis pathways. A comparison of LdcC and CadA from *K. pneumoniae* 52145 found a shared sequence identity of 88.1 % and 94.7 % and a similarity of 93 % and 97.8 %, respectively. Comparison of CadA to the *V. vulnificus* homolog showed a similar result with sequence identity of 74.6 % and similarity of 87 %. The genome of *P. aeruginosa* PAO1 encodes a gene referred to as *ldcA*, encoding a lysine decarboxylase. A comparison of LdcC and CadA to LdcA revealed 39.9 % and 38.6 % identity and 57 % and 56.2 % similarity, respectively.

LdcC and CadA are both PLP-dependent decarboxylases, meaning that both feature a lysine residue (in *E. coli* K12 K367) within the structure that forms covalent interaction known as a Schiff base, with their coenzyme pyridoxal 5'-phosphate that is essential for their function. Alignment of the LdcC from *K. pneumoniae* 52145 with that of *E. coli* K12 indicates the presence of a conserved lysine residue at position 367 of the amino acid sequence, that aligns with the known modified residue in the LdcC of *E. coli* K12 at position 367 (Figure 5.2B). Alignment of CadA from *K. pneumoniae* 52145 with that from *E. coli* K12, identifies a conserved lysine residue at position 369, that aligns with the known modified residue in the CadA of *E. coli* K12 at position 367 (Figure 5.2B). Analysis of the LdcC and CadA amino acids sequences with InterPro predicts the PLP attachment site motif consists of residues 362-376 of the LdcC sequence and residues 364-378 of the CadA sequence, with lysine 367 and 369 being the PLP-modified residues for each enzyme, supporting the observations made when aligning homologous sequences. Despite their wide range of substrates and evolutionary divergence fold type I PLP-dependent enzymes maintain a conserved set of residues critical for co-factor binding. Within the active site of *E. coli* CadA, it is known that PLP has five sets of interactions with residues of the active site. PLP forms hydrogen bonds with residues T220, S221,

S364, and H366, within the monomer it is covalently linked to (Kanjee et al., 2011). In addition, it also forms hydrogen bonds with T398, T399, and S400, within the second monomer of the dimer (Kanjee et al., 2011). Alignment of the CadA sequence from *K. pneumoniae* and that of *E. coli* K12 found that all residues are conserved (Figure 5.2B). Additionally, PLP interacts with D330, W333, H245, and A332. Alignment indicates that all residues are conserved in *K. pneumoniae* CadA (Figure 5.2B). The alignment of the LdcC sequence with both CadA sequences, shows the same residues are conserved (Figure 5.2B).

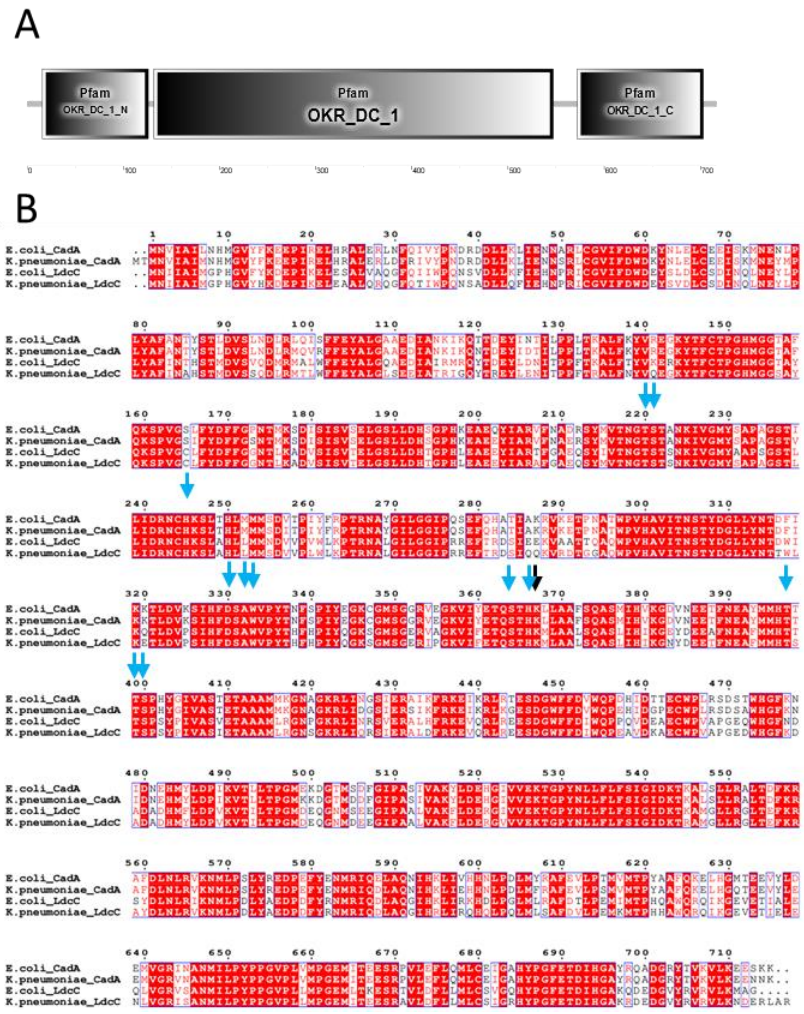

Figure 5.2. Functional residues of LdcC and CadA are highly conserved between *E. coli* K12 and *K. pneumoniae* 52145. (A) The predicted domains of the *K. pneumoniae* CadA protein. OKR_DC_1_N: N-terminal domain. OKR_DC_1: major domain. OKR_DC_1_C: C-terminal domain. **(B)** Protein sequence alignment of *K. pneumoniae* 52145 CadA and LdcC with CadA from *E. coli* K12. Black arrow: Indicates PLP-modified lysine residue. Blue arrow: Indicates residues conserved residues known to be involved in PLP interaction in *E. coli*. Domains were predicted with SMART. Sequence alignment was generated with Clustal Omega and visualised with ESPript 3.0.

5.3.2.2 Analysis of the CadB antiporter

The cadaverine acid resistance system requires an antiporter for the exchange of lysine/cadaverine. This is facilitated by CadB, which is composed of 444 amino acids (Figure 5.3A) with a molecular mass of 47.7 kDa. *K. pneumoniae* 52145 CadB consists of seven cytoplasmic segments, twelve transmembrane segments, and six periplasmic segments (Table 5.1 and Figure 5.3B).

Table 5.1. Regions of CadC protein and corresponding residues.

Domain	Residues
Cytoplasmic	1-6, 59-93, 140-145, 209-219, 284-322, 372-382, 425-444
Transmembrane	7-28, 40-58, 94-115, 121-139, 146-169, 189-208, 220-246, 258-283, 323-344, 350-371, 383-401, 407-424
Periplasmic	29-39, 116-120, 170-188, 247-257, 345-349, 402-406

Sequence alignment with CadB from *E. coli* K12 revealed an amino acid identity of 93 % and a sequence similarity of 97.7 %. A similar result was observed when compared to the CadB of *S. enterica* (91.7 % identity/ 95.9 % similarity) and *V. vulnificus* (64.7 % identity/ 80.4 % similarity). Several residues that are involved in cadaverine uptake and lysine/cadaverine antiporter activity have been identified in *E. coli* (Table 1.1). Alignment with the CadB from *E. coli* K12 and that of *K. pneumoniae* 52145 found that all residues relating to function are conserved in the *K. pneumoniae* sequence (Figure 5.3C).

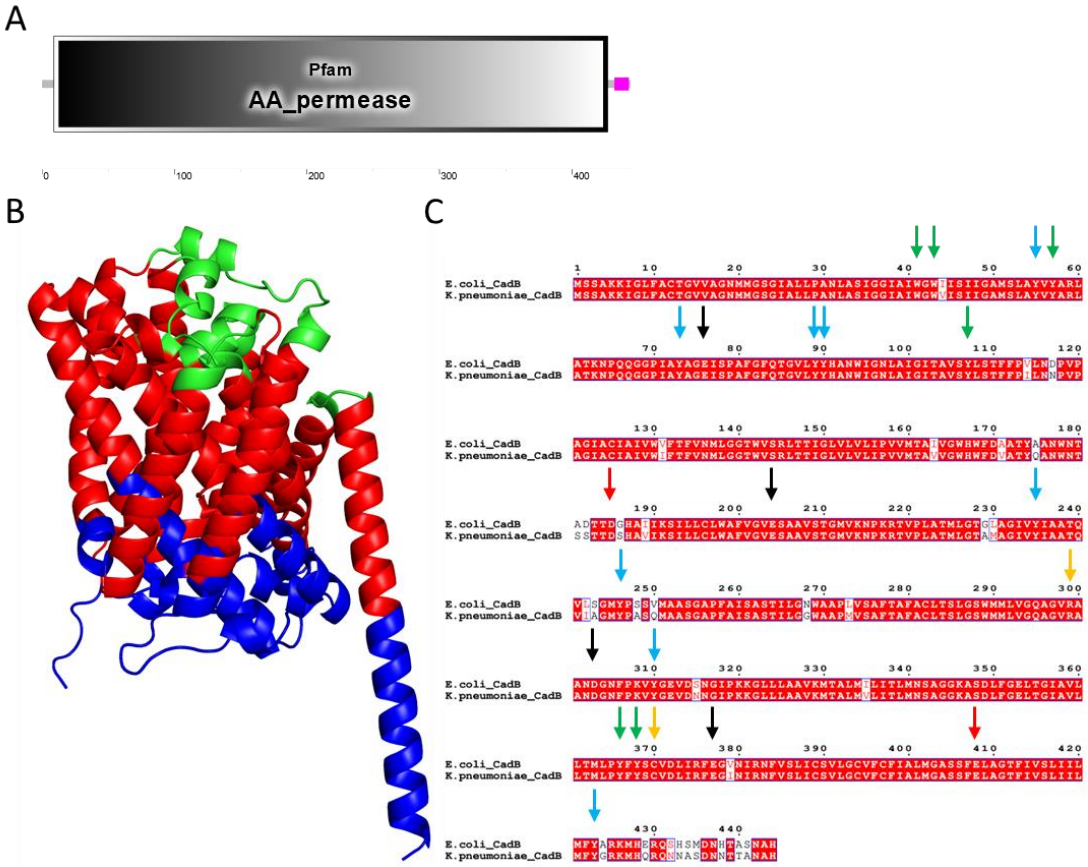

Figure 5.3. Amino acid sequence of CadB is highly conserved between *E. coli* K12 and *K. pneumoniae* 52145. (A) The predicted domains of the CadB protein from *K. pneumoniae* 52145. **(B)** AlphaFold Database 3D predicted structure. Blue: residues found within the cytoplasm. Red: Transmembrane residues. Green: residues found within the periplasm. **(C)** Protein sequence alignment of *K. pneumoniae* 52145 CadB with CadB from *E. coli* K12. Black arrow: Indicates conserved acidic residues associated with uptake and excretion. Red arrow: Indicates conserved acidic residues associated with uptake only. Blue arrows: Indicates conserved aromatic residues associated with uptake and excretion. Green arrow: Indicates conserved aromatic residues associated with uptake only. Yellow arrow: Indicates additional conserved residues associated with uptake and/or excretion. Domains were predicted with SMART Sequence alignment was generated with EMBOSS NEEDLE and visualised with ESPript 3.0.

5.3.2.3 Analysis of the CadC regulator

The expression of the *cadB* and *cadA* genes is tightly regulated by the CadC transcriptional regulator located within the cytoplasmic membrane. CadC is composed of 522 amino acids, with a predicted molecular mass of 57.8 kDa. InterPro predicts the cytoplasmic region spans residues 1-169 with the DNA-binding effector domain spanning residues 11-100 within this region. InterPro analysis predicted that residues 30E, 49S, 50R, 67V, 70Q, 78S, 79L, 92T and 97G

are involved in DNA binding. The trans-membrane domain is predicted to be comprised of residues 170-192 and the periplasmic domain residues 193-522. Of note the CadC C-terminal domain 1, that is the N-terminal subdomain of the C-terminal periplasmic domain, is predicted to be composed of residues 202-333. Additionally, the Mobi database predicts a disordered region, toward the C-terminal end of the cytoplasmic domain, spanning amino acids 118-161, this is the disordered linker region between the cytoplasmic and transmembrane domains. The CadC of *K. pneumoniae* 52145 is ten amino acids longer than the CadC from *E. coli* K12. Alignment of the two sequences found a shared sequence identity of 65.9 % and a similarity of 78.9 %. BLASTp of the amino acid sequence found the sequence encoded by *K. pneumoniae* 52145 is highly similar to other species of *Klebsiella* such as *K. africana* (98.66 % identity), *K. quasipneumoniae* (96.55 % identity) and *K. variicola* (94.71 % identity). The sequence was also highly similar to those encoded by *Serratia liquefaciens* (99.81 % identity), *Providencia stuartii* (99.81 % identity), and *Raoultella terrigena* (81.3 % identity). The regulation of the expression of the *cadBA* genes, by CadC, is controlled through the sensing of extracellular pH by its periplasmic domain. Several residues in CadC of *E. coli* have been identified as essential for pH sensing and the pH-dependent expression of the *cad* operon (Table 1.2). Pairwise alignment of the CadC from *K. pneumoniae* 52145 and *E. coli* K12 showed the majority of periplasmic residues are conserved (Figure 5.4B). However, several residues are not. The first two are G284 and Q266, mutation of both residues in *E. coli* confers pH-independent *cadBA* expression, while Q266 confers lysine independence (Table 1.2). S294 aligns with the G284 in the *E. coli* sequence (Figure 5.4B). Aligned to Q266 of *E. coli* CadC is a charged H276 of the *K. pneumoniae* CadC (Figure 5.4B). The third residue that is not conserved is the negatively charged E468. Mutation of this residue abolishes acid-induced expression of *cadBA* (Table 1.2). Alignment found that a L478, aligns with the *E. coli* E468 residue (Figure 5.4B). The final residue P499 when mutated confers pH-independent *cadBA* expression (Table 1.2). Alignment found that N509 of the *K. pneumoniae* sequence aligns with P499 in the *E. coli* sequence (Figure 5.4B).

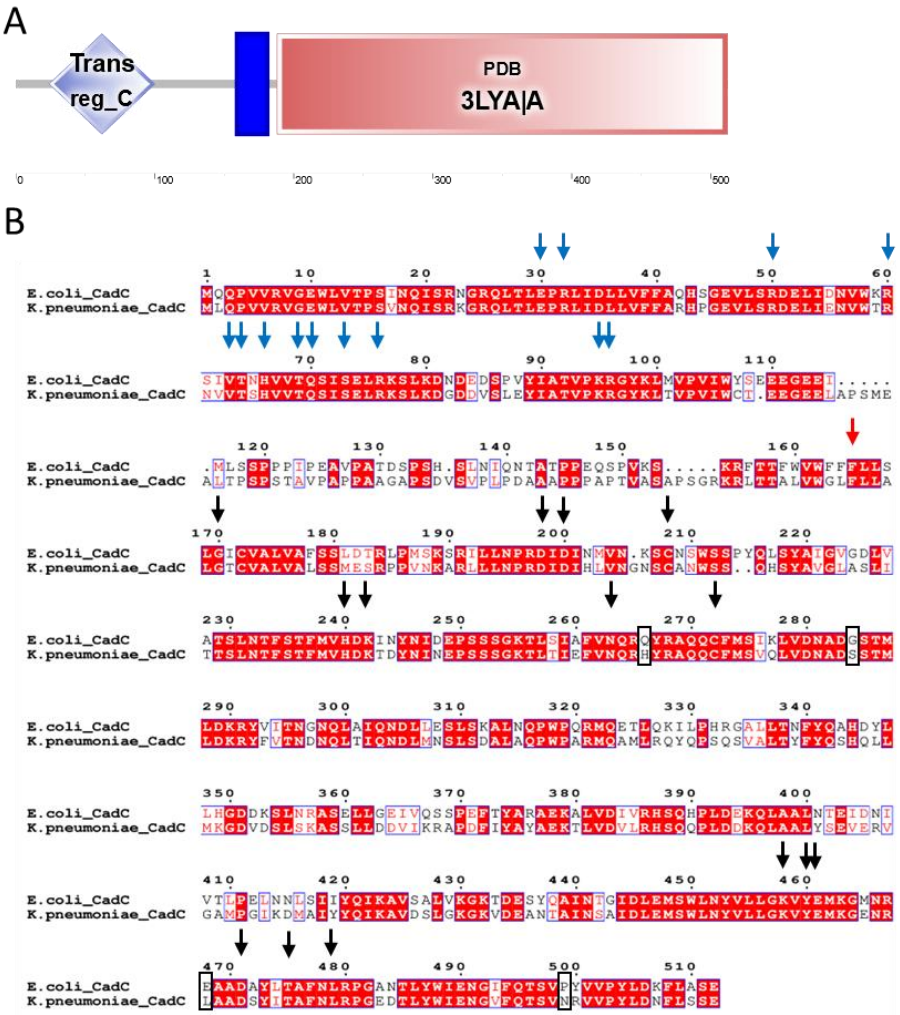

Figure 5.4. Several residues required for pH sensing are not conserved between the CadC of *E. coli* K12 and *K. pneumoniae* 52145. (A) Predicted domains of CadC from *K. pneumoniae* 52145. Transreg_C: C-terminal domain. Blue rectangle: transmembrane region. 3LYA|A: Periplasmic domain. Referencing *E. coli* K12 CadC periplasmic domain crystal structure in the PDB database. **(B)** Protein sequence alignment of *K. pneumoniae* 52145 CadC with CadC from *E. coli* K12. Black arrows: Indicate conserved residues found in the periplasmic domain relating to pH sensing. Red arrows: Indicate conserved residues found in the transmembrane domain. Blue arrow: Indicate conserved residues found in the cytoplasmic domain, relating to DNA binding. Black boxes: Indicate non-conserved residues that are known to have a phenotype when mutated in *E. coli*. Domains were predicted with SMART. Sequence alignment was generated with EMBOSS NEEDLE and visualised with ESPript 3.0.

Following the observation that several key residues of the CadC of *E. coli* are not conserved in the amino acid sequence encoded by *K. pneumoniae* 52145, a comparison of the sequence was carried out against other members of the *Klebsiella* genus (Figure 5.5) The CadC from *K. pneumoniae* 52145 and *E. coli* K12 were aligned alongside CadC encoded by type and/or reference strains,

that have complete genome sequences available, of *K. aerogenes*, *K. variicola*, *K. oxytoca*, *K. grimontii* and *K. africana* found that variability in the conservation of these four residues across the different species (Figure 5.5). The G284 of the *E. coli* K12 sequence is not conserved in either strains of *K. pneumoniae* and *K. variicola* (Figure 5.5), G284 is also not conserved in *K. africana* (Figure 5.5). However, there appears to be a conservation substitution with all strains of these three species having serine present at the aligned position with G284 (Figure 5.5). There is however conservation present in the strains of *K. aerogenes*, *K. michiganensis, K. grimontti* and *K. oxytoca* (Figure 5.5) Q266 of the *E. coli* sequence is not conserved in any of the aligned sequences of CadC (Figure 5.5), however, the substituted histidine residue is conserved in the CadC sequences across the *Klebsiella* genus (Figure 5.5). P499 of the *E. coli* K12 sequence is not conserved in any species of *Klebsiella* (Figure 5.5). In *K. variicola* and *K. africana* there is a substitution of asparagine, the same as the sequences from all three *K. pneumoniae strains* (Figure 5.5). In *K. aerogenes*, *K. michiganesis*, *K. grimontii* and *K. oxytoca* there appears to a threonine at the aligned position (Figure 5.5). E468 of the *E. coli* K12 sequence, similarly to G284, is not conserved across all species of the *Klebsiella* genus, but a subset of those aligned (Figure 5.5). G284 is found conserved in *K. aerogenes*, *K. michiganensis, K. grimontti* and *K. oxytoca* (Figure 5.5), while there is conservation of the substitution in *K. pneumoniae, K. africana* and *K. variicola,* all of which feature a leucine at the aligned position (Figure 5.5).

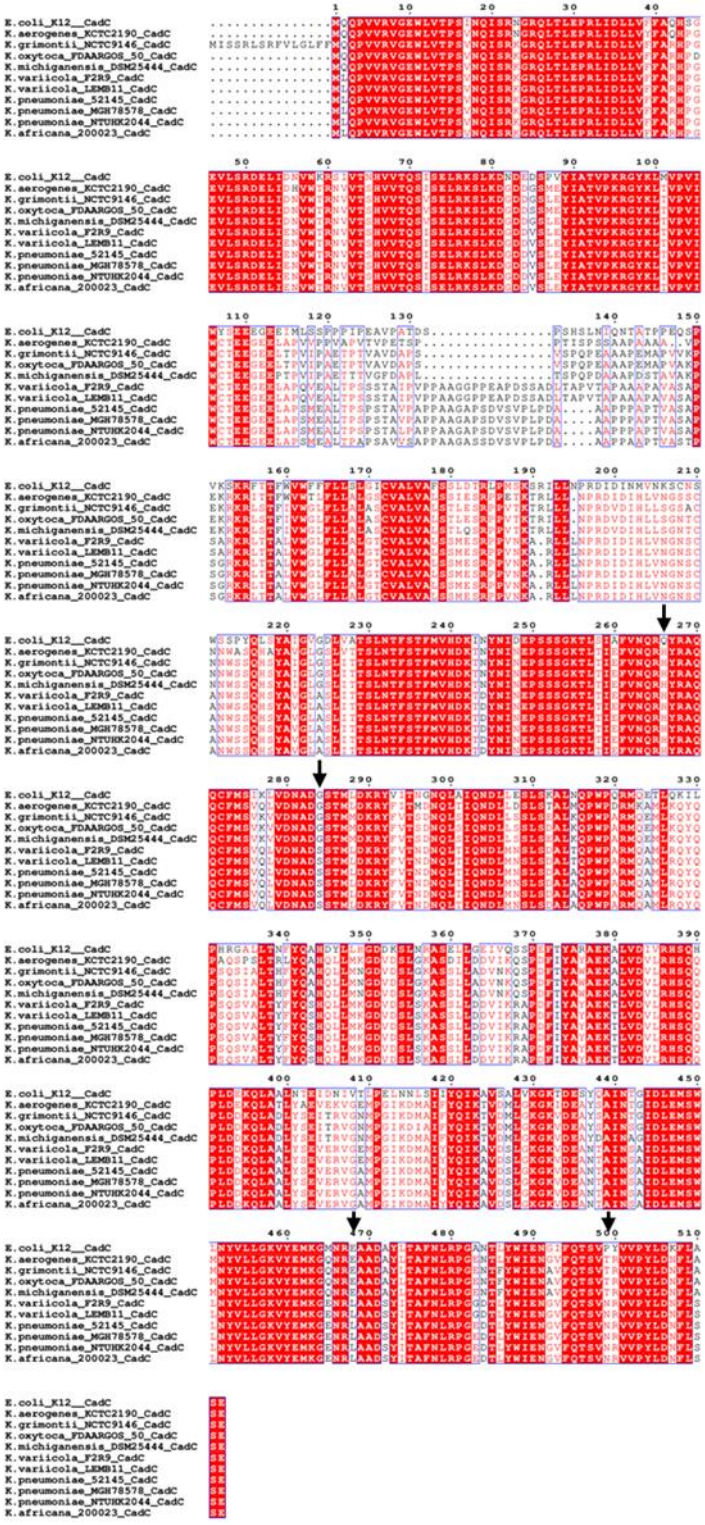

Figure 5.5. 266Q, G284, E468 and P499 of *E. coli* K12 CadC are not completely conserved in *Klebsiella* species. Sequence alignment of the CadC sequence from E. coli K12, *K. pneumoniae* and species of *Klebsiella* including *K. aerogenes, K. grimontii, K. oxytoca, K. michiganensis, K. variicola* and *K. africana*. Black arrows: indicate residues in the *E. coli* K12 CadC sequence associated with function. Sequence alignment was generated with Clustal Omega and visualised with ESPript 3.0.

Of the previously discussed residues relating to CadC function, in *E. coli,* alignment found that those in the cytoplasmic domain, involved in DNA binding, all are completely conserved across the species of *Klebsiellla* (Figure 5.5) Of the remaining residues within the periplasmic domain, that are conserved between *E. coli* K12 and *K. pneumoniae* 52145 CadC, all are completely conserved apart from the glycine present at position 170 in the CadC of *E. coli* (Figure 5.5). The residue is conserved across all strains of *K. pneumoniae* and in *K. aerogenes*, *K. africana* and *K. variicola* (Figure 5.5). While the residue differs at the aligned position in CadC from *K. michiganensis, K. grimontii* and *K. oxytoca* (Figure 5.5).

In addition to pH sensing, two cysteine residues are key to the acid-inducible function of CadC in *E. coli*. Alignment established that C208 and C272 are conserved in the cadC of *K. pneumoniae* at positions 220 and 282 (Figure 5.4B). Interaction with LysP, a lysine permease that mediates lysine uptake for cadaverine synthesis, is also a key regulatory element. In *E. coli* K12, residue F165, is known to be required for LysP/CadC interaction (Tetsch et al., 2008). When the CadC of *K. pneumoniae* and *E. coli* are aligned, there appears to be a conserved phenylalanine residue at position 176 (Figure 5.4B), suggesting a possibly similar interaction between LysP/CadC in *K. pneumoniae* 52145 as in *E. coli* K12. To allow for expression of the *cadBA* genes, the cytoplasmic DNA binding domain must interact with the cadC1 and C2 sites, of the *cadBA* promoter. Several residues have been identified, in the CadC of *E. coli* K12, as being required for *cadBA* induction under stress conditions (Table 1.3). A comparison of the two CadC amino acid sequences found that all of these residues are conserved within the amino acid sequence of CadC from *K. pneumoniae* 52145 (Figure 5.4B).

5.3.2.4 LysP sequence conservation and CadC interaction

LysP is responsible for the regulation of *cadBA* expression. The LysP of *K. pneumoniae* 52145 is predicted to be 489 amino acids and has a molecular weight of 53.7 kDa. InterPro suggests the amino acid permease domain is spans

residues 21-476 and is comprised of 12 transmembrane segments (Table 5.2 and Figure 5.6A and B).

Table 5.2. Regions of LysP protein and their corresponding residues

Domain	Residues
Cytoplasmic	1-20, 67-102, 150-160, 225-244, 313-347, 395-414, 468-489
Transmembrane	21-43, 49-66, 103-125, 131-149, 161-182, 202-224, 245-267, 287-312, 348-365, 371-394, 415-435, 447-467
Periplasmic	44-48, 126-130, 183-201, 268-286, 366-370, 436-446

The amino acid permease conserved signature is predicted to span residues 46-77 and is part of the second transmembrane segment. Alignment of LysP from *K. pneumoniae* 52145 with that of *E. coli* K12 found a shared amino acid identity of 93.5 % and a similarity of 97.5 %. Several residues have been identified, in *E. coli*, as essential for proper CadC inhibition. The mutation of Y102, W106, and F216 significantly impair *cadBA* expression under inducing conditions (Rauschmeier et al., 2014). Additionally, the replacement of E222 results in strong inhibition of CadC. Alignment of the LysP from *K. pneumoniae* 52145 and *E. coli* K12 revealed that all three residues are conserved in the sequence encoded by *K. pneumoniae* (Figure 5.6C). Mutation of E230, E438, D443, and D446 all result in LysP being unable to inhibit CadC (Rauschmeier et al., 2014). However, all variants are still pH-dependent for *cadBA* expression. Alignment of the two LysP sequences revealed that all four amino acids are conserved in *K. pneumoniae* (Figure 5.6C). Taken together this suggests that, if LysP in *K. pneumoniae* 52145 requires the same amino acid residues for function, then the LysP should interact with CadC and regulate *cadBA* expression, similarly to that shown in *E. coli*. Overall, the components of the *cad* acid resistance system are relatively well conserved, compared to that found in *E. coli.* However, the substitution of several amino acids previously identified as being required for function may suggest, that in *K. pneumoniae* there may be altered expression and activity of the system compared to that seen in *E. coli.*

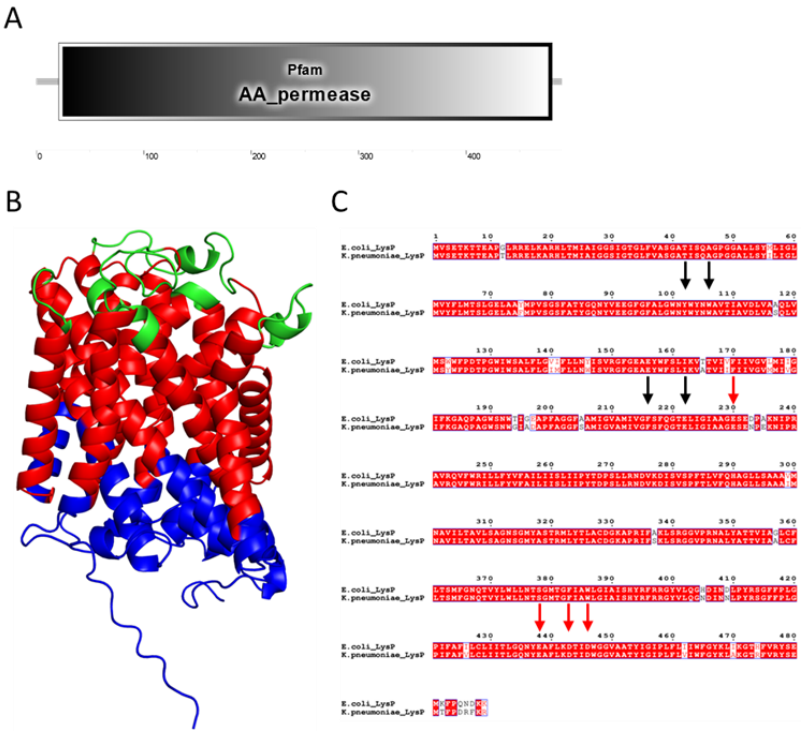

Figure 5.6. The amino acid sequence of LysP is highly conserved between *E. coli* K12 and *K. pneumoniae* 52145. **(A)** Predicted domains of LysP from *K. pneumoniae* 52145. AA_permease: amino acid permease domain. **(B)** AlphaFold DB predicted 3D monomeric structure of LysP. Residues are coloured by their cell position. Blue: residues found within the cytoplasm. Red: Transmembrane residues. Green: residues found within the periplasm. **(C)** Protein sequence alignment of *K. pneumoniae* 52145 LysP with LysP from *E. coli* K12.Black arrows: Indicate conserved residues, that when mutated, in E. coli, result in increased CadC inhibition. Red arrows: Indicate conserved residues that when mutated, in *E. coli*, result in lysine independent *cadBA* expression. Sequence alignment was generated with EMBOSS NEEDLE and visualised with ESPript 3.0.

5.3.2.5 Gene regulation of the *cadBA* genes

The expression of *cadBA* is a tightly regulated process in *E. coli* with expression being controlled by H-NS binding. This binding occurs in low GC-rich regions of the genome. The overall GC content of the *K. pneumoniae* 52145 genome is approximately 57%. The GC content of the 365 bp region between the stop codon of *cadC* and the start codon of *cadB* is 35%. This AT richness is indicative of potential H-NS binding. In *E. coli* there are five H-NS sites located between -25 and -324 bp of the transcriptional start site of *cadB.* To include all H-NS sites 508 bp was selected downstream of the cadB start codon was selected for alignment. The two sequences share 60 % sequence identity (Figure 5.7).

However, the H-NS site sequences are not completely conserved within the *K. pneumoniae* genome. Further molecular analysis would be required to determine the location and sequence of these sites (Figure 5.7).

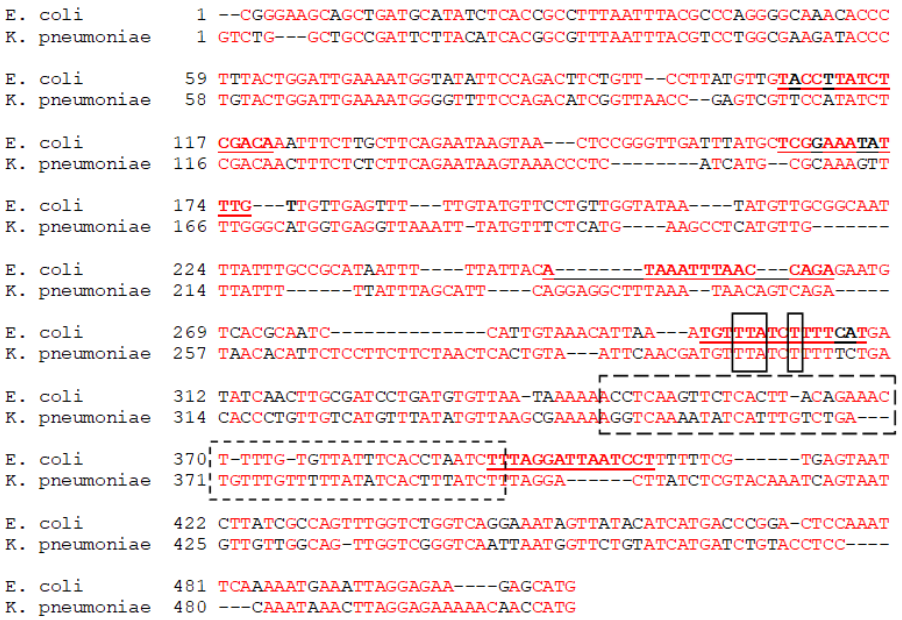

Figure 5.7. Regulatory elements with the *cadBA* promoter region are partially conserved. Alignment of nucleotides 508 bp upstream of the *cadB* start codon from *K. pneumoniae* 52145 and *E. coli* K12. Bold underlined text: The five predicted H-NS sites within the *E. coli* K12 sequence. Solid black boxes: Represent residues of the *E. coli* 41-mer site that directly interact with CadC DNA binding domain. Dashed black boxes represent the CadC2 sequence, in *E. coli* K12. Sequence alignment was generated with EMBOSS NEEDLE and visualised using BoxShade.

H-NS binding sites also correlate with curvature of the DNA helix (Küper and Jung, 2005), so the same 508 bp sequence encompassing the 3' end of the *cadC* gene and the intergenic region between the *cadC* and *cadB* genes was tested for its curvature/bendability, alongside the same region from *E. coli*, using Bend.it Server (Vlahoviček et al., 2003) (Figure 5.8). This predicts the curvature of DNA and is expressed as degrees per helical turn (10.5 °/helical turn = 1 °/basepair). Experimentally tested curvature ranges between 5-25 °/helical turn, while straight motifs are below 5 °/helical turn (Küper and Jung, 2005). There are five regions in the *E. coli* region with intrinsic curvature, indicated by peaks of >5 °/helical turn (Figure 5.8B), as shown by Kuper and Jung (2005). Similar to *E. coli*, prediction using the *K. pneumoniae* sequence suggests there

be several stretches of nucleotides within this region that have intrinsic curvature, these being residues 67-85, 168-199, 282-303, 309-325, and 341-367 (Figure 5.8A). This taken together with the AT-richness of the sequence suggests that it is likely H-NS similarly regulates *cadBA* expression in *K. pneumoniae,* but further investigation is needed to confirm this.

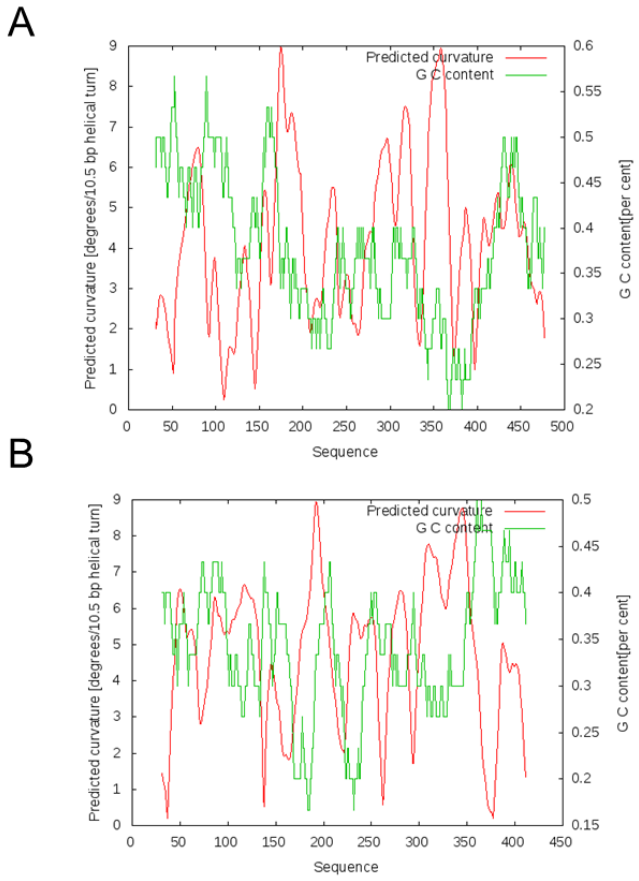

Figure 5.8. The 3' end of cadC ORF and the intergenic region between *cadC* and *cadB* in *K. pneumoniae* 52145 have intrinsic curvature. (A) Prediction of intrinsic curvature in *K. pneumoniae* 52145 comprising 140 bp of the 3' end of the *cadC* ORF and the 368 bp comprising the intergenic region and the start codon of the *cadB* ORF. **(B)** The prediction of intrinsic curvature present within the 3' end of *cadC* ORF and the intergenic region between *cadC* and *cadB* in *E. coli* K12, as stated by Kuper and Jung (2005). Comprising 141bp of the 3' end of the *cadC* ORF and the 367 bp comprising the intergenic region and the start codon of the *cadB* ORF. Curvature predictions were carried out using the Bend.it webserver.

cadBA expression is also regulated by the ToxR-like CadC. In *E. coli* CadC binds to two specific sequences known as cadC1 and C2 that lie in the intergenic region between *cadC* and *cadB*. The alignment of the 508 bp region from *K. pneumoniae* with the *E. coli* sequence shows neither the C1 site nor the C2 site

is completely conserved within *K. pneumoniae* 52145 (Figure 5.7). Initially, the quasi-palindromic sequence of cadC1 was suggested as being essential for CadC interaction (Küper and Jung, 2005). This has now been narrowed down to the specific consensus sequence 5'-T-T-A-x-x-x-x-T-3' (Schlundt et al., 2017). The alignment of this sequence with that of *V. vulnificus* and *V. cholerae* previously indicated the conservation of the consensus sequence in these species (Schlundt et al., 2017). Alignment of the sequence between cadC and B of *E. coli* K12 and *K. pneumoniae* 52145 also indicates that there is complete conservation of one of these consensus sequences (Figure 5.7). This suggests a similar interaction between the CadC regulator and the *cadBA* promoter in *K. pneumoniae*. Together this information suggests that the *cadBA* genes may be regulated similarly to those found in *E. coli* and the *vibrio* species.

5.3.3 Expression of cadaverine synthesis genes in *K. pneumoniae* 52145

5.3.3.1 Expression of the *cadCBA* and *ldcC* genes

In *E. coli* the expression of the *cadBA* genes is regulated by CadC, the binding of H-NS to the *cadBA* promoter and surrounding area and indirectly through, LysP. In *E. coli* the *cadC* gene is constitutively expressed independently of *cadBA,* while the *cadBA* genes are expressed from the same promoter upstream of the *cadBA* ORFs under acidic pH and in the presence of lysine (Neely and Olson, 1996). To investigate the expression of the *cadA* gene in *K. pneumoniae* 52145, primers were designed to amplify a product of 153 bp (Figure 5.9). The expression of the believed to be constitutive *ldcC* gene was also assessed, and primers were designed to amplify an RT-PCR product of 174 bp (Figure 5.9). The *rpoB* gene was used as an expression control, with primers amplifying a product of 120 bp. RNA was extracted from *K. pneumoniae* 52145 grown in LB broth to mid exponential phase altered to a pH of 4, 5.5 and 7.5, to determine the effect of external pH on lysine decarboxylase expression. The *rpoB* gene was shown to be expressed across the pH range, as expected, indicated by the presence of a 120 bp RT-PCR product (Figure 5.9B). The *ldcC*

gene was shown to be expressed at each pH, indicated by the presence of a 174 bp band on the gel (Figure 5.9B), as expected by our hypothesis that *ldcC* would be constitutively expressed. The *cadA* gene was also shown to be expressed at each pH tested, including pH 7.5, indicated by the presence of 153 bp RT-PCR product (Figure 5.9B). This suggests either that the induction of *cadBA* expression occurs at a higher pH compared to *E. coli* or that regulation of the *cadBA*, varies in *K. pneumoniae*, potentially allowing pH-independent or basal expression.

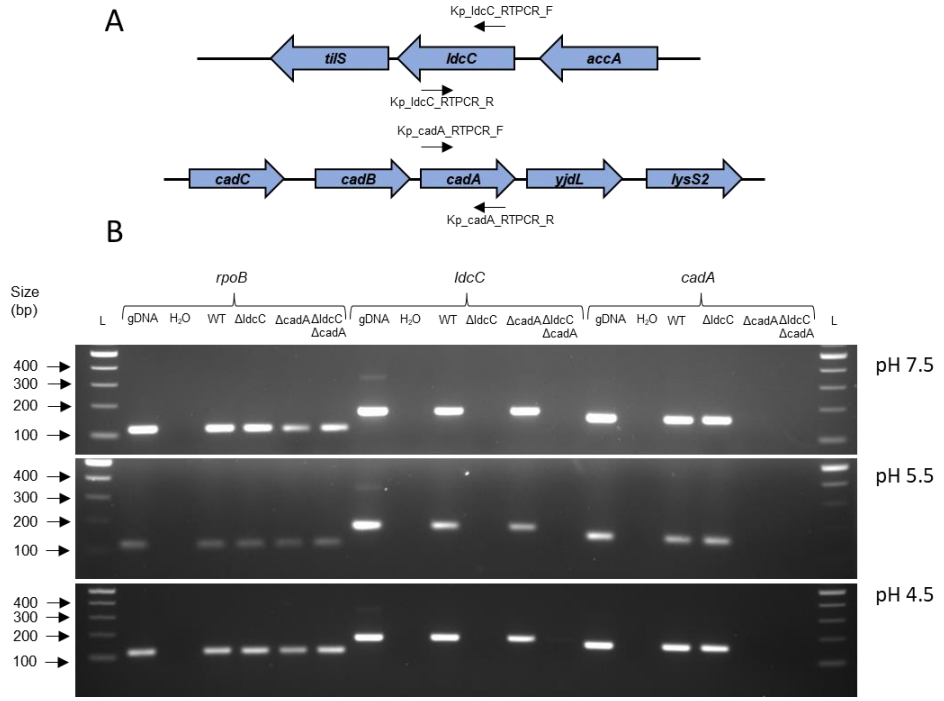

Figure 5.9. *ldcC* and *cadA* genes of *K. pneumoniae* 52145 are expressed at neutral and acidic pH. (A) Diagram of the predicted amplification within the *ldcC* and *cadA* genes of *K. pneumoniae* 52145, indicating the primer pair used and annealing sites. **(B)** Reverse transcriptase PCR performed on RNA isolated from exponentially growing *K. pneumoniae* 52145 wild type and cadaverine deletion strains, grown in LB broth altered to pH 7.5, 5.5 and 4.5 using primers to amplify internally of the *rpoB*, *ldcC* and *cadA* genes. The Kp_rpoB_RTPCR_F and Kp_rpoB_RTPCR_R pair were used for the *rpoB* gene amplifying a 120 bp product. Kp_ldcC_RTPCR_F and Kp_ldcC_RTPCR_R pair were used for the *ldcC* gene amplifying a product of 174 bp. The Kp_cadA_RTPCR_F and Kp_cadA_RTPCR_R pair were used for the *cadA* gene amplifying a product of 152 bp. L: 100 bp ladder. gDNA: Wild type genomic DNA positive control. H_2O: negative control. WT: RNA extracted from wild type strain. Δ*ldcC*: RNA extracted from Δ*ldcC* strain. Δ*cadA*: RNA extracted from Δ*cadA* strain. Δ*ldcC* Δ*cadA*: RNA extracted from Δ*ldcC* Δ*cadA* strain. RT-PCR is representative of two independent repeats.

5.3.3.2 Co-transcription of genes

With the confirmation of the expression of the *cadA* gene in *K. pneumoniae* 52145, it was next decided to investigate whether the *cadCBA* genes and the downstream *yjdL* and *lysS2* are expressed as polycistronic mRNA. In *E. coli* there is only coexpression of the *cadBA* genes, while in *K. pneumoniae* NTUH-K2044 it has been demonstrated that the *cadBA* genes are coexpressed with the downstream genes *yjdL* and *lysS2* (Hsieh et al., 2010). To confirm whether the genes are co-expressed with one another in the 52145 strain primers were designed to amplify across the junctions between genes (Figure 5.10A). The primers spanning the 365 bp *cadC*/*B* intergenic region, produce a product of 632 bp, the pair amplifying across the 76 bp *cadB*/*A* intergenic region produces a 484 bp product, the pair for the 59 bp *cadA*/*yjdL* intergenic region generate a product of 450 bp and the pair amplifying across the 331 bp *yjdL*/*lysS2* intergenic region generate a product of 882 bp. As expected, the RT-PCR using the *cadC*/*B* primer pair did not generate a product, showing that the *cadC* of *K. pneumoniae* 52145 is transcribed independently of *cadB* and *cadA* (Figure 5.10B). Amplification across the intergenic regions for *cadB*/*A*, *cadA*/*yjdL,* and *yjdL*/*lysS2* all generated the expected 484, 450, and 882 bp products, respectively (Figure 5.10B). This confirms that the *cadB*, *cadA*, *yjdL,* and *lysS2* in *K. pneumoniae* 52145 are transcribed as a single unit.

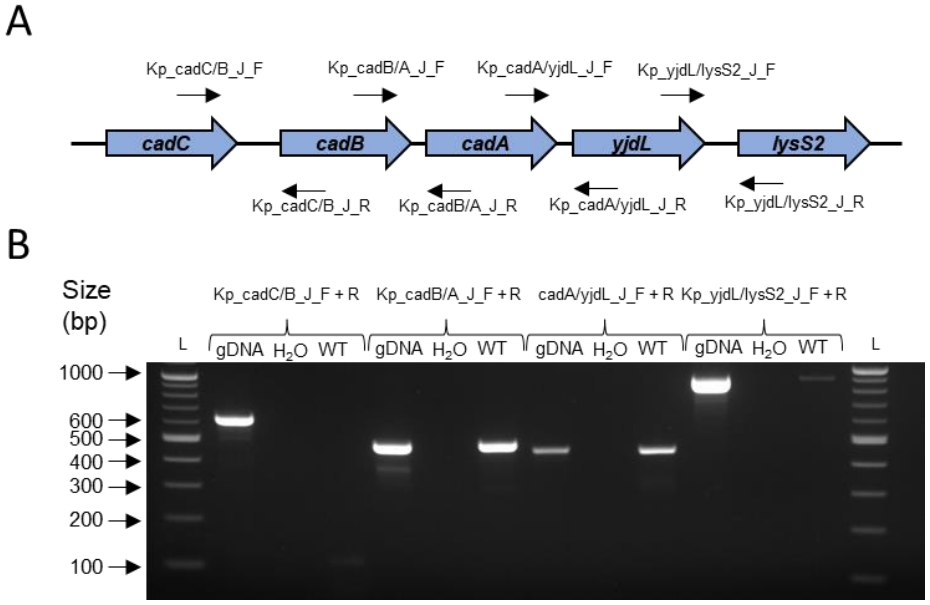

Figure 5.10. The *cadBA* genes are co-expressed in *K. pneumoniae* 52145.(A) Diagram of the predicted amplification across the intergenic regions of between the genes of the *cadCBA* operon and the downstream *yjdL* and *lysS2* genes of *K. pneumoniae* 52145, indicating the primer pair used and their annealing site. **(B)** Reverse transcriptase PCR performed on RNA isolated from wild type *K. pneumoniae* 52145 grown in LB broth pH 5.5 using the cadC/B_J_F and cadC/B_J_R, cadB/A_J_F and cadB/A_J_R, cadA/yjdL_J_F and cadA/yjdL_J_R, yjdL/lysS2_J_F and yjdL/lysS2_J_F primer pairs to amplify across the intergenic region between the *cadC*/*B*, *cadB*/*A*, *cadA*/*yjdL* and *yjdL*/*lysS2* genes generating 632 bp, 484 bp, 450 bp, 882 bp products, respectively. L: 100 bp ladder. gDNA: Wild type genomic DNA positive control. H_2O: negative control. WT: RNA extracted from wild type strain. RT-PCR is representative of two independent repeats.

5.3.4 Confirmation of the Δ*ldcC*, Δ*cadA,* and Δ*ldcC* Δ*cadA* deletions in *K. pneumoniae* 52145

To investigate the role of cadaverine in *K. pneumoniae* 52145 deletions were made in the constitutive and inducible pathways using the same methodology as other deletion strains, by Xuedi Liu, a previous member of the Hobley group. Gene deletions in the Δ*ldcC*, Δ*cadA,* and Δ*ldcc* Δ*cadA* strains were verified by PCR. Confirmation of Δ*ldcC* used the Kp_ldcC_UpF1 and Kp_ldcC_DwnR1 primer pair (Figure 5.11A), amplifying a product of 3.9 Kbp in the wild type and 1.8 Kbp in Δ*ldcC* deletion strain. Confirmation of the Δ*cadA* strain used the Kp_cadA_UpF1 and Kp_cadA_DwnR1 primer pair (Figure 5.11A), amplifying a 4 Kbp product from wild type gDNA and 1.9 Kbp product from the Δ*cadA*. Amplification generated the expected 1.8 and 1.9 Kbp products from the Δ*ldcC*

Δ*cadA* strain. Both sets of primers were used on the wild type and each deletion strain to confirm the presence of each gene or the successful deletion. The wild type strain produced the expected 3.9 and 4 Kbp products for the *ldcC* and *cadA* genes, respectively (Figure 5.11B). Final confirmation of deletion strains was carried out by Sanger sequencing of the deletion region (Section 2.5.1). Additionally, WGS was also carried out (Section 2.5.3). Sequencing of the deletion regions and WGS found a complete absence of the *ldcC* and *cadA* genes, in the respective strains, confirming the successful deletion of the cadaverine synthesis genes. Successful deletion of *ldcC* and *cadA* genes indicates that cadaverine is not essential for the survival of *K. pneumoniae* 52145.

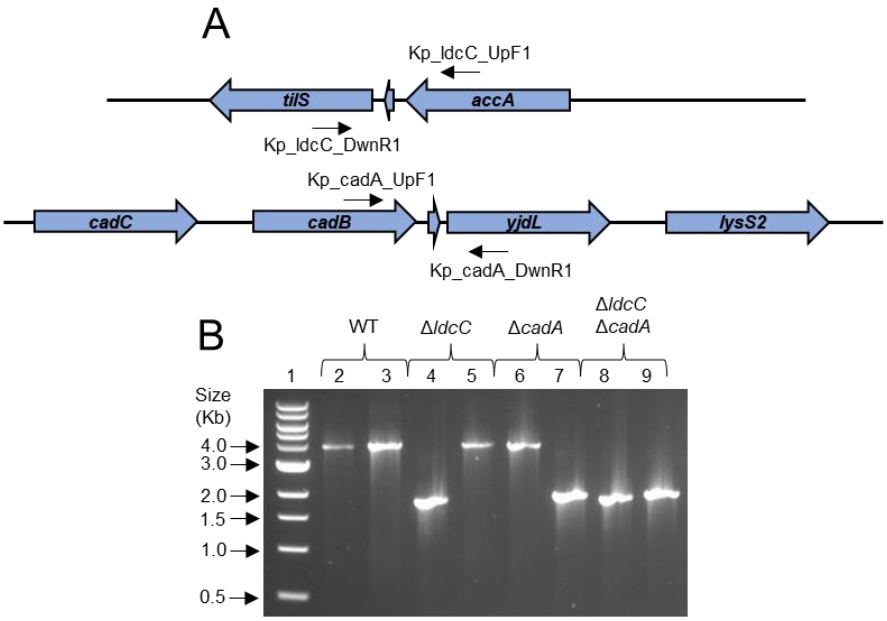

Figure 5.11. Confirmation of the deletion of *ldcC* and *cadA* genes of *K. pneumoniae* 52145. (A) Diagram of the amplification across the chromosomal region containing the *ldcC* and *cadA* genes showing the primers used to confirm the deletion of each gene. **(B)** Agarose gel confirming the successful deletion of *ldcC* and *cadA* genes *K. pneumoniae* 52145. To confirm the Δ*ldcC* the Kp_ldcC_UpF1 and Kp_ldcC_DwnR1 pair were used, generating 3.9 Kbp and 1.8 Kbp products for the wild type and Δ*ldcC*, respectively. To confirm the Δ*cadA* the Kp_cadA_UpF1 and Kp_cadA_DwnR1 were used, generating 4 Kbp and 1.9 Kbp products for the wild type and Δ*cadA* respectively. Lane 1: 1 Kbp ladder. Lane 2/4/6/8: Amplification of the *ldcC* gene. Lane 3/5/7/9: Amplification of the *cadA* gene. WT: Genomic DNA extracted from *K. pneumoniae* 52145 wild type. Δ*ldcC*: Genomic DNA extracted from the Δ*ldcC* strain. Δ*cadA*: Genomic DNA extracted from the Δ*cadA* strain. Δ*ldcC* Δ*cadA*: Genomic DNA extracted from the Δ*ldcC* Δ*cadA* strain.

5.3.5 Point mutations in *K. pneumoniae* 52145 wild type and Δ*ldcC*, Δ*cadA,* and Δ*ldcC* Δ*cadA* deletion strains.

Sequencing revealed point mutations with the deletion regions of the Δ*ldcC*, Δ*cadA* and Δ*ldcC* Δ*cadA* and WGS later confirmed this. This also found the Δ*ldcC* strain has five SNPs, five insertions, and one deletion. Of the five SNPs four occurred in the wild type and all the insertions were shared. The single additional SNP and deletion in the Δ*ldcC* strain (Table 5.3), are in the same ORF (BN49_4137), a gene annotated as encoding a predicted glyoxylase I family protein. The SNP is not predicted to cause structural damage to the protein. The frameshift, however would result in a dysfunctional protein. These mutations are shared with the Δ*ldcC* Δ*cadA* strain (Table 5.3) suggesting an introduction by the pGPI-SceI-Δ*ldcC* deletion vector. Fourteen SNPs were observed in the Δ*cadA* strain with eleven occurring in the sequenced wild type genome. Ten insertions were observed with nine occurring in the wild type. The two additional SNPs occurred in ORFs and were shared with the Δ*ldcC* Δ*cadA* strain (Table 5.3). The additional insertion was found to occur within an intergenic region (Table 5.3). For the Δ*ldcC* Δ*cadA,* fifteen SNPs were present with ten occurring in the wild type. An additional twelve insertions were observed, with ten of these being shared with the wild type. The Δ*ldcC* Δ*cadA* harboured a single deletion found within the BN49_4137 ORF (Table 5.3).. Analysis with Missense 3D suggests that N341T does not result in structural damage. Additionally, N341 does not appear involved in CadB function (Section 5.3.2.2) suggesting that this mutation may have little effect on protein function or structure. A mutation was observed in the downstream *yjdL* gene (BN49_1543). If the protein were still to be translated, Missense3D suggests there would be no significant impact on protein structure. The shared presence of these SNPs confirms they were introduced by the pGPI-SceI-Δ*cadA* deletion vector. There are two additional SNPs present in the Δ*ldcC* Δ*cadA* strain.

Table 5.3. Point mutations unique to the *K. pneumoniae* cadaverine deletion strains

***K. pneumoniae* Δ*ldcC* mutations**					
Nucleotide position	Allele in WT (amino acid residue)	Allele in ddc (amino acid residue)	Gene	Description	Possible effect on the structure of the protein
4379929	A (I86)	G T (86)	BN49_RS22765	VOC family protein	No structural damage
4379991	TG	T (Deletion)	BN49_RS22765	VOC family protein	Frameshift at position 65 of amino acid sequence
***K. pneumoniae* Δ*cadA* mutations**					
348718	C	CT	Intergenic	Downstream of *asd* encoding aspartate-semialdehyde dehydrogenase and the *glgB* gene, predicted to encode 1,4-alpha-glucan-branching enzyme	
1581727	A (N341)	C (T341)	BN49_RS09170 (*cadB*)	cadaverine/lysine antiporter	No structural damage
1584331	T	C	BN49_RS09180 (*yjdL*)	dipeptide permease DtpD	No structural damage
5438737	G	C	Intergenic	Upstream of *rnpA*, encoding ribonuclease P protein component	
***K. pneumoniae* Δ*ldcC* Δ*cadA* mutations**					
348718	C	CT	Intergenic	Downstream of *asd* encoding aspartate-semialdehyde dehydrogenase and the *glgB* gene, predicted to encode 1,4-alpha-glucan-branching enzyme	

1581727	A (N341)	C (T341)	BN49_RS09170 (*cadB*)	cadaverine/lysine antiporter	No structural damage
1584331	T (M1)	C (T1)	BN49_RS09180 (*yjdL*)	dipeptide permease DtpD	No structural damage
4379929	A	G	BN49_RS22765	VOC family protein	No structural damage
4379991	TG	T	BN49_RS22765	VOC family protein	Frameshift at position 65 of amino acid sequence
4382414	A	G	Intergenic	Downstream of *accA*, encoding Acetyl-coenzyme A carboxylase carboxyl transferase subunit alpha, and upstream of the *ldcC,* constitutive lysine decarboxylase	
4534031	G (A702)	T (A702)	BN49_RS23450 (*aroD*)	type I 3-dehydroquinate dehydratase	Synonymous mutation
4650326	G	GT	BN49_RS23995 (*rsmC*)	16S rRNA (guanine(1207)-N(2))-methyltransferase RsmC	Frameshift at position 165 of amino acid sequence

5.3.6 Genetic complementation of cadaverine biosynthesis mutants

Attempts were made to genetically complement the Δ*ldcC,* Δ*cadA* and Δ*ldcC* Δ*cadA* strains by cloning the *ldcC* and *cadA* genes into the pGEMT vector. Gene insertions were confirmed by diagnostic digest and sequencing. The expected products from the digestion of pGEMT-*ldcC* with EcoRI and ScaI were 2.8 Kbp for the gene insert and 1.8 and 1.1 Kbp for the pGEMT backbone fragments. The expected products of pGEMT-*cadA* digestion with SalI and ScaI were 3 Kbp for the gene insert and 1.8 Kbp and 1.2 Kbp for the pGEMT fragments. Each of the four pGEMT-*ldcC* and pGEMT-*cadA* vectors showed the expected fragment sizes, confirming the presence of the correct insertions into pGEMT. Sequencing found no point mutations present in any of the inserted sequences. Following confirmation, vectors were transformed into *K. pneumoniae* 52145 wild type and deletion strains. Their presence was confirmed by diagnostic digest (Figure 5.12) that found the correct transformation of each vector into the required deletion strain.

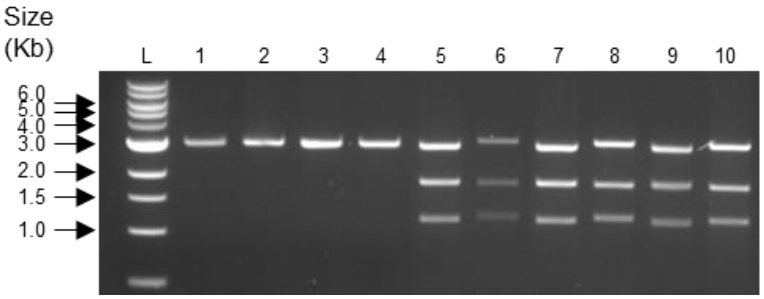

Figure 5.12. Confirmation of vectors for genetic complementation of Δ*ldcC*, Δ*cadA,* and Δ*ldcC* Δ*cadA*. Restriction digest of pGEMT vectors for the complementation of cadaverine biosynthesis mutants, purified from wild type, Δ*ldcC*, Δ*cadA,* and Δ*ldcC* Δ*cadA*, following transformation. pGEMT-*ldcC* were digested with EcoRI and ScaI generating products of 2.8, 1.8, and 1.1 Kbp. pGEMT-*cadA* were digested with SalI and ScaI to generate products of 3, 1.8 and 1.2 Kbp. L: 1 Kbp ladder. Lane 1: pGEMT purified from the WT strain. Lane 2: pGEMT purified from the Δ*ldcC* strain. Lane 3: pGEMT purified from the Δ*cadA* strain. Lane 4: pGEMT purified from the Δ*ldcC* Δ*cadA* strain. Lane 5: pGEMT-*ldcC* purified from the WT strain. Lane 6: pGEMT-*cadA* purified from the WT strain. Lane 7: pGEMT-*ldcC* purified from the Δ*ldcC* strain. Lane 8: pGEMT-*cadA* purified from the Δ*cadA* strain. Lane 9: pGEMT-*ldcC* purified from the Δ*ldcC* Δ*cadA* strain. Lane 10: pGEMT-*cadA* purified from the Δ*ldcC* Δ*cadA* strain.

5.3.7 *K. pneumoniae* 52145 synthesises cadaverine

K. pneumoniae 52145 encodes the genes for constitutive and acid-inducible cadaverine synthesis. Along with those for 1, 3-diaminopropane, putrescine and spermidine. It is hypothesised that *K. pneumoniae* may synthesise the spermidine analogues, norspermidine and aminopropylcadaverine. To confirm the polyamines produced by *K. pneumoniae* 52145 HPLC analysis (Section 2.10) was carried out by Aaron Franklin in Dr Patrick Moynihan's laboratory at The University of Birmingham. Alongside samples known polyamine standards were assessed (Figure 5.13). 1, 3-diaminopropane is detected at approximately 15.9 minutes, putrescine is detected at 16 minutes, cadaverine at 16.1 minutes, the internal standard 1, 7-diaminoheptane is detected at 16.5 minutes and spermidine is detected at 17 minutes.

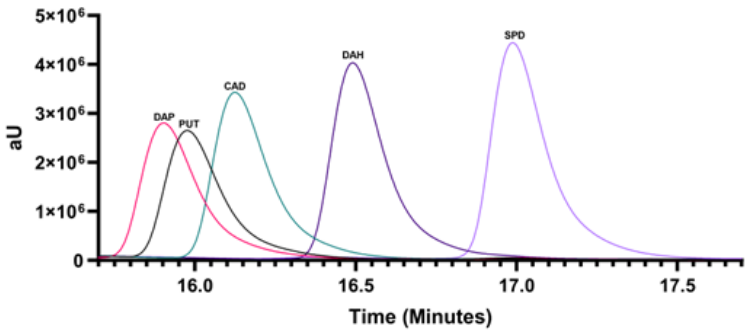

Figure 5.13. Retention times of 1, 3-diaminopropane, putrescine, cadaverine, 1, 7-diaminoheptane and spermidine polyamine standards. Separation of polyamines standards and the corresponding retention times of 1, 3-diaminopropane, DAP; putrescine, PUT; cadaverine; CAD, 1, 7-diaminoheptane, DAH; spermidine, SPD.

All samples analysed feature a peak corresponding to the retention time of the added internal standard 1, 7-diaminoheptane (Figure 5.14). This was used to determine the relative abundance of each polyamine in each sample. Growth of the wild type, Δ*ldcC*, Δ*cadA* and Δ*ldcC* Δ*cadA* strains in M9 broth at pH 6.5 (Figure 5.14A-D) and 5.5 (Figure 5.14A-D) generated detectable levels of putrescine and spermidine relative abundance of putrescine appears to be far greater than that of spermidine, under both conditions, for all strains (Figure 5.14A-D) and 5.5 (Figure 5.15A-D). This confirms the synthesis of both putrescine and spermidine in *K. pneumoniae* 52415.

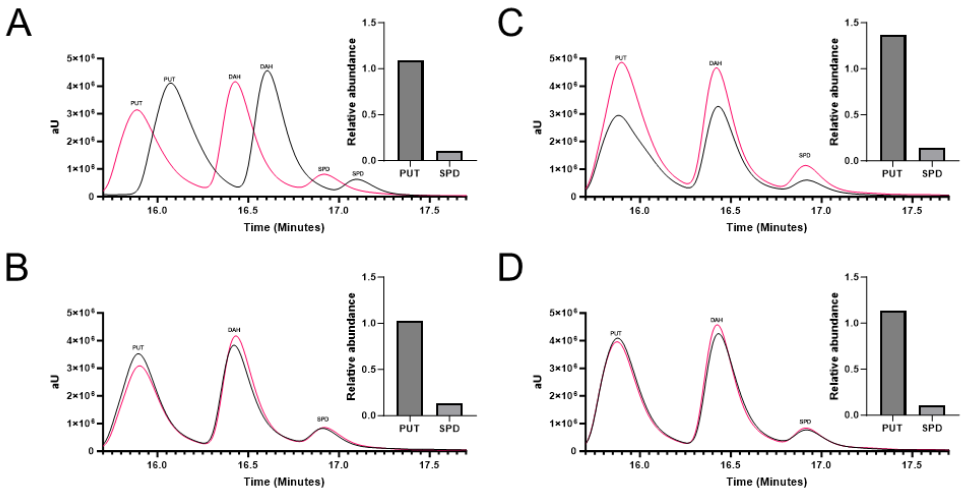

Figure 5.14. Putrescine and spermidine are synthesised at pH 6.5 and stationary phase in *K. pneumoniae* 52145. Comparison of the detection of polyamines produced by *K. pneumoniae* **(A)** wild type, **(B)** Δ*ldcC*, **(C)** Δ*cadA*, **(D)** Δ*ldcC* Δ*cadA* strains, when grown at pH 6.5, by HPLC and their relative abundance. Cells were grown in M9 minimal media, devoid of exogenous polyamines. 15 µl of 0.4 mM 1,7-diaminoheptane was added to each sample as an internal standard. Polyamines were extracted with trichloroacetic acid: HCl extraction and derivatised with dansyl chloride. PUT, putrescine; DAH, 1, 7-diaminoheptane; SPD, spermidine. The data presented represents two biological repeats.

There do not appear to be detectable levels of cadaverine in the wild type, Δ*ldcC,* or Δ*cadA* strains at pH 6.5 (Figure 5.14A-C). This may be due to the vast abundance of putrescine detected, obscuring the lesser prevalent diamines such as cadaverine. Cadaverine is not detected in Δ*ldcC* Δ*cadA* strain sample either when grown at pH 6.5 (Figure 5.14D). While it is plausible that the vast abundance of putrescine may mask the detection of cadaverine in the previously discussed strains this is likely not the case with the Δ*ldcC* Δ*cadA,* as there is a loss of both lysine decarboxylase enzymes, preventing cadaverine synthesis via the known metabolic pathways. Growth of the wild type strain in M9 at pH 5.5 results in detectable cadaverine, indicated by the shoulder formed on the putrescine peak for the wild type derived sample (Figure 5.15A). This confirms that *K. pneumoniae* 52145 synthesises cadaverine and suggests that acid induction of cadaverine synthesis is occurring during growth. The relative abundance of cadaverine, in the wild type, is similar to that of putrescine when grown at pH 5.5 (Figure 5.15A). It is worth noting that the relative abundance of putrescine at pH 5.5 is nearly half that seen at pH 6.5.

This factor may allow for more accurate detection of cadaverine, present in the sample. Cadaverine is not detected in the Δ*ldcC* strain when grown at pH 5.5 (Figure 5.15B). Considering, the Δ*ldcC* strain still maintains the acid-inducible CadA, lysine decarboxylase, this could be seen as unusual. There is a significant presence of putrescine, indicated by the relative abundance (Figure 5.15B). This suggests that again putrescine may be obscuring the detection of cadaverine. As expected, there does not appear to be any significant cadaverine produced by the Δ*cadA* and Δ*ldcC* Δ*cadA* strains when grown at pH 5.5 (Figure 5.15C and D) which can be attributed to the loss of acid-inducible lysine decarboxylase. Both strains also produce putrescine and spermidine, with the relative abundance of putrescine being greater than that of spermidine (Figure 5.15C and D).

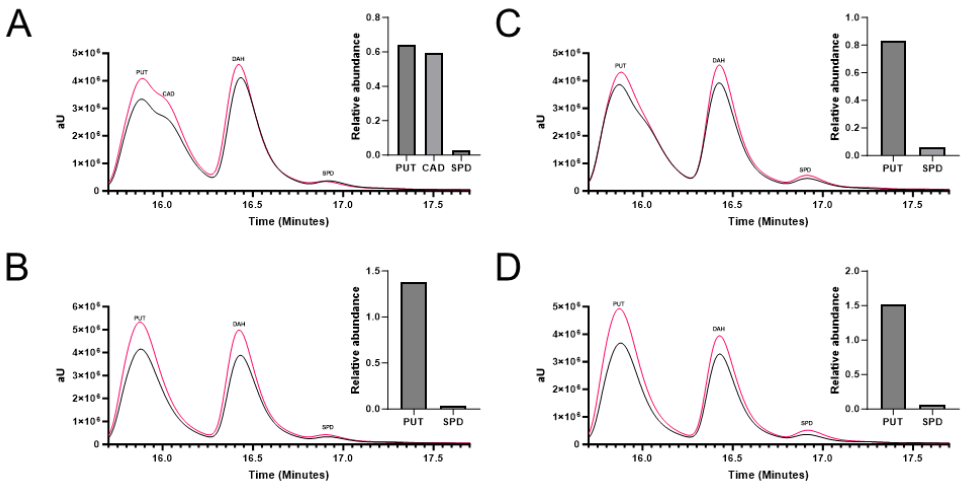

Figure 5.15. Cadaverine is synthesised at pH 5.5 and stationary phase in K. pneumoniae 52145. Comparison of the detection of polyamines produced by K. pneumoniae **(A)** wild type, **(B)** Δ*ldcC*, **(C)** Δ*cadA*, **(D)** Δ*ldcC* Δ*cadA* strains, when grown at pH 5.5, by HPLC and their relative abundance. Cells were grown in M9 minimal media, devoid of exogenous polyamines. 15 µl of 0.4 mM 1,7-diaminoheptane was added to each sample as an internal standard. Polyamines were extracted with trichloroacetic acid: HCl extraction and derivatised with dansyl chloride. PUT, putrescine; CAD, cadaverine; DAH, 1, 7-diaminoheptane; SPD, spermidine. The data presented represents two biological repeats.

Analysis of *K. pneumoniae* Δ*speAB,* Δ*speABC* and Δ*speABCE* strains revealed that cadaverine is synthesised when grown at pH 6.5 figures (Figure 5.16A-C). In addition to cadaverine, there are also detectable levels of 1, 3-diaminopropane in the Δ*speABC* and Δ*speABCE* strains (Figure 5.16B and C),

lacking putrescine synthesis. This supports the idea, that when there is a significant abundance of putrescine separation of other diamines becomes difficult. The relative abundance of cadaverine appears to be less than that of 1, 3-diaminopropane, in both strains (Figure 5.16B and C). As expected, the Δ*speABC* and Δ*speABCE* strains, show a loss of detectable putrescine (Figure 5.16B and C). This is due to a loss of both putrescine synthesis pathways. The Δ*speAB* strain still produces putrescine (Figure 5.16A), due to the presence of the ornithine pathway being present. Analysis of the sample derived from the Δ*speABC* strain revealed the presence of a polyamine, with a retention time comparable to spermidine (Figure 5.16B). However, this strain lacking the *speABC* genes, should be incapable of putrescine synthesis and would subsequently be unable to synthesise spermidine. In addition to this, deletion of the *speABC* genes along with *speE*, results in the loss of this detectable peak (Figure 5.16C). This suggests spermidine synthase may be acting on cadaverine, in the absence of putrescine, to synthesise aminopropylcadaverine.

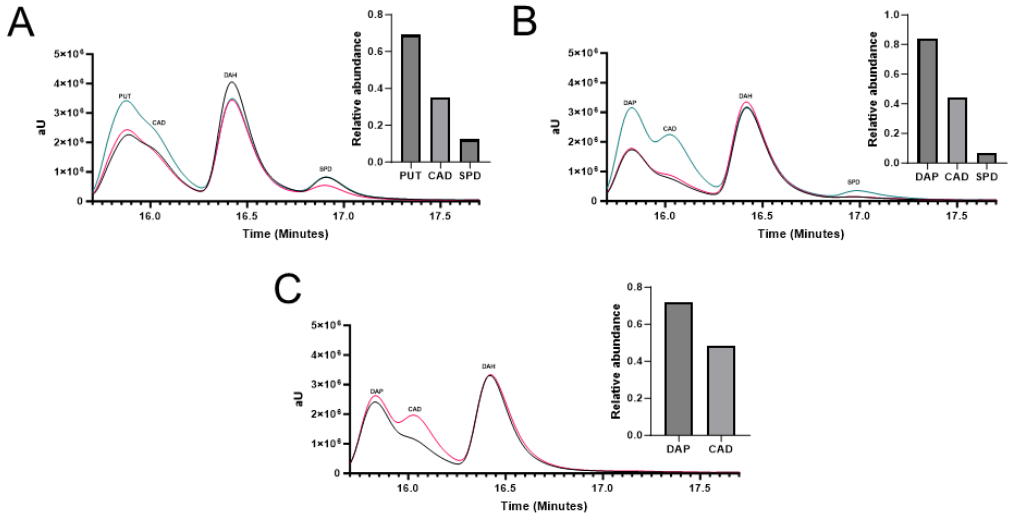

Figure 5.16. Cadaverine is synthesised at pH 6.5 and stationary in *K. pneumoniae* 52145 and is possibly converted into aminopropylcadaverine. Comparison of the detection of polyamines produced by *K. pneumoniae* **(A)** Δ*speAB*, **(B)** Δ*speABC*, **(C)** Δ*speABCE* strains, when grown at pH 6.5, by HPLC and their relative abundance. Cells were grown in M9 minimal media, devoid of exogenous polyamines. 15 µl of 0.4 mM 1,7-diaminoheptane was added to each sample as an internal standard. Polyamines were extracted with trichloroacetic acid: HCl extraction and derivatised with dansyl chloride. DAP, 1, 3-diaminopropane; PUT, putrescine; CAD, cadaverine; DAH, 1, 7-diaminoheptane; SPD, spermidine. Data presented for the Δ*speAB* and Δ*speABC* strains represents three biological repeats. The data presented for the Δ*speABCE* strain represents two biological

5.3.8 Deletion of *cadA* results in loss of acid-inducible cadaverine production

To confirm LDC activity in *K. pneumoniae* 52145 and indirectly the secretion of cadaverine for pH maintenance the wild type and cadaverine deletion strains were grown in lysine decarboxylase broth (Section 2.11). During incubation, the anaerobic conditions result in acid production, by fermentation, which lowers the pH of the media resulting in a purple to yellow colour change. The acidic conditions and excess of L-lysine in the media promote the expression of LDC. The resulting cadaverine production and export raise the pH of the media. This changes the colour of the broth back to purple. This can infer whether there is acid-inducible LDC activity and cadaverine production. The growth of the wild type and the Δ*ldcC* deletion strain in LDC broth resulted in the purple colouration of media (Figure 5.17). This suggests that *K. pneumoniae* 52145 has acid-inducible lysine decarboxylase activity and produces cadaverine to maintain pH homeostasis. Growth of the Δ*cadA* and Δ*ldcC* Δ*cadA* deletion strains in LDC broth resulted in the yellow colouration of media (Figure 5.17), implying the presence of an acidic environment. This confirms a loss of acid-inducible lysine decarboxylase activity when the *cadA* gene is deleted. Interestingly, the *ldcC* gene is intact in the Δ*cadA* strain, suggesting that the constitutive lysine decarboxylase cannot complement the loss of *cadA*. This confirms that *K. pneumoniae* 52145, is capable of acid lysine decarboxylase activity and that cadaverine is used to maintain pH in acidic environments.

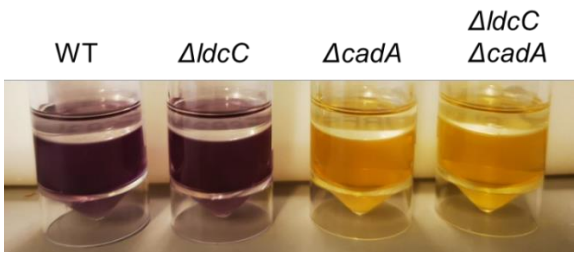

Figure 5.17. Deletion of the *cadA* gene results in the loss of acid-inducible lysine decarboxylase activity. Comparison of the lysine decarboxylase activity of cadaverine deletion strains using lysine decarboxylase broth. Left to right: *K. pneumoniae* 52145 Wild type, Δ*ldcC*, Δ*cadA*, Δ*ldcC* Δ*cadA* grown in Lysine decarboxylase broth overlaid with 2 ml of mineral oil incubated for 24 hours at 37 °C. The images presented are representative of three independent repeats.

5.3.9 Genetic complementation with *cadA* does not restore lysine decarboxylase activity

Genetic complementation of the Δ*ldcC*, Δ*cadA* and Δ*ldcC* Δ*cadA* was attempted and lysine decarboxylase activity was assessed using LDC broth. To test whether the pGEM-T-based vectors negatively impacted cell viability, all were transformed into wild type *K. pneumoniae* 52145. The empty pGEM-T and complementation vectors did not affect the wild type or cadaverine deletion strain viability or the known lysine decarboxylase activity of the wild type or Δ*ldcC* strain (Figure 5.18B). Transformation of pGEMT-*cadA* into the Δ*cadA* and Δ*ldcC* Δ*cadA* deletion strains was unable to restore the acid-inducible lysine decarboxylase activity (Figure 5.18A), with the LDC broth remaining acidic and visibly yellow. This suggests that genetic complementation with *cadA* gene does not restore acid-inducible lysine decarboxylase activity. Transformation of the pGEMT-*ldcC* vector into the Δ*ldcC* strain did not affect lysine decarboxylase activity (Figure 5.18A), with the Δ*ldcC* strain phenocopying the wild type strain in LDC broth. Complementation with the *ldcC* gene did not restore the lysine decarboxylase activity of the Δ*cadA* or Δ*ldcC* Δ*cadA* deletion strains (Figure 5.18A). This confirms the importance of *cadA* in the *cadCBA* operon acid resistance system, and that additional factors may play a role in *cadA* expression.

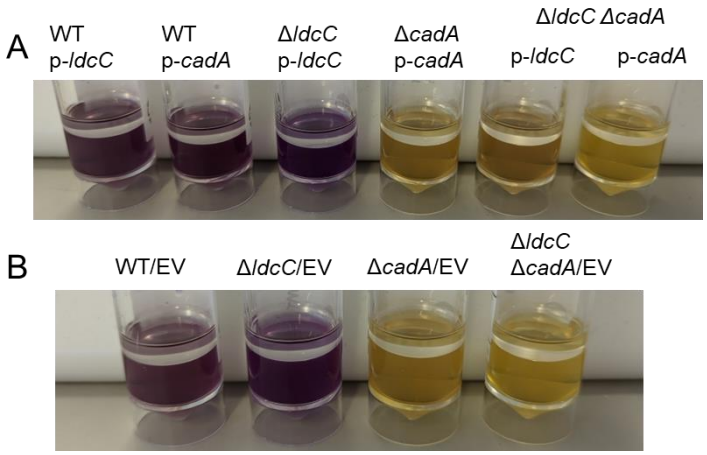

Figure 5.18. The loss of inducible lysine decarboxylase activity cannot be genetically complemented. (A) Comparison of the lysine decarboxylase activity of genetically complemented cadaverine deletion strains using lysine decarboxylase broth. Left to right: *K. pneumoniae* 52145 Wild type + pGEMT-*ldcC*, WT + pGEMT-*cadA*, Δ*ldcC* + pGEMT-*ldcC*, Δ*cadA* + pGEMT-*cadA*, Δ*ldcC* Δ*cadA* + pGEMT-*ldcC* + pGEMT-*cadA*. **(B)** Comparison of the lysine decarboxylase activity of *K. pneumoniae* 52145 wild type and cadaverine deletion strains containing empty pGEMT vectors (EV). Images are representative of two biological repeats.

5.3.10 Deletion of cadaverine synthesis genes does not alter *K. pneumoniae* hypermucoviscous phenotype

As with the *K. pneumoniae* 52145 Δ*dat* and Δ*ddc* strains (Section 4.3.5) capsule formation was first investigated. Before the assessment of capsule mucoviscosity, it was observed that the Δ*ldcC*, Δ*cadA* and Δ*ldcC* Δ*cadA* strains did not appear to exhibit any growth defects, colonies had the same mucoid appearance, and when centrifuged all showed the same capsulated pellet as the wild type strain. The string test was used to assess the hypermucoviscous phenotype of the cadaverine synthesis mutants (Section 2.13). All strains tested, excluding the Δ*manC* and Δ*speE*, formed strings on LB and M9 minimal agar (Figure 5.19). All strains displayed longer strings when grown on M9 minimal agar (Figure 5.19B) than LB agar (Figure 5.19A). When grown on either LB or M9 minimal media there was no significant difference in the string lengths of the Δ*ldcC*, Δ*cadA* and Δ*ldcC* Δ*cadA* strains when compared to *K. pneumoniae* 52145 wild type strain (Figure 5.19). These observations show that cadaverine is not required for capsule synthesis or the hypermucoviscous phenotype of *K. pneumoniae* 52145.

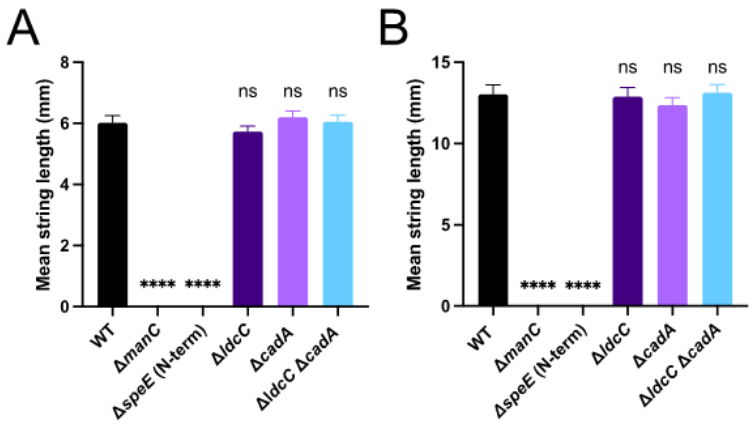

Figure 5.19. Deletion of the *ldcC* and *cadA* genes does not impact capsule formation or the hypermucoviscous phenotype of *K. pneumoniae* 52145. Comparison of the mean string length produced when an inoculation loop is moved vertically from a colony of 2-4 mm in diameter grown on **(A)** LB or **(B)** M9 minimal agar for *K. pneumoniae* 52145 wild type, Δ*ldcC*, Δ*cadA* and Δ*ldcC* Δ*cadA* strains. Δ*manC* and Δ*speE* (N-term) were used as negative controls. *manC* encodes Mannose-1-phosphate guanylyltransferase and Δ*speE* encodes spermidine synthase, deletion of both genes results in a loss of typical hypercapsulated phenotype. Values presented are the mean and SEM of ten measurements from three independent experiments. **** = p-value ≤ 0.0001 (unpaired T-test with Welch's correction).

5.3.11 Cadaverine synthesis promotes growth in acidic conditions

While the combination of the analysis of gene expression, growth in LDC broth and HPLC (Section 5.3.3.1, 5.3.7 and 5.3.8) have all determined that *K. pneumoniae* 52145 expresses the inducible LDC and produces cadaverine it does not give an indication to the degree protection cadaverine provides against low environmental pH. To determine the effects of varying pH on the growth kinetics strains were grown in LB broth altered to pH 7, 5.5, 4 and 3 (Section 2.12). Growth of all deletion strains at pH 7.5 and 5.5 demonstrate similar kinetics, when compared to the wild type (Figure 5.20A and B), with there being no significant differences in the growth rate (Table 9.3) and doubling time (Table 9.3). Growth of all strains appears to slow following 4 hours of incubation (Figure 5.20A and B) with all reaching a plateau in optical density at approximately 6 hours (Figure 5.20A and B) and strains reach a comparative final optical density (Figure 5.20A and B). Growth at pH 4 does somewhat impact the kinetics of the wild type (Figure 5.20AC), it was found to

significantly decrease the exponential growth rate (Table 9.3) when compared to those obtained at pH 7.5 and 5.5 (P = 0.0012 and 0.0014), and significantly increasing the doubling time (Table 9.3) when compared to those at pH 7.5 and 5.5 (P = 0.0054 and 0.0041). A similar observation was seen with the Δ*ldcC* strain (Figure 5.20C), there appears to be a significant decrease in the exponential growth rate (Table 9.3), when compared to the rates observed at pH 7.5 and 5.5 (P = 0.0028 and 0.0021) and an increase in doubling time (Table 9.3) when compared to those observed at pH 7.5 and 5.5 (P = 0.0090 and 0.0066). The growth of the Δ*ldcC* strain appears to phenocopy the wild type strain at pH 4 (Figure 5.20C), with no significant difference in growth rate or doubling time (Table 9.3). Both strains appear to reach a similar final optical density following the 8-hour growth period (Figure 5.20C), an optical density similar to that obtained when both strains are grown at pH 7.5 and 5.5 (Figure 5.20A-C). Growth of the Δ*cadA* and Δ*ldcC* Δ*cadA* strains at pH 4 has a greater effect on growth compared to the wild type and Δ*ldcC* (Figure 5.20C). Determination of the growth rates of both strains (Table 9.3), revealed them to be significantly decreased when compared to the wild type grown under the same conditions (P = 0.0344 and 0.0255). While visibly there appears to be a difference in the doubling time of both strains (Table 9.3), neither appears to be significantly different to the doubling time of the wild type, grown under the same conditions.

Growth of the Δ*cadA* and Δ*ldcC* Δ*cadA* strains at pH 4, decreases the maximum optical density achieved after the eight hours of growth (Figure 5.20C), while the wild type and Δ*ldcC* achieve a similar, final optical density to those seen at pH 7.5 and 5.5 (Figure 5.20A-C). None of the strains reach a plateau in optical density, similar to that observed at pH 7.5 and 5.5 (Figure 5.20A-C). Optical densities appear to be unchanged when subjected to pH 3 (Figure 5.20D), suggesting a lack of survival and growth. When enumerated at the end of the eight hours, little to no colonies were recovered from each culture (data not shown), suggesting all strains had limited survival at pH 3. This data indicates that the inducible lysine decarboxylase supports the growth of *K. pneumoniae*

52145 in pH as low as 4 but cannot provide protection, or at least under these conditions, to pH 3.

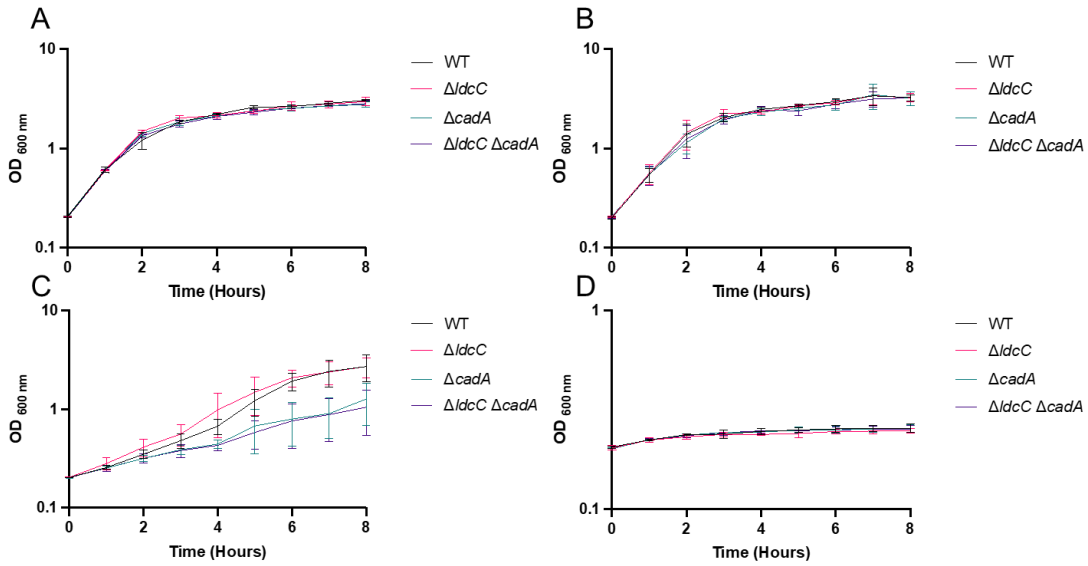

Figure 5.20. The *cadA* gene promotes growth at pH 4. Comparison of growth kinetics of *K. pneumoniae* 52145 wild type and the Δ*ldcC*, Δ*cadA*, Δ*ldcC* Δ*cadA* at pH **(A)** 7.5, **(B)** 5.5, **(C)** 4 and **(D)** 3. The OD_{600nm} was measured every hour across and 8-hour period. Values represent the mean and SEM of three independent experiments.

5.3.12 Loss of cadaverine synthesis does not increase susceptibility to Oxidative stress

The *cadBA* genes of *V. vulnificus* are induced under oxidative stress in *V. vulnificus* and *E. coli* (Akhova et al., 2021; Kang et al., 2007) suggesting cadaverine protects against ROS. Along with this and the previous rationale with the 1, 3-diaminopropane strains, the contribution of cadaverine to oxidative stress resistance in *K. pneumoniae* was investigated (Section 2.15.1). As expected, the size of the inhibitory zone was proportional to the concentration of hydrogen peroxide used, increasing as concentration increased (Figure 5.21). The diameter of Inhibitory zones for Δ*ldcC*, Δ*cadA* and Δ*ldcC* Δ*cadA* at each concentration of H_2O_2 were identical to those of the wild type at the same concentration (Figure 5.21) and therefore were not significantly different to the wild type across all hydrogen peroxide concentrations tested. Indicating that loss of cadaverine synthesis does not increase susceptibility to oxidative stress, and that cadaverine is not utilised as

an antioxidant in *K. pneumoniae*. The possibility that cadaverine acts as a ROS scavenger cannot be completely disregarded, as *K. pneumoniae* 52145 encodes several other polyamine synthesis pathways. An abundance of other polyamines may negate any negative phenotype arising from the loss of cadaverine synthesis, however, it could be possible that another polyamine of those synthesised carries out this role in *K. pneumoniae.*

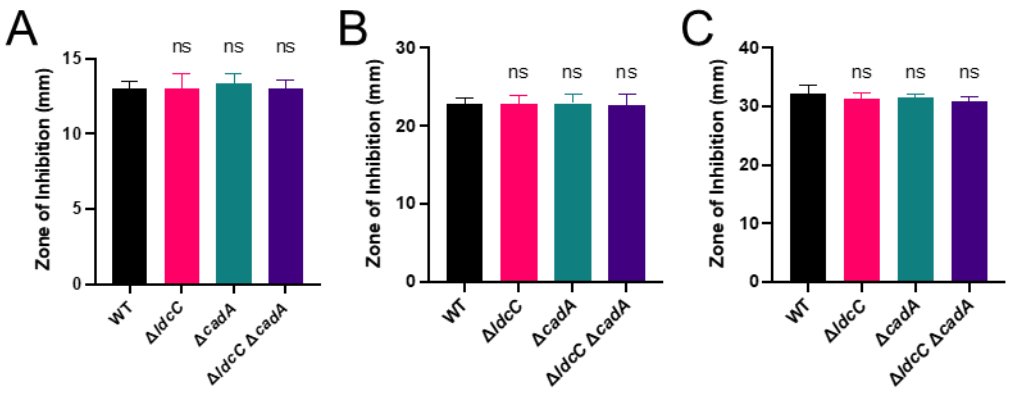

Figure 5.21. Cadaverine does not protect against oxidative stress induced by H_2O_2. Comparison of survival of *K. pneumoniae* wild type and Δ*ldcC*, Δ*cadA* and Δ*ldcC* Δ*cadA* strains, in the presence of **(A)** 3 %, **(B)** 10 % and **(C)** 30 % (v/v) hydrogen peroxide. The inhibitory effect of hydrogen peroxide was assessed by disk diffusion assay. The values presented represent the mean and SEM of three independent experiments. Statistical analysis was measured using an unpaired T-test with Welch's correction.

5.3.13 Deletion of *cadA* results in altered growth kinetics in the presence of nitrite

Previous investigation has found that cadaverine protects against nitrosative stress in uropathogenic *E. coli* (Bower and Mulvey, 2006). Drawing on parallels between UPEC and *K. pneumoniae* it was decided to investigate the possibility of cadaverine in protection against RNS. The effect of nitrosative stress was investigated by two methods (Section 2.15.2). The first utilised acidified nitrite to induce nitrosative stress. Nitrite in the presence of hydrogen ions forms nitrous acid. This ultimately forms nitric oxide and dinitrogen oxide, inducing nitrosative stress (Equation 5.1). The second utilised sodium nitroprusside, a compound that readily releases nitric oxide from its structure.

$$NO_2^- + H^+ \rightarrow HNO_2$$

$$2HNO_2 \rightarrow N_2O_3 + H_2O$$

$$N_2O_3 \rightarrow NO_2 + NO$$

Equation 5.1. The formation of reactive nitrogen species from nitrite in the presence of hydrogen ions.

Initially, the effect of nitrosative stress on cadaverine deletion strains was assessed using acidified sodium nitrite (Figure 5.22). It was found that all cadaverine deletion strains appear to grow similarly to the wild type at pH 5.5 and in the absence of sodium nitrite (Figure 5.22), the same as what was previously observed (Section 5.3.11). Growth of all strains slows following 4 hours of incubation (Figure 5.22) and continues until reaching a plateau at 6 hours of incubation (Figure 5.22). All strains reach a comparative final optical density following 8 hours of incubation (Figure 5.22). All four strains had comparative exponential growth rates and doubling times (Table 9.4) similar to those previously observed at pH 5.5 (Section 5.3.11). The addition of sodium nitrite, to pH 5.5 media, results in a change in the growth kinetics of all four strains (Figure 5.22). The Δ*ldcC* strain appears to phenocopy the wild type strain (Figure 5.22), with optical densities identical across all time points. Acidified sodium nitrite appears to significantly decrease the growth rate of the wild type, compared to the rate obtained in its absence (P = 0.0003). A similar observation was made with the Δ*ldcC* strain (P = 0.0008). Both strains have identical, non-significantly different, exponential growth rates and doubling times (Table 9.4). Both strains reach a similar final optical density, following 8-hour incubation (Figure 5.22).

Growth of the Δ*cadA* and Δ*ldcC* Δ*cadA* strains in the presence of acidified nitrite has a greater effect on growth kinetics than that observed for the wild type and Δ*ldcC* strains. Both strains phenocopying one another (Figure 5.22) and optical density values are lower than those obtained with the WT and Δ*ldcC* strains (Figure 5.22), under the same conditions. Comparison of the growth rate of the

Δ*cadA* (Table 9.4) in the presence and absence of sodium nitrite revealed the rate to be significantly decreased when acidified nitrite was present (P = 0.0002) However, compared to the wild type under the same conditions there appears to be no significant difference. A similar observation was made with the Δ*ldcC* Δ*cadA* strain, the presence of sodium nitrite significantly decreases the growth rate compared to that in its absence (P = 0.0007). However, there appears to be no significant difference between the wild type and the Δ*ldcC* Δ*cadA*, in the presence of acidified sodium nitrite. Despite the lack of statistical significance between the Δ*cadA*/Δ*ldcC* Δ*cadA* strains and the wild type, there is a clear difference in growth kinetics between the two strains and the wild type. None of the four strains reaches a stationary phase, like that observed in the absence of sodium nitrite, and all reach a lower average final optical density following 8 hours of incubation.

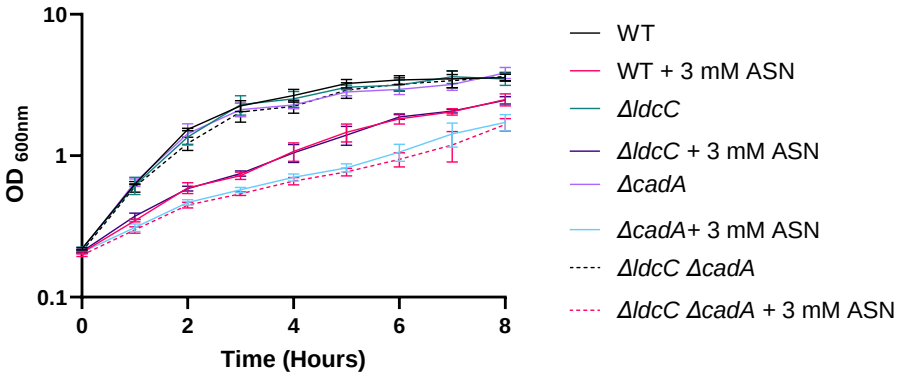

Figure 5.22. Deletion of the Δ*cadA* gene impacts growth kinetics in the presence of acidified sodium nitrite. Comparison of the planktonic growth kinetics of *K. pneumoniae* wild type and the Δ*ldcC*, Δ*cadA* and Δ*ldcC* Δ*cadA* cadaverine deletion strains in LB broth (pH 5.5) supplemented with 3 mM sodium nitrite. The OD_{600nm} was measured every hour across 8 hours. Values represent the mean and SEM of three independent experiments.

Following the observations made with acidified sodium nitrite, another approach was taken to assess the effect of nitrosative stress on the cadaverine deletion strains. This involved the application of sodium nitroprusside at pH 5.5 (Figure 5.23A) and 7.5 (Figure 5.23B). The application of sodium nitroprusside alters the growth kinetics of all strains when compared to the presence of sodium ferrocyanide (Figure 5.23) and the effect is further exacerbated by the

presence of acidic pH (Figure 5.23A). At the two pHs, the growth kinetics of the wild type and the Δ*ldcC* strain, are highly similar (Figure 5.23) and there is no significant difference between the presence of sodium nitroprusside and sodium ferrocyanide. At pH 7.5 all of the cadaverine deletion strains phenocopy the wild type strain when sodium nitroprusside and ferrocyanide are present (Figure 5.23B). All strains approach a plateau at approximately 6 hours (Figure 5.23B). All strains reach a lower maximum optical density when sodium nitroprusside is present compared to those recorded with sodium ferrocyanide (Figure 5.23B).

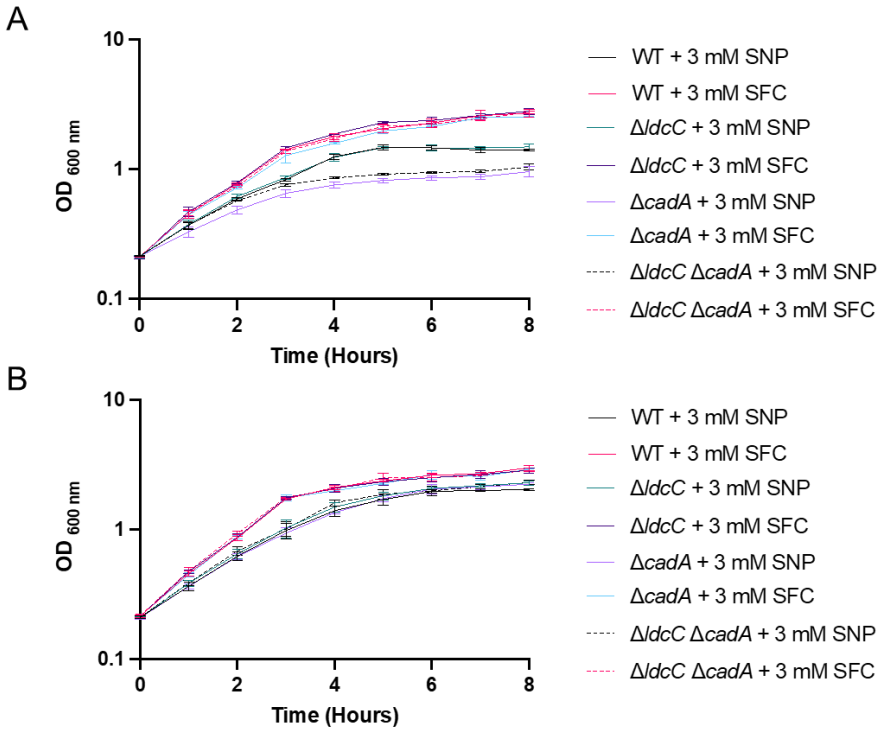

Figure 5.23. Deletion of the Δ*cadA* gene impacts growth kinetics in the presence of sodium nitroprusside at pH 5.5. Comparison of the planktonic growth kinetics of *K. pneumoniae* wild type and the Δ*ldcC*, Δ*cadA* and Δ*ldcC* Δ*cadA* cadaverine deletion strains in LB broth at pH **(A)** 5.5 and **(B)** 7.5 supplemented with 3 mM sodium nitroprusside or sodium ferrocyanide. The OD_{600nm} was measured every hour across 8 hours. Values represent the mean and SEM of three independent experiments.

The presence of sodium nitroprusside at the acidic pH, results in altered growth kinetics of the Δ*cadA* and Δ*ldcC* Δ*cadA* strains when compared to the wild type and Δ*ldcC*. The Δ*cadA* strain appears to reach lower optical densities across the entire time course when compared to those of the wild type (Figure 5.23A).

The maximum optical density reached by the Δ*cadA* and Δ*ldcC* Δ*cadA* strains, in the presence of acidic pH and sodium nitroprusside is less than those of the wild type and Δ*ldcC* (Figure 5.23A) and less than those observed when acidified nitrite (Figure 5.22) was the source of nitrosative stress. Both strains appear to begin reaching a plateau in optical density following 4 hours of incubation (Figure 5.23A). Interestingly the Δ*ldcC* Δ*cadA* strain behaves similarly to the wild type for the first 2-3 hours of incubation at pH 5.5 (Figure 5.23A) and in the presence of sodium ferrocyanide.

When the growth rate of Δ*cadA* in the presence of sodium nitroprusside (Table 9.4) is compared to that in the presence of sodium ferrocyanide (Table 9.4), at the same pH, there is a significant decrease (P = 0.0001). There is also a significant decrease when compared to the growth rate (Table 9.4) and doubling time of the wild type at pH 5.5 in the presence of sodium nitroprusside (Table 9.4) (P = 0.0008 and 0.0007). Similarly, the addition of sodium nitroprusside at pH 5.5 decreases the growth rate of the Δ*ldcC* Δ*cadA* strain (Table 9.4), compared to when sodium ferrocyanide is present (P= 0.0017). Contradictory to the observation with the Δ*cadA* strain there is no significant difference between the growth rate when compared with the wild type, in the presence of sodium nitroprusside. Despite the lack of statistical significance between the Δ*ldcC* Δ*cadA* and the wild type strain, there is a clear effect induced by sodium nitroprusside in combination with the acidic pH. The Δ*ldcC* Δ*cadA* strain reached a lower final optical density than the wild type, appearing to match the Δ*cadA* growth kinetics, after 3 hours of growth. The application of sodium ferrocyanide does not significantly reduce the growth rate of any strain compared to the wild type. This suggests that the reductions in growth rate observed are due to a release of nitric oxide and not the structure of the sodium nitroprusside.

To determine whether exogenous cadaverine could alleviate the effects of acidified sodium nitrite, cadaverine was administered to the growth medium before incubation. Preliminary data generated using the wild type and the Δ*ldcC* Δ*cadA* strain suggests that exogenous cadaverine cannot alleviate the

effect of acidified sodium nitrite (Figure 5.24) with the cadaverine deletion strain appearing to show similar growth kinetics in the presence and absence of cadaverine (Figure 5.24) with a similar observation being made with the wild type (Figure 5.24). The growth kinetics observed with the wild type in the presence of acidified nitrite and cadaverine do not mirror those of the wild type only exposed to pH 5.5 (Figure 5.20B) but instead mirror those previously seen in the presence of acidified nitrite (Figure 5.22). This suggests that exogenous cadaverine cannot alleviate the effects of acidified sodium nitrite and the effect seen may not be linked to RNS quenching. Taken together these results suggests that the susceptibility seen may be tied to the acidic pH and not solely nitrosative stress. With a possible explanation being linked to altered buffer capability following deletion of *cadA*.

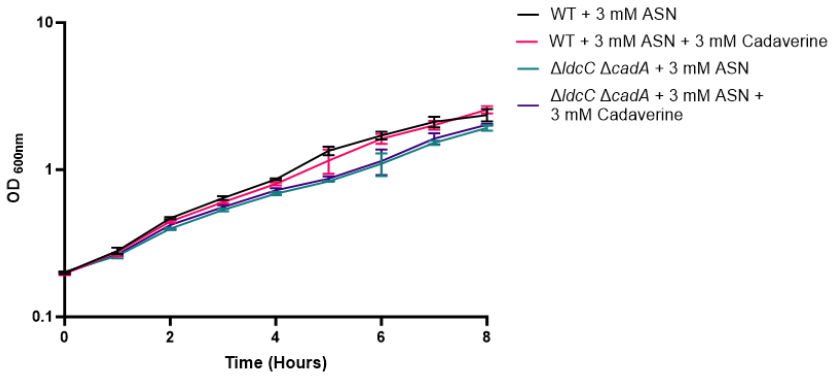

Figure 5.24. Preliminary data suggests that exogenous cadaverine is unable to alleviate the effect of acidified nitrite on *K. pneumoniae* 52145. Comparison of the growth of *K. pneumoniae* 52145 wild type and Δ*ldcC* Δ*cadA* in LB broth (pH 5.5) in the presence of acidified sodium nitrite and additional 125 µM cadaverine. The OD_{600nm} was measured every hour across 8 hours.

5.3.14 Deletion of cadaverine synthesis does not impact biofilm formation of *K. pneumoniae* 52145

As with 1, 3-diaminopropane in *A. baumannii* and *K. pneumoniae* (Section 3.3.15 and 4.3.7) biofilm formation was assessed in the cadaverine deletion strains. The *K. pneumoniae* 52145 wild type strain formed the greatest amount of biofilm, of all strains tested (Figure 5.25). As expected, the Δ*ompA* strain formed the least and significantly less biofilm than the wild type strain (Figure

5.25). The Δ*ldcC*, Δ*cadA* and Δ*ldcC* Δ*cadA* strains all formed comparative levels of biofilm (Figure 5.25), that were marginally less, but not significantly different to the wild type. This suggests that cadaverine is not required for biofilm formation in *K. pneumoniae* 52145.

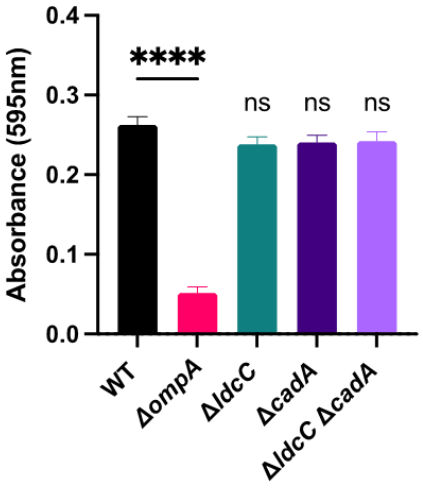

Figure 5.25. Deletion of the *ldcC* and *cadA* genes does not affect the biofilm formation of *K. pneumoniae* 52145 in MES-buffered M9 minimal salt media (pH 6.5). Comparison of biofilm formed by *K. pneumoniae* 52145 wild type and cadaverine deletion strains in a 96-well plate. Biofilm was quantified with crystal violet staining and absorbance measurement at 595 nm. Δ*ompA* was used as a negative control. Deletion of the OmpA in *K. pneumoniae* significantly decreases biofilm formation. The values presented represent the mean and SEM of four independent experiments. Each experiment was comprised of 36 wells per strain/condition across three technical replicates. **** = p-value ≤ 0.0001 (Mann-Whitney).

5.3.15 Loss of cadaverine synthesis does not alter susceptibility to antibiotics

Cadaverine synthesis has been shown to decrease susceptibility to antibiotics in *E. coli,* with this being linked to protection against antimicrobial-induced ROS (Akhova et al., 2021). Similar to the 1, 3-diaminopropane mutants, the effect of the Δ*ldcC* and Δ*cadA* deletion on antimicrobial MICs was investigated. The MICs for all antibiotics tested were the same between strains other than that of the MIC of meropenem for Δ*ldcC* strain and the MIC for gentamicin for all three cadaverine deletion strains, compared to the wild type strain (Table 5.4). Despite these differences the MICs are within one doubling dilution of the wild

type suggesting there is no difference between them and that cadaverine does not play a role in antibiotic susceptibility.

Table 5.4 The MIC of antimicrobials determined for *K. pneumoniae* 52145 wild type, Δ*ldcC*, Δ*cadA* and Δ*ldcC* Δ*cadA* strains

Antibiotic	WT	Δ*ldcC*	Δ*cadA*	Δ*ldcC* Δ*cadA*
	Antibiotic MIC (µg/ml)			
Meropenem	1	0.5	1	1
Ampicillin	2	2	2	2
Gentamicin	1	2	2	2
Colistin	8	8	8	8
Trimethoprim	32	32	32	32
Tetracycline	1	1	1	1
The values presented represent the MIC obtained from three independent experiments. MIC values were excluded if greater than one doubling dilution of the predominant value obtained according to the convention normally used in the published literature				

5.3.16 Deletion of cadaverine synthesis does not alter *in vivo* virulence of *K. pneumoniae* in *Galleria mellonella* infection model

As with the previous polyamine deletion strains, the potential role of cadaverine in the virulence of *K. pneumoniae* was assessed by *G. mellonella* infection model. Infection of larvae with 1 x 10^5 larvae of the wild type strain and the Δ*ldcC* resulted in the death of 23 % of infected larvae 24 hours post-infection (Figure 5.26A). Infection with the Δ*cadA* and Δ*ldcC ΔcadA* strains resulted in the death of 13.3 % and 16.7 %, 24 hours post-infection (Figure 5.26A), respectively. Infection with the wild type, Δ*ldcC* and Δ*cadA* strains, resulted in the death of 53.3 % of larvae for each strain tested (Figure 5.26A). Infection of larvae with the Δ*ldcC* Δ*cadA* strain resulted in the death of a total of 43.3 %, 72 hours post-infection (Figure 5.26A). Larvae were also infected with an inoculum of 1 x 10^6 of each strain (Figure 5.26B). Infection with the wild type resulted in the death of 57 % of infected larvae 24 hours post-infection (Figure 5.26B). While infection with the Δ*ldcC* resulted in the deaths of 67 % of infected larvae (Figure 5.26B) and 63.3 % of those infected with the Δ*cadA* and

Δ*ldcC* Δ*cadA* strains (Figure 5.26B). By 72 hours post the wild type strain had killed a total of 83.3 % of infected larvae (Figure 5.26B). Infection with the Δ*ldcC* and Δ*cadA* strains resulted in the deaths of a total of 87 % of larvae infected with each strain, 72 hours post-infection (Figure 5.26B). The Δ*ldcC* Δ*cadA* strain killed 97 % of infected larvae by 72 hours post-infection (Figure 5.26B). There was no significant difference in bacterial killing of larvae, at either inoculum, by any of the cadaverine biosynthesis mutants when compared to the wild type. This suggests that the deletion of cadaverine synthesis does not attenuate the virulence of *K. pneumoniae* and that cadaverine is not required for the full virulence of *K. pneumoniae*. Injection with PBS did not result in the deaths of any larvae, therefore ruling out the possibility deaths were attributable to mechanical trauma or the injection with PBS as a vehicle for the inoculum.

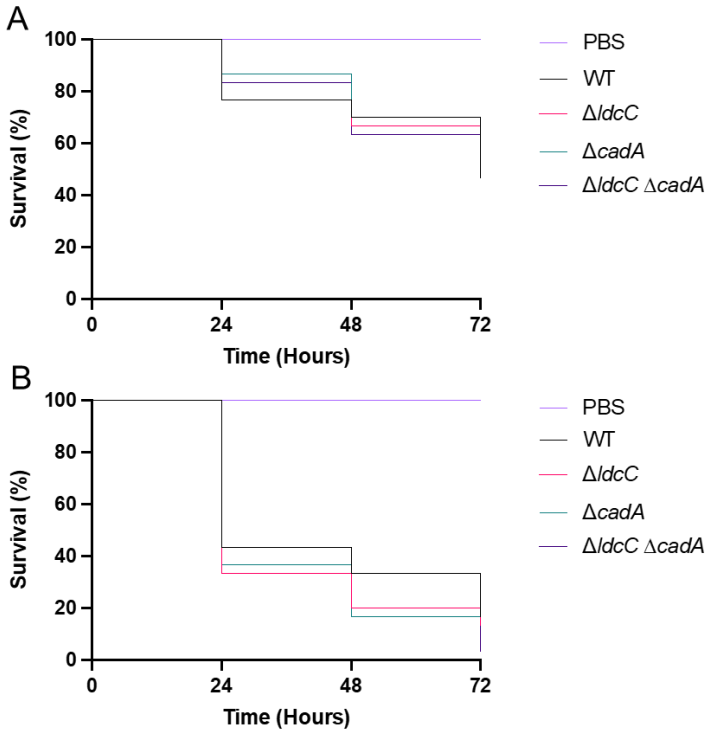

Figure 5.26. Cadaverine synthesis is not required for the virulence of *K. pneumoniae* 52145. Comparison of the percentage survival of *G. mellonella* 72 hours post-infection with a **(A)** 1 x 10^5 and **(B)** 1 x 10^6 CFU inoculum of *K. pneumoniae* 52145 wild type, Δ*ldcC*, Δ*cadA*, Δ*ldcC* Δ*cadA*. A vehicle and trauma control group were injected with PBS. A total of thirty larvae, across three independent groups of ten, were infected in each group. Statistical significance was determined using the log-rank Mantel-Cox test.

5.4 Chapter discussion

5.4.1 Cadaverine contributes to acid tolerance in *K. pneumoniae* 52145

Part of this chapter's investigation focused on cadaverine's involvement in the acid stress resistance of *K. pneumoniae* 52145. Growth in LDC broth confirmed acid-inducible LDC activity in the 52145 strain (Figure 5.17). This is expected as it is well known the CadCBA system responds to acidic pH in *E. coli*, *S. Typhimurium,* and *Vibrio* (Merrell and Camilli, 2000; Park et al., 1996). Different amino acid-based decarboxylase/antiporter systems protect against different acidic pH ranges (Gong et al., 2003; Kashiwagi et al., 1991; Park et al., 1996). The range at which cadaverine protects *K. pneumoniae* is unknown but what has been previously demonstrated is that cadaverine can protect against extreme acid shock (pH 3) (Hsieh et al., 2010). Growth of *K. pneumoniae* at pH 5.5, 4, and 3 highlights the possible pH at which cadaverine buffering and protection becomes relevant in *K. pneumoniae*, with the deletion of *cadA* significantly affecting growth at pH 4 (Figure 5.20). This gives new evidence to indicate the possible pH at which cadaverine offers protection and suggests possible environments where cadaverine may support growth. This raises the question: where does *K. pneumoniae* utilise this resistance? *K. pneumoniae* encounters acidic pH following phagocytosis (Cano et al., 2015). It could be hypothesised that cadaverine aids intracellular survival. However, several pieces of evidence go against this. Previous evidence shows *K. pneumoniae* requires vacuole acidification for intracellular survival (Cano et al., 2015). Therefore, it seems counterproductive to buffer against this. In *Salmonella* the *cadBA* genes are downregulated during similar acidification (Chakraborty et al., 2015). It is reasonable to hypothesise that cadaverine is not utilised during vacuole acidification. Acid tolerance is commonly associated with gastrointestinal pathogens. In the GI tract, short-chain fatty acids are abundant. It is possible these could diffuse across the plasma membrane

resulting in cytoplasmic acidification. Therefore, I hypothesise that cadaverine may promote GI tract colonisation by *K. pneumoniae*. The formation of a stable population within the GI tract would allow for a potential reservoir of *K. pneumoniae* within the gut. Evidence suggests that *K. pneumoniae* gut colonisation can be a prerequisite for infection (Gorrie et al., 2017).

To supplement the investigation into cadaverine and acid tolerance the expression of the *cadA* gene was assessed under neutral to mild acidic conditions. Though limited, it showed *cadA* expression at pH 5.5 and 4.5 (Figure 5.9B). What could be seen as unexpected is the expression of the *cadA* gene at pH 7.5. This is in stark contrast to what has been observed in *E. coli* where the *cadBA* genes are inhibited at pH 7.5 (Neely and Olson, 1996). This suggests that *cadA* expression in *K. pneumoniae* may differ from that in *E. coli*. I hypothesise two possible explanations for this. The first lies in the regulation of *cadBA* expression. Three pH-sensing residues are not conserved between the *E. coli* and *K. pneumoniae* CadC amino acid (Figure 5.5). Mutation of these residues results in a constant induced state of the *cadBA* genes (Dell et al., 1994). A lack of conservation may allow the *cadBA* genes of *K. pneumoniae* 52145 to be in this "on-state". A second and what I believe to be a more favourable hypothesis could be that there is a basal expression of the *cadBA* genes under non-inducing conditions similar to *Vibrio* (Merrell and Camilli, 2000). It is unclear what the biological significance of this would be in *K. pneumoniae.* In *Vibrio* it is believed basal level expression allows for low-level synthesis of cadaverine as a substitute for constitutive LdcC as *Vibrio* lacks this enzyme (Merrell and Camilli, 2000). *K. pneumoniae* encodes the biosynthesis constitutive form of lysine decarboxylase (LdcC), suggesting that *cadA* basal expression may not fulfil the substitutive role as in *Vibrio*. A comprehensive investigation into gene expression is needed to determine whether this is the case. Future investigation will allow for an understanding of *cadBA* gene expression and regulation that influences this in *K. pneumoniae,* and how this may differ from CadCBA systems in other species. This will give a greater understanding of how this system is utilised and how it may contribute to host colonisation.

5.4.2 Synthesis of spermidine analogues from cadaverine

Investigation with HPLC analysis confirmed the presence of cadaverine within *K. pneumoniae* 52145 (Figure 5.15) which was expected given this species encodes both the constitutive and inducible pathways. Unexpectedly HPLC analysis detected a triamine at the approximate retention time for spermidine in the putrescine/spermidine null Δ*speABC* strain. Currently, there is no information regarding the enzymatic specificity of the *K. pneumoniae* spermidine synthase, SpeE. This led me to hypothesise SpeE could be acting upon another diamine due to a lack of putrescine. In the case of cadaverine, this would produce aminopropylcadaverine. As previously stated, SpeE in other species can act on diamines other than putrescine (Bowman et al., 1973; Igarashi et al., 1986). To further investigate this, deletion of the *speE* gene in the Δ*ldcC* Δ*cadA* background or deletion of the cadaverine synthesis genes in the Δ*speABC* strain along with further HPLC analysis would determine whether cadaverine is being utilised for triamine synthesis. As previously stated, LC-MS could establish the structure of the triamine. This further investigation would give a more complete understanding of polyamine synthesis and utilisation *in K. pneumoniae*.

5.4.3 Cadaverine contributes to nitrosative stress resistance

Following the investigation into acid tolerance, the involvement of cadaverine in nitrosative stress resistance was assessed. This investigation provides evidence for a novel role of the acid-inducible synthesis pathway in resistance to nitrosative stress in *K. pneumoniae*. When grown at pH 5.5 with sodium nitrite the effect of nitrosative stress is exacerbated in the Δ*cadA* and Δ*ldcC* Δ*cadA* strains (Figure 5.22). This finding is in agreement with previous work that established the *cadCBA* operon to be involved in resistance to RNS in both uropathogenic *E. coli* and *S*. Typhimurium (Bower and Mulvey, 2006; Mühlig et al., 2014). While it provides evidence for this, it does not elucidate the mechanism by which this occurs. I initially hypothesised that cadaverine might

quench RNS similar to how polyamines act as ROS scavengers (Akhova and Tkachenko, 2020; Das and Misra, 2004; Gaboriau et al., 2005). However, preliminary work with exogenous cadaverine suggests this may not be the case (Figure 5.24). Cadaverine synthesis and excretion are known for their buffering capability due to the diamine's basic nature and consumption of protons within the cytoplasm. I now believe a more plausible hypothesis could be that the increased susceptibility is due to a lack of buffering capacity. The acidification of nitrite results in nitrous acid formation. This could diffuse across the membrane and dissociate into the neutral cytoplasm lowering the internal pH. Cadaverine synthesis would buffer the cytoplasm potentially mitigating the effect of this and the excretion of cadaverine and buffering of the extracellular environment would potentially reduce the formation of nitrous acid and RNS. To further investigate this hypothesis, the intracellular pH could be assessed in the presence and absence of ASN. A possible method for this could be pH-sensitive green fluorescent protein (Mühlig et al., 2014) or pH-sensitive fluorogenic dyes to detect internal pH change. This poses the question: is cadaverine synthesised in response to nitrosative stress or due to the acidic media? The results of growth with SNP could shed some light on this. These show that growth at pH 5.5 with SNP results in similar kinetics to growth with ASN (Figure 5.23A). When grown at pH 7.5 all strains grow similarly in the presence of SNP (Figure 5.23B). When grown at pH 5.5 the acidic conditions and abundance of lysine in the LB broth would allow for full induction of the *cadBA* genes. The effect seen across all strains at pH 7.5 could be due to a lack of cadaverine induction and buffering of the cytoplasm due to a lack of acidic pH. To further investigate these differences RT-qPCR could be carried out to determine if nitrosative stress induced by these agents causes *cadBA* expression. This would give a better understanding of the regulation of cadaverine synthesis under these conditions and the connection between cadaverine and RNS. Resistance to RNS may be important in the context of *K. pneumoniae* infection. Cadaverine has previously been linked to UPEC infection (Bower et al., 2009). With *K. pneumoniae* being a urinary tract pathogen cadaverine synthesised by *K. pneumoniae* may similarly contribute to UTIs.

Further investigation and understanding of how cadaverine protects against RNS and the implications of this *in vivo* will give an insight into how this affects *K. pneumoniae* during infection and how this pathogen adapts by potentially utilising cadaverine. Ultimately greater understanding of this could offer a novel therapeutic approach to treat *K. pneumoniae* infections in the future.

5.4.4 Limitations

HPLC analysis has demonstrated that cadaverine is synthesised by *K. pneumoniae*. However, the growth conditions before polyamine extraction could be regarded as suboptimal. It is well-established that induction of the *cadBA* genes is directly tied to external pH but also the presence of external lysine. Further HPLC analysis with additional lysine and optimisation would allow for a complete understanding of cadaverine synthesis in *K. pneumoniae*. Expression analysis with RT-PCR only indicates whether or not genes are expressed under a given condition, and it does not show the effect of induction. To fully explore the expression of *cadBA* RT-qPCR should be utilised, as initially planned. The genetic complementation of the *cadA* deletion was unsuccessful. This lack of complementation is likely due to a lack of *cadA* expression. Either due to the included predicted promoter being inappropriate or additional regulatory factors acting on *cadA.* Ideally, the expression of the *cadA* gene from the complementation vector should have been verified to conclude the reasoning for a lack of complementation. In hindsight, a more suitable approach for complementation could have been to complement the entire *cadCBA* operon, either through a plasmid or by introduction into the chromosome. A possible method for this could be Tn7 transposon insertion into the attTn7 site (Llobet et al., 2015). This would mean *cadBA* would be under the control of their native promoters. An added benefit of chromosomal insertion would not be that the copy number of a plasmid does not interfere with the system or the cell as a whole.

5.4.5 Conclusion

In this chapter, I aimed to investigate the role of cadaverine in *K. pneumoniae* 52145. This has built on the understanding that polyamines are important in stress responses and provides the first indication that cadaverine may play a role in nitrosative stress resistance in *K. pneumoniae,* possibly allowing for survival and infection within specific host environments. Additionally, it provides further insight into cadaverine and acid resistance in *K. pneumoniae* and though limited gives new evidence on the regulation and expression of the inducible pathway indicating that it may differ from that of *E. coli.* However, further investigation into gene expression and HPLC analysis under a variety of additional conditions will be needed to assess this. HPLC analysis has shed light on the actions of SpeE in *K. pneumoniae* and gives the first evidence that this enzyme has the potential to act upon other diamines. Overall, this investigation indicates that cadaverine remains a viable therapeutic target for future investigation and highlights specific areas of future investigation that may be beneficial in the use of these novel therapeutics.

Chapter 6 Analysis of 1, 3-diaminopropane synthesis enzymes

6.1 Chapter introduction

There are growing concerns surrounding antimicrobial resistance of bacterial pathogens. The WHO has deemed carbapenem-resistant *Enterobacteriaceae* and *A. baumannii* of critical concern for the investigation of new antimicrobials and treatment options (Tacconelli et al., 2018). A possible approach to this is the targeting of polyamine synthesis. The most successful inhibitor is DL-α-difluoromethylornithine used to treat African sleeping sickness (LoGiudice et al., 2018). Among others are the SpeD inhibitors MGBG and SAM486a and the LDC inhibitors DFML and MFML (Kallio et al., 1981; Levine, 2001; Wallace and Fraser, 2004). Polyamine synthesis has been identified in several bacterial pathogens making it a viable therapeutic target. 1, 3-diaminopropane is a promising candidate for this as it appears to play a significant role in the virulence of *A. baumannii*. An added benefit of targeting this pathway would be that it is not present within humans, avoiding any cross-reactivity of a therapeutic with the host. Two enzymes are involved in 1, 3-diaminopropane synthesis. These being L-2, 4-diaminobutyrate:2-ketoglutarate 4-aminotransferase and L-2, 4-diaminobutyrate decarboxylase. Currently little is known about their 3D structures. To further investigate the possibility of targeting these enzymes as a therapeutic approach understanding of their 3D structures is required.

6.2 Research aims

- Construct expression vectors for the Dat and Ddc of *A. baumannii* 17978 and *K. pneumoniae* 52145
- Crystallise and solve the protein structure of Dat and Ddc to aid in the investigation of inhibitory compounds for each enzyme

- Determine whether Dat and Ddc form multimeric structures using a bacterial two-hybrid system

6.3 Chapter results

6.3.1 Expression and purification of *K. pneumoniae* and *A. baumannii* Dat and Ddc

To allow for the investigation of novel inhibitors of Dat and Ddc an experimentally derived 3D structure is required. Therefore, it was originally planned to express and purify the 1, 3-diaminopropane synthesis enzymes from *K. pneumoniae* and *A. baumannii* allowing for crystallisation and solving of the 3D structure.

6.3.1.1 Construction and confirmation of expression vectors

To begin the *dat* and *ddc* genes were cloned into pET28a and pET41c with restriction-free cloning. This involved designing primers to amplify genes allowing for the addition of 5' and 3' overhangs complementary to the pET28a or 41c vector. The amplified DNA then acted as a "megaprimer" for the amplification of the vector sequence, resulting in an incorporated gene sequence within the vector. For cloning into pET41c restriction cloning was utilised with amplified DNA featuring XhoI and NdeI restriction site overhangs. The presence of each gene insert was confirmed by a diagnostic digest of plasmids using a variety of enzymes. pET28a-*dat*$_{Kp}$ was digested with HincII and was expected to produce products of approximately 4.7 Kbp and 1.9 Kbp (Figure 6.1.A). pET28a-*ddc*$_{Kp}$ and pET41c-*ddc*$_{Kp}$ were digested with XmaI and were expected to produce fragments of 4.4 Kbp and 2.3 Kbp for pET28a (Figure 6.1.B) and 4.1 Kbp and 2.3 Kbp for pET41c (Figure 6.1.C). Digestion with XmaI resulted in an unexpected product at approximately >6 Kbp. It is possibly linearised plasmid, as a result of incomplete digestion. pET28a-*dat*$_{Ab}$ and pET41c-*dat*$_{Ab}$ were digested with NcoI, which generated two fragments of approximately 6 Kbp and 0.5 Kbp (Figure 6.1.A and C). pET28a-*ddc*$_{Ab}$ and

pET41c-*ddc*$_{Ab}$ were digested with HincII, to give two fragments of approximately 4 Kbp and 2.8 Kbp for pET28a and 3.7 Kbp and 2.7 Kbp for pET41c (Figure 6.1.A and C). All digested vectors showed the presence of the desired gene insertions in the pET28a and pET41c expression vectors. Restriction-based insertion of the *K. pneumoniae dat* gene into pET41c could not be carried out, as an XhoI site was found within the gene sequence, cutting at position 1255 of the nucleotide sequence. Therefore, restriction-free insertion into the pET41c vector was attempted but was found to be unsuccessful. Final confirmation insertions and detection of mutations were carried out using sequencing. This found that all vectors had the correct gene insertion.

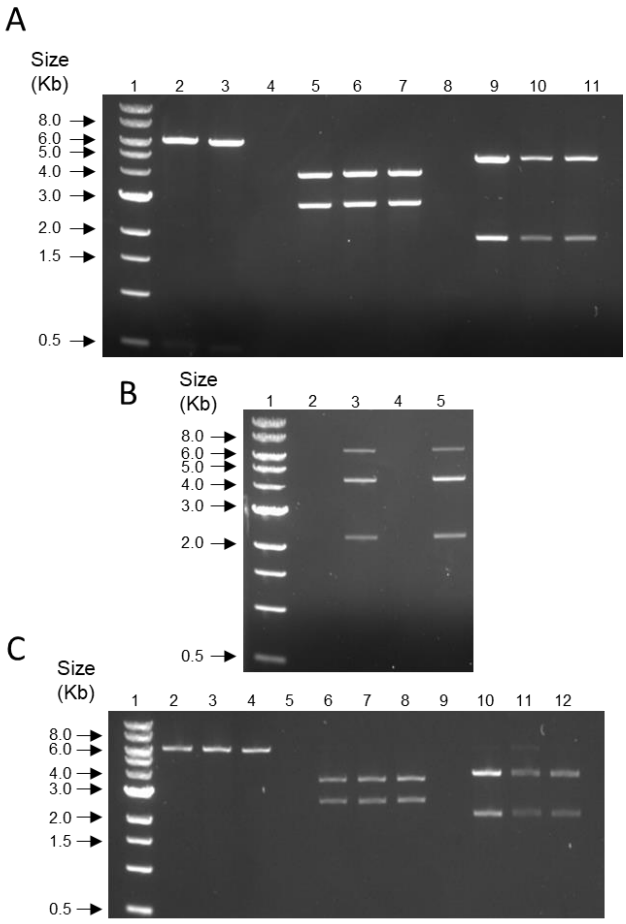

Figure 6.1. Confirmation of the pET28a and pET41c expression vectors. (A) Restriction digest of pET28a expression vectors for the expression of Dat and Ddc from *A. baumannii* 17978 and *K. pneumoniae* separated by gel electrophoresis. Lane 1: 1 Kbp ladder. Lane 2-3: pET28a-dat_{Ab} digested with NcoI generating products of 6 Kbp and 0.5 Kbp. Lane 6-7: pET28a-ddc_{Ab} digested with HincII generating products of 4 Kbp and 2.8 Kbp. Lane 9-11 pET28a-dat_{Kp} digested with HincII generating products of 4.7 Kbp and 1.9 Kbp**. (B)** Restriction digest of pET28a expression vector for the expression of *K. pneumoniae* 52145 Ddc. Lane 1: 1 Kbp ladder. Lane 3/5 pET28a-ddc_{Kp} digested with XmaI generating products of 4.1 Kbp and 2.3 Kbp and the unexpected, linearized vector at approximately 6.4 Kbp. **(C)** Restriction digest of pET41c expression vectors for the expression of Dat from *K. pneumoniae* 52145 and both Dat and Ddc from *A. baumannii* 17978. Lane 1: 1 Kbp ladder. Lane 2-4: pET41c-dat_{Ab} digested with NcoI generating products of 6 Kbp and 0.5 Kbp. Lane 6-8: pET41c-ddc_{Ab} digested with HincII generating products of 3.7 Kbp and 2.7 Kbp. Lane 10-11: pET41c-ddc_{Kp} digested with XmaI generating 4.1 Kbp and 2.3 Kbp products.

6.3.1.2 Expression and purification of 1, 3-diaminopropane synthesis enzymes

As stated, the impact of the COVID-19 pandemic prevented proper investigation into the 3D structure of Dat and Ddc. However, the expression of

these proteins was attempted by several MSc students supervised by Dr David Scott. This utilised the previously made expression vectors, constructed by myself. These vectors pET28a-*dat*$_{Kp}$, pET41c-*ddc*$_{Kp}$, pET28a-*dat*$_{Ab}$, pET41c-*ddc*$_{Ab}$, were transformed into the *E. coli* BL21(DE3) pLysS, here on referred to simply as *E. coli* BL21 and expression and purification were carried out. The subsections of section 6.3.1.2 are an overview of the data generated by each MSc student.

6.3.1.2.1 Expression and purification of *K. pneumoniae* Dat

The expression and purification of Dat from *K. pneumoniae* was carried out by MSc student, Narasimhan Raghunathan. SDS-PAGE following IPTG induction revealed successful expression and recovery of the Dat enzyme from *E. coli* BL21 (Figure 6.2). This was then followed by purification using Ni-NTA affinity chromatography. SDS-PAGE revealed specific banding for the expressed Dat protein, illustrated as the presence of a thick band (Figure 6.5), with no discernible banding present in the flow through. This suggests successful expression and purification of the Dat enzyme from *K. pneumoniae* 52145.

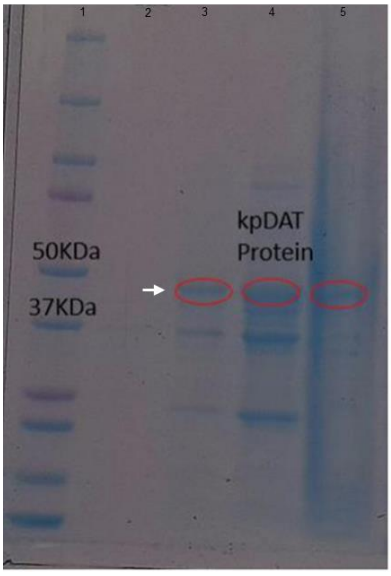

Figure 6.2. The *K. pneumoniae* Dat can be expressed in *E. coli* BL21. Protein expression following IPTG induction and growth at 25°C for 18 hours. Lane 1: 10-250 kDa Protein MW ladder. Lane 2: Dat present in lysate pre-induction. Lane 3: Dat present in lysate post-induction. Lane 4: Dat present in the supernatant of cell lysate. Lane 5: Dat present in pellet of cell lysate. Arrow indicates protein of interest (POI) Figure adapted from Raghunathan (2023).

6.3.1.2.2 Expression and purification of *A. baumannii* Dat

The expression and purification of Dat from *A. baumannii* was carried out by MSc student, Zeyu Ying. SDS-PAGE analysis of IPTG-induced cells following 18 hours of incubation at 25 °C revealed little to no detectable protein, suggesting these to be inappropriate for the expression of *A. baumannii* Dat (Figure 6.3A). Induction at 37 °C for 3 hours was revealed to be successful and expression of the *A. baumannii* Dat enzyme in *E. coli* BL21 was observed by SDS-PAGE (Figure 6.3B). This was followed by affinity chromatography. SDS-PAGE revealed that purification had been successful with the presence of purified protein indicated by the intense banding (Figure 6.5).

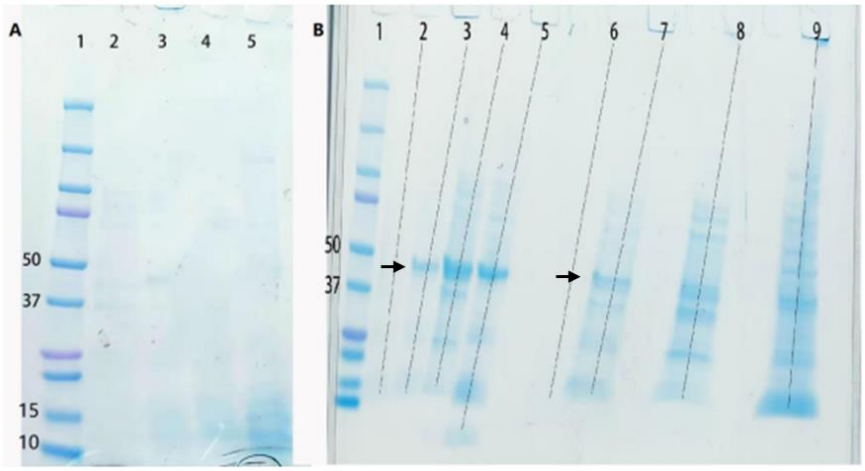

Figure 6.3. The *A. baumannii* Dat can be expressed in *E. coli* BL21. (A) Protein expression following IPTG induction and growth at 25°C for 18 hours. Lane 1: 10-250 kDa Protein MW ladder. Lane 2: Dat present pre-induction. Lane 3: Dat present post-induction. Lane 4: Dat present in the supernatant of the cell lysate. Lane 5: Dat present in pellet of cell lysate. **(B)** Protein expression in two separate cultures following IPTG induction and growth at 37 °C for 3 hours. Lane 1: 10-250 kDa Protein MW ladder. Lanes 2-5 represent the analysis of "culture 1" and Lanes 6-9 represent the analysis of expression in "culture 2". Lanes 2 and 6: Dat present pre-induction. Lanes 3 and 7: Dat present post-induction. Lanes 4 and 8: Dat present in the supernatant of the cell lysate. Lanes 5 and 9: Dat present in the pellet of cell lysate. Arrow indicates POI. Figure adapted from Ying (2023).

6.3.1.2.3 Expression and purification of *K. pneumoniae* and *A. baumannii* Ddc

The expression and purification of Ddc from *K. pneumoniae* and *A. baumannii* were carried out by MSc student, Ruqayyah Adebisi Adelakin. Initial verification

of expression by SDS-PAGE revealed that induction had successfully expressed both Ddc enzymes, as illustrated by the intense banding (Figure 6.4). Following this, both proteins underwent purification using affinity chromatography. SDS-PAGE revealed the presence of the Ab Ddc protein as indicated by the intense staining present on the SDS gel (Figure 6.5). The initial affinity chromatography resulted in a loss of the Kp Ddc product, further expression and purification were carried out (Data not shown). The data generated by each MSc student confirms the successful expression and purification of the Dat and Ddc enzymes of *K. pneumoniae* and *A. baumannii*, from the expression vectors generated as part of my PhD. It also indicates a sufficient quality and concentration of each protein to allow for further downstream assessment, such as crystallisation.

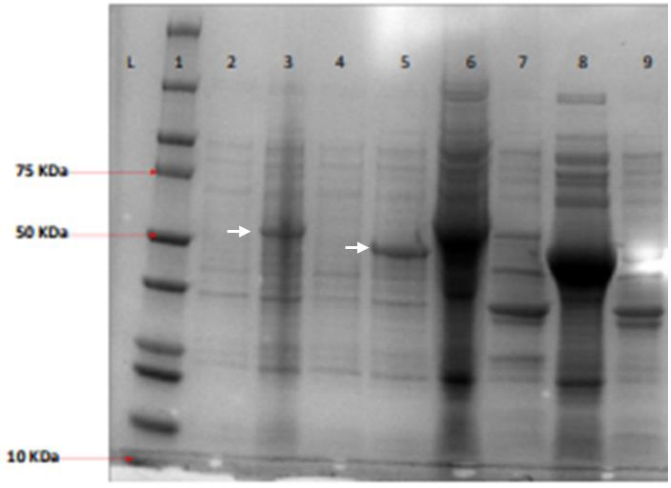

Figure 6.4. The Ddc from *K. pneumoniae* and *A. baumannii* can be expressed in *E. coli* BL21. Protein expression of the Ddc following IPTG induction and growth at 25°C for 18 hours. Lane 1: 10-250 kDa Protein MW ladder. Lane 2: Ab Ddc present pre-induction. Lane 3: Ab Ddc present following induction. Lane 4: Kp Ddc present pre-induction. Lane 5: Kp Ddc present following induction. Lane 6: Ab Ddc present in the supernatant of cell lysate. Lane 7: Ab Ddc present in the pellet of cell lysate. Lane 8: Kp Ddc present in the supernatant of cell lysate. Lane 9: Kp Ddc present in the pellet of cell lysate. Arrow indicates POI. Figure adapted from Adelakin (2023).

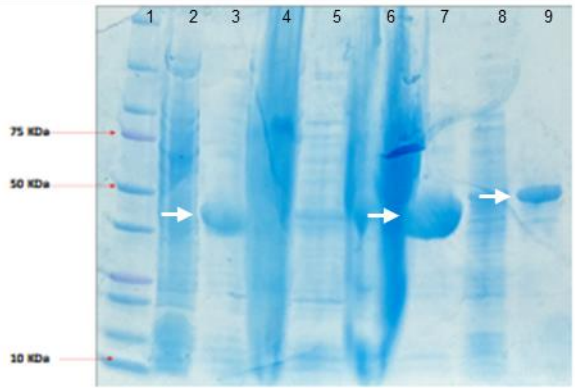

Figure 6.5. SDS-PAGE of 1, 3-diaminopropane synthesis enzymes following affinity chromatography. SDS-PAGE of affinity chromatography purified Ab and Kp Dat and Ab Ddc. Lane 1: 10-250 kDa Protein MW ladder. Lane 2: Ab Dat flowthrough. Lane 3: Ab Dat elution. Lane 6: Kp Dat Flowthrough Lane 7: Kp Dat elution. Lane 8: Ab Ddc flowthrough. Lane 9: Ab Ddc elution. Arrow indicates POI. Figure adapted from Adelakin (2023).

6.3.2 Analysis of protein interactions with the bacterial two-hybrid system

6.3.2.1 Construction and confirmation of BACTH vectors

Proteins are capable of forming both homo- and hetero-multimeric structures and it has been suggested that the Dat and Ddc enzymes form tetrameric and dimeric structures, respectively (Ikai and Yamamoto, 1997; Yamamoto et al., 1992). EctB, a homolog of Dat, required for ectoine biosynthesis in *C. salexigens* DSM 3043 was also found to be a tetramer (Hillier et al., 2020). It was decided that the bacterial two-hybrid system would be used to determine the possible homo and hetero interactions between the Dat and Ddc enzymes of *K. pneumoniae* and *A. baumannii*. To do this, genes were amplified to include XbaI and KpnI sites on the 5' and 3' ends of the amplified products to allow for restriction cloning into pUT28c and pKT25 vectors, in frame with the T18/T25 sequences (Figure 6.6).

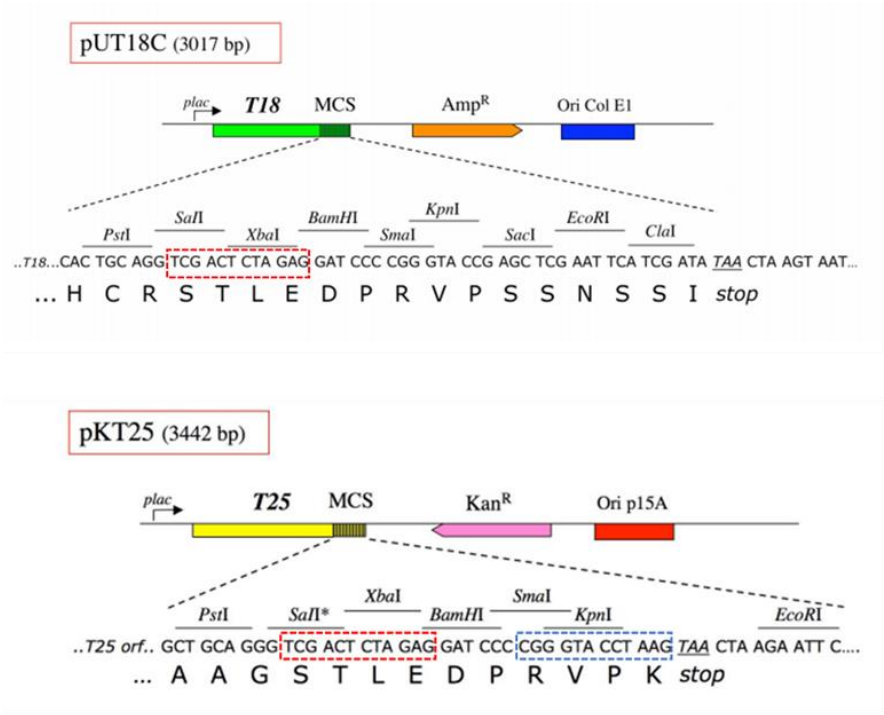

Figure 6.6. Diagram of BACTH vector MCS sequences. The MCS of pUT18C and pKT25 show the restriction endonuclease sites. Overhang sequences added to primers are highlighted. (Red) XbaI restriction site and additional bases. (Blue) KpnI restriction site and additional bases.

Vectors were subsequently transformed into the cloning strain *E. coli* DH5α. The correct insertion was determined by PCR and diagnostic digests. All pUT18C and pKT25 were digested with XbaI and KpnI, to excise the gene insertion from the plasmid backbone. The pUT18C and pKT25 backbones were expected to give a product of 3.0 Kbp and 3.4 Kbp, respectively (Figure 6.7). The gene fragments for *K. pneumoniae dat* and *ddc* were expected to be 1.3 and 1.4 Kbp, respectively (Figure 6.7). The gene fragments for *A. baumannii dat* and *ddc* were expected to be 1.3 and 1.5 Kbp, respectively (Figure 6.7). All digested vectors were found to contain the correct gene insertion as indicated by the sizes of the banding patterns (Figure 6.7).

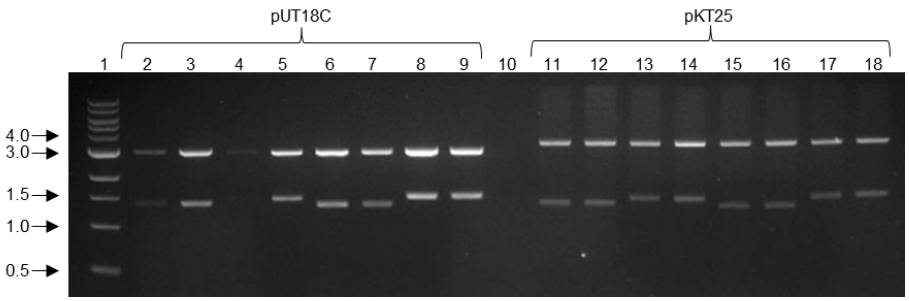

Figure 6.7. Confirmation of the BACTH vectors. Restriction digest of pUT18C and pKT25 BACTH vectors encoding *dat* and *ddc* from *K. pneumoniae* and *A. baumannii*, with XbaI and KpnI. Expected products for the pUT18C and pKT25 backbones were 3.0 Kbp and 3.4 Kbp. For genes expected products were 1.3 and 1.4 Kbp for dat_{Kp} and ddc_{Kp} and 1.3 and 1.5 Kbp for dat_{Ab} and ddc_{Ab}. Lane 1: 1 Kbp ladder. Lane 2-3: pUT18C-dat_{Kp}. Lane 4-5: pUT18C-ddc_{Kp}. Lane 6-7: pUT18C-dat_{Ab}. Lane 8-9: pU18C-ddc_{Ab}. Lane 11-12: pKT25-dat_{Kp}. Lane 13-14: pKT25-ddc_{Kp}. Lane 15-16: pKT25-dat_{Ab}. Lane 17-18: pKT25-ddc_{Ab}. Digestions were carried out on vectors isolated from two different colonies.

This confirms the successful insertion of gene fragments into the pUT18C and pKT25 vectors. Vector insertions were sequenced to determine the presence of point mutations. This found no point mutations had been introduced. Following confirmation of inserts, vectors were co-transformed into the cAMP auxotroph *E. coli* BTH101. Colony PCR confirmed the successful co-transformation of all combinations of the bacterial two-hybrid vectors in *E. coli* BTH101.

6.3.2.2 BACTH analysis of Dat and Ddc interactions

The BACTH system relies on the catalytic domain of *Bordetella pertussis* adenylate cyclase which is composed of two distinct complementary fragments, T25 and T18, that are not functionally active when separated. When genes of interest are cloned into the pKT25 and pUT18C and expressed in-frame with either fragment, chimeric fusion proteins are formed. When protein interaction occurs T25 and T18 functionality is restored, and cAMP is produced. Functional complementation of the T18 and T25, in an *E. coli* strain lacking adenylate cyclase activity, results in gene expression of β-galactosidase allowing the utilisation of lactose. Protein interactions are determined by growth on agar plates supplemented with X-gal. This is hydrolysed by β-galactosidase giving rise to the colourless galactose and 4-chloro-3-brom-

indigo, which forms an intense blue precipitate. This can be used to infer the presence of β-galactosidase activity and protein interactions.

pUT18C and pKT25 encoding the *A. baumannii* and *K. pneumoniae dat* and *ddc* genes were co-transformed into *E. coli* BTH101 in varying combinations. Empty pUT18C and pKT25 acted as a negative interaction control, while pUT18C-Zip and pKT25-Zip encoding an isoleucine zipper acted as the positive interaction control (Section 2.21). As expected, the combination of pUT18C-Zip and pKT25-Zip encoding the T18 and T25-Zip fusion proteins led to a strong positive interaction, indicated by the hydrolysis of X-gal and the subsequent blue pigmentation (Figure 6.8.) The pUT18C and pKT25 empty vector combination was negative for interactions as bacterial growth was white in appearance, confirming the inability of the T18 and T25 to functionally complement without being part of an interacting chimeric fusion protein (Figure 6.8). *E. coli* expressing the combinations of *K. pneumoniae* T18-Dat/T25-Dat and T18-Ddc/T25-Ddc fusions resulted in blue pigmentation (Figure 6.8). *E. coli* expressing the combination of *A. baumannii* T18-Dat/T25-Dat and T18-Ddc/T25-Ddc resulted in blue pigmented *E. coli* (Figure 6.8). This suggests that the Dat and Ddc of *K. pneumoniae* and *A. baumannii* form homomultimeric structures. Expression of the *K. pneumoniae* and *A. baumannii* T18-Dat and T-25-Dat fusion proteins also results in a positive interaction, indicating cross-species interaction suggesting that residues involved in multimerisation are conserved between these two species. A similar result was observed with the expression of the Ddc fusion proteins (Figure 6.8). Expression of Dat and Ddc together showed growth with white pigmentation suggesting heteromultimers are not formed. These results confirm the

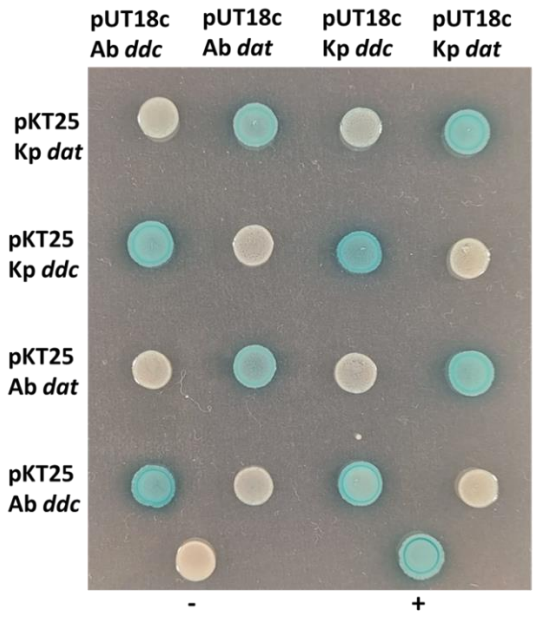

Figure 6.8. Dat and Ddc form homomultimeric structures but do not form heteromultimeric structures. The investigation of protein: protein interactions of L-2,4-diaminobutyrate:2-ketoglutarate 4-aminotransferase (Dat) and L-2,4-Diaminobutyrate decarboxylase (Ddc) using bacterial two-hybrid system. Dat and Ddc were cloned into pUT18c and pKT25 bacterial two hybrid vectors. Resulting in Dat and Ddc tagged with T25 and T18 fragments. β-galactosidase activity was assessed on Nutrient agar supplemented with 40 µg/ml X-gal, incubated at 37°C for 72 hours. +: *E. coli* BTH101 containing pUT18c-Zip and pKT25-Zip were used as a positive control. -: *E. coli* BTH101 containing the empty pUT18c and pKT25 was used as a negative control. Images are representative of two biological repeats.

6.3.2.3 Quantification of β-galactosidase activity

To quantify the β-galactosidase activity and subsequently, the interactions between hybrid Dat and Ddc proteins, the Miller ONPG assay was employed (Section 2.21.2). This utilises ONPG as a substrate for β-galactosidase to quantify enzymatic activity. The hydrolysis of ONPG forms o-nitrophenol producing a yellow colour. When ONPG is in excess, the production of o-nitrophenol per unit of time is directly proportional to the concentration of β-galactosidase within the cell. The β-galactosidase activity was expressed as Miller units (Equation 2.1). *E. coli* expressing the T18-Zip and T-25-Zip fusion proteins had the greatest β-galactosidase activity compared to all other combinations (Figure 6.9). *E. coli* containing the pUT18C and pKT25 empty vectors had significantly less ($P = 0.0064$), β-galactosidase activity compared

with the T18-Zip and T-25-Zip expressing *E. coli* (Figure 6.9). *E. coli* expressing combinations of T18 and T25 fusions of the same enzyme, showed significantly more β-galactosidase activity than in *E. coli* containing the empty vectors amd no significant difference to those containing Zip fusions (Figure 6.9). This suggests that Dat and Ddc form homomultimeric structures and that Dat and Ddc from other species are capable of interacting with each other (Figure 6.9). *E. coli* expressing combinations of T18 and T25 fusions of different enzymes, showed significantly less β-galactosidase activity when compared with the activity in *E. coli* expressing the Zip fusions, with no significant difference with the *E. coli* containing the empty vectors (Figure 6.9). Suggesting that Dat and Ddc do not form heteromultimeric structures, corroborating what was previously observed when screened for β-galactosidase activity on X-gal supplemented agar.

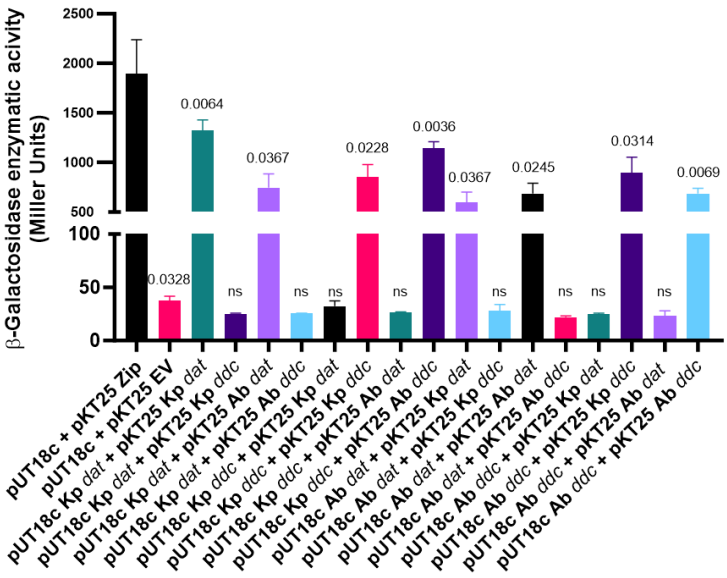

Figure 6.9. Dat and Ddc interact to form homomultimeric structures. Comparison of the β-galactosidase activity of *E. coli* BTH101 harbouring pUT18C and pKT25 expressing Dat and Ddc T18 and T25 chimeric proteins. *E. coli* BTH101 containing pUT18C and pKT25 vectors were grown overnight. Cells were resuspended in Z-buffer and the OD_{600nm} was measured. Cells were permeabilised with SDS and chloroform and ONPG solution was added. The time to form sufficient colour change was measured. Reactions were quenched with Na_2CO_3 and the reaction time was recorded. The OD_{420nm} and OD_{550nm} were recorded for each reaction mixture. The β-galactosidase activity was expressed as Miller units. The values presented represent the mean and SEM of three independent experiments. Statistical analysis was measured using an unpaired T-test with Welch's correction.

6.3.3 *In silico* analysis of Dat and Ddc

6.3.3.1 Analysis of the Dat and Ddc from *A. baumannii* 17978

The Dat of *A. baumannii* 17978 is predicted to comprise 457 amino acids, with a calculated molecular mass of 48.8 kDa. The Ddc of *A. baumannii* 17978 is predicted to comprise 510 amino acids, with a calculated molecular mass of 56.2 kDa. The sequence of Dat was first analysed with InterPro to predict features present within the sequence. It predicted that the major domain consists of residues 71-338 (Figure 6.10) and the small domain is comprised of residues 24-70 and 339-443 (Figure 6.10). The PLP-attachment site, found within the major domain, is predicted to consist of residues 257-294 (Figure 6.10). InterPro predicted of the PLP-dependent decarboxylase domain of Ddc spans residues 82-428 (Figure 6.11), with the predicted PLP-attachment site being comprised of residues 313-333 (Figure 6.11). InterPro also predicts the presence of two coil structures the first comprised of residues 228-248 and the second 479-499 (Figure 6.11).

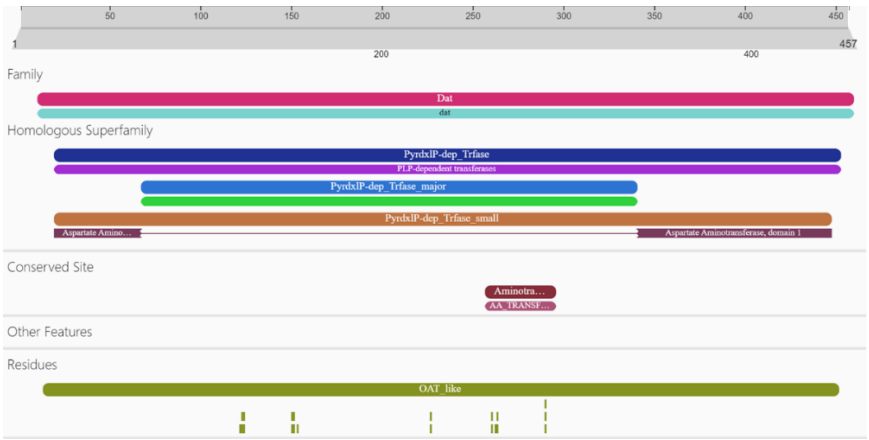

Figure 6.10. The predicted domains and features of the Dat protein in *A. baumannii* 17978. Family: 2,4-diaminobutyrate 4-transaminase. Homologous superfamily: PLP-dependent transferase, small domain, and major domains. Conserved site: aminotransferase class III PLP-binding site. Residues: OAT_like domain and predicted Cofactor binding pocket and PLP-binding residues. Predictions were made with and adapted from InterPro.

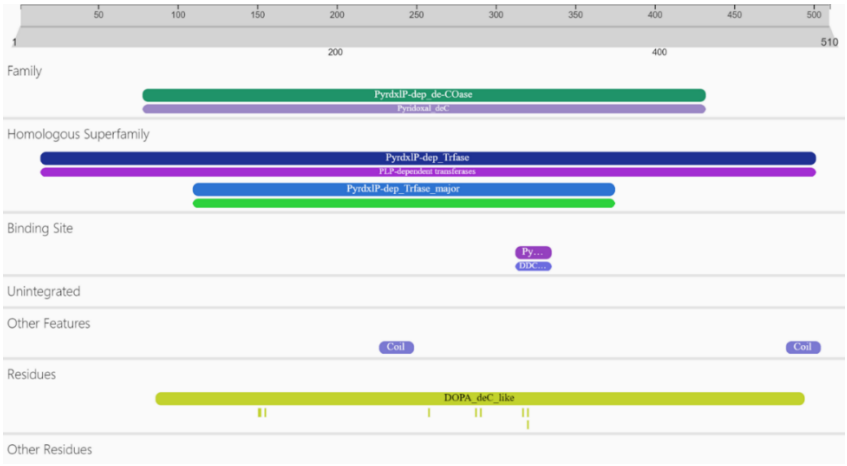

Figure 6.11. The predicted domains and features of the Ddc protein in *A. baumannii* 17978. InterPro predicts family: PLP-dependent decarboxylase. Binding site: PLP-binding site. Coil: coiled-coil structures. DOPA_deC_like: DOPA decarboxylase family and predicted residues for PLP binding residues and the catalytic lysine residue. Predictions were made with and adapted from InterPro.

The Dat and Ddc amino acid sequences were analysed with BLASTp. This found the Dat and Ddc amino sequences are similar to those encoded by *Glaesserella parasuis* (82.68 % and 82.55 % identity) and *Moraxella bovis* (80.09 % and 83.66 % identity), as examples. The evidence of polyamine synthesis in either of these organisms is limited however *G. parasusis* is a member of the Pasteurellaceae family, the same as that of *H. influenzae* that is known to encode 1, 3-diaminopropane synthesis enzymes. As for *M. bovis,* it is of the same family as *Acinetobacter.* Therefore, it is reasonable to speculate that these organisms share these synthesis enzymes through evolutionary means. The Dat sequence was compared to specific homologues. Comparison of Dat with EctB encoded by *C. salexigens*, one of the few Dat homologous to have a known crystal structure found Dat to be moderately similar to EctB (36.2 % identity/ 53.9 % similarity). Pyoverdine synthesis also requires L-2,4-diaminobutyrate:2-ketoglutarate 4-aminotransferase activity, in the form of PvdH. Dat shares 53.5 % identity and 67.9 % similarity with the PvdH of *P. aeruginosa* PAO1. While there appears to be a degree of difference within the protein sequences of Dat and its homologues in other species, residues relating to enzymatic function and structure are likely conserved. Very little is known about the 3D structure of Dat.

The structure of EctB has been well characterised, with annotation of residues relating to PLP-binding, substrate-binding pockets, dimeric and tetrameric interfaces, and the small and large domains (Hillier et al., 2020). To determine if these residues are conserved between EctB and Dat the sequences were aligned. PLP-dependent enzymes feature a lysine residue within their structure that is modified by PLP. Alignment found that K289 of Dat aligns with the known modified lysine residue of EctB, suggesting this is the site of Schiff base formation. Investigation with InterPro agreed with this observation (Figure 6.10). Further comparison revealed several residues relating to PLP-binding are conserved between the Dat and EctB sequences (Figure 6.12). Those that were not completely conserved were found to be of similar properties. Hydrophobic tyrosine and methionine appear to position 152 and 155, respectively, with tyrosine aligning similarly hydrophobic phenylalanine and methionine with valine in EctB (Figure 6.12). A similar observation can be seen with the hydrophobic valine at position 262 and the uncharged threonine at position 315, with valine aligning with isoleucine and threonine with asparagine of EctB (Figure 6.12). One amino acid, relating to PLP-binding (A126) was not fully, or conservatively, conserved between the two sequences (Figure 6.12). There was also found to be a high degree of conservation of residues relating to the substrate binding pocket in EctB, these being Y31, G61, A62, G63, L91, D92, E227, E232, T317, R319, E414, and R424 of the Dat sequence (Figure 6.12). There was found to be one residue, relating to the EctB binding pocket, not completely, but conservatively conserved, between the two sequences, this being the uncharged T315 in Dat, which aligns with the uncharged asparagine in EctB (Figure 6.12). Alignment also showed that several residues involved in EctB dimerization are conserved. These being W309, P311, V28, G122, P296, F318 in *A. baumannii* Dat.

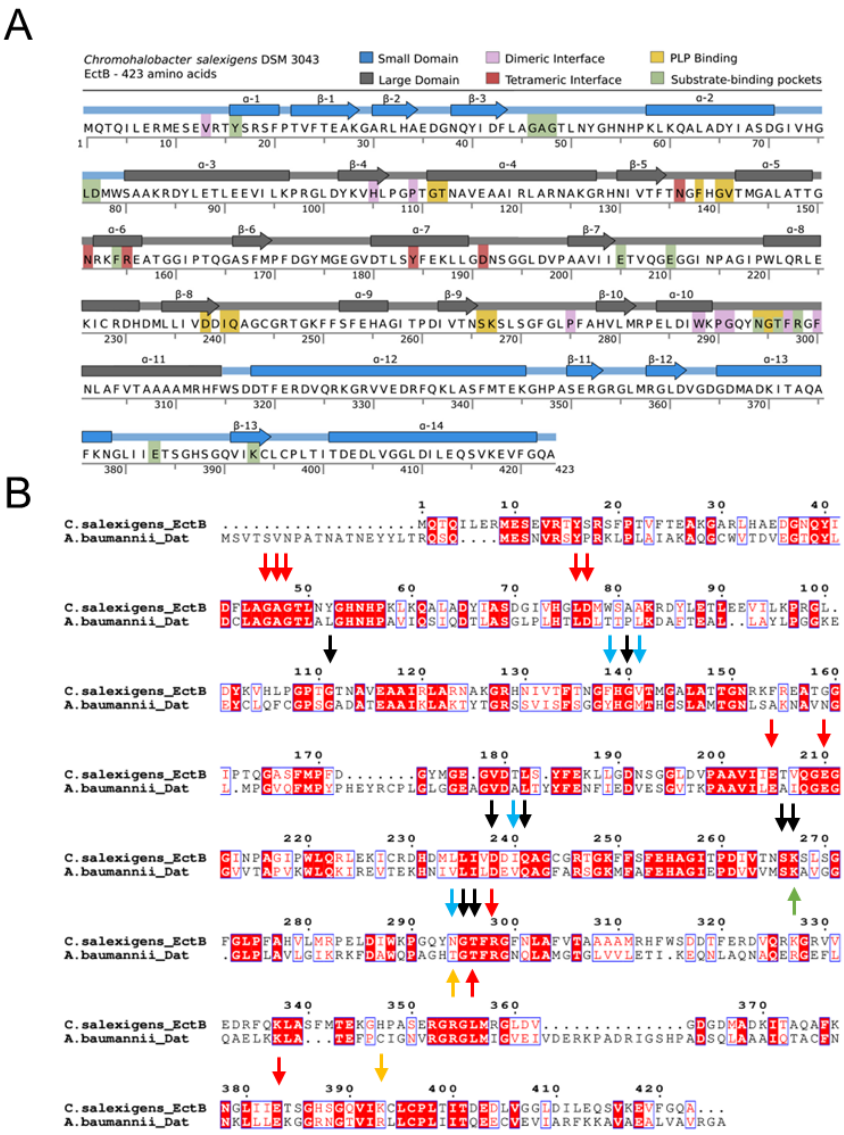

Figure 6.12. Residues involved in PLP-binding and substrate binding pocket are conserved between EctB of *C. salexigens* and *A. baumannii*. (A) The structural overview of the EctB from *C. salexigens* DSM 3043 featuring the domains and amino acid residues relating to function and structure. Figure adapter from Hillier et al 2020. **(B)** Protein sequence alignment of *A. baumannii* 17978 Dat with EctB from *C. salexigens* DSM 3043. Green arrow: indicates PLP-modified lysine residue. Black arrows: indicate conserved residues that are involved in PLP-binding in *C. salexigens* DSM 3043. Blue arrow: indicates similar amino acid, at that position, to those involved in PLP binding. Red arrow indicates conserved residues that are related to substrate-binding pockets. Yellow arrow indicates a similar amino acid, at that position, related to substrate binding pockets. White character within the red box: indicates conserved amino acid identity. Red character: indicates similarity of amino acid. Sequence alignment was generated with EMBOSS NEEDLE and visualised with ESPript 3.0.

The Ddc of *A. baumannii* was next investigated. The amino acid sequence was compared to other group II decarboxylases these being Glutamate decarboxylase alpha from *E. coli* and tyrosine decarboxylase from *Enterococcus faecalis.* Similar to PLP-dependent aminotransferases such as Dat, PLP-dependent decarboxylases also feature a modified lysine residue within their active sites. Alignment of sequences found that a conserved lysine residue was present at position 319 (Figure 6.13). Suggesting this is the residue involved in Schiff base formation, which is supported by InterPro. PLP-dependent decarboxylases feature a tetrapeptide sequence assigned to the active site, -S(N, T)-X-H-K, that includes the modified lysine residue. Comparisons of the Ddc from *A. baumannii* with other group II decarboxylases found the sequence in Ddc was -D-F-H-K-, with the possible serine, asparagine or threonine being substituted for aspartic acid (Figure 6.13). Analysis of the amino acid sequence of Ddc was carried out with InterPro. This predicted that based on homology, residues G153, T154, N157, T258, D287, W290, and D316 are involved in PLP binding.

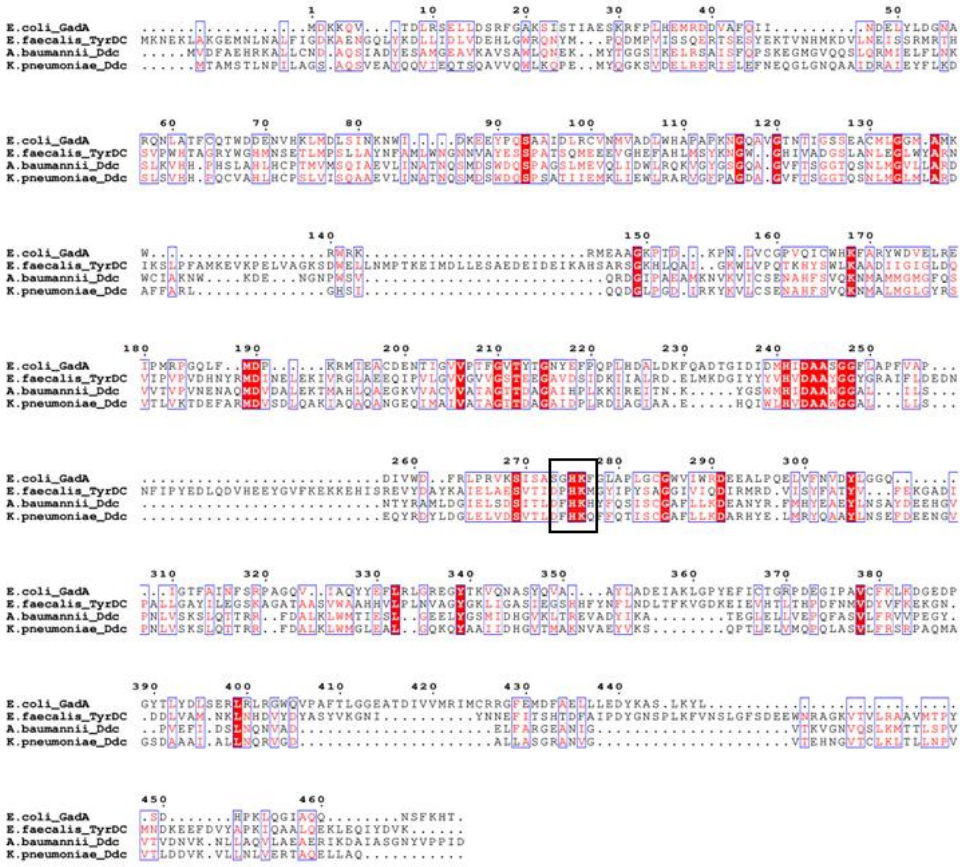

Figure 6.13. The -S(N, T)-X-H-K tetrapeptide sequence is not completely conserved in Ddc of *A. baumannii* 17978 and *K. pneumoniae* 52145. Protein multiple sequence alignment of *K. pneumoniae* and *A. baumannii* Ddc with *E. coli* glutamate decarboxylase alpha (GadA) and *E. faecalis* tyrosine decarboxylase (TyrDC). Boxed residues: The -S(N, T)-X-H-K tetrapeptide sequence with the lysine in the sequence being the PLP-modified residue. Sequence alignment was generated with Clustal Omega and visualised with ESPript 3.0.

6.3.3.2 Analysis of the Dat and Ddc from *K. pneumoniae* 52145

The *dat* gene in *K. pneumoniae* 52145 is codes for an amino acid sequence composed of 461 amino acids, with a molecular mass of 49.9 kDa. The amino acid sequence coded by *ddc* is composed of 493 amino acids, with a calculated molecular mass of 54.0 kDa. Investigation of the Dat amino acid sequence was carried out using InterPro. Dat is comprised of two domains, referred to as the major and small domains (Figure 6.14). Analysis revealed that the major domain of the Dat monomer includes residues 77-344 of the amino acid sequence domains (Figure 6.14). The small domain consists of residues 31-76 and 345-450 domains (Figure 6.14). Further investigation suggests the presence of the PLP attachment region consists of residues 263-300, that

encode the lysine residue for PLP interaction domains (Figure 6.14). InterPro revealed the Ddc of *K. pneumoniae* is comprised of a PLP-dependent decarboxylase domain which spans residues 68-419 (Figure 6.15). Based on similarity to the DOPA decarboxylase family, InterPro predicts residues G152, T153, N156, T249, D278, W281 and D307 to be involved in PLP binding (Figure 6.15). InterPro also suggests there be a coil structure composed of residues 473-493 (Figure 6.15).

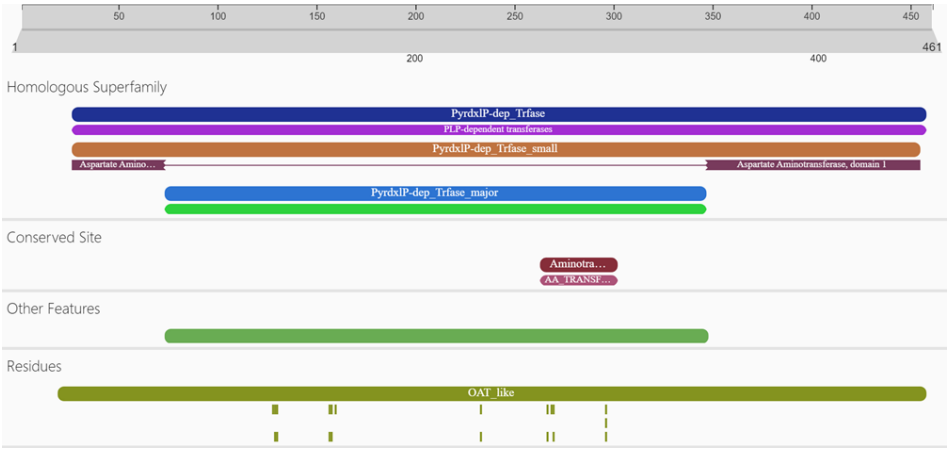

Figure 6.14. The predicted domains and features of the Dat protein in *K. pneumoniae* 52145. Family: 2,4-diaminobutyrate 4-transaminase. Homologous superfamily: PLP-dependent transferase, small domain and major domains. Conserved site: aminotransferase class III PLP-binding site. Residues: OAT_like domain and predicted Cofactor binding pocket and PLP-binding residues. Predictions were made with and adapted from InterPro.

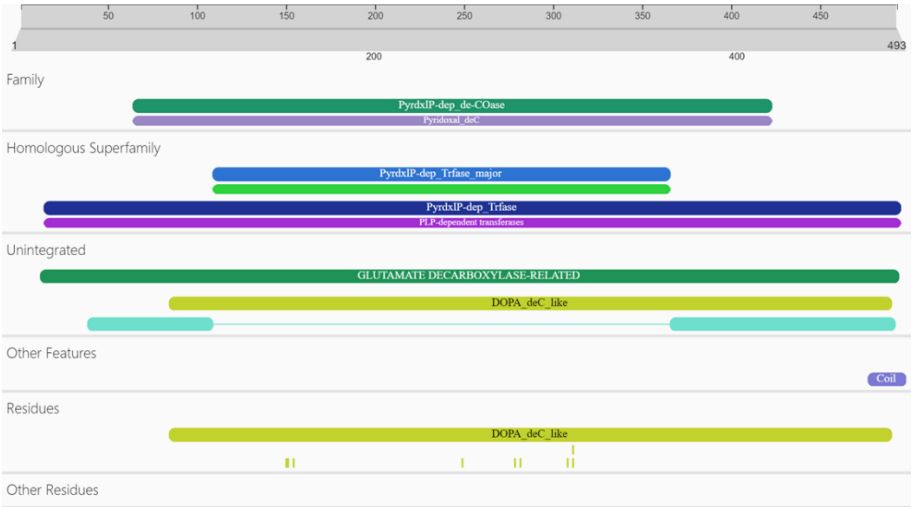

Figure 6.15. The predicted domains and features of the Ddc protein in *K. pneumoniae* 52145. InterPro predicts family: PLP-dependent decarboxylase. Binding site: PLP-binding site. Coil: coiled-coil structures. DOPA_deC_like: DOPA decarboxylase family and predicted residues for PLP binding residues and the catalytic lysine residue. Predictions were made with and adapted from InterPro.

Dat and Ddc were compared to homologues found in species, where Dat homologues had previously been characterised. When *K. pneumoniae* Dat was compared to the amino acid sequences of Dat from *A. baumannii* 17978 and *H. influenzae* ATCC 51907 both of which have shown to be functional, it was found the Dat of *K. pneumoniae* was longer compared to the 445 and 454 amino acids of Dat from *A. baumannii* and *H. influenzae*, respectively. Alignment found the Dat of *K. pneumoniae* is comparatively similar to the *A. Baumannii* Dat (63.9 % identity/ 76.6 % similarity) and *H. influenzae* Dat (62.2 % identity/ 76.9% similarity). BLASTp of *K. pneumoniae* Dat found that the amino acid sequence of Dat was similar to, the amino acid sequences encoded by *Providencia stuartii* (99.78 % identity), *Raoutella terrigena* (95.66 % identity) and *Pectobacterium carotovorum* (91.76 %). *P. stuartii* and *R. terrigena* are Enterobacteriaceae and *P. carotovorum* is a former member of the *Erwinia* genus of the Enterobacteriaceae suggesting these homologues are shared through evolution.

Comparison of the Ddc amino acid sequence from *K. pneumoniae* to the Ddc of *A. baumannii* and *H. influenzae* found the *K. pneumoniae* Ddc to be shorter compared to the 510 and 511 amino acid sequences of Ddc from *A. baumannii*

and *H. influenzae*, respectively. Similar to Dat, the Ddc of *K. pneumoniae* was similar to the *A. baumannii* (52.2 % identity/ 69.9 % similarity) and *H. influenzae* (52.2 % identity/ 67.5 % similarity) Ddc homologues. Analysis by BLASTp found that the amino acid sequence of *K. pneumoniae* Ddc was most similar to, excluding the *Klebsiella* genus, that found in *Providencia stuartii* (99.58 % identity), *Raoutella ornithinolytica* (93.1 % identity) and *Enterobacter cloacae* (91.89 %). Similarly to the sequence of Dat homologous sequences to Ddc are also found in members of the Enterobacteriaceae and closely related families again suggesting an evolutionary link between 1, 3-diaminopropane in these species and suggesting that 1, 3-diaminopropane synthesis is widespread among Enterobacteriaceae. The *K. pneumoniae* Dat was aligned with PvdH of *P. aeruginosa* PAO1 and shared 51.9 % identity and 69.3 % similarity. A comparison of the Dat of *K. pneumoniae* and the EctB of *C. salexigens* and *H. elongata* found that both show the least similarity to Dat when compared to other homologues examined, with 37.9 % identity and 54.2 % similarity and 35.9 % identity and 52.3 % similarity to EctB of *C. salexigens* and *H. elongata*, respectively.

There is no information regarding the modified lysine residue of the Dat or Ddc of *K. pneumoniae* 52145. The predicted pyroxidal binding lysine residue of *A. baumannii's* Dat is Lysine 289. Alignment of the *K. pneumoniae* sequence reveals a conserved lysine residue at position 295 of the amino acid sequence, suggesting this is lysine residue involved in Schiff base formation (Figure 6.16). InterPro supports this as it predicted the same catalytic residue. The Dat from *K. pneumoniae* 52145 was aligned with EctB of *C. salexigens.* This was done to determine the conservation of residues relating to protein structure and function. This established that several of the residues required for PLP-binding in EctB are completely conserved in Dat, these being G131, G160, Q269, D266, S294, K295, T323 and G322 in the amino acid sequence (Figure 6.16). While several PLP-binding residues differ, they are still amino acids of similar properties (Figure 6.16). A similar result was observed for residues involved in substrate binding pockets the residues were conserved in the Dat amino acid

sequence. Alignment also showed that several residues involved in EctB dimerisation are conserved. These are V34, P129, G302, W315, P317, G318, F324 in the *K. pneumoniae* Dat sequence.

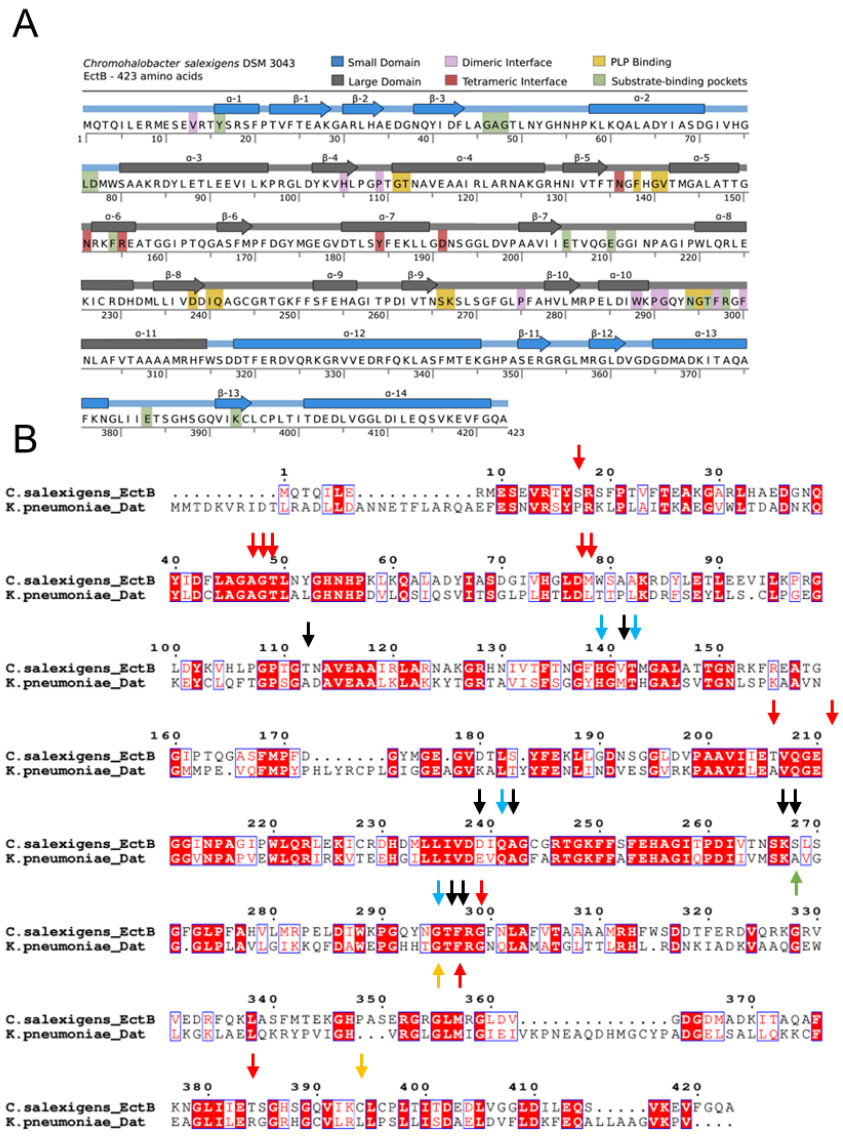

Figure 6.16. Residues involved in PLP-binding and the substrate-binding pocket are conserved between EctB of *C. salexigens* and *K. pneumoniae*. (A) The structural overview of the EctB from *C. salexigens* DSM 3043 featuring the domains and amino acid residues relating to function and structure. Figure adapted from Hillier et al (2020). **(B)** Protein sequence alignment of *K. pneumoniae* 52145 Dat with EctB from *C. salexigens* DSM 3043. Green arrow: indicates PLP-modified lysine residue. Black arrows: indicate conserved residues that are involved in PLP-binding in *C. salexigens* DSM 3043. Blue arrow: indicates similar amino acid, at that position, to those involved in PLP binding. Red arrow indicates conserved residues that are related to substrate-binding pockets. Yellow arrow indicates a similar amino acid, at that position, related to substrate binding pockets. White character within red box: indicates conserved amino acid identity. Red character: indicates similarity of amino acid. Sequence alignment was generated with EMBOSS NEEDLE and visualised with ESPript 3.0.

The amino acid sequence of Ddc from *K. pneumoniae* was aligned with the Ddc of *A. baumannii*, which has somewhat been characterised but does not have a solved crystal structure, along with other well-characterised group II decarboxylase enzymes, to determine the presence of conserved residues. The predicted modified lysine of the Ddc of *A. baumannii* is K319 (Figure 6.13). Alignment of the *K. pneumoniae* Ddc amino acid sequence found there is a conserved lysine residue at position 310 of the amino acid sequence (Figure 6.13). Suggesting this to be the residue involved in Schiff base formation. Analysis with InterPro supports this prediction as it predicted the same residue. As for the tetrapeptide sequence assigned to the active site, -S(N, T)-X-H-K alignment with Ddc of *A. baumannii* and the glutamate and tyrosine decarboxylases from *E. coli* and *E. faecalis,* respectively revealed the presence of this sequence in the sequence of Ddc from *K. pneumoniae*. Of the sequence, the Histidine residue is conserved but the possible serine, asparagine, or threonine are substituted for aspartate in *K. pneumoniae* (Figure 6.13).

6.3.4 Prediction of Dat 3D structure

6.3.4.1 Analysis of 3D prediction

To begin investigating the possible structure of Dat and Ddc the monomeric structures of each protein from *K. pneumoniae* and *A. baumannii* were predicted using ColabFold. This generated highly confident structural predictions for the Dat monomers of both *K. pneumoniae* and *A. baumannii*. ColabFold produces five predicted structures from a given amino acid sequence. Alongside structural prediction, there are several other important readouts. The first is pLDDT, which is derived from the LDDT score, a superposition-free score, it measures the percentage of correctly predicted interatomic distances. Regions with pLDDT scores between 70-90 % are considered highly confident. 50-70 % are considered low confidence and caution should be taken. Regions with pLDDT <50 % should not be interpreted. The second result is the predicted aligned error score (PAE). This is a measure of expected positional error at residue x if the predicted and actual structures

are aligned on residue y and are most practical for determining the positional arrangement of domains within a protein. The predicted Dat monomeric structure is presented in Figure 6.17A. There appears to be a high level of confidence throughout the predicted model, with a PLDDT score >80 % (Figure 6.17B and C). The predicted model does show some low confidence, concerning the pLDDT score, from residues 1-20 (Figure 6.17B and C). The predicted *A. baumannii* Dat monomeric structure Figure 6.18A also shows high confidence, with PLDDT being primarily >80 % (Figure 6.18B and C). Similarly, to the Dat of *K. pneumoniae* there is low confidence found in the N-terminus, from residues 1-12 and at the last two residues of the C-terminus (Figure 6.18B and C).

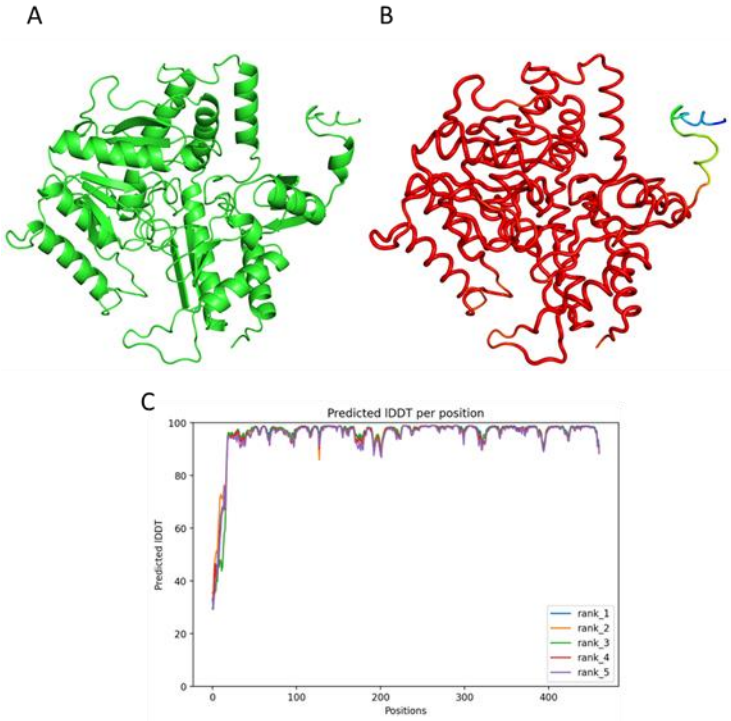

Figure 6.17. The predicted monomeric structure of Dat from *K. pneumoniae* 52145. (A) represents the predicted structure of Dat. **(B)** represents the structure coloured by B-factor which in this case represents pLDDT score. **(C)** pLDDT plot for all five of the predicted structures of *K. pneumoniae* Dat, Rank_1-5 corresponds to the five models constructed by the algorithm. Structures were predicted with ColabFold and visualised using pyMOL.

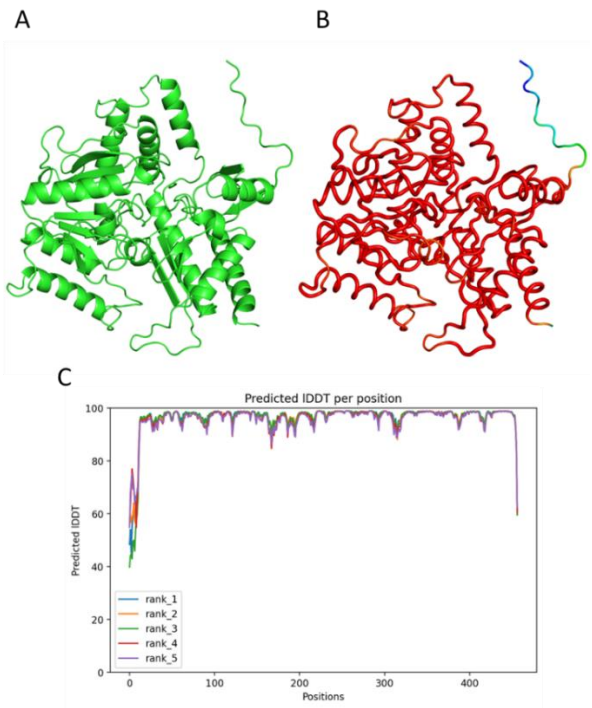

Figure 6.18. The predicted monomeric structure of Dat from *A. baumannii* 17978. (A) represents the predicted structure of Dat. **(B)** represents the structure coloured by B-factor which in this case represents pLDDT score. **(C)** pLDDT plot for all five of the predicted structures of *A. baumannii* Dat, Rank_1-5 corresponds to the five models constructed by the algorithm. Structures were predicted with ColabFold and visualised using pyMOL.

Initially, the predicted structures of the *K. pneumoniae* and *A. baumannii* Dat were aligned to one another (Figure 6.19). This was done using, using PDB 3D pairwise alignment with only one of the five predicted structures. This gave the root mean squared deviation (RMSD) and the template modelling score (TM-Score). The former is a measure of the distance between the C-alpha atoms of two superimposed structures, given in angstroms, with a lower score being better. TM-Score is a measure of topological similarity. It varies from RMSD as it weights smaller distance error stronger than larger. The TM-Score is therefore sensitive to global topology as opposed to local variation. For this a score closest to one is desirable. This generated an RMSD of 1.41 and a TM-Score of 0.98. The five predicted structures for each Dat were aligned to the EctB from *C. salexigens* DSM 3043 (PDB: 6RL5) (Figure 6.20). For the *K. pneumoniae* Dat the median RMSD score was 1.48 (range: 1.47-1.49) while the median TM-Score was 0.95 (range: 0.95). For the *A. baumannii* Dat, the median

RMSD was 1.57 (range 1.56-1.58). The median TM-score was 0.95 (range 0.95). This TM-Score suggests that the structures are nearly identical which would be expected if using an experimentally derived Dat structure as homologous enzymes would share the same fold and structure. This highlights how accurate and supports the confidence of the predicted 3D structure produced by ColabFold.

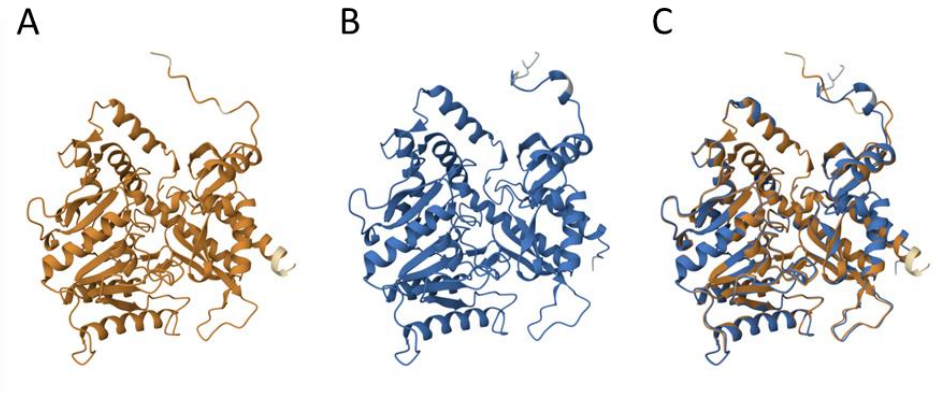

Figure 6.19. Alignment of the ColabFold predicted 3D structures of Dat from *K. pneumoniae* 52145 and *A. baumannii* 17978. (A) 3D prediction of *K. pneumoniae* Dat **(B)** 3D prediction of *A. baumannii* Dat **(C)** Superimposition of the two predicted structures. RMSD: 1.41 TM-Score: 0.98.

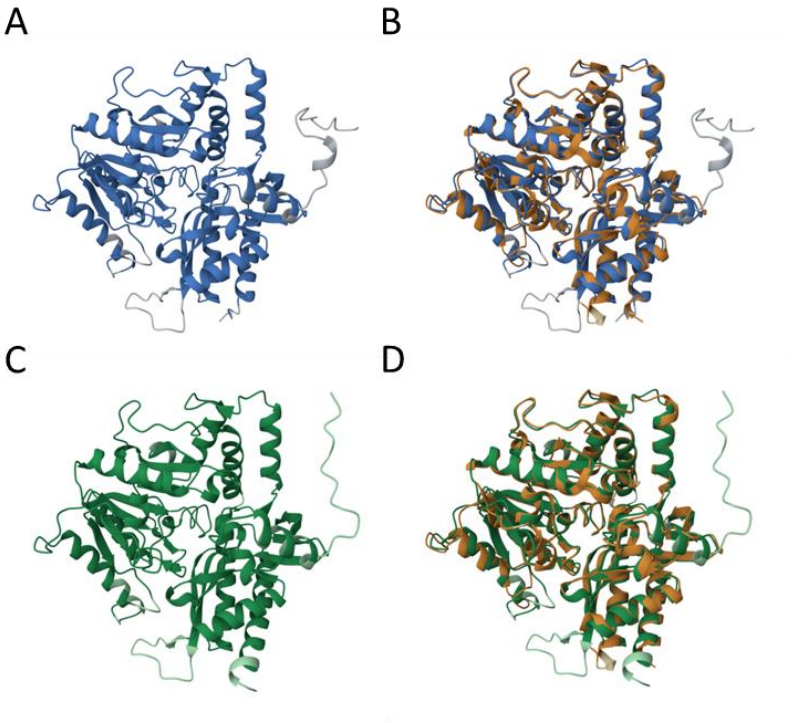

Figure 6.20. Alignment of the ColabFold predicted 3D structures of L-2, 4-diaminobutyrate:2-ketoglutarate 4-aminotransferase from *K. pneumoniae* 52145 and *A. baumannii* 17978 with the 3D structure of EctB (6RL5) from *C. salexigens* DSM 3034. (A) Predicted monomeric structure of Dat from *K. pneumoniae* 52145 **(B)** superimposition of Dat from K. *pneumoniae* and EctB from *C. salexigens* DSM 3034. **(C)** Predicted monomeric structure of Dat from *A. baumannii* 17978 **(D)** superimposition of Dat from *A. baumannii* 17978 and EctB from *C. salexigens* DSM 3034.

6.3.4.2 Fold and topology of Dat 3D prediction

The folding of the 3D prediction is consistent with the aminotransferase type-I fold. The Dat monomers of both species formed two distinct domains these being the large and small. In both enzymes, the large domain forms a distinct α/β/α confirmation. This is comprised of α-helices that sandwich a seven-stranded β-sheet of mixed topology (5X 1X -2X -1X -1X -1). The small domains differ between structures. The *K. pneumoniae* Dat features two β-sheets and six α-helices. The *A. baumannii* Dat features two β-sheets and five α-helices.

6.3.5 Prediction of the Ddc 3D monomeric structure

6.3.5.1 Analysis of 3D prediction

As with Dat, the 3D monomeric structure of Ddc from *K. pneumoniae* and *A. baumannii* was predicted using ColabFold. The predicted structure *of K. pneumoniae* Ddc (Figure 6.21A) shows a high level of confidence (Figure 6.21B and C). However, there are regions of lower confidence (<80 %) these span residues 1-9, 38-45, 333-349, and 421-428 (Figure 6.21B and C). The *A. baumannii* Ddc predicted structure (Figure 6.21A) has the confidence of primarily >80% (Figure 6.22B and C). However, there are also some lower confidence regions. These include the C and N-termini with an additional region spanning approximately residues 339-370 (Figure 6.22B and C).

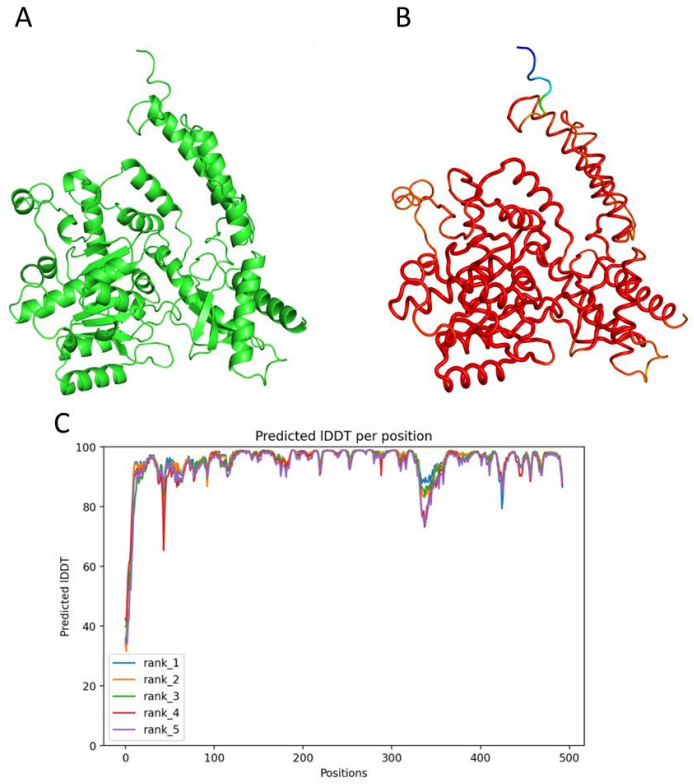

Figure 6.21. The predicted monomeric structure of Ddc from *K. pneumoniae* 52145. (A) represents the predicted structure of Ddc. **(B)** represents the structure coloured by B-factor which in this case represents pLDDT score. **(C)** pLDDT plot for all five of the predicted structures of *K. pneumoniae* Dat, Rank_1-5 corresponds to the five models constructed by the algorithm. Structures were predicted with ColabFold and visualised using pyMOL.

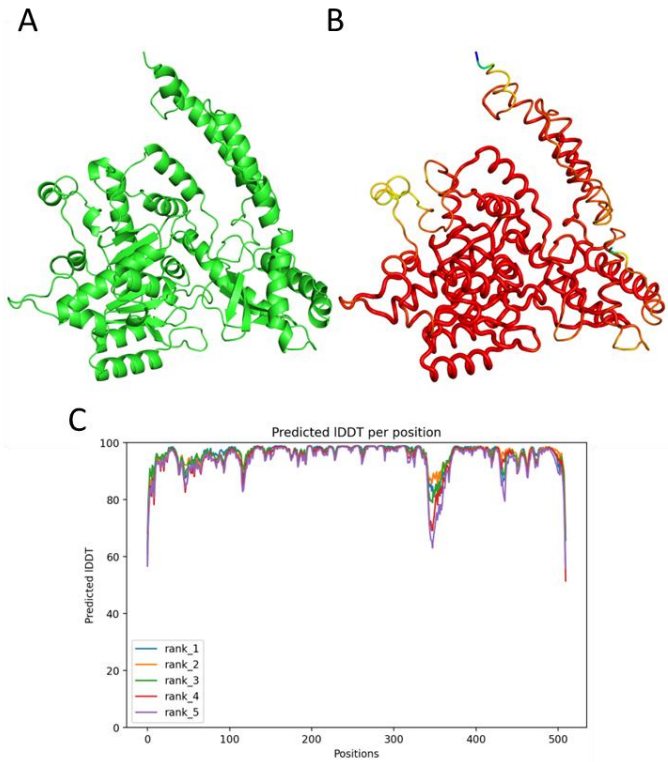

Figure 6.22. The predicted monomeric structure of Ddc from *A. baumannii* 17978. (A) represents the predicted structure of Ddc. **(B)** represents the structure coloured by B-factor which in this case represents pLDDT score. **(C)** pLDDT plot for all five of the predicted structures of *A. baumannii* Ddc, Rank_1-5 corresponds to the five models constructed by the algorithm. Structures were predicted with ColabFold and visualised using pyMOL.

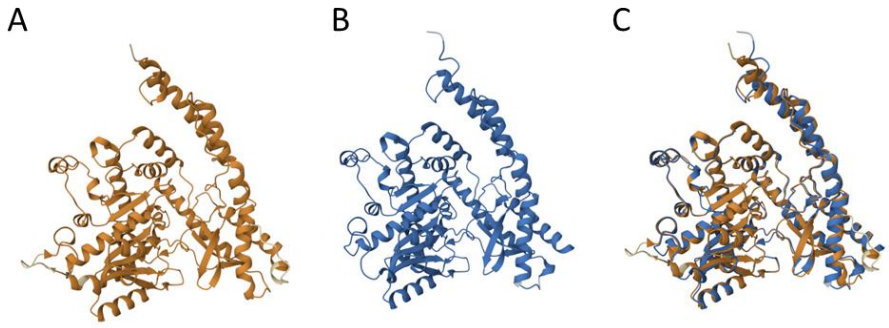

Figure 6.23. Alignment of the ColabFold predicted 3D structures of Ddc from *K. pneumoniae* 52145 and *A. baumannii* 17978. (A) 3D prediction of *K. pneumoniae* Ddc **(B)** 3D prediction of *A. baumannii* Ddc **(C)** Superimposition of the two predicted structures. RMSD: 1.04 TM-Score: 0.95.

The predicted Ddc structures were aligned with one another. This gives an RMSD of 1.04 and a TM-Score of 0.95 (Figure 6.23). Due to no crystal structure for an L-2, 4-diaminobutyrate decarboxylase homolog, predicted Ddc

structures were compared to several structurally related proteins. Initially, the predicted 3D structures of both Ddc enzymes were assessed with FoldSeek to determine closely related 3D structures. From this several structures were selected, and the predicted structures were aligned. The RMSD and TM-Scores are presented in Table 6.1. The alignment with both species' Ddc enzymes with DfoJ generated the lowest RMSD and the highest TM-Score. The worst RMSD value and TM-Scores the alignments to GadA and Tdc. The TM-Scores reflect that all analysed sequences are of the same fold despite being biologically different enzymes. The increasing RMSD scores could primarily be seen as a result of the reduced protein sequence identity between the protein sequences used.

Table 6.1 Comparison of the predicted 3D structure of Ddc with group II decarboxylases

Protein and bacterial species	Reference (Uniprot and PDB ID)	Sequence identity (%)	Median RMSD (Å)	Median TM-Score
Putative lysine decarboxylase (DfoJ) *Erwinia amylovora*	D4I245 5O5C	Kp Ddc: 40 Ab Ddc: 37	1.35 (1.32-1.37) 1.50 (1.49-1.53)	0.96 (0.96-0.97) 0.97 (0.97)
Pyridoxal-dependent decarboxylase *Sphaerobacter thermophilus*	D1C7D8 4RIT	Kp Ddc: 30 Ab Ddc: 28	2.16 (2.12-2.27) 2.18 (2.12-2.2)	0.93 (0.93) 0.93 (0.93-0.94)
Tyrosine decarboxylase (Tdc) *Enterococcus faecalis*	Q838D6 7CWX	Kp Ddc: 20 Ab Ddc 23	2.65 (2.65-2.69) 2.76 (2.75-2.82)	0.66 (0.66) 0.67 (0.67)
Glutamate decarboxylase alpha (GadA) *Escherichia coli*	P69908 1XEY	Kp Ddc: 15 Ab Ddc 14	3.12 (3.08-3.18) 3.02 (3.01-3.03)	0.8 (0.79-0.8) 0.71 (0.71)

6.3.5.2 Fold and topology

Before structural prediction, InterPro highlighted that the Ddc enzymes both feature PLP-transferase major domain, the same as in Dat (Figure 6.11 and Figure 6.15). The folded structure of both Ddc enzymes appears to be that of

fold type I. This is expected as group II decarboxylases commonly have this fold type. The structure of both enzymes has a major domain with the distinct α/β/α confirmation featuring a β sheet of seven strands with mixed topology (5X 1X -2X -1X -1X -1).

6.3.6 Prediction of the 3D multimeric structure of Dat and Ddc

L-2,4-diaminobutyrate:2-ketoglutarate 4-aminotransferase is a member of the class III PLP-dependent aminotransferase family of enzymes, which are largely believed to form functional dimers in solution. It was previously suggested that the aminotransferase may be a tetramer (Ikai and Yamamoto, 1997). Recently Hillier et al (2020) purified and solved the structure of L-2, 4-diaminobutyrate: 2-ketoglutarate 4-aminotransferase from *Chromohalobacter salexigens* DSM 3043, involved in ectoine synthesis. It was established the structure was a tetramer, comprised of two dimers. Other Class III aminotransferases such as, PuuE and GabT are also known homotetramers. Taken with the observations with BACTH analysis it was hypothesised that Dat forms a multimeric structure, this potentially being a tetramer. Expression and purification of the decarboxylase from *A. calcoaceticus* suggests that it may form a dimeric structure (Yamamoto et al., 1992). However, this has not been confirmed by X-ray crystallography. With Ddc being a group II decarboxylase and now known to be a fold-I type enzyme it is reasonable to hypothesise that it forms a dimeric structure at the very least.

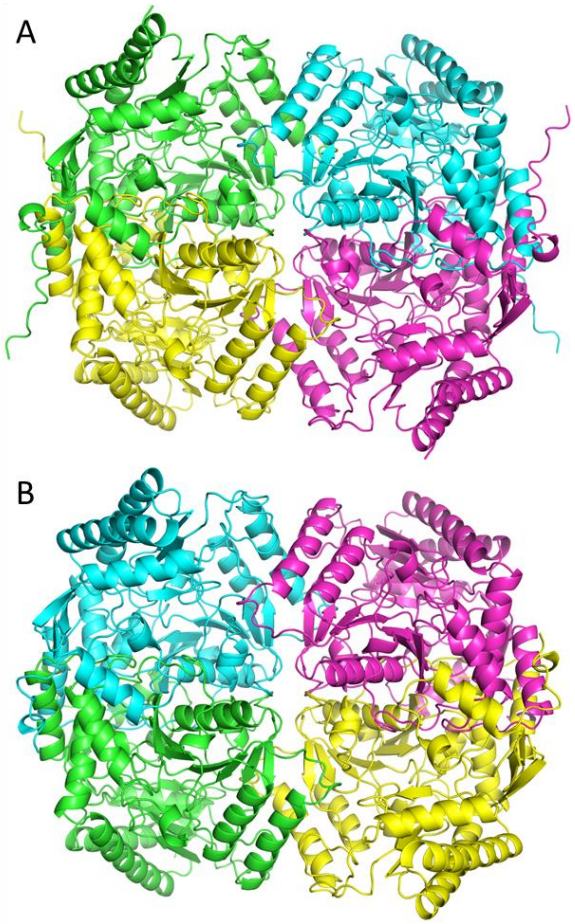

Figure 6.24. Dat forms a tetrameric structure. (A) The predicted tetrameric structure of Dat from *K. pneumoniae* 52145 **(B)** The predicted tetrameric structure of Dat from *A. baumannii.* Individual chains are coloured separately. Structures were predicted using ColabFold and presented using PyMOL.

To begin the prediction of the dimeric structure of Dat from both organisms was attempted. This produced predictions for the dimeric structures of both aminotransferases suggesting that both enzymes dimerise, similar to EctB and other fold-I type enzymes. Following this, attempts were made to predict the possible tetrameric structures of both enzymes and ColabFold produced predicted tetrameric structures for both (Figure 6.24). The dimeric structures of both Ddc enzymes were also predicted using ColabFold (Figure 6.25). This was able to produce two highly confident models for each protein. This supports the suggestion of Yamamoto et al (1992) that Ddc may form heterodimers. The high level of confidence within the monomeric structures and their 3D alignments and the high level of the quaternary structure suggest

that these predicted structures may be a close approximation of an experimentally solved 3D structure.

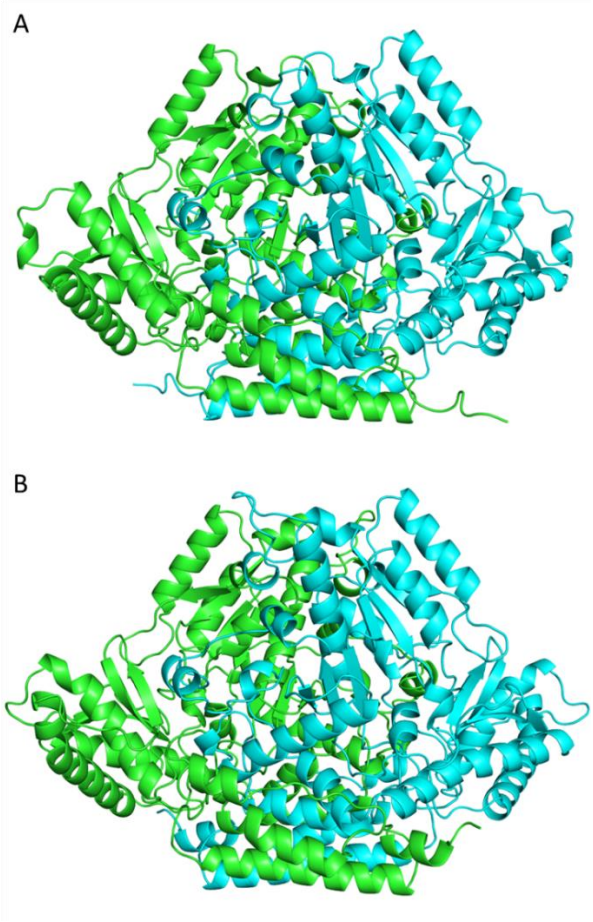

Figure 6.25. Ddc forms dimeric structure. (A) The predicted dimer structure of Ddc from *K. pneumoniae* 52145 **(B)** The predicted dimeric structure of Ddc from *A. baumannii.* Individual chains are coloured separately. Structures were predicted using ColabFold and presented using PyMOL.

6.4 Chapter discussion

This chapter sought to investigate the 3D structures of Dat and Ddc to support novel therapeutic investigations in the future. 3D structural prediction with ColabFold has revealed the possible structures of the Dat and Ddc enzymes from *A. baumannii* and *K. pneumoniae.* The ColabFold-generated structures show high levels of confidence and are highly similar to known 3D structures of homologues or closely related enzymes. Inspection of the 3D monomeric structures revealed both Dat and Ddc are type-I fold enzymes. This is expected

as Dat is a class-III aminotransferase and Ddc is a group II decarboxylase and both commonly have this fold type (Liang et al., 2019). It must be stated that, even though ColabFold has produced highly confident predictions, these predicted structures cannot replace experimentally derived structures. The bioinformatics analysis presented in this chapter will however be useful in the future structural determination of both enzymes and publication of this work. The prediction of multimeric structures is expected as enzymes of the fold I type commonly form multimeric structures as this forms the active site (Liang et al., 2019). Analysis of protein interactions with the BACTH system confirmed these interactions. This evidence confirms the previous suggestions that each forms multimeric structures (Ikai and Yamamoto, 1997; Yamamoto et al., 1992). Analysis with BACTH also revealed a homo-interaction between the monomers of *K. pneumoniae* and *A. baumannii*. This is most likely due to the high degree of conservation between the amino acid sequences of both species. This is expected as residues required for such function and structure are usually evolutionarily conserved. This is supported by the observation that most of the known residues involved in dimeric interaction in EctB are conserved in Dat (Sections 6.3.3.1 and 6.3.3.2).

The results obtained by the MSc biotechnology students provide proof of concept for the expression of all four enzymes in an *E. coli* system and their subsequent purification. Once purified, further investigation should continue with protein crystallisation and X-ray crystallography, as initially planned. X-ray crystallography could utilise the facilities present at the Dimond Lightsource at Harwell, with the collaboration of Professor Andrew Lovering at the University of Birmingham, as initially planned for this project. If this were to be successful, the investigation could eventually move on to identifying possible inhibitory compounds. As for a novel inhibitor, there are two main approaches to enzyme inhibition these being reversible and irreversible. In terms of polyamine synthesis irreversible inhibition is the approach behind many current polyamine synthesis inhibitors. For Dat and Ddc this would utilise structural homologues of the enzyme substrates that have been modified with additional

groups, that when acted upon by the targeted enzyme would result in irreversible covalent modification of the active site. To begin investigating this chemical databases such as ZINC could be used to mine for similar compounds to the Dat and Ddc substrates. Followed by virtual screening experiments and then high throughput screening of these compounds on enzymatic activity. The analysis of the amino acid sequences of Dat and Ddc revealed a high level of homology between *A. baumannii* and *K. pneumoniae* but also to other bacterial species. The high degree of sequence homology suggests that if a therapeutic were to be developed it is likely to target enzymes from both species and could be used to target other bacterial species. For example, to inhibit PvdH, which is required for pyoverdine synthesis in *P. aeruginosa,* or to inhibit Dat or Ddc in other species of the *Acinetobacter* complex.

6.4.1 Conclusion

In this chapter, I initially set out to solve the 3D structure of the Dat and Ddc enzymes. However, due to complications of the COVID-19 pandemic much of the protein work could not be completed. This investigation has given a foundation for continued investigation into solving the 3D structure of the Dat and Ddc enzymes. It has generated expression strains, determined optimal conditions for expression and given details on the structure of both enzymes. Taken together this information will be valuable for future experimental structure determination. Continued investigation will potentially allow for identifying novel therapeutic compounds that target either the Dat or Ddc to allow for new therapeutic approaches to *K. pneumoniae* and *A. baumannii* infection.

Chapter 7 Discussion

The work completed in this thesis was focused on two main aims. The first was to investigate the role of polyamines in *A. baumannii* and *K. pneumoniae, to* potentially establish a link between these molecules and the virulence of both species. The second was to investigate the 1, 3-diaminopropane synthesis enzymes and solve their 3D structure, to aid in the search for a novel therapeutic compound to target and block synthesis.

Investigation provided in Chapter 3 shows for the first time that deletion of 1, 3-diaminopropane synthesis results in cell septation and growth defects. I believe this suggests a link between the diamine and cell division or that deletion may indirectly impact on this process, potentially through altered metabolism or gene expression. This new information indicates that 1, 3-diaminopropane may have a greater role in *A. baumannii* biology beyond regulating motility and biofilm formation. It has also shown that 1, 3-diaminopropane contributes to *A. baumannii* biofilm formation and corroborates the previous findings regarding motility. The involvement of 1, 3-diaminopropane in motility and biofilm formation suggests this diamine plays a significant role in *A. baumannii* lifestyle changes. Motility and biofilm formation are important for *A. baumannii* infection. Further investigation may lead to novel therapeutic approaches for treating future *A. baumannii* infections. A major question before this investigation was how the loss of 1, 3-diaminopropane synthesis attenuates virulence. This study has shed new light on this, indicating that this is due to increased susceptibility to innate immune system AMPs.

Chapter 4 shows that 1, 3-diaminopropane is synthesised by *K. pneumoniae* 52145. It also provides the first evidence for the involvement of this diamine in biofilm formation. Much of the investigation presented in this chapter suggests that 1, 3-diaminopropane is not involved in several of the investigated phenotypes including virulence, narrowing down potential future investigation. I believe targeting 1, 3-diaminopropane synthesis in this species

could be an anti-biofilm instead of an anti-virulence strategy. With a possibility, this could be used to eradicate abiotic biofilms that form on medical equipment and aid in infection.

Chapter 5 was focused on the role of cadaverine in *K. pneumoniae.* It provides evidence for the potential role of cadaverine in nitrosative stress resistance. Additionally, this investigation has provided a further understanding of cadaverine's involvement in acidic stress resistance. It gives details on the pH range cadaverine provides resistance and information on the expression of the system in this species, suggesting this may differ from that of *E. coli*. These findings suggest cadaverine may contribute to host colonisation and resistance to stress conditions encountered during infection. Further investigation may establish how these contribute *in vivo* to identify novel strategies for targeting cadaverine synthesis to tackle *K. pneumoniae* colonisation and infection.

One of the initial aims was to determine the 3D structure of Dat and Ddc enzymes. However, due to the COVID-19 pandemic, this could not be fulfilled. Despite this the investigation in Chapter 6 has provided insight into the structure and functional residues of the Dat and Ddc enzymes. This analysis will be useful in the experimental determination of the Dat and Ddc structures, in the future. As for conducting this work, the construction of expression vectors and preliminary protein expression and purification provide a basis for this investigation.

In conclusion, this work has highlighted novel roles of 1, 3-diaminopropane in both *A. baumannii* and *K. pneumoniae*. This investigation also has given a new understanding of cadaverine in *K. pneumoniae* while building on previous knowledge. This provides a basis for further investigation of polyamine biology in *A. baumannii* and *K. pneumoniae*. It also gives possible avenues of exploration for the potential use of these synthesis pathways as therapeutic targets. Antimicrobial resistance is an ongoing and significantly growing problem across the world. This ever-increasing threat calls for investigating and developing novel therapeutic strategies to treat infection in the future.

Chapter 8 References

Adelakin, R.A., 2023. Expression and bioinformatics analysis of L-2,4-diaminobutyrate decarboxylase of Klebsiella pneumoniae and Acinetobacter baumannii in Escherichia coli. M. Sc. Thesis. The University of Nottingham.

Ahmad, I., Nadeem, A., Mushtaq, F., Zlatkov, N., Shahzad, M., Zavialov, A. V., Wai, S.N., Uhlin, B.E., 2023. Csu pili dependent biofilm formation and virulence of Acinetobacter baumannii. npj Biofilms Microbiomes 2023 91 9, 1–17.

Akhova, A., Nesterova, L., Shumkov, M., Tkachenko, A., 2021. Cadaverine biosynthesis contributes to decreased Escherichia coli susceptibility to antibiotics. Res. Microbiol. 172, 103881.

Akhova, A. V., Tkachenko, A.G., 2020. Multifaceted role of polyamines in bacterial adaptation to antibiotic-mediated oxidative stress. Microbiol. Soc. Korea 56, 103–110.

Al-Shehri, S.S., 2021. Reactive oxygen and nitrogen species and innate immune response. Biochimie 181, 52–64.

Altschul, S.F., Gish, W., Miller, W., Myers, E.W., Lipman, D.J., 1990. Basic local alignment search tool. J. Mol. Biol. 215, 403–410.

Álvarez, D., Merino, S., Tomás, J.M., Benedí, V.J., Albertí, S., 2000. Capsular polysaccharide is a major complement resistance factor in lipopolysaccharide O side chain-deficient Klebsiella pneumoniae clinical isolates. Infect. Immun. 68, 953–955.

Andrejko, M., Mak, P., Siemińska-Kuczer, A., Iwański, B., Wojda, I., Suder, P., Kuleta, P., Regucka, K., Cytryńska, M., 2021. A comparison of the production of antimicrobial peptides and proteins by Galleria mellonella larvae in response to infection with two Pseudomonas aeruginosa strains differing in the profile of secreted proteases. J. Insect Physiol. 131, 104239.

Appleyard, R.K., 1954. Segregation of New Lysogenic Types during Growth of a Doubly Lysogenic Strain Derived from Escherichia Coli K12. Genetics 39, 440–52.

Armalytė, J., Čepauskas, A., Šakalytė, G., Martinkus, J., Skerniškytė, J., Martens, C., Sužiedėlienė, E., Garcia-Pino, A., Jurėnas, D., 2023. A polyamine acetyltransferase regulates the motility and biofilm formation of Acinetobacter baumannii. Nat. Commun. 2023 141 14, 1–11.

Ashurst, J. V., Dawson, A., 2023. Klebsiella Pneumonia. StatPearls.

Aubert, D.F., Hamad, M.A., Valvano, M.A., 2014. A markerless deletion method for genetic manipulation of burkholderia cenocepacia and other multidrug-resistant gram-negative bacteria. Methods Mol. Biol. 1197, 311–327.

Ayoola, M.B., Shack, L.A., Lee, J.H., Lim, J., Eoh, H., Swiatlo, E., Phanstiel, O., Nanduri, B., 2022. Difluoromethylornithine (DFMO) and AMXT 1501 inhibit capsule biosynthesis in pneumococci. Sci. Rep. 12.

Ayoola, M.B., Shack, L.A., Nakamya, M.F., Thornton, J.A., Swiatlo, E., Nanduri, B., 2019. Polyamine Synthesis Effects Capsule Expression by Reduction of Precursors in Streptococcus pneumoniae. Front. Microbiol. 10, 1996.

Bach, S., de Almeida, A., Carniel, E., 2000. The Yersinia high-pathogenicity island is present in different members of the family Enterobacteriaceae. FEMS Microbiol. Lett. 183, 289–294.

Bachman, M.A., Oyler, J.E., Burns, S.H., Caza, M., Lépine, F., Dozois, C.M., Weiser, J.N., 2011. Klebsiella pneumoniae yersiniabactin promotes respiratory tract infection through evasion of lipocalin 2. Infect. Immun. 79, 3309–3316.

Barry, D.P., Asim, M., Leiman, D.A., de Sablet, T., Singh, K., Casero, R.A., Chaturvedi, R., Wilson, K.T., 2011. Difluoromethylornithine Is a Novel Inhibitor of Helicobacter pylori Growth, CagA Translocation, and Interleukin-8 Induction. PLoS One 6, 17510.

Bartholomew, T.L., Kidd, T.J., Pessoa, J.S., Álvarez, R.C., Bengoechea, J.A., 2019. 2-Hydroxylation of Acinetobacter baumannii Lipid A Contributes to Virulence. Infect. Immun. 87.

Bateman, A., Martin, M.J., Orchard, S., Magrane, M., Ahmad, S., Alpi, E., Bowler-Barnett, E.H., Britto, R., Bye-A-Jee, H., Cukura, A., Denny, P., Dogan, T., Ebenezer, T.G., Fan, J., Garmiri, P., da Costa Gonzales, L.J., Hatton-Ellis, E., Hussein, A., Ignatchenko, A., ...Zhang, J., 2023. UniProt: the Universal Protein Knowledgebase in 2023. Nucleic Acids Res. 51, D523–D531.

Berman, H., Henrick, K., Nakamura, H., 2003. Announcing the worldwide Protein Data Bank. Nat. Struct. Mol. Biol. 2003 1012 10, 980–980.

Berman, H.M., Westbrook, J., Feng, Z., Gilliland, G., Bhat, T.N., Weissig, H., Shindyalov, I.N., Bourne, P.E., 2000. The Protein Data Bank. Nucleic Acids Res. 28, 235–242.

Bertani, B., Ruiz, N., 2018. Function and biogenesis of lipopolysaccharides. EcoSal Plus 8.

Bialek-Davenet, S., Criscuolo, A., Ailloud, F., Passet, V., Jones, L., Delannoy-Vieillard, A.S., Garin, B., Hello, S. Le, Arlet, G., Nicolas-Chanoine, M.H., Decré, D., Brisse, S., 2014. Genomic Definition of Hypervirulent and Multidrug-Resistant Klebsiella pneumoniae Clonal Groups. Emerg. Infect. Dis. 20, 1812.

Blanco, P., Hernando-Amado, S., Reales-Calderon, J.A., Corona, F., Lira, F., Alcalde-Rico, M., Bernardini, A., Sanchez, M.B., Martinez, J.L., 2016. Bacterial Multidrug Efflux Pumps: Much More Than Antibiotic Resistance Determinants. Microorg. 2016, Vol. 4, Page 14 4, 14.

Blaschke, U., Skiebe, E., Wilharm, G., 2021. Novel Genes Required for Surface-Associated Motility in Acinetobacter baumannii. Curr. Microbiol. 2021 784 78, 1509–1528.

Blattner, F.R., Plunkett, G., Bloch, C.A., Perna, N.T., Burland, V., Riley, M., Collado-Vides, J., Glasner, J.D., Rode, C.K., Mayhew, G.F., Gregor, J., Davis, N.W., Kirkpatrick, H.A., Goeden, M.A., Rose, D.J., Mau, B., Shao, Y., 1997. The Complete Genome Sequence of Escherichia coli K-12. Science (80-.). 277, 1453–1462.

Boll, J.M., Tucker, A.T., Klein, D.R., Beltran, A.M., Brodbelt, J.S., Davies, B.W., Trent, M.S., 2015. Reinforcing lipid a acylation on the cell surface of acinetobacter baumannii promotes cationic antimicrobial peptide resistance and desiccation survival. MBio 6, 1–11.

Böttcher, F., Ober, D., Hartmann, T., 1994. Biosynthesis of pyrrolizidine alkaloids: putrescine and spermidine are essential substrates of enzymatic homospermidine formation. Can. J. Chem. 72, 80–85.

Bower, J.M., Gordon-Raagas, H.B., Mulvey, M.A., 2009. Conditioning of Uropathogenic Escherichia coli for Enhanced Colonization of Host. Infect. Immun. 77, 2104.

Bower, J.M., Mulvey, M.A., 2006. Polyamine-Mediated Resistance of Uropathogenic Escherichia coli to Nitrosative Stress. J. Bacteriol. 188, 928.

Bowman, W.H., White Tabor, C., Herbert Tabor, A., 1973. Spermidine Biosynthesis Purification and properties of propylamine transferase from Escherichia coli. J. Biol. Chem. 248, 2480–2486.

Brameyer, S., Rösch, T.C., El Andari, J., Hoyer, E., Schwarz, J., Graumann, P.L., Jung, K., 2019. DNA-binding directs the localization of a membrane-integrated receptor of the ToxR family. Commun. Biol. 2019 21 2, 1–10.

Bridges, A.A., Bassler, B.L., 2021. Inverse regulation of vibrio cholerae biofilm dispersal by polyamine signals. Elife 10.

Brossard, K.A., Campagnari, A.A., 2012. The Acinetobacter baumannii Biofilm-Associated Protein Plays a Role in Adherence to Human Epithelial Cells. Infect. Immun. 80, 228.

Buchner, S., Schlundt, A., Lassak, J., Sattler, M., Jung, K., 2015. Structural and Functional Analysis of the Signal-Transducing Linker in the pH-Responsive One-Component System CadC of Escherichia coli. J. Mol. Biol. 427, 2548–2561.

Camarena, L., Bruno, V., Euskirchen, G., Poggio, S., Snyder, M., 2010. Molecular Mechanisms of Ethanol-Induced Pathogenesis Revealed by RNA-Sequencing. PLoS Pathog. 6, 1–14.

Campos, M.A., Vargas, M.A., Regueiro, V., Llompart, C.M., Albertí, S., Bengoechea, J.A., 2004. Capsule polysaccharide mediates bacterial resistance to antimicrobial peptides. Infect. Immun. 72, 7107–7114.

Cano, V., March, C., Insua, J.L., Aguiló, N., Llobet, E., Moranta, D., Regueiro, V., Brennan, G.P., Millán-Lou, M.I., Martín, C., Garmendia, J., Bengoechea, J.A., 2015. Klebsiella pneumoniae survives within macrophages by avoiding delivery to lysosomes. Cell. Microbiol. 17, 1537–1560.

Chae, T.U., Kim, W.J., Choi, S., Park, S.J., Lee, S.Y., 2015. Metabolic engineering of Escherichia coli for the production of 1,3-diaminopropane, a three carbon diamine. Sci. Reports 2015 51 5, 1–13.

Chakraborty, S., Mizusaki, H., Kenney, L.J., 2015. A FRET-Based DNA Biosensor Tracks OmpR-Dependent Acidification of Salmonella during Macrophage Infection. PLoS Biol. 13.

Chattopadhyay, M.K., Tabor, C.W., Tabor, H., 2003. Polyamines protect Escherichia

coli cells from the toxic effect of oxygen. Proc. Natl. Acad. Sci. U. S. A. 100, 2261–2265.

Chattopadhyay, M.K., Tabor, C.W., Tabor, H., 2009. Polyamines are not required for aerobic growth of Escherichia coli: Preparation of a strain with deletions in all of the genes for polyamine biosynthesis. J. Bacteriol. 191, 5549–5552.

Cheng, H.Y., Chen, Y.S., Wu, C.Y., Chang, H.Y., Lai, Y.C., Peng, H.L., 2010. RmpA Regulation of Capsular Polysaccharide Biosynthesis in Klebsiella pneumoniae CG43. J. Bacteriol. 192, 3144.

Choby, J.E., Howard-Anderson, J., Weiss, D.S., 2020. Hypervirulent Klebsiella pneumoniae – clinical and molecular perspectives. J. Intern. Med. 287, 283.

Choby, J.E., Howard-Anderson, J., Weiss, D.S., 2019. Hypervirulent *Klebsiella pneumoniae* – clinical and molecular perspectives. J. Intern. Med. joim.13007.

Choi, C.H., Lee, J.S., Lee, Y.C., Park, T.I., Lee, J.C., 2008. Acinetobacter baumannii invades epithelial cells and outer membrane protein A mediates interactions with epithelial cells. BMC Microbiol. 8, 216.

Choi, K.H., Schweizer, H.P., 2006. mini-Tn7 insertion in bacteria with single attTn7 sites: example Pseudomonas aeruginosa. Nat. Protoc. 2006 11 1, 153–161.

Clemmer, K.M., Bonomo, R.A., Rather, P.N., 2011. Genetic analysis of surface motility in Acinetobacter baumannii. Microbiology 157, 2534.

Corral, J., Pérez-Varela, M., Sánchez-Osuna, M., Cortés, P., Barbé, J., Aranda, J., 2021. Importance of twitching and surface-associated motility in the virulence of Acinetobacter baumannii. Virulence 12, 2201–2213.

Correa, W., Manrique-Moreno, M., Behrends, J., Patiño, E., Marella, C., Peláez-Jaramillo, C., Garidel, P., Gutsmann, T., Brandenburg, K., Heinbockel, L., 2014. Galleria mellonella native and analogue peptides Gm1 and ΔGm1. II) Anti-bacterial and anti-endotoxic effects. Biochim. Biophys. Acta - Biomembr. 1838, 2739–2744.

Das, K.C., Misra, H.P., 2004. Hydroxyl radical scavenging and singlet oxygen quenching properties of polyamines. Mol. Cell. Biochem. 262, 127–133.

Dell, C.L., Neely, M.N., Olson, E.R., 1994. Altered pH lysine signalling mutants of cadC, a gene encoding a membrane-bound transcriptional activator of the Escherichia coli cadBA operon. Mol. Microbiol. 14, 7–16.

Demarre, G., Guérout, A.M., Matsumoto-Mashimo, C., Rowe-Magnus, D.A., Marlière, P., Mazel, D., 2005. A new family of mobilizable suicide plasmids based on broad host range R388 plasmid (IncW) and RP4 plasmid (IncPα) conjugative machineries and their cognate Escherichia coli host strains. Res. Microbiol. 156, 245–255.

Deng, W., Fu, T., Zhang, Z., Jiang, X., Xie, J., Sun, H., Hu, P., Ren, H., Zhou, P., Liu, Q., Long, Q., 2020. L-lysine potentiates aminoglycosides against Acinetobacter baumannii via regulation of proton motive force and antibiotics uptake. Emerg. Microbes Infect. 9, 639.

Di Martino, P., Cafferini, N., Joly, B., Darfeuille-Michaud, A., 2003. Klebsiella pneumoniae type 3 pili facilitate adherence and biofilm formation on abiotic

surfaces. Res. Microbiol. 154, 9–16.

Di Salvo, M., Puccio, S., Peano, C., Lacour, S., Alifano, P., 2019. RhoTermPredict: An algorithm for predicting Rho-dependent transcription terminators based on Escherichia coli, Bacillus subtilis and Salmonella enterica databases. BMC Bioinformatics 20, 1–11.

Dodds, D.R., 2017. Antibiotic resistance: A current epilogue. Biochem. Pharmacol.

Dong, J.F., Liu, C.W., Wang, P., Li, L., Zou, Q.H., 2022. The type VI secretion system in Acinetobacter baumannii clinical isolates and its roles in antimicrobial resistance acquisition. Microb. Pathog. 169, 105668.

El-Halfawy, O.M., Valvano, M.A., 2014. Putrescine reduces antibiotic-induced oxidative stress as a mechanism of modulation of antibiotic resistance in Burkholderia cenocepacia. Antimicrob. Agents Chemother. 58, 4162–4171.

Eryilmaz-Erem, E., Yalcin, S., Ozan, F., Saatci, E., Yildiz, S.S., Ture, Z., Kilinc-Toker, A., Celik, I., 2023. An outbreak analysis of wound infection due to Acinetobacter baumannii in earthquake-trauma patients. Am. J. Infect. Control.

Espinel, I.C., Guerra, P.R., Jelsbak, L., 2016. Multiple roles of putrescine and spermidine in stress resistance and virulence of Salmonella enterica serovar Typhimurium. Microb. Pathog. 95, 117–123.

Europen Centre for Disease Prevention and Control, 2023. Antimicrobial resistance in the EU/EEA (EARS-Net) Annual Epidemiological Report for 2022. Stockholm.

Fang, C.T., Chuang, Y.P., Shun, C.T., Chang, S.C., Wang, J.T., 2004. A Novel Virulence Gene in Klebsiella pneumoniae Strains Causing Primary Liver Abscess and Septic Metastatic Complications. J. Exp. Med. 199, 697–705.

Fang, C.T., Lai, S.Y., Yi, W.C., Hsueh, P.R., Liu, K.L., 2010. The Function of wzy_K1 (magA), the Serotype K1 Polymerase Gene in Klebsiella pneumoniae cps Gene Cluster. J. Infect. Dis. 201, 1268–1269.

Flannagan, R.S., Linn, T., Valvano, M.A., 2008. A system for the construction of targeted unmarked gene deletions in the genus Burkholderia. Environ. Microbiol. 10, 1652–1660.

Flemming, H.C., Wingender, J., Szewzyk, U., Steinberg, P., Rice, S.A., Kjelleberg, S., 2016. Biofilms: an emergent form of bacterial life. Nat. Rev. Microbiol. 2016 149 14, 563–575.

Fredlund, J.O., Johansson, M.C., Dahlberg, E., Oredsson, S.M., 1995. Ornithine Decarboxylase and S-Adenosylmethionine Decarboxylase Expression during the Cell Cycle of Chinese Hamster Ovary Cells. Exp. Cell Res. 216, 86–92.

Gaboriau, F., Vaultier, M., Moulinoux, J.P., Delcros, J.G., 2005. Antioxidative properties of natural polyamines and dimethylsilane analogues. Redox Rep. 10, 9–18.

Gales, A.C., Seifert, H., Gur, D., Castanheira, M., Jones, R.N., Sader, H.S., 2019. Antimicrobial Susceptibility of Acinetobacter calcoaceticus–Acinetobacter baumannii Complex and Stenotrophomonas maltophilia Clinical Isolates: Results From the SENTRY Antimicrobial Surveillance Program (1997–2016). Open Forum Infect. Dis. 6, S34.

Garneau-Tsodikova, S., Labby, K.J., 2016. Mechanisms of Resistance to Aminoglycoside Antibiotics: Overview and Perspectives. Medchemcomm 7, 11.

Goetz, D.H., Holmes, M.A., Borregaard, N., Bluhm, M.E., Raymond, K.N., Strong, R.K., 2002. The Neutrophil Lipocalin NGAL Is a Bacteriostatic Agent that Interferes with Siderophore-Mediated Iron Acquisition. Mol. Cell 10, 1033–1043.

Gong, S., Richard, H., Foster, J.W., 2003. YjdE (AdiC) Is the Arginine:Agmatine Antiporter Essential for Arginine-Dependent Acid Resistance in Escherichia coli. J. Bacteriol. 185, 4402.

Gorrie, C.L., Mirc Eta, M., Wick, R.R., Edwards, D.J., Thomson, N.R., Strugnell, R.A., Pratt, N.F., Garlick, J.S., Watson, K.M., Pilcher, D. V., McGloughlin, S.A., Spelman, D.W., Jenney, A.W.J., Holt, K.E., 2017. Gastrointestinal Carriage Is a Major Reservoir of Klebsiella pneumoniae Infection in Intensive Care Patients. Clin. Infect. Dis. An Off. Publ. Infect. Dis. Soc. Am. 65, 208.

Gutierrez, E., Shin, B.S., Woolstenhulme, C.J., Kim, J.R., Saini, P., Buskirk, A.R., Dever, T.E., 2013. eif5A promotes translation of polyproline motifs. Mol. Cell 51, 35–45.

Hamad, M.A., Skeldon, A.M., Valvano, M.A., 2010. Construction of Aminoglycoside-Sensitive Burkholderia cenocepacia Strains for Use in Studies of Intracellular Bacteria with the Gentamicin Protection Assay. Appl. Environ. Microbiol. 76, 3170.

Hamana, K., 1996. Distribution of diaminopropane and acetylspermidine in Enterobacteriaceae. Can. J. Microbiol. 42, 107–114.

Hamana, K., Matsuzaki, S., 1992. Diaminopropane occurs ubiquitously in acinetobacter as the major polyamine. J. Gen. Appl. Microbiol 38, 191–194.

Hameed, F., Khan, M.A., Muhammad, H., Sarwar, T., Bilal, H., Rehman, T.U., 2019. Plasmid-mediated mcr-1 gene in Acinetobacter baumannii and Pseudomonas aeruginosa: first report from Pakistan. Rev. Soc. Bras. Med. Trop. 52, e20190237.

Han, Y.L., Wen, X.H., Zhao, W., Cao, X.S., Wen, J.X., Wang, J.R., Hu, Z. De, Zheng, W.Q., 2022. Epidemiological characteristics and molecular evolution mechanisms of carbapenem-resistant hypervirulent Klebsiella pneumoniae. Front. Microbiol. 13, 1003783.

Hanahan, D., 1983. Studies on transformation of Escherichia coli with plasmids. J. Mol. Biol. 166, 557–580.

Haneburger, I., Eichinger, A., Skerra, A., Jung, K., 2011. New Insights into the Signaling Mechanism of the pH-responsive, Membrane-integrated Transcriptional Activator CadC of Escherichia coli. J. Biol. Chem. 286, 10681.

Hanfrey, C.C., Pearson, B.M., Hazeldine, S., Lee, J., Gaskin, D.J., Woster, P.M., Phillips, M.A., Michael, A.J., 2011. Alternative spermidine biosynthetic route is critical for growth of Campylobacter jejuni and is the dominant polyamine pathway in human gut microbiota. J. Biol. Chem. 286, 43301–43312.

Harding, C.M., Kinsella, R.L., Palmer, L.D., Skaar, E.P., Feldman, M.F., 2016. Medically Relevant Acinetobacter Species Require a Type II Secretion System and Specific Membrane-Associated Chaperones for the Export of Multiple Substrates and

Full Virulence. PLOS Pathog. 12, e1005391.

Harding, C.M., Pulido, M.R., Di Venanzio, G., Kinsella, R.L., Webb, A.I., Scott, N.E., Pachón, J., Feldman, M.F., 2017. Pathogenic Acinetobacter species have a functional type I secretion system and contact-dependent inhibition systems. J. Biol. Chem. 292, 9075.

Harding, C.M., Tracy, E.N., Carruthers, M.D., Rather, P.N., Actis, L.A., Munson, R.S., 2013. Acinetobacter baumannii Strain M2 Produces Type IV Pili Which Play a Role in Natural Transformation and Twitching Motility but Not Surface-Associated Motility. MBio 4.

Hassan, K.A., Naidu, V., Edgerton, J.R., Mettrick, K.A., Liu, Q., Fahmy, L., Li, L., Jackson, S.M., Ahmad, I., Sharples, D., Henderson, P.J.F., Paulsen, I.T., 2019. Short-chain diamines are the physiological substrates of PACE family efflux pumps. Proc. Natl. Acad. Sci. U. S. A. 116, 18015–18020.

Herbst, E.J., Snell, E.E., 1949. The nutritional requirements of Hemophilus parainfluenzae 7901. J. Bacteriol. 58, 379.

Higashi, K., Ishigure, H., Demizu, R., Uemura, T., Nishino, K., Yamaguchi, A., Kashiwagi, K., Igarashi, K., 2008. Identification of a Spermidine Excretion Protein Complex (MdtJI) in Escherichia coli. J. Bacteriol. 190, 872.

Higashi, K., Kashiwagi, K., Taniguchi, S., Terui, Y., Yamamoto, K., Ishihama, A., Igarashi, K., 2006. Enhancement of +1 frameshift by polyamines during translation of polypeptide release factor 2 in Escherichia coli. J. Biol. Chem. 281, 9527–9537.

Hillier, H.T., Altermark, B., Leiros, I., 2020. The crystal structure of the tetrameric DABA-aminotransferase EctB, a rate-limiting enzyme in the ectoine biosynthesis pathway. FEBS J. 287, 4641–4658.

Hobley, L., Kim, S.H., Maezato, Y., Wyllie, S., Fairlamb, A.H., Stanley-Wall, N.R., Michael, A.J., 2014. Norspermidine Is Not a Self-Produced Trigger for Biofilm Disassembly. Cell 156, 844.

Hobley, L., Li, B., Wood, J.L., Kim, S.H., Naidoo, J., Ferreira, A.S., Khomutov, M., Khomutov, A., Stanley-Wall, N.R., Michael, A.J., 2017. Spermidine promotes Bacillus subtilis biofilm formation by activating expression of the matrix regulator slrR. J. Biol. Chem. 292, 12041–12053.

Hsieh, P.F., Lin, H.H., Lin, T.L., Wang, J.T., 2010. CadC Regulates cad and tdc Operons in Response to Gastrointestinal Stresses and Enhances Intestinal Colonization of Klebsiella pneumoniae. J. Infect. Dis. 202, 52–64.

Iacovelli, A., Oliva, A., Siccardi, G., Tramontano, A., Pellegrino, D., Mastroianni, C.M., Venditti, M., Palange, P., 2023. Risk factors and effect on mortality of superinfections in a newly established COVID-19 respiratory sub-intensive care unit at University Hospital in Rome. BMC Pulm. Med. 23, 1–13.

Igarashi, K., Kashiwagi, K., 2010. Characteristics of cellular polyamine transport in prokaryotes and eukaryotes. Plant Physiol. Biochem. 48, 506–512.

Igarashi, K., Kashiwagi, K., 2018. Effects of polyamines on protein synthesis and growth of Escherichia coli. J. Biol. Chem. 293, 18702.

Igarashi, K., Kashiwagi, K., 2021. Functional roles of polyamines and their metabolite acrolein in eukaryotic cells. Amino Acids 53, 1473–1492.

Igarashi, K., Kashiwagi, K., Hamasaki, H., Miura, A., Kakegawa, T., Hirose, S., Matsuzaki, S., 1986. Formation of a compensatory polyamine by Escherichia coli polyamine-requiring mutants during growth in the absence of polyamines. J. Bacteriol. 166, 128.

Ikai, H., Yamamoto, S., 1994. Cloning and expression in Escherichia coli of the gene encoding a novel L-2,4-diaminobutyrate decarboxylase of Acinetobacter baumannii. FEMS Microbiol. Lett. 124, 225–228.

Ikai, H., Yamamoto, S., 1997. Identification and Analysis of a Gene Encoding L-2,4-Diaminobutyrate:2-Ketoglutarate 4-Aminotransferase Involved in the 1,3-Diaminopropane Production Pathway in Acinetobacter baumannii. J. Bacteriol. 179, 5118–5125.

Ikai, H., Yamamoto, S., 1998. Two genes involved in the 1,3-diaminopropane production pathway in Haemophilus influenzae. Biol. Pharm. Bull. 21, 170–173.

Inchai, J., Pothirat, C., Bumroongkit, C., Limsukon, A., Khositsakulchai, W., Liwsrisakun, C., 2015. Prognostic factors associated with mortality of drug-resistant Acinetobacter baumannii ventilator-associated pneumonia. J. Intensive Care 3, 1–8.

Insua, J.L., Llobet, E., Moranta, D., Pérez-Gutiérrez, C., Tomás, A., Garmendia, J., Bengoechea, J.A., 2013. Modeling Klebsiella pneumoniae Pathogenesis by Infection of the Wax Moth Galleria mellonella. Infect. Immun. 81, 3552.

Ittisoponpisan, S., Islam, S.A., Khanna, T., Alhuzimi, E., David, A., Sternberg, M.J.E., 2019. Can Predicted Protein 3D Structures Provide Reliable Insights into whether Missense Variants Are Disease Associated? J. Mol. Biol. 431, 2197–2212.

Iyer, R., Williams, C., Miller, C., 2003. Arginine-Agmatine Antiporter in Extreme Acid Resistance in Escherichia coli. J. Bacteriol. 185, 6556.

Jackson-Litteken, C.D., Venanzio, G. Di, Le, N.H., Scott, N.E., Djahanschiri, B., Distel, J.S., Pardue, E.J., Ebersberger, I., Feldman, M.F., 2022. InvL, an Invasin-Like Adhesin, Is a Type II Secretion System Substrate Required for Acinetobacter baumannii Uropathogenesis. MBio 13.

Jacobs, A.C., Hood, I., Boyd, K.L., Olson, P.D., Morrison, J.M., Carson, S., Sayood, K., Iwen, P.C., Skaar, E.P., Dunman, P.M., 2010. Inactivation of phospholipase D diminishes Acinetobacter baumannii pathogenesis. Infect. Immun. 78, 1952–1962.

Jin, L., Wang, R., Gao, H., Wang, Q., Wang, H., 2021. Identification of a novel hybrid plasmid encoding KPC-2 and virulence factors in klebsiella pneumoniae sequence type 11. Antimicrob. Agents Chemother. 65.

Johnson, L., Mulcahy, H., Kanevets, U., Shi, Y., Lewenza, S., 2012. Surface-Localized Spermidine Protects the Pseudomonas aeruginosa Outer Membrane from Antibiotic Treatment and Oxidative Stress. J. Bacteriol. 194, 813.

Joshi, G.S., Spontak, J.S., Klapper, D.G., Richardson, A.R., 2011. Arginine catabolic mobile element encoded speG abrogates the unique hypersensitivity of

Staphylococcus aureus to exogenous polyamines. Mol. Microbiol. 82, 9–20.

Jumper, J., Evans, R., Pritzel, A., Green, T., Figurnov, M., Ronneberger, O., Tunyasuvunakool, K., Bates, R., Žídek, A., Potapenko, A., Bridgland, A., Meyer, C., Kohl, S.A.A., Ballard, A.J., Cowie, A., Romera-Paredes, B., Nikolov, S., Jain, R., Adler, J., ...Hassabis, D., 2021. Highly accurate protein structure prediction with AlphaFold. Nat. 2021 5967873 596, 583–589.

Kallio, A., Mccann, P.P., Bey, P., 1981. DL-a-(Difluoromethyl)arginine: A Potent Enzyme-Activated Irreversible Inhibitor of Bacterial Arginine Decarboxylasest. Biochemistry 20, 3163–3166.

Kanafani, Z.A., Kanj, S.S., 2024. Acinetobacter infection: Treatment and prevention. In: Calderwood, S.B. (Ed.), UpToDate. Wolters Kluwer.

Kang, I.-H., Kim, J.-S., Kim, E.-J., Jeong K, L., 2007. Cadaverine protects Vibrio vulnificus from superoxide stress. J. Microbiol. Biotechnol. 17, 176–179.

Kanjee, U., Gutsche, I., Alexopoulos, E., Zhao, B., El Bakkouri, M., Thibault, G., Liu, K., Ramachandran, S., Snider, J., Pai, E.F., Houry, W.A., 2011. Linkage between the bacterial acid stress and stringent responses: the structure of the inducible lysine decarboxylase. EMBO J. 30, 931.

Kanjee, U., Houry, W.A., 2013. Mechanisms of Acid Resistance in Escherichia coli. Annu. Rev. Microbiol. 67, 65–81.

Karampatakis, T., Tsergouli, K., Behzadi, P., 2023. Carbapenem-Resistant Klebsiella pneumoniae: Virulence Factors, Molecular Epidemiology and Latest Updates in Treatment Options. Antibiot. 2023, Vol. 12, Page 234 12, 234.

Karatan, E., Duncan, T.R., Watnick, P.I., 2005. NspS, a Predicted Polyamine Sensor, Mediates Activation of Vibrio cholerae Biofilm Formation by Norspermidine. J. Bacteriol. 187, 7434.

Kashiwagi, K., Suzuki, T., Suzuki, F., Furuchi, T., Kobayashi, H., Igarashis, K., 1991. Coexistence of the Genes for Putrescine Transport Protein and Ornithine Decarboxylase at 16 min on Escherichia coli Chromosome 266, 20922–20927.

Kidd, T.J., Mills, G., Sá-Pessoa, J., Dumigan, A., Frank, C.G., Insua, J.L., Ingram, R., Hobley, L., Bengoechea, J.A., 2017. A Klebsiella pneumoniae antibiotic resistance mechanism that subdues host defences and promotes virulence. EMBO Mol. Med. 9, 430.

Kim, J.H., Kim, H.J., Kim, Y.H., Jeon, J.M., Song, H.S., Kim, J., No, S.Y., Shin, J.H., Choi, K.Y., Park, K.M., Yang, Y.H., 2016. Functional Study of Lysine Decarboxylases from Klebsiella pneumoniae in Escherichia coli and Application of Whole Cell Bioconversion for Cadaverine Production. J. Microbiol. Biotechnol. 26, 1586–1592.

Kim, J.S., Choi, S.H., Lee, J.K., 2006. Lysine decarboxylase expression by Vibrio vulnificus is induced by SoxR in response to superoxide stress. J. Bacteriol. 188, 8586–8592.

Kim, S.H., Wang, Y., Khomutov, M., Khomutov, A., Fuqua, C., Michael, A.J., 2016. The essential role of spermidine in growth of Agrobacterium tumefaciens is determined by the 1,3-diaminopropane moiety. ACS Chem. Biol. 11, 491.

Kingsford, C.L., Ayanbule, K., Salzberg, S.L., 2007. Rapid, accurate, computational discovery of Rho-independent transcription terminators illuminates their relationship to DNA uptake. Genome Biol. 8, 1–12.

Küper, C., Jung, K., 2005. CadC-Mediated Activation of the cadBA Promoter in Escherichia coli. J. Mol. Microbiol. Biotechnol. 10, 26–39.

Kurihara, S., Sakai, Y., Suzuki, H., Muth, A., Phanstiel IV, O., Rather, P.N., 2013. Putrescine Importer PlaP Contributes to Swarming Motility and Urothelial CellInvasion in Proteus mirabilis. J. Biol. Chem. 288, 15668.

Kurihara, S., Suzuki, H., Oshida, M., Benno, Y., 2011. A Novel Putrescine Importer Required for Type 1 Pili-driven Surface Motility Induced by Extracellular Putrescine in Escherichia coli K-12. J. Biol. Chem. 286, 10185.

Kurihara, S., Suzuki, H., Tsuboi, Y., Benno, Y., 2009a. Dependence of swarming in Escherichia coli K-12 on spermidine and the spermidine importer. FEMS Microbiol. Lett. 294, 97–101.

Kurihara, S., Tsuboi, Y., Oda, S., Kim, H.G., Kumagai, H., Suzuki, H., 2009b. The Putrescine Importer PuuP of Escherichia coli K-12. J. Bacteriol. 191, 2776.

Latour, Y.L., Gobert, A.P., Wilson, K.T., 2020. The Role of Polyamines in the Regulation of Macrophage Polarization and Function. Amino Acids 52, 151.

Lawlor, M.S., O'Connor, C., Miller, V.L., 2007. Yersiniabactin is a virulence factor for Klebsiella pneumoniae during pulmonary infection. Infect. Immun. 75, 1463–1472.

Lee, J., Sperandio, V., Frantz, D.E., Longgood, J., Camilli, A., Phillips, M.A., Michael, A.J., 2009. An Alternative Polyamine Biosynthetic Pathway Is Widespread in Bacteria and Essential for Biofilm Formation in Vibrio cholerae. J. Biol. Chem. 284, 9899–9907.

Lee, S.B., Park, J.H., Kaevel, J., Sramkova, M., Weigert, R., Park, M.H., 2009. The effect of hypusine modification on the intracellular localization of eIF5A. Biochem. Biophys. Res. Commun. 383, 497–502.

Lehrer, R.I., Rosenman, M., Harwig, S.S.S.L., Jackson, R., Eisenhauer, P., 1991. Ultrasensitive assays for endogenous antimicrobial polypeptides. J. Immunol. Methods 137, 167–173.

Lerner, T.R., Lovering, A.L., Bui, N.K., Uchida, K., Aizawa, S.I., Vollmer, W., Sockett, R.E., 2012. Specialized Peptidoglycan Hydrolases Sculpt the Intra-bacterial Niche of Predatory Bdellovibrio and Increase Population Fitness. PLoS Pathog. 8, 1002524.

Lery, L.M.S., Frangeul, L., Tomas, A., Passet, V., Almeida, A.S., Bialek-Davenet, S., Barbe, V., Bengoechea, J.A., Sansonetti, P., Brisse, S., Tournebize, R., 2014. Comparative analysis of Klebsiella pneumoniae genomes identifies a phospholipase D family protein as a novel virulence factor. BMC Biol. 12.

Letunic, I., Khedkar, S., Bork, P., 2021. SMART: recent updates, new developments and status in 2020. Nucleic Acids Res. 49, D458–D460.

Levine, M., 2001. Lysine decarboxylase inhibitors for the prevention and treatment of periodontal disease. US 6,187,296 B1.

Li, J., Beuerman, R., Verma, C.S., 2020. Mechanism of polyamine induced colistin resistance through electrostatic networks on bacterial outer membranes. Biochim. Biophys. Acta - Biomembr. 1862, 183297.

Liang, J., Han, Q., Tan, Y., Ding, H., Li, J., 2019. Current advances on structure-function relationships of pyridoxal 5'-phosphate-dependent enzymes. Front. Mol. Biosci. 6, 387990.

Liu, N., Benedik, M.J., Delcour, A.H., 1997. Disruption of polyamine modulation by a single amino acid substitution on the L3 loop of the OmpC porin channel. Biochim. Biophys. Acta - Biomembr. 1326, 201–212.

Liu, Y.C., Cheng, D.L., Lin, C.L., 1986. Klebsiella pneumoniae Liver Abscess Associated With Septic Endophthalmitis. Arch. Intern. Med. 146, 1913–1916.

Llobet, E., March, C., Giménez, P., Bengoechea, J.A., 2009. Klebsiella pneumoniae OmpA Confers Resistance to Antimicrobial Peptides. Antimicrob. Agents Chemother. 53, 298.

Llobet, E., Martínez-Moliner, V., Moranta, D., Dahlström, K.M., Regueiro, V., Tomása, A., Cano, V., Pérez-Gutiérrez, C., Frank, C.G., Fernández-Carrasco, H., Insua, J.L., Salminen, T.A., Garmendia, J., Bengoechea, J.A., 2015. Deciphering tissue-induced Klebsiella pneumoniae lipid a structure. Proc. Natl. Acad. Sci. U. S. A. 112, E6369–E6378.

Llobet, E., Tomás, J.M., Bengoechea, J.A., 2008. Capsule polysaccharide is a bacterial decoy for antimicrobial peptides. Microbiology 154, 3877–3886.

Lob, S.H., Hoban, D.J., Sahm, D.F., Badal, R.E., 2016. Regional differences and trends in antimicrobial susceptibility of Acinetobacter baumannii. Int. J. Antimicrob. Agents 47, 317–323.

Loehfelm, T.W., Luke, N.R., Campagnari, A.A., 2008. Identification and Characterization of an Acinetobacter baumannii Biofilm-Associated Protein. J. Bacteriol. 190, 1036.

LoGiudice, N., Le, L., Abuan, I., Leizorek, Y., Roberts, S., 2018. Alpha-Difluoromethylornithine, an Irreversible Inhibitor of Polyamine Biosynthesis, as a Therapeutic Strategy against Hyperproliferative and Infectious Diseases. Med. Sci. 6, 12.

Lohinai, Z., Keremi, B., Szöko, E., Tábi, T., Szabo, C., Tulassay, Z., DiCesare, J.C., Davis, C.A., Collins, L.M., Levine, M., 2015. Biofilm Lysine Decarboxylase, a New Therapeutic Target for Periodontal Inflammation. J. Periodontol. 86, 1176–1184.

Long, Q., Zhou, W., Zhou, H., Tang, Y., Chen, W., Liu, Q., Bian, X., 2023. Polyamine-containing natural products: structure, bioactivity, and biosynthesis. Nat. Prod. Rep.

López-Martín, M., Dubern, J.F., Alexander, M.R., Williams, P., 2021. AbaM Regulates Quorum Sensing, Biofilm Formation, and Virulence in Acinetobacter baumannii. J. Bacteriol. 203.

Ma, C., McClean, S., 2021. Mapping global prevalence of acinetobacter baumannii and recent vaccine development to tackle it. Vaccines 9.

March, C., Cano, V., Moranta, D., Llobet, E., Pérez-Gutiérrez, C., Tomás, J.M., Suárez, T., Garmendia, J., Bengoechea, J.A., 2013. Role of Bacterial Surface Structures on the Interaction of Klebsiella pneumoniae with Phagocytes. PLoS One 8, e56847.

Martins-Sorenson, N., Snesrud, E., Xavier, D.E., Cacci, L.C., Iavarone, A.T., McGann, P., Riley, L.W., Moreira, B.M., 2020. A novel plasmid-encoded mcr-4.3 gene in a colistin-resistant Acinetobacter baumannii clinical strain. J. Antimicrob. Chemother. 75, 60.

Ménard, G., Rouillon, A., Cattoir, V., Donnio, P.Y., 2021. Galleria mellonella as a Suitable Model of Bacterial Infection: Past, Present and Future. Front. Cell. Infect. Microbiol. 11, 782733.

Mendes, A.C., Novais, Â., Campos, J., Rodrigues, C., Santos, C., Antunes, P., Ramos, H., Peixe, L., 2018. mcr-1 in Carbapenemase-Producing Klebsiella pneumoniae with Hospitalized Patients, Portugal, 2016–2017. Emerg. Infect. Dis. 24, 762.

Merino, S., Camprubi, S., Alberti, S., Benedi, V.J., Tomas, J.M., 1992. Mechanisms of Klebsiella pneumoniae resistance to complement-mediated killing. Infect. Immun. 60, 2529–2535.

Merrell, D.S., Camilli, A., 2000. Regulation of Vibrio cholerae genes required for acid tolerance by a member of the "ToxR-like" family of transcriptional regulators. J. Bacteriol. 182, 5342–5350.

Michael, A.J., 2016. Biosynthesis of polyamines and polyamine-containing molecules. Biochem. J.

Miller, jeffrey H., 1972. Experiments in molecular genetics. Cold Spring Harbor Laboratory, New York.

Millward, M.J., Joshua, A., Kefford, R., Aamdal, S., Thomson, D., Hersey, P., Toner, G., Lynch, K., 2005. Multi-centre Phase II trial of the polyamine synthesis inhibitor SAM486A (CGP48664) in patients with metastatic melanoma. Invest. New Drugs 23, 253–256.

Minton, K.W., Tabor, H., Tabor, C.W., 1990. Paraquat toxicity is increased in Escherichia coli defective in the synthesis of polyamines. Proc. Natl. Acad. Sci. U. S. A. 87, 2851.

Mirdita, M., Schütze, K., Moriwaki, Y., Heo, L., Ovchinnikov, S., Steinegger, M., 2022. ColabFold: making protein folding accessible to all. Nat. Methods 2022 196 19, 679–682.

Miyamoto, S., Kashiwagi, K., Ito, K., Watanabe, S.I., Igarashi, K., 1993. Estimation of polyamine distribution and polyamine stimulation of protein synthesis in Escherichia coli. Arch. Biochem. Biophys. 300, 63–68.

Morris, B., 2017. Investigating the role of polyamines in Klebsiella pneumoniae. MRes Thesis. Queens University Belfast.

Morris, D.R., Pardee, A.B., 1966. Multiple pathways of putrescine biosynthesis in Escherichia coli. J. Biol. Chem. 241, 3129–3135.

Moubareck, C.A., Halat, D.H., 2020. Insights into Acinetobacter baumannii: A Review of Microbiological, Virulence, and Resistance Traits in a Threatening

Nosocomial Pathogen. Antibiotics 9.

Mühlig, A., Behr, J., Scherer, S., Müller-Herbst, S., 2014. Stress Response of Salmonella enterica Serovar Typhimurium to Acidified Nitrite. Appl. Environ. Microbiol. 80, 6373.

Murphy, C.N., Mortensen, M.S., Krogfelt, K.A., Clegg, S., 2013. Role of Klebsiella pneumoniae Type 1 and Type 3 Fimbriae in Colonizing Silicone Tubes Implanted into the Bladders of Mice as a Model of Catheter-Associated Urinary Tract Infections. Infect. Immun. 81, 3009.

Mussi, M.A., Gaddy, J.A., Cabruja, M., Arivett, B.A., Viale, A.M., Rasia, R., Actis, L.A., 2010. The Opportunistic Human Pathogen Acinetobacter baumannii Senses and Responds to Light. J. Bacteriol. 192, 6336.

Nagy, E., Losick, R., Kahnea, D., 2019. Robust Suppression of Lipopolysaccharide Deficiency in Acinetobacter baumannii by Growth in Minimal Medium. J. Bacteriol. 201.

Nakada, Y., Itoh, Y., 2003. Identification of the putrescine biosynthetic genes in Pseudomonas aeruginosa and characterization of agmatine deiminase and N-carbamoylputrescine amidohydrolase of the arginine decarboxylase pathway. Microbiology 149, 707–714.

Nakamya, M.F., Ayoola, M.B., Shack, L.A., Mohamed, M., Swiatlo, E., Nanduri, B., 2021a. Arginine Decarboxylase Is Essential for Pneumococcal Stress Responses. Pathogens 10, 1–13.

Nakamya, M.F., Ayoola, M.B., Shack, L.A., Swiatlo, E., Nanduri, B., 2021b. The effect of impaired polyamine transport on pneumococcal transcriptome. Pathogens 10.

Needleman, S.B., Wunsch, C.D., 1970. A general method applicable to the search for similarities in the amino acid sequence of two proteins. J. Mol. Biol. 48, 443–453.

Neely, M.N., Olson, E.R., 1996. Kinetics of expression of the Escherichia coli cad operon as a function of pH and lysine. J. Bacteriol. 178, 5522.

Nishimura, K., Lee, S.B., Park, J.H., Park, M.H., 2012. Essential role of eIF5A-1 and deoxyhypusine synthase in mouse embryonic development. Amino Acids 42, 703.

Novović, K., Jovčić, B., 2023. Colistin Resistance in Acinetobacter baumannii: Molecular Mechanisms and Epidemiology. Antibiotics 12.

Özgür, E.S., Horasan, E.S., Karaca, K., Ersöz, G., Nayci Atiş, S., Kaya, A., 2014. Ventilator-associated pneumonia due to extensive drug-resistant Acinetobacter baumannii: Risk factors, clinical features, and outcomes. Am. J. Infect. Control 42, 206–208.

Paczosa, M.K., Mecsas, J., 2016. Klebsiella pneumoniae: Going on the Offense with a Strong Defense. Microbiol. Mol. Biol. Rev. 80, 629.

Paridaens, R., Uges, D.R.A., Barbet, N., Choi, L., Seeghers, M., Van Der Graaf, W.T.A., Groen, H.J.M., Dumez, H., Van Buuren, I., Muskiet, F., Capdeville, R., Van Oosterom, A.T., De Vries, E.G.E., 2000. A phase I study of a new polyamine

biosynthesis inhibitor, SAM486A, in cancer patients with solid tumours. Br. J. Cancer 83, 594.

Park, M.H., Kar, R.K., Banka, S., Ziegler, A., Chung, W.K., 2022. Post-translational formation of hypusine in eIF5A: implications in human neurodevelopment. Amino Acids 54, 485–499.

Park, Y.K., Bearson, B., Bang, S.H., Bang, I.S., Foster, J.W., 1996. Internal pH crisis, lysine decarboxylase and the acid tolerance response of Salmonella typhimurium. Mol. Microbiol. 20, 605–611.

Patel, C.N., Wortham, B.W., Lines, J.L., Fetherston, J.D., Perry, R.D., Oliveira, M.A., 2006. Polyamines are essential for the formation of plague biofilm. J. Bacteriol. 188, 2355–2363.

Pathak, S.N., Porter, C.W., Dave, C., 1977. Morphological Evidence for an Antimitochondrial Action by Methylglyoxal-bis(guanylhydrazone)1. Cancer Res. 37, 2246–2250.

Patiño-Ruiz, M., Ganea, C., Călinescu, O., 2022. Prokaryotic Na+/H+ Exchangers—Transport Mechanism and Essential Residues. Int. J. Mol. Sci. 2022, Vol. 23, Page 9156 23, 9156.

Paysan-Lafosse, T., Blum, M., Chuguransky, S., Grego, T., Pinto, B.L., Salazar, G.A., Bileschi, M.L., Bork, P., Bridge, A., Colwell, L., Gough, J., Haft, D.H., Letunić, I., Marchler-Bauer, A., Mi, H., Natale, D.A., Orengo, C.A., Pandurangan, A.P., Rivoire, C., Sigrist, C.J.A., Sillitoe, I., Thanki, N., Thomas, P.D., Tosatto, S.C.E., Wu, C.H., Bateman, A., 2023. InterPro in 2022. Nucleic Acids Res. 51, D418–D427.

Pegg, A.E., 2016. Functions of Polyamines in Mammals. J. Biol. Chem. 291, 14904.

Pegg, A.E., Lockwood, D.H., Williams-Ashman, H.G., 1970. Concentrations of putrescine and polyamines and their enzymic synthesis during androgen-induced prostatic growth. Biochem. J. 117, 17.

Pelechano, V., Alepuz, P., 2017. eIF5A facilitates translation termination globally and promotes the elongation of many non polyproline-specific tripeptide sequences. Nucleic Acids Res. 45, 7326.

Penwell, W.F., Degrace, N., Tentarelli, S., Gauthier, L., Gilbert, C.M., Arivett, B.A., Miller, A.A., Durand-Reville, T.F., Joubran, C., Actis, L.A., 2015. Discovery and Characterization of New Hydroxamate Siderophores, Baumannoferrin A and B, produced by Acinetobacter baumannii. ChemBioChem 16, 1896–1904.

Perchat, N., Dubois, C., Mor-Gautier, R., Duquesne, S., Lechaplais, C., Roche, D., Fouteau, S., Darii, E., Perret, A., 2022. Characterization of a novel β-alanine biosynthetic pathway consisting of promiscuous metabolic enzymes. J. Biol. Chem. 298.

Perez Mora, B., Giordano, R., Permingeat, V., Calderone, M., Arana, N., Müller, G., Rodríguez, R.E., Krasauskas, R., Mussi, M.A., 2023. BfmRS encodes a regulatory system involved in light signal transduction modulating motility and desiccation tolerance in the human pathogen Acinetobacter baumannii. Sci. Reports 2023 131 13, 1–13.

Pistocchi, R., Kashiwagi, K., Miyamoto, S., Nukui, E., Sadakata, Y., Kobayashi, H.,

Igarashit, K., 1993. Characteristics of the Operon for a Putrescine Transport System That Maps at 19 Minutes on the Escherichia coli Chromosome*. J. Biol. Chem. 268, 146–152.

Pomakova, D.K., Hsiao, C.B., Beanan, J.M., Olson, R., MacDonald, U., Keynan, Y., Russo, T.A., 2012. Clinical and phenotypic differences between classic and hypervirulent Klebsiella pneumonia: An emerging and under-recognized pathogenic variant. Eur. J. Clin. Microbiol. Infect. Dis. 31, 981–989.

Pormohammad, A., Mehdinejadiani, K., Gholizadeh, P., Mohtavinejad, N., Dadashi, M., Karimaei, S., Safari, H., Azimi, T., 2020. Global prevalence of colistin resistance in clinical isolates of Acinetobacter baumannii: A systematic review and meta-analysis. Microb. Pathog. 139, 103887.

Poulin, R., Lu, L., Ackermann, B., Bey, P., Pegg, A.E., 1992. Mechanism of the irreversible inactivation of mouse ornithine decarboxylase by alpha-difluoromethylornithine. Characterization of sequences at the inhibitor and coenzyme binding sites. J. Biol. Chem. 267, 150–158.

Prlić, A., Bliven, S., Rose, P.W., Bluhm, W.F., Bizon, C., Godzik, A., Bourne, P.E., 2010. Pre-calculated protein structure alignments at the RCSB PDB website. Bioinformatics 26, 2983–2985.

Radi, R., 2013. Peroxynitrite, a Stealthy Biological Oxidant. J. Biol. Chem. 288, 26464.

Rafei, R., Dabboussi, F., Hamze, M., Eveillard, M., Lemarié, C., Mallat, H., Rolain, J.M., Joly-Guillou, M.L., Kempf, M., 2014. First report of blaNDM-1-producing Acinetobacter baumannii isolated in Lebanon from civilians wounded during the Syrian war. Int. J. Infect. Dis. 21, 21–23.

Raghunathan, N., 2023. High level expression and purification of recombinant kpDAT protein from E. coli for structure elucidation. M. Sc. Thesis. The University of Nottingham.

Rauschmeier, M., Schüppel, V., Tetsch, L., Jung, K., 2014. New Insights into the Interplay Between the Lysine Transporter LysP and the pH Sensor CadC in Escherichia Coli. J. Mol. Biol. 426, 215–229.

Regenass, U., Helmut, M., Stanek, J., Mueller, M., Kramer, D., Porter, C.W., 1994. CGP 48664, a new S-adenosylmethionine decarboxylase inhibitor with broad spectrum antiproliferative and antitumor activity. Cancer Res. 54.

Repizo, G.D., Gagné, S., Foucault-Grunenwald, M.L., Borges, V., Charpentier, X., Limansky, A.S., Gomes, J.P., Viale, A.M., Salcedo, S.P., 2015. Differential Role of the T6SS in Acinetobacter baumannii Virulence. PLoS One 10.

Ribeiro, C.A., Rahman, L.A., Holmes, L.G., Woody, A.M., Webster, C.M., Monaghan, T.I., Robinson, G.K., Mühlschlegel, F.A., Goodhead, I.B., Shepherd, M., 2021. Nitric oxide (NO) elicits aminoglycoside tolerance in Escherichia coli but antibiotic resistance gene carriage and NO sensitivity have not co-evolved. Arch. Microbiol. 203, 2541.

Rice, L.B., 2008. Federal Funding for the Study of Antimicrobial Resistance in Nosocomial Pathogens: No ESKAPE. J. Infect. Dis. 197, 1079–1081.

Robert, X., Gouet, P., 2014. Deciphering key features in protein structures with the new ENDscript server. Nucleic Acids Res. 42, W320–W324.

Rumbo, C., Tomás, M., Moreira, E.F., Soares, N.C., Carvajal, M., Santillana, E., Beceiro, A., Romero, A., Bou, G., 2014. The Acinetobacter baumannii Omp33-36 Porin Is a Virulence Factor That Induces Apoptosis and Modulates Autophagy in Human Cells. Infect. Immun. 82, 4666.

Russell, D., Snyder, S.H., 1968. Amine synthesis in rapidly growing tissues: ornithine decarboxylase activity in regenerating rat liver, chick embryo, and various tumors. Proc. Natl. Acad. Sci. U. S. A. 60, 1420.

Russo, T.A., Luke, N.R., Beanan, J.M., Olson, R., Sauberan, S.L., MacDonald, U., Schultz, L.W., Umland, T.C., Campagnari, A.A., 2010. The K1 capsular polysaccharide of Acinetobacter baumannii strain 307-0294 is a major virulence factor. Infect. Immun. 78, 3993–4000.

Russo, T.A., Marr, C.M., 2019. Hypervirulent Klebsiella pneumoniae. Clin. Microbiol. Rev. 32.

Russo, T.A., Olson, R., Fang, C.T., Stoesser, N., Miller, M., MacDonald, U., Hutson, A., Barker, J.H., La Hoz, R.M., Johnson, J.R., Backer, M., Bajwa, R., Catanzaro, A.T., Crook, D., De Almeida, K., Fierer, J., Greenberg, D.E., Klevay, M., Patel, P., Ratner, A., Wang, J.T., Zola, J., 2018. Identification of Biomarkers for Differentiation of Hypervirulent Klebsiella pneumoniae from Classical K. pneumoniae. J. Clin. Microbiol. 56, 776–794.

Russo, T.A., Olson, R., MacDonald, U., Beanan, J., Davidsona, B.A., 2015. Aerobactin, but not yersiniabactin, salmochelin, or enterobactin, enables the growth/survival of hypervirulent (hypermucoviscous) Klebsiella pneumoniae ex vivo and in vivo. Infect. Immun. 83, 3325–3333.

Russo, T.A., Olson, R., MacDonald, U., Metzger, D., Maltese, L.M., Drake, E.J., Gulick, A.M., 2014. Aerobactin Mediates Virulence and Accounts for Increased Siderophore Production under Iron-Limiting Conditions by Hypervirulent (Hypermucoviscous) Klebsiella pneumoniae. Infect. Immun. 82, 2356.

Sakamoto, A., Terui, Y., Yamamoto, T., Kasahara, T., Nakamura, M., Tomitori, H., Yamamoto, K., Ishihama, A., Michael, A.J., Igarashi, K., Kashiwagi, K., 2012. Enhanced biofilm formation and/or cell viability by polyamines through stimulation of response regulators UvrY and CpxR in the two-component signal transducing systems, and ribosome recycling factor. Int. J. Biochem. Cell Biol. 44, 1877–1886.

Sakamoto, A., Terui, Y., Yoshida, T., Yamamoto, T., Suzuki, H., Yamamoto, K., Ishihama, A., Igarashi, K., Kashiwagi, K., 2015. Three Members of Polyamine Modulon under Oxidative Stress Conditions: Two Transcription Factors (SoxR and EmrR) and a Glutathione Synthetic Enzyme (GshA). PLoS One 10.

Sarathy, J.P., Lee, E., Dartois, V., 2013. Polyamines Inhibit Porin-Mediated Fluoroquinolone Uptake in Mycobacteria. PLoS One 8, e65806.

Sato, K., Akiyama, M., Sakakibara, Y., 2021. RNA secondary structure prediction using deep learning with thermodynamic integration. Nat. Commun. 2021 121 12, 1–9.

Schlundt, A., Buchner, S., Janowski, R., Heydenreich, T., Heermann, R., Lassak, J., Geerlof, A., Stehle, R., Niessing, D., Jung, K., Sattler, M., 2017. Structure-function analysis of the DNA-binding domain of a transmembrane

transcriptional activator. Sci. Rep. 7.

Schneider, B.L., Reitzer, L., 2012. Pathway and Enzyme Redundancy in Putrescine Catabolism in Escherichia coli. J. Bacteriol. 194, 4080.

Schuller, A.P., Wu, C.C.C., Dever, T.E., Buskirk, A.R., Green, R., 2017. eIF5A Functions Globally in Translation Elongation and Termination. Mol. Cell 66, 194.

Scott, P., Deye, G., Srinivasan, A., Murray, C., Moran, K., Hulten, E., Fishbain, J., Craft, D., Riddell, S., Lindler, L., Mancuso, J., Milstrey, E., Bautista, C.T., Patel, J., Ewell, A., Hamilton, T., Gaddy, C., Tenney, M., Christopher, G., Petersen, K., Endy, T., Petruccelli, B., 2007. An outbreak of multidrug-resistant Acinetobacter baumannii-calcoaceticus complex infection in the US military health care system associated with military operations in Iraq. Clin. Infect. Dis. 44, 1577–1584.

Semenec, L., Cain, A.K., Dawson, C.J., Liu, Q., Dinh, H., Lott, H., Penesyan, A., Maharjan, R., Short, F.L., Hassan, K.A., Paulsen, I.T., 2023. Cross-protection and cross-feeding between Klebsiella pneumoniae and Acinetobacter baumannii promotes their co-existence. Nat. Commun. 2023 141 14, 1–18.

Sheldon, J.R., Skaar, E.P., 2020. Acinetobacter baumannii can use multiple siderophores for iron acquisition, but only acinetobactin is required for virulence. PLoS Pathog. 16, e1008995.

Shiba, T., Mizote, H., Kaneko, T., Nakajima, T., Yasuo, K., sano, I., 1971. Hypusine, a new amino acid occurring in bovine brain: Isolation and structural determination. Biochim. Biophys. Acta - Gen. Subj. 244, 523–531.

Short, F.L., Liu, Q., Shah, B., Clift, H.E., Naidu, V., Li, L., Prity, F.T., Mabbutt, B.C., Hassan, K.A., Paulsen, I.T., 2021. The Acinetobacter baumannii disinfectant resistance protein, AmvA, is a spermidine and spermine efflux pump. Commun. Biol. 4.

Sievers, F., Wilm, A., Dineen, D., Gibson, T.J., Karplus, K., Li, W., Lopez, R., McWilliam, H., Remmert, M., Söding, J., Thompson, J.D., Higgins, D.G., 2011. Fast, scalable generation of high-quality protein multiple sequence alignments using Clustal Omega. Mol. Syst. Biol. 7, 539.

Skiebe, E., de Berardinis, V., Morczinek, P., Kerrinnes, T., Faber, F., Lepka, D., Hammer, B., Zimmermann, O., Ziesing, S., Wichelhaus, T.A., Hunfeld, K.P., Borgmann, S., Gröbner, S., Higgins, P.G., Seifert, H., Busse, H.J., Witte, W., Pfeifer, Y., Wilharm, G., 2012. Surface-associated motility, a common trait of clinical isolates of Acinetobacter baumannii, depends on 1,3-diaminopropane. Int. J. Med. Microbiol. 302, 117–128.

Smani, Y., Dominguez-Herrera, J., Pachón, J., 2013. Association of the Outer Membrane Protein Omp33 With Fitness and Virulence of Acinetobacter baumannii. J. Infect. Dis. 208, 1561–1570.

Smith, M.G., Gianoulis, T.A., Pukatzki, S., Mekalanos, J.J., Ornston, L.N., Gerstein, M., Snyder, M., 2007. New insights into Acinetobacter baumannii pathogenesis revealed by high-density pyrosequencing and transposon mutagenesis. Genes Dev. 21, 601.

Soksawatmaekhin, W., Uemura, T., Fukiwake, N., Kashiwagi, K., Igarashi, K., 2006.

Identification of the cadaverine recognition site on the cadaverine-lysine antiporter CadB. J. Biol. Chem. 281, 29213–29220.

Solovyev, V., Salamov, A., 2011. Automatic Annotation of Microbial Genomes and Metagenomic Sequences. In: Li, R.W. (Ed.), Metagenomics and Its Applications in Agriculture, Biomedicine and Environmental Studies. Nova Science Publishers, pp. 61–78.

Spellberg, B., Rex, J.H., 2013. The value of single-pathogen antibacterial agents. Nat. Rev. Drug Discov.

Srinivasan, V.B., Venkataramaiah, M., Mondal, A., Vaidyanathan, V., Govil, T., Rajamohan, G., 2012. Functional Characterization of a Novel Outer Membrane Porin KpnO, Regulated by PhoBR Two-Component System in Klebsiella pneumoniae NTUH-K2044. PLoS One 7.

Stahl, J., Bergmann, H., Göttig, S., Ebersberger, I., Averhoff, B., 2015. Acinetobacter baumannii Virulence Is Mediated by the Concerted Action of Three Phospholipases D. PLoS One 10.

Stanek, J., Caravatti, G., Frei, J., Furet, P., Mett, H., Schneider, P., Regenass, U., 1993. 4-Amidinoindan-1-one 2'-Amidinohydrazone: A New Potent and Selective Inhibitor of S-Adenosylmethionine Decarboxylase. J. Med. Chem 36, 2168–2171.

Struve, C., Bojer, M., Krogfelt, K.A., 2008. Characterization of Klebsiella pneumoniae type 1 fimbriae by detection of phase variation during colonization and infection and impact on virulence. Infect. Immun. 76, 4055–4065.

Struve, C., Bojer, M., Krogfelt, K.A., 2009. Identification of a conserved chromosomal region encoding Klebsiella pneumoniae type 1 and type 3 fimbriae and assessment of the role of fimbriae in pathogenicity. Infect. Immun. 77, 5016–5024.

Sturgill, G., Rather, P.N., 2004. Evidence that putrescine acts as an extracellular signal required for swarming in Proteus mirabilis. Mol. Microbiol. 51, 437–446.

Svensson, L., Poljakovic, M., Demirel, I., Sahlberg, C., Persson, K., 2018. Host-Derived Nitric Oxide and Its Antibacterial Effects in the Urinary Tract. Adv. Microb. Physiol. 73, 1–62.

Swigoňová, Z., Mohsen, A.W., Vockley, J., 2009. Acyl-CoA Dehydrogenases: Dynamic History of Protein Family Evolution. J. Mol. Evol. 69, 176.

Tacconelli, E., Carrara, E., Savoldi, A., Harbarth, S., Mendelson, M., Monnet, D.L., Pulcini, C., Kahlmeter, G., Kluytmans, J., Carmeli, Y., Ouellette, M., Outterson, K., Patel, J., Cavaleri, M., Cox, E.M., Houchens, C.R., Grayson, M.L., Hansen, P., Singh, N., ...Zorzet, A., 2018. Discovery, research, and development of new antibiotics: the WHO priority list of antibiotic-resistant bacteria and tuberculosis. Lancet Infect. Dis. 18, 318–327.

Tarkkanen, A.M., Virkola, R., Clegg, S., Korhonen, T.K., 1997. Binding of the type 3 fimbriae of Klebsiella pneumoniae to human endothelial and urinary bladder cells. Infect. Immun. 65, 1546–1549.

Terui, Y., Higashi, K., Tabei, Y., Tomitori, H., Yamamoto, K., Ishihama, A., Igarashi, K., Kashiwagi, K., 2009. Enhancement of the Synthesis of RpoE and StpA by

Polyamines at the Level of Translation in Escherichia coli under Heat Shock Conditions. J. Bacteriol. 191, 5348.

Terui, Y., Higashi, K., Taniguchi, S., Shigemasa, A., Nishimura, K., Yamamoto, K., Kashiwagi, K., Ishihama, A., Igarashi, K., 2007. Enhancement of the Synthesis of RpoN, Cra, and H-NS by Polyamines at the Level of Translation in Escherichia coli Cultured with Glucose and Glutamate. J. Bacteriol. 189, 2359.

Terui, Y., Saroj, S.D., Sakamoto, A., Yoshida, T., Higashi, K., Kurihara, S., Suzuki, H., Toida, T., Kashiwagi, K., Igarashi, K., 2014. Properties of putrescine uptake by PotFGHI and PuuP and their physiological significance in Escherichia coli. Amino Acids 46, 661–670.

Tetsch, L., Koller, C., Dönhöfer, A., Jung, K., 2011. Detection and function of an intramolecular disulfide bond in the pH-responsive CadC of Escherichia coli. BMC Microbiol. 11, 74.

Tetsch, L., Koller, C., Haneburger, I., Jung, K., 2008. The membrane-integrated transcriptional activator CadC of Escherichia coli senses lysine indirectly via the interaction with the lysine permease LysP. Mol. Microbiol. 67, 570–583.

The European Committee on Antimicrobial Susceptibility Testing, 2024. EUCAST Disk Diffusion Test Manual v12.0.

Thongbhubate, K., Nakafuji, Y., Matsuoka, R., Kakegawa, S., Suzuki, H., 2021. Effect of Spermidine on Biofilm Formation in Escherichia coli K-12. J. Bacteriol. 203.

Thurlow, L.R., Joshi, G.S., Clark, J.R., Spontak, J.S., Neely, C.J., Maile, R., Richardson, A.R., 2013. Functional Modularity of the Arginine Catabolic Mobile Element Contributes to the Success of USA300 Methicillin-Resistant Staphylococcus aureus. Cell Host Microbe 13, 100–107.

Tipton, K.A., Chin, C.Y., Farokhyfar, M., Weiss, D.S., Rathera, P.N., 2018. Role of Capsule in Resistance to Disinfectants, Host Antimicrobials, and Desiccation in Acinetobacter baumannii. Antimicrob. Agents Chemother. 62.

Tkachenko, A.G., Akhova, A. V., Shumkov, M.S., Nesterova, L.Y., 2012. Polyamines reduce oxidative stress in Escherichia coli cells exposed to bactericidal antibiotics. Res. Microbiol. 163, 83–91.

Tomaras, A.P., Dorsey, C.W., Edelmann, R.E., Actis, L.A., 2003. Attachment to and biofilm formation on abiotic surfaces by Acinetobacter baumannii: Involvement of a novel chaperone-usher pili assembly system. Microbiology 149, 3473–3484.

Tuon, F.F., Penteado-Filho, S.R., Amarante, D., Andrade, M.A., Borba, L.A., 2010. Mortality rate in patients with nosocomial Acinetobacter meningitis from a Brazilian hospital. Brazilian J. Infect. Dis. 14, 437–440.

Tuttobene, M.R., Müller, G.L., Blasco, L., Arana, N., Hourcade, M., Diacovich, L., Cribb, P., Tomás, M., Nieto-Peñalver, C.G., Mussi, M.A., 2021. Blue light directly modulates the quorum network in the human pathogen Acinetobacter baumannii. Sci. Rep. 11, 13375.

Uzairue, L.I., Rabaan, A.A., Adewumi, F.A., Okolie, O.J., Folorunso, J.B., Bakhrebah, M.A., Garout, M., Alfouzan, W.A., Halwani, M.A., Alamri, A.A., Halawani, S.A., Alshahrani, F.S., Hasan, A., Mutair, A. Al, Alhumaid, S., Etafo, J., Utip, I., Odoh,

I.M., Uwaezuoke, N.S., 2022. Global Prevalence of Colistin Resistance in Klebsiella pneumoniae from Bloodstream Infection: A Systematic Review and Meta-Analysis. Pathogens 11.

Van Den Ent, F., Löwe, J., 2006. RF cloning: a restriction-free method for inserting target genes into plasmids. J. Biochem. Biophys. Methods 67, 67–74.

Varadi, M., Anyango, S., Deshpande, M., Nair, S., Natassia, C., Yordanova, G., Yuan, D., Stroe, O., Wood, G., Laydon, A., Zídek, A., Green, T., Tunyasuvunakool, K., Petersen, S., Jumper, J., Clancy, E., Green, R., Vora, A., Lutfi, M., Figurnov, M., Cowie, A., ...Velankar, S., 2022. AlphaFold Protein Structure Database: massively expanding the structural coverage of protein-sequence space with high-accuracy models. Nucleic Acids Res. 50, D439–D444.

Vlahoviček, K., Kaján, L., Pongor, S., 2003. DNA analysis servers: plot.it, bend.it, model.it and IS. Nucleic Acids Res. 31, 3686.

Wallace, H.M., Fraser, A. V., 2004. Inhibitors of polyamine metabolism: Review article. Amin. Acids 2004 264 26, 353–365.

Weber, B.S., Miyata, S.T., Iwashkiw, J.A., Mortensen, B.L., Skaar, E.P., Pukatzki, S., Feldman, M.F., 2013. Genomic and Functional Analysis of the Type VI Secretion System in Acinetobacter. PLoS One 8, 55142.

Webster, C.M., Woody, A.M., Fusseini, S., Holmes, L.G., Robinson, G.K., Shepherd, M., 2022. Proton motive force underpins respiration-mediated potentiation of aminoglycoside lethality in pathogenic Escherichia coli. Arch. Microbiol. 204, 120.

Wijers, C.D.M., Pham, L., Menon, S., Boyd, K.L., Noel, H.R., Skaar, E., Gaddy, J.A., Palmer, L.D., Noto, M.J., 2021. Identification of two variants of *Acinetobacter baumannii* 17978 with distinct genotypes and phenotypes. Infect. Immun.

Willsey, G.G., Ventrone, S., Schutz, K.C., Wallace, A.M., Ribis, J.W., Suratt, B.T., Wargo, M.J., 2018. Pulmonary surfactant promotes virulence gene expression and biofilm formation in Klebsiella pneumoniae. Infect. Immun. 86.

Wisplinghoff, H., Paulus, T., Lugenheim, M., Stefanik, D., Higgins, P.G., Edmond, M.B., Wenzel, R.P., Seifert, H., 2012. Nosocomial bloodstream infections due to Acinetobacter baumannii, Acinetobacter pittii and Acinetobacter nosocomialis in the United States. J. Infect. 64, 282–290.

Wortham, B.W., Oliveira, M.A., Fetherston, J.D., Perry, R.D., 2010. Polyamines are Required for the Expression of Key Hms proteins Important for Yersinia pestis Biofilm Formation. Environ. Microbiol. 12, 2034.

Wu, H., Min, J., Ikeguchi, Y., Zeng, H., Dong, A., Loppnau, P., Pegg, A.E., Plotnikov, A.N., 2007. Structure and mechanism of spermidine synthases. Biochemistry 46, 8331–8339.

Xie, Y., Kang, M., Tao, C., Guo, L., Ye, Y., Fan, H., 2010. Molecular Epidemiology of an Outbreak of Multidrug-Resistant Acinetobacter baumannii in an Intensive Care Unit of Victims of the Wenchuan Earthquake. Lab. Med. 41, 292–295.

Yamamoto, S., Suemoto, Y., Seito, Y., Nakao, H., Shinoda, S., 1986. The presence of l-2,4-diaminobutyric acid decarboxylase activity in Vibrio species: A new biosynthetic pathway for 1,3-diaminopropane. FEMS Microbiol. Lett. 35, 289–

293.

Yamamoto, S., Tsuzaki, Y., Tougou, K., Shinoda, S., 1992. Purification and characterization of L-2,4-diaminobutyrate decarboxylase from Acinetobacter calcoaceticus. J. Gen. Microbiol. 138, 1461–1465.

Yamashita, T., Nishimura, K., Saiki, R., Okudaira, H., Tome, M., Higashi, K., Nakamura, M., Terui, Y., Fujiwara, K., Kashiwagi, K., Igarashi, K., 2013. Role of polyamines at the G1/S boundary and G2/M phase of the cell cycle. Int. J. Biochem. Cell Biol. 45, 1042–1050.

Yang, J., Wencewicz, T.A., 2022. In Vitro Reconstitution of Fimsbactin Biosynthesis from Acinetobacter baumannii. ACS Chem. Biol. 17, 2923–2935.

Ying, Z., 2023. Expression of Virulence-Associated Protein from Acinetobacter baumannii in Escherichia coli for Crystallographic Analysis: Methods and Challenges. . M. Sc. Thesis. The University of Nottingham.

Yoshida, M., Kashiwagi, K., Kawai, G., Ishihama, A., Igarashi, K., 2002. Polyamines enhance synthesis of the RNA polymerase σ38 subunit by suppression of an amber termination codon in the open reading frame. J. Biol. Chem. 277, 37139–37146.

Yoshida, M., Kashiwagi, K., Shigemasa, A., Taniguchi, S., Yamamoto, K., Makinoshima, H., Ishihama, A., Igarashi, K., 2004. A unifying model for the role of polyamines in bacterial cell growth, the polyamine modulon. J. Biol. Chem. 279, 46008–46013.

Yoshida, T., Sakamoto, A., Terui, Y., Takao, K., Sugita, Y., Yamamoto, K., Ishihama, A., Igarashi, K., Kashiwagi, K., 2016. Effect of Spermidine Analogues on Cell Growth of Escherichia coli Polyamine Requiring Mutant MA261. PLoS One 11, 159494.

Zhou, K., Xiao, T., David, S., Wang, Q., Zhou, Y., Guo, L., Aanensen, D., Holt, K.E., Thomson, N.R., Grundmann, H., Shen, P., Xiao, Y., 2020. Novel Subclone of Carbapenem-Resistant Klebsiella pneumoniae Sequence Type 11 with Enhanced Virulence and Transmissibility, China. Emerg. Infect. Dis. 26, 289.

Chapter 9 Appendix

Table 9.1. Growth rates and doubling times for *A. baumannii* 17978 wild type and Δ*ddc* strains

Strain	Average growth rate per hour	Average doubling time (Hours)
Growth rates and doubling times for *A. baumannii* and Δ*ddc* growth analysis		
WT	0.852 ± 0.015	0.814 ± 0.017
Δ*ddc*	0.626 ± 0.015	1.109 ± 0.031
Growth rates and doubling times 1, 3-diaminopropane complementation		
WT	1.279 ± 0.139	0.549 ± 0.064
WT+ dap	0.857 ± 0.009	0.809 ± 0.008
Δ*ddc*	0.646 ± 0.012	1.074 ± 0.020
Δ*ddc* + dap	1.060 ± 0.013	0.654 ± 0.008
Growth rates and doubling times for putrescine and cadaverine complementation		
WT	1.090 ± 0.004	0.636 ± 0.002
WT + put	0.842 ± 0.024	0.824 ± 0.024
WT + cad	0.854 ± 0.026	0.812 ± 0.025
Δ*ddc*	0.635 ± 0.022	1.093 ± 0.039
Δ*ddc* + put	0.662 ± 0.018	1.047 ± 0.028
Δ*ddc* + cad	0.638 ± 0.015	1.088 ± 0.026
Growth rates and doubling for triamine complementation		
WT	1.076 ± 0.015	0.644 ± 0.009
WT + spd	1.077 ± 0.011	0.644 ± 0.006
WT + spm	1.070 ± 0.28	0.648 ± 0.017
Δ*ddc*	0.643 ± 0.025	1.080 ± 0.042
Δ*ddc* + spd	0.649 ± 0.018	1.069 ± 0.031
Δ*ddc* + spm	0.652 ± 0.028	1.066 ± 0.047

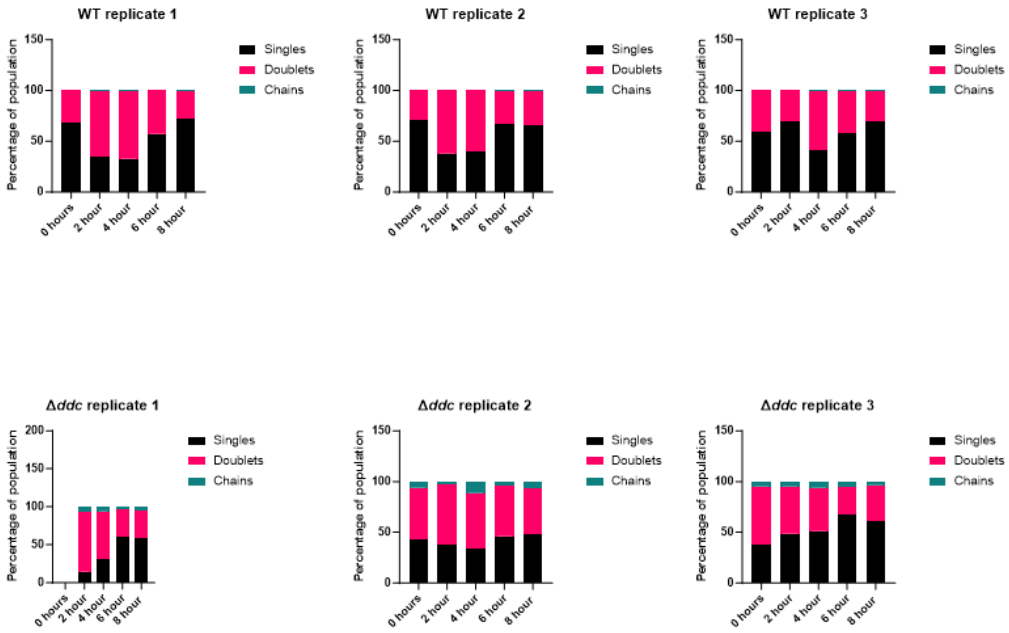

Figure 9.1. The Δ*ddc* strain has a septation defect and forms chains in planktonic culture. Comparison of the cells present within wild type planktonic culture (Top) and a Δ*ddc* planktonic culture (Bottom) grown for 8 hours. Cultures were observed by phase contrast microscopy every 2 hours. Imaged cells were counted at every timepoint (N=>500) and reported as a percentage of a whole. The data presented is the counts for each biological replicate.

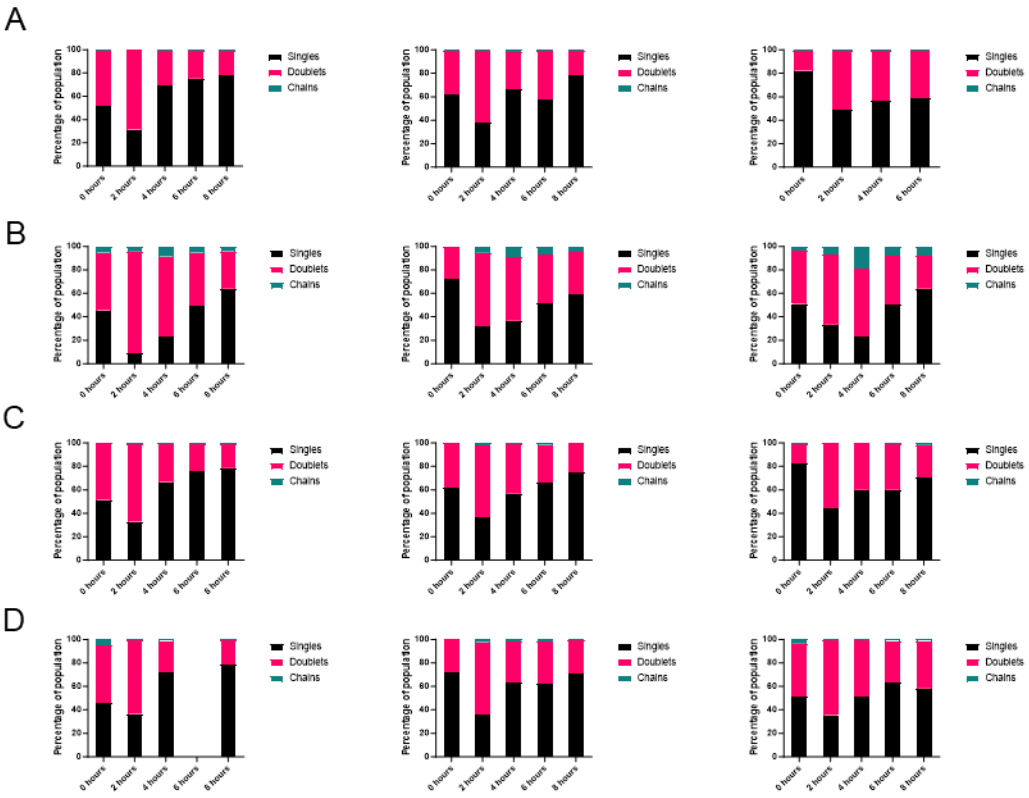

Figure 9.2. 1, 3-diaminopropane complements the septation defect of the Δ*ddc* strain. Comparison of the cells present within **(A)** wild type and **(B)** Δ*ddc* planktonic cultures and **(C)** wild type and **(D)** Δ*ddc* cultures supplemented with 125 µM 1, 3-diaminopropane grown for 8 hours. Cultures were observed by phase contrast microscopy every 2 hours. Imaged cells were counted at every timepoint (N=>500) and reported as a percentage of a whole. The data presented is the counts for each biological replicate.

Table 9.2. Growth rate and doubling times for *K. pneumoniae* 52145 wild type, Δ*dat* and Δ*ddc* strains

Strain	**Average growth rate per hour**	**Average doubling time (Hours)**
pH 7.5		
Wild type	0.581 ± 0.020	1.195 ± 0.042
Δ*dat*	0.590 ± 0.007	1.175 ± 0.014
Δ*ddc*	0.581 ± 0.004	1.194 ± 0.009
pH 5.5		
Strain	Average growth rate per hour	Average doubling time (Hours)
Wild type	0.611 ± 0.014	1.134 ± 0.026
Δ*dat*	0.612 ± 0.009	1.134 ± 0.016
Δ*ddc*	0.586 ± 0.008	1.183 ± 0.017
pH 4		
Strain	Average growth rate per hour	Average doubling time (Hours)

Wild type	0.298 ± 0.075	2.492 ± 0.667
Δ*dat*	0.300 ± 0.081	2.504 ± 0.712
Δ*ddc*	0.301 ± 0.066	2.404 ±0.470

Table 9.3. Growth rates and doubling times for the *K. pneumoniae* 52145 wild type, Δ*ldcC*, Δ*cadA* and Δ*ldcC* Δ*cadA* strains

Strain	Average exponential growth rate per hour	Average exponential doubling time (Hours)
pH 7.5		
Wild type	0.584 ± 0.005	1.186 ± 0.010
Δ*ldcC*	0.589 ± 0.014	1.178 ± 0.029
Δ*cadA*	0.574 ± 0.011	1.208 ± 0.023
Δ*ldcC* Δ*cadA*	0.573 ± 0.013	1.211 ± 0.027
pH 5.5		
Wild type	0.634 ± 0.031	1.095 ± 0.053
Δ*ldcC*	0.624 ± 0.024	1.112 ± 0.042
Δ*cadA*	0.609 ± 0.031	1.141 ± 0.058
Δ*ldcC* Δ*cadA*	0.626 ± 0.029	1.109 ± 0.053
pH 4		
Wild type	0.359 ± 0.039	1.952 ± 0.198
Δ*ldcC*	0.391 ± 0.040	1.789 ± 0.180
Δ*cadA*	0.209 ± 0.055	3.577 ± 1.022
Δ*ldcC* Δ*cadA*	0.196 ± 0.054	3.813 ± 1.027

Table 9.4. Growth rates and doubling times for the *K. pneumoniae* 52145 wild type, Δ*ldcC*, Δ*cadA* and Δ*ldcC* Δ*cadA* strains when exposed to acidified nitrite, sodium nitroprusside and ferrocyanide

Strain	Average growth rate per hour	Average doubling time (Hours)
Average growth rates in the presence of acidified sodium nitrite		
WT	0.624 ± 0.039	1.115 ± 0.068
WT + ASN	0.303 ± 0.010	2.291 ± 0.079
Δ*ldcC*	0.616 ± 0.048	1.133 ± 0.085
Δ*ldcC* + ASN	0.299 ± 0.008	2.323 ± 0.060
Δ*cadA*	0.588 ± 0.021	1.181 ± 0.042
Δ*cadA* + ASN	0.247 ± 0.029	2.852 ± 0.358
Δ*ldcC* Δ*cadA*	0.591 ± 0.041	1.179 ± 0.079
Δ*ldcC* Δ*cadA* + ASN	0.238 ± 0.032	2.961 ± 0.366
Average growth rates in the presence of acidified sodium nitrite (pH 5.5)		
WT + SNP	0.389 ± 0.015	1.782 ± 0.067
WT + SFC	0.541 ± 0.028	1.284 ± 0.066
Δ*ldcC* + SNP	0.389 ± 0.011	1.785 ± 0.049
Δ*ldcC* + SFC	0.552 ± 0.18	1.257 ± 0.043
Δ*cadA* + SNP	0.273 ± 0.010	2.543 ± 0.093
Δ*cadA* + SFC	0.446 ± 0.014	1.557 ± 0.048
Δ*ldcC* Δ*cadA* + SNP	0.350 ± 0.016	1.984 ± 0.089

Δ*ldcC* Δ*cadA* + SFC	0.461 ± 0.014	1.505 ± 0.045
Average growth rates in the presence of acidified sodium nitrite (pH 7.5)		
WT + SNP	0.378 ± 0.004	1.833 ± 0.018
WT + SFC	0.590 ± 0.006	1.174 ± 0.011
Δ*ldcC* + SNP	0.422 ± 0.007	1.644 ± 0.029
Δ*ldcC* + SFC	0.584 ± 0.018	1.188 ± 0.036
Δ*cadA* + SNP	0.427 ± 0.012	1.626 ± 0.045
Δ*cadA* + SFC	0.581 ± 0.017	1.195 ± 0.036
Δ*ldcC* Δ*cadA* + SNP	0.444 ± 0.021	1.566 ± 0.072
Δ*ldcC* Δ*cadA* + SFC	0.580 ± 0.004	1.195 ± 0.009